Function of IQD proteins in shoot organ growth

A Thesis submitted to the University of East Anglia for the degree of Doctor of Philosophy

Emma Mckechnie-Welsh

John Innes centre

Norwich,UK

January 2021

Abstract

A large family of *IQ67-domain* (*IQD*) genes encode calmodulin-binding proteins conserved throughout the evolution of land plants. Their functional role in plants is however largely unstudied. Recent research has linked different *IQD* family members to roles in plant defence and the control of growth and developmental processes, including fruit shape. IQD proteins also show interesting cellular localisations, among which association with microtubules has been highlighted as key for modulation of specific developmental processes. Furthermore, there is evidence for regulation of *IQDs* by a variety of transcription factors and plant hormones vital for controlling plant growth, supporting the importance of IQD protein function downstream in cellular processes regulating growth.

The basis of my project was to study a set of closely related *IQD* genes that were linked to plant growth, using gain and loss of function in the model plant *Arabidopsis thaliana*. This hoped to unveil redundant function and facilitate the study of cellular and molecular processes underlying IQDs' regulation of plant growth, which is applicable to crop species. Research also sought to investigate the relationship between IQD function and chemical signals associated with the gene family, such as phytohormones and calcium.

The results reported gave insight into the role of IQDs in oriented organ growth, with links to oriented cell division and auxin transport. Whilst unable to fully define the molecular basis of *IQD* function in plant growth, the work validated IQDs as molecular players involved in fundamental cellular processes of plant growth and raised novel hypotheses to explain the role of *IQD* genes in plant growth regulation.

Acknowledgments

I would like to foremost thank my supervisor Robert Sablowski for guidance throughout my PhD, particularly in motivating me to persevere when it felt like lots of work had made little progress. Your huge repertoire of knowledge in plant developmenthas helped direct experimental ideas and to expand my reading, as well as your scripting development for analysis of microscope data supporting my experimental results.

I would also like to thank Christine Faulkner and Myriam Charpentier for guidance and support throughout my PhD on my advisory committee, as well as Myriamfor sharing essential seed lines to explore the link to calcium. Huge thanks go to collaborators Katharina Burstenbinder and Dolf Weijers who so readily shared plant materials and had useful discussions that massively boosted my early project progressions.

I would like to thank all the lab members who have been present throughout my four years for helping me develop my skills and troubleshoot problems. Particular thanks to Max Bush for helping keep the lab orderly (and always knowing where to find something!) as well as helping me with any experiments or plant care if needed. Thanks go to fellow PhD student Marco D'Ario for which many discussions over hypothesis were had as well as moments to laugh alongside work.

As well as Marco, I would like to thank the huge array of other PhD students and researchers at the John Innes Centre whose friendliness and positive attitude in work made it a great environment. Many becoming friends, who provided the best kind of support outside of work, as they knew exactly what you were going through, creating so many fun memories to look back on my time spent in Norwich.

I would also like to thank my friends and family who supported from a far and always believed in me, as well as offering welcome retreats during visits where I couldn't over think work. Special thanks to my wonderful housemates and boyfriend who couldn't escape me during my thesis writing period alongside house arrest and a world pandemic.

I would like to thank the support staff such as the media kitchen, horticultural service and microscopy department for unknowing amounts of help with my research. Finally, I am grateful to the BBSRC for funding my PhD and giving me the opportunity to access amazing research facilities and gain the skills and knowledge that I have been able to.

Contents

Table of Figures

Abbreviations

ARF	AUXIN RESPONSE FACTOR protein
BIFC	Bimolecular fluorescence complementation
CaMBP	Calmodulin binding protein
CER	control environment room
ChIP-seq	Chromatin Immunoprecipitation - High Throughput sequencing

CL	constant light
CM	calmodulin protein
CML	calmodulin like protein
CMU	Cellulose-microtubule-uncoupling protein
CMT	cortical microtubule
CUC	CUP-SHAPED COTYLEDON
Col-0	Columbia
CSC	cellulose-synthase complex
CVr	coefficient of variation of cell radii
DAG	days after germination
DAPI	4,6’-diamino-2-phenylindole
Dex	dexamethasone
DMSO	Dimethyl sulfoxide
EGTA	ethylene glycol-bis(β-aminoethyl ether)-N,N,N′,N′-tetraacetic acid
FM4-64	(*N*-(3-Triethylammoniumpropyl)-4-(6-(4-(Diethylamino) Phenyl) Hexatrienyl) Pyridinium Dibromide)
FP	forward primer
GA	Gibberellic acid
GFP	green fluorescent protein
GRN	gene regulatory networks
GUS	β-glucuronidase enzyme
hr	hour/hours
IP-MS	immunoprecipitation – mass spectrometry
IQD/SUN	IQ-67 domain
MAP	microtubule associated protein
min	minutes
mPS-PI	modified pseudo-Schiff-propidium iodide stain
PAM	protospacer adjacent motif where cas9 enzyme cuts
PC	pavement cell
PCR	polymerase chain reaction
PIN	PIN-FORMED protein
PM	plasma membrane
PPB	pre-prophase band
QTL	quality trait locus
RFP	red fluorescent protein
RGA	REPRESSOR OF ga1-3

RNA	ribonucleic acid
RP	reverse primer
RZ	rib zone
RT-qPCR	Quantitative reverse transcription PCR
SAM	Shoot apical meristem
SD	short day
TF	transcription factor
UTR	untranslated region
YFP	yellow fluorescent protein
WT	wild type
2,4-D	2,4-Dichlorophenoxyacetic acid

Chapter 1 Introduction

1.1 Introduction

Growth can be defined simplistically as an irreversible increase in size. Regulation of plant growth involves controlling fundamental cellular processes to generate new plant tissue in structures with specific sizes and shapes, each adapted for optimal function supporting plant growth in vastly different environments. This regulation has evolved through a highly complex arrayof interlinking pathways, connecting signalling molecules, such as phytohormones and calcium, with a diverse array of proteins eventually converging on modification of the cell machinery. A vast amount of research has sought to unpick the entangled mechanisms of plant growth regulation, however large numbers of genes with relevant function remain unstudied, leaving the complex jig-saw puzzle fragmented.

1.1.1 Cell Division and Expansion

A large proportion of genes in plants are involved in controlling their adaptive growth and development. The diversity of plant organ shapes would not be possible without the complex and tightly regulated mechanisms established in plants to control cell division. As soon as cell division is initiated in the embryo during germination the process is under a high level of control.

The plant must be able to control when each cell begins division as well as tightly regulating when a dividing cell moves from phase to phase in the cell cycle to control organ development and overall growth rate. These control processes involve many molecular and signalling components in plants. Essential regulatory proteins are identified as cyclins. D-type cyclins (CyCD) are key for transition into several cell cycle stages (Cockcroft, E. C. et al. 2000; Riou-Khamlichi, C. et al., 1999) as well as A-type cyclins in conjunction with CYCLIN DEPENDENT KINASE A (CDKA) and B-type cyclin’s interactions with CDKB. Cyclins are regulated through transcriptional control as well as ubiquitination-induced degradation, and control entry to, and rate of, cell division in a responsive way to environmental stimuli and plant growth hormones for optimal growth (Genschik, P.et al. 2014).

Genes with repressive function in cell cycle progression are important too, with several KIP-RELATED PROTEINS (KRP) shown to inhibit CDK activity through binding cyclins (Boudolf, V. et al. 2004).

The rate of cell division in different tissues is important. Great variation in division rates is required depending on whether cells are part of an emerging organ or dividing for gradual growth of a mature organ. Meristem cell regions are the epicentre of cell division, enabling generation of all the plants' organs. In a developing embryo, a shoot apical meristem (SAM) and root meristem are established, which subsequently sustain the growth of the shoot and root, respectively. The shoot apical meristem is maintained by the division of stem cells in the central zone, which replenish cells in the peripheral zone and rib zone for organ outgrowth. These two zones of the SAM generate the lateral organs and stem, respectively. Due to the constantly replenished source of stem cells, plants, unlike many other organisms, undergo indeterminate growth (Gaillochet, C. et al. 2015). During organ initiation the initial growth phase largely involves rapid cycles of cell division providing a patterned cell population, which undergoes expansion to establish the defined shape and size of an organ. The proliferative phase and timing of the switch to growth predominantly by expansion is tightly regulated (Sablowski, R. and Dornelas, M.C. 2014).

There is a complex relationship between cell division and expansion. Individual cell sizes and shapes vary dramatically, both between different tissues within a plant and between different plant species. This is achieved by plants through coordinated control of cell expansion and division (Sablowski, R. and Dornelas, M.C. 2014). For cell expansion to take place, both cytoplasm and vacuole expansion must be coordinated with relaxation of the cell wall, before cellulose components are added to restore the wall thickness (Wolf, S. et al., 2012). The growth of any given section of cell wall can be defined as isotropic or anisotropic, depending on whether it is expanding at the same rate in all directions, therefore isotropic, or varying rates in different directions, so expanding anisotropically (Rasmussen C. G. et al. 2013).

A more complex definition of growth is the number of cell divisions, directional plane in which cells divide, symmetry of division and cell expansion, controlling cell size and shape, combine to dictate the final shape and size of a growing organ. Plant organs are diverse in shape and size. Extensive research has uncovered genetic components, divergent and overlapping, expressed in different plant organs. Through controlling both expression and transport of

regulators, growth is controlled spatially and temporally. Key regulators identified in plants include phytohormones, transcriptionfactors and calcium signaling, with microtubule arrays being a molecular component involved in both cellular processes underlying growth: cell division and expansion. Despite intensive research, how a plant keeps track of organ size and shape remains one of the most fundamental un-answered questions in biology (Johnson, K. and Lenhard, M. 2011; Sablowski, R., 2014; Zhu, M. and Roeder, HK. A. 2020). While the subset of growth regulator components used during development of different organs varies, bio-mechanical tissue responses involving microtubule arrays are potentially a universal control mechanism in plant morphogenesis (O. Hamant et al. 2008; Zhu, M. 2020).

1.2 Elements underpinning regulation of growth

1.2.1 Phytohormones

Phytohormones are prominent growth regulators across plants (Davies, P. J., 2010; Liu, K. et al., 2006). Six have been identified to have enormous importance for control of plant growth and differentiation; auxin, giberellins, cytokynins, ethylene, abscisic acid and brassinosteroids (Davies, P. J., 2010). The location and concentration of these chemical compounds, in varying combinations, can elicit very specific gene expression patterns through molecular interactions with their respective receptor proteins. Phytohormones are important for stimulation of plant growth as well as tempering growth according to adverse environmental conditions.

Ethylene and Abscisic acid (ABA) largely regulate plant growth in response to stress. Ethylene function is also linked to germination, gravitropism, fruit ripening and organ senescence. The hormone interacts with phytohormone auxin in restricting root growth and tempering plant growth upon detection of salinity stress (Wang, F. et al. 2013; Jian-Jun, T. et al. 2015). ABA is important for seed development and retardation of plant growth in response to drought stress (Nakashima, K., et al. 2013)

Other phytohormones function largely in concert with one another to both promote and restrict apical and subapical plant organ growth, balancing the rate of growth throughout development. Gibberellic acid (GA) functions in multiple

aspects of plant growth throughout development including germination, organ elongation growth and transition to flowering. The compound promotes both cell division and expansion (Achard P. et al.2009; Ubeda-Tomas S. et al. 2008).

The dwarfing of Brassinosteroid-deficient plants, caused by reduced cell proliferation and expansion, identifies the hormone also has ability to regulate both cellular processes (Fridman, Y. Savaldi-Goldstein, S. 2013). Brassinosteroids have been cited as organ growth promoting and restricting due to synergistic or negative regulatory interactions with other growth hormones. This demonstrates the importance of combined readouts for a plants' growth response to hormones (Singh, A.P. Savaldi-Goldstein, S. 2015).

Cytokynin primarily influences plant growth via regulating cell proliferation, functioning in cell cycle progression at G1/S and G2/M. It has largely opposing effects on growth in the shoot and root, promoting sustained proliferation in the shoot meristem, promoted by nitrogen (Q. Shen et al. 2013), while driving differentiation and entry in endoreduplication in the root. Cytokynin's promotion of shoot growth is largely linked to auxin function, and both phytohormones are required for induction of cell proliferation in cell cultures (Schaller, E. et al. 2014).

Auxin is arguably the most influential hormone in plant shoot growth processes, being linked to any given shoot organs' growth. This encompasses initiation and promotion of organ growth, patterning the array of lateral organs, as well as regulating the fine details of an organ, such as flat lying leaf lamina and leaf margin complexity (Maugarny-Calès, A. and Patrick Laufs, P. 2018). As with cytokinin, auxin synergistically impacts root growth. Auxin contributes to plant growth via multiple controls on cell division and expansion in a complex fashion involving multiple downstream elements. While differential function is brought about by expression of different interactors/ downstream auxin signalling components in specific cell types, the hormone is also able to have such a wide range of growth functions through complex regulation of spatio-temporal auxin concentration. Both synthesis and transport are tightly regulated (Perrot-Rechenmann, C. 2010).

1.2.1.1 Auxin transport in Plant Growth

The importance of auxin gradients throughout plant development has led to in-depth studies of auxin transport. A family of auxin exporters, PIN-FORMED (PIN) proteins, of which seven members exist in *Arabidopsis thaliana*, were

identified. Polar plasma membrane (PM) localisation of these exporters largely drives auxin gradients throughout the plant shoot and root, with additional auxin efflux proteins such as AUXIN1/LIKE-AUX1 (AUX/LAX) family reinforcing these gradients (Swarup, R. Benjamin, P. 2012).

Research has centred on PIN1 behaviour, for which strong links to organ patterning and growth have been made. Auxin gradients are thought to self-reinforce through auxin up-regulating PIN1 expression and PIN1 in each cell orientating towards neighbour cells with the highest auxin concentration (Jonsson, H. et al. 2006). Recent literature has looked further at patterning in growing tissues and whether PIN orientation is also influenced by stress patterns. High resolution imaging in the SAM has shown that PIN1 localises strongest at PMs under stress, implicating tissue stress patterns direct auxin transporter PM localisation (Heisler M.G. et al. 2010), and PIN1 reorientates around ablation sites, sites of unnaturally introduced extreme mechanical stress.

1.2.1.2 Auxin and Phyllotaxis

Computational studies of phyllotactic patterns consider timing between organ initiation, or plastochron, space between initiation sites and the size and shape of both the structure a pattern forms on and initiating objects (Douady, S. Couder, Y. 1996).

Recent models for organ patterning around a growing meristem are based on spatial inhibition fields created by newly formed primordia. Modelling generates a vast range of physically observed plant phyllotaxis by systems with two modes of inhibition, one immediate short-range inhibition and another long-range inhibition that is gradually introduced. Importantly, inhibition decreases overtime, with the newest primordia imposing the highest inhibition. Whilst it is widely accepted that initiating primordia inhibit others from initiating nearby, a biological mechanism has not been clarified (Smith, R.S. et al. 2006).

A well-studied event in organ patterning is the concentration of PIN1 at sites where new organ primordia will initiate (Reinhardt, D. et al. 2003). Studies of the transport of auxin in developing primordia have validated auxin availability as a candidate for inhibition. Auxin in epidermal cells near a primordium initiation site will be transported towards the forming primordia and have depleted auxin levels introducing an inhibition field. During outgrowth, primordia also export auxin from the epidermis to the central vasculature, allowing the site to

persist in inhibiting new primordia around them overtime. As the meristem grows, old primordia are displaced to an increasing distance away from the zone in which primordia may initiate, decreasing their influence over time. An auxin concentration threshold may therefore position successive primordia based on the positions of previously initiated ones (Smith, R.S. Guyomarc'h, S. et al. 2006).

The importance of the auxin exporter PIN1 in plant growth is underlined by severe growth defects in the *pin1* mutant, presenting an almost complete loss of ability to initiate lateral shoot organs from the stem, thus the PIN-FORMED name due to the pin-head link appearance of the shoot's bare apex (Reinhardt, D. et al. 2003). Indeed, mutations resulting in deficiencies in all of the four key plant growth regulating hormones cause severe and pleotropic growth defects, or growth arrest in the case of cytokinin (Fridman, Y. Savaldi-Goldstein, S. 2013; Dill, A et al. 2004; Skylar, A. et al. 2010), highlighting their central role in the regulation of cellular processes involved in growth. Plant hormones often perform this role by regulating the activity of transcription factors to initiate cascades of gene expression.

1.2.2 Transcription factor regulation of shoot development

A genes' regulation, whether it be transcriptionally or post-transcriptionally, is often interlinked with a large number of other genes which are part of gene regulatory networks (GRNs). The genes positioned at the hubs of these networks often encode transcription factors (TFs) that regulate RNA Polymerase II activity. It is the expression of the multiple genes downstream of transcription factors whose molecular interactions modify cellular processes impacting plant organ growth. Due to TFs' central roles in GRNs, forward genetic screens have revealed multiple TFs that are important for shoot organ growth and cause notable phenotypic variation in plants with single mutations. Examples of TFs in Arabidopsis linking to phytohormone growth regulation include the DELLA protein RGA and the brassinosteroid response factor BRASSINAZOLE RESISTANT(BZR).

REPRESSOR OF ga1-3 (RGA) works to repress the gibberellin signalling pathway, whilst gibberellin induces degradation of RGA. RGA therefore is important in GA homeostasis and to carry out the functions of the growth hormone. The activity of RGA along with other DELLA proteins results in repressed growth (Swain, S. M. and Singh, D. P., 2005). Unlike most TFs, RGA does not directly

bind to DNA and is recruited to DNA sites though interaction with other TFs (Hirsch, S. and Oldroyd, G. 2009) regulating expression of genes near DNA sites to which it is targeted to (Park, J et al. 2013). RGA interacts with hundreds to thousands of different loci that mediate its function in regulating organ growth (Serrano-Mislata et al 2017). BZR binds many gene targets involved in the downstream growth responses of brassinosteroids (BR) and is activated through phosphorylation in a kinase pathway following detection of BR by its receptor; such post-transcriptional regulation is common in gene regulatory networks (Kim, T-W. and Wang, Z-Y. 2010).

Whilst the upstream elements controlling plant growth and differentiation, such as hormones and transcription factors, have been identified through the drastic phenotypes of the corresponding mutant plants, the investigation of genes targeted by transcription factors is much less advanced. The growth processes that identified TFs modify cannot often be fully explained based on the functional characterisation of downstream targets currently known. Functional redundancy, and the complexity of multiple protein interactors involvement in any given process controlling plant growth, means that many novel genes with direct roles in plant organ growth remain undiscovered.

1.2.3 The role of microtubule arrays in cell and tissue growth

As briefly introduced, microtubules (MTs) are molecular components involved in both cell division and expansion. To perform their functions, microtubules organise into a wide range of different structures. Before mitosis, the cortical microtubules re-arrange to form the pre-prophase band (PPB), which is believed to direct the subsequent position of cell division planes, through recruitment of proteins that identify the sites of cell plate formation. During mitosis, MTs form the spindle involved in dividing genetic materials between two daughter cells, and during cytokinesis, cell plate formation requires another dynamic microtubule array, the phragmoplast, which directs the deposition of new cell wall components (Rasmussen C. G. et al. 2013).

In plant cells not undergoing division, MTs organise in the cell's periphery (cortical region) to form the Cortical Microtubule Array (CMT array). The CMTs functions in cell expansion, connecting the internal cell machinery geared towards production of cell wall components, and in particular the cellulose synthase complex (CSC), to the sites the cell wall where these components are delivered.

These cell wall components are required to fortify elongating cell walls following their expansion. In addition, they also direct anisotropic expansion through establishment of cell wall anisotropy, by fortifying specific regions of the cell wall more than others, which become more resistant to expansion versus more relaxed cell wall regions (Crowell, E.F. et al. 2010). Microtubules, therefore, are elements that orient both cell expansion and division. As such important molecular components throughout cellular processes driving organ growth, understanding how their function is regulated can inform on mechanisms of regulating plant growth.

One important factor that influences MT behaviour is mechanical stress. Because the walls of neighbouring cells are attached to each other, plant cells have to adjust their size and shape to those of their neighbours during tissue growth. This constraint puts the cell walls under stress. Interestingly, CMT arrays organise in patterns according to the directions of highest stress. This was first proposed through microtubule arrays' positioning perpendicular to the plane of cell elongation in anisotropically expanding cells under uniform turgor pressure. This microtubule pattern was suggested to occur through re-organisation in the direction of highest stress, directing deposition of cell wall material to fortify the walls under stress (Crowell, E.F et al. 2010). Imaging microtubules in the shoot apical meristem also showed correlation between CMT patterns and tissue stress patterns, as well as their re-arrangement following induction of artificial stress (Landrein, B. 2013).

Thus, stress patterns generated in growing tissues need to be considered to understand the regulation of plant morphogenesis. The function of microtubules and cell wall plasticity in organogenesis (Heisler, M.G., 2020), tension in the outer epidermal cell layer and coordinating growth of inner tissues (Mirabet, V. et al. 2011) and contribution of mechanical signals and microtubule behaviour to flat leaf lamina growth (Zhao, F. et al. 2020) point to plant's use of mechanical signals to control growth, in part through microtubule behaviour. Despite the identification of microtubules as primary elements responsive to mechanical signals during growth, a mechanism by which stress issensed and the information conveyed to microtubules is yet to be discovered.

Studies of microtubule's dynamic behaviour, and modelling of this (Allard, J.F. et al. 2010), postulated that their arrangement across the cell surface is largely self-organising. Individual microtubules grow at one end, denoted plus (+) end, and shrink at the other, denoted minus (–) end. Changes may occur in

growth and shrinkage according to stress felt at the cell wall. Furthermore, collision of a growing MT with other microtubules can lead to loss of the MT in a so-called catastrophe event, where the rate of shrinkage markedly out-paces growth. Because of this, new MTs that are in line with most other microtubules have a greater chance of growth, reinforcing any emerging pattern that begins to form (Landrein, B. Hamant, O. 2013). Modelling incorporating microtubule dynamics has been used to assess contribution of cell wall curvature, cell shape and PM association of MTs to patterns of CMT arrays in cells (Mirabet V et al. 2018) besides importance of experimentally confirmed microtubule dynamics.

Plants have also evolved a large variety of microtubule-associated proteins (MAPs), which facilitate the re-organisation of microtubules or stabilise the structures formed (Gardiner, 2013; Struk and Dhonukshe, 2014). Candidates for proteins important in CMT array organisation are structural and motor MAPS, plasma membrane-microtubule linkers and T-tubulin. The microtubule severing MAP Katanin is also important for both stabilising array configurations and promoting changes in conformation according to external stimuli. Severing is preferential at microtubule cross-over sites, because microtubule bundling behaviour decreases the availability of cut sites where microtubules are at low angles to one another (Deinum, E.E et al. 2017). Multiple MAPs likely work in concert with one another. For example, SPIRAL2, a minus end associated MAP important for stabilisation, determines the time period in which katanin cut sites are available, allowing katanin to facilitate rapid re-organisation in response to external stimuli (Nakamura, M. et al. 2018).

In animals, research also links microtubule dynamics to progression through the cell cycle, dependent on MAP phosphorylation levels (Niculescu, A.B. et al. 1998; Moon, D-O. et al. 2008). Aurora kinases are well studied in animals for their function in mitosis and meiosis, including promotion of microtubule polymerisation in spindle growth. Two classes of Aurora kinase are present in plants and, whilst less characterised, the family is also strongly implicated in cell cycle progression and microtubule dynamics. Plant aurora kinases localise at spindle microtubules, centromeres and the cell plate. While loss of function appeared lethal, knockdown lines had increased endoreduplication and reduced lateral roots, attributed to persistent periclinal rather than anti-clinal divisions. This links microtubule dynamics to progression through the cell cycle and asymmetric division planes (Van Damme,D. et al. 2011; Petrovska, B. et al. 2012).

Whilst MAP function is often regulated via phosphorylation, Ca2+/

calmodulin interactions with MAPs are also proposed to regulate re-arrangement of cortical arrays (Cyr, R. J and Palevitz, B. A. 1995). Despite this, few MAPs that bind Ca++ or Ca++ sensors have been studied. Only one, KINESIN-LIKE CaM BINDING PROTEIN KCBP, is well-studied and linked to plant growth (Buschmann,H. et al. 2015), indicating that MAPs important for regulation of microtubule behaviour remain un-characterised.

Microtubule behaviour directing cell division planes is also regulated by the phytohormone auxin in the embryo and during lateral root initiation (Lucas, M., et al.2013; Yoshida S, Prusinkiewicz P, et al. 2014). Modelling emphasised local polar auxin signalling and CMT behaviour, particularly at cell edges, are important for correct cell division plane positioning (Chakrabortty B, et al. 2018).

In summary, regulation of microtubule organisation and dynamics is complex and impacted on by multiple factors, including cell geometry, MAPs and phytohormones. Such mechanisms highlight the importance of fine-tuning microtubule behaviour, which must change alignment throughout tissue growth. The family of MAPs and mechanisms regulating microtubule behaviour can be expanded on in pursuit of understanding a plants' ability to tightly regulate growth.

1.2.4 Calcium signalling

Many different proteins have evolved for detection and response to calcium signals in plants; calcium dependent protein kinases (CDPKs), Calmodulin (CM) and Calmodulin like (CML) proteins as well as calcineurin B-like (CBL) proteins. CM and CML proteins are particularly relevant in the context of my research. In line with the potential complexity of calcium signalling in plants, a huge variety of calmodulin (CM) and calmodulin like (CML) proteins exist. Arabidopsis has 7 *AtCaM* genes with identical isoforms. Four isoforms, whilst highly conserved, are distinct and vary by up to 4 amino acids (McCormack and Braam, 2003). A diverse range of 50 CML proteins are also expressed. These vary structurally, whilst still possessing multiple EF-hand motifs as their functional domains (Ranty, B., Aldon, D. and Galaud, J. P., 2006). Interactor proteins of these calcium messengers are even greater in number.

CM/CML proteins possess EF-hand domains with negatively charged amino acid side chains to interact with positive Ca++ cations. Upon Ca++ binding the protein folding changes, altering the protein's surface charge and shape, in turn directing differential protein-protein interactions. Calmodulin interacting domains such as the IQ67 domain theoretically confer the ability to interact with all

such proteins however, given that proteins with IQ67 domains interact with only a subset of the CM and CML families in in-vitro interaction assays, protein folding and the regions surrounding the interacting domain may further define CM/CML protein binding specificity (Wendrch, J. 2018, Burstenbinder, K. et al. 2017). Further to this, expression of calmodulin interacting proteins and CM/CML proteins are likely spatially controlled to designate interacting partners for specific functions, as well as CM/CML transcript levels being regulated differentially by detection of stress, hormones and throughout development, allowing the control of multiple divergent functions by a single molecule.

Through binding to interactor proteins, CM/CML proteins transduce calcium signals to direct the correct cellular response corresponding to the event which generated the calcium signal (Tuteja, N. and Mahajan, S., 2007). An important development in the calcium signalling field has been the discovery of differential calcium signals, based on differences in frequency and duration of raises in calcium concentration (Wakelam, M.J.O. and Berridge, M.J. 2007). Calcium is maintained at very low cytoplasmic concentrations, however high concentrations are present in intracellular compartments such as the vacuole, endoplasmic reticulum and apoplast. Controlled entry into the cytoplasm through a vast array of different calcium channels, activated by different means, facilitates a large diversity of signals generated from different stimuli, as well as in highly specific regions within the cell. Combined, this again allows the use of a conserved simple signalling molecule to regulate specific processes in plant growth.

Due to the contrast between cytosolic and compartmentalised calcium concentrations, activation of any given channel results in very rapid changes in cytosolic Ca++ levels. These calcium signals are also able to propagate quickly through plant tissues. Such a rapid and mobile signal places calcium as an ideal molecule for sessile plants' responses to environmental stress, and indeed, increased cytosolic calcium concentration has been reported among the most rapid responses to a variety of abiotic and biotic stresses. Research has also identified CM and CMLs in stress signal transduction, such as responses to temperature changes. CMs regulate cold responsive genes as well as CM3 regulating HEAT SHOCK FACTORs, with *cm3* mutation reducing levels of HEAT SHOCK PROTEIN and tolerance in plants. CM/CML members are highly upregulated in drought/ osmotic stress as well as wounding. Mutations in calcium channels impair plants' responses to pathogens, as well as CM/CML proteins

identified downstream in molecular signaling pathways for plant defense (Kai H. Edel, K.H. et al. 2017).

Calcium sensor proteins have also been linked to growth processes involving responses to environmental stimuli, including photomorphogenic growth in response to light (Kushwaha, R. et al. 2008). Further to this, CML proteins have been identified as components in trichome development (S. Dobney, S. et al 2009) and flowering time through moderation of FLOWERING LOCUS C (FLC) (Tsai, Y.C. et al. 2007). Growth related functions of CM/CML proteins defined in literature are in very specific stand-alone growth processes. Such functions would not indicate a requirement for moderation of CM/CML levels throughout plant development, which would indicate more universal roles in plant growth. As stated, few MAPs have been confirmed to interact with calcium signalling components. These could provide an avenue to uncover more substantial roles of calcium signalling in shoot growth.

1.3 IQ67-domain family

The *IQ67-domain* (*IQD*) gene family is conserved across dicotyledons and monocotyledon species. The conservation across divergent plant species suggests important roles. In fact, based on the discovery of *IQD*-like genes in *Physcomitrella patens*, it has been proposed that the *IQD* gene family evolved 450–700 million years ago, very early in the evolution of land plants (Zhao, Y. & Mooney, S. D. A., 2009; Wu, M. L. et al., 2016). All members of the IQDs are composed of different combinations of a subset of conserved modules which could confer their function, although yet to be defined (Abel, S., et al., 2005, Wu M. et al. 2016). Those with similar module components are placed in *IQD* subfamilies. Extensive phylogenetic analysis of *IQD*s in different species (Feng, L. et al. 2014; Abel, S. et al. 2005; Cai, R. et al. 2016; Wu M. et al. 2016) has led to division into five sub-families (Figure 1.1). Interestingly, the proteins are more highly conserved within each sub-family than to other IQDs in the same species but in different sub families. Combined, this information indicates divergent function of IQDs across sub-families.

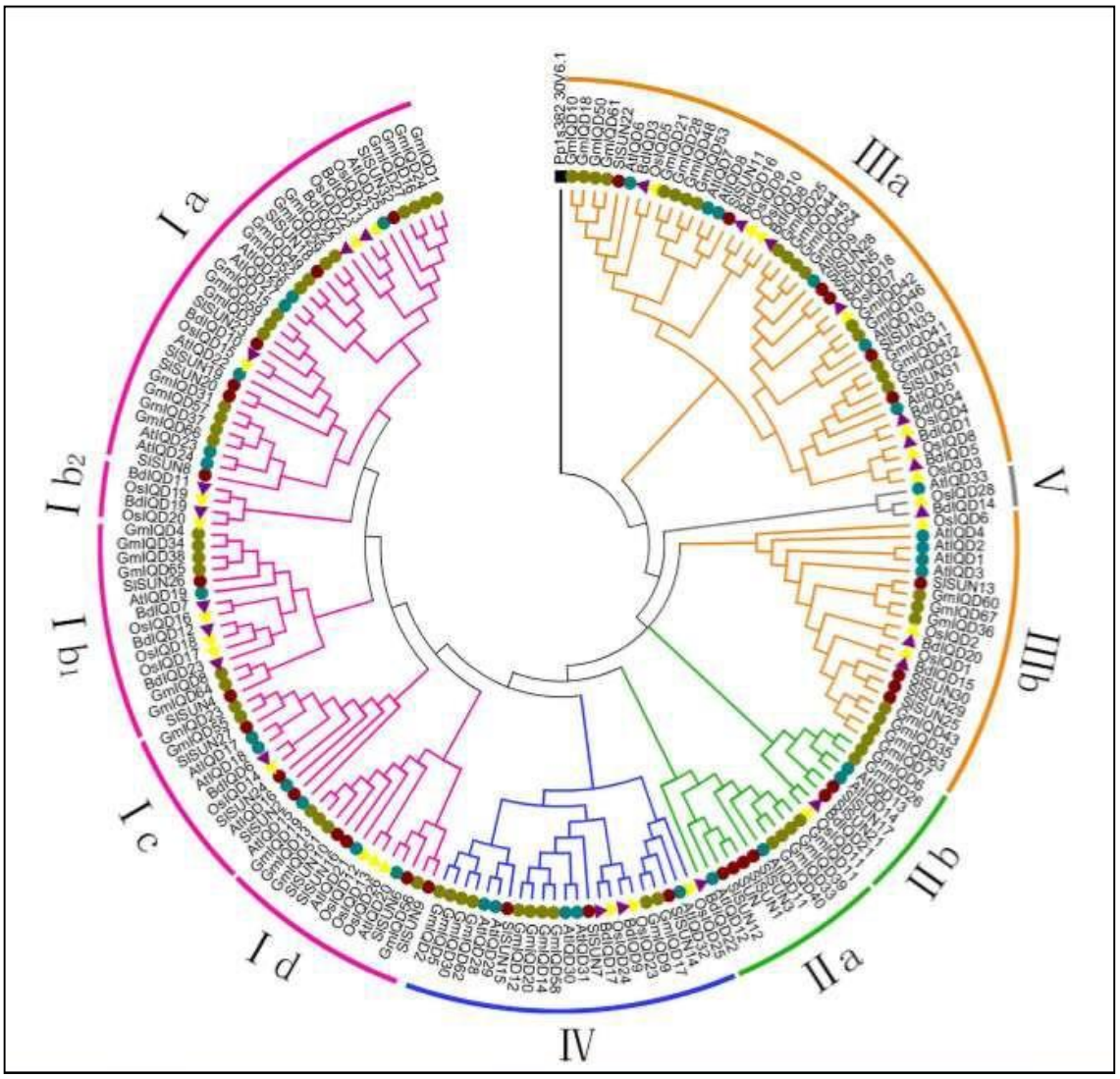

1. 1: Phylogenetic tree of the *IQD* gene family in Arabidopsis, soyabean, tomato, rice and Brachypodium. The 33 members in Arabidopsis span all 5 subfamilies, with multiple members in each likely conferring functional redundancy. Large families exist in both dicot and monocot species. Taken from Feng L, Chen Z, Ma H, Chen X, Li Y, et al. (2014) The IQD Gene Family in Soybean: Structure, Phylogeny, Evolution and Expression. PLoS ONE 9(10): e110896. doi:10.1371/journal.pone.0110896. open access publication distributed under the terms of the Creative Commons Attribution License.

IQDs also display a variety of interesting cellular localisations which suggest roles in multiple cellular processes. Almost all IQD family members have been shown to associate with microtubules. As well as this, certain members show localisation to membrane micro-domains, whilst all appear to tether non-discriminatorily at the plasma membrane. Some IQDs also have a variety of nuclear localisations, with GFP fusions observed at the nuclear envelope, nucleus, nucleolus or in nuclear bodies. Protein size would indicate a requirement for active import, and indeed nuclear localisation signals have been identified

(Burstenbinder, K., 2017). Through sequence analysis and predicted protein structure, IQDs' microtubule and PM localisation has been proposed to be mediated by basic amino acids generating positively charged patches on the proteins. Basic amino acids aid electrostatic interactions with the acidic phospholipid membrane and tail motif of tubulin subunits (Drevensek, S. et al.2012; Scott A.M. et al 2013). A high isoelectric point of IQD proteins (~10.3) is a hallmark of the family (Abel, S. et. Al 2005). Membrane tethering of IQD proteins is possibly further stabilised by *S*-acylation, for which sites have been predicted (Burstenbinder, K. 2017).

In spite of their high conservation, being present in almost all land plant species, and intriguing subcellular localisations suggesting function in cellular processes controlling plant growth, little has been published regarding the function of IQD proteins in plant cells. Arabidopsis has a large *IQD* family comprising of 33 members, consistent with the large family sizes also annotated in crop species (Figure 1.1). Examination of expression data available on ARAPORT shows high expression levels of several members in the shoot apical meristem, encouraging research into their possible developmental roles in the shoot (Tian et. al., 2014).

1.3.1 Calcium and IQDs

The *IQD* family received its name because all family members contain 1-3 copies of a conserved calcium-independent calmodulin binding domain called IQ67. IQD proteins also contain 1-4 copies of the 1-5-10 and 1-8-14 calcium-dependent calmodulin binding domains (CaMBD). These domains can overlap with the IQ67 domains (Abel, S., et al. 2005). CaMBDs are rich in basic amino acids that form interactions with the negative hydrophobic pockets of Calmodulin, exposed upon calcium binding. Currently only one identified calmodulin binding protein (CaMBP), which is also a microtubule associated protein (MAP), KINESIN-LIKE CaM BINDING PROTEIN (KCBP/ZWI), has a characterised role in plant development (Buschmann, H. et al. 2015). Calmodulins (CMs) are however identified as messenger proteins used by the plant to control microtubule organisation in response to external and internal signals, making it likely that other CaMBP-MAPS have roles in adaptive growth control. IQDs are calmodulin-binding MAPs and have been shown to interact with other microtubule associated proteins, such as Kinesin light chain related protein 1 (KLCR1/CMU) and SPIRAL2

(Wendrich, J. R. et. al., 2018) making them ideal candidates for mediating the effects of Ca++ on microtubule arrays (Burstenbinder, K., 2013, 2017).

Due to the large number of calmodulin binding sites in IQDs, their function is likely to be regulated by calcium signals via changes in calmodulin interactions. Establishing whether intracellular calcium levels affects calmodulin interactions with IQDs, IQD association with other elements such as microtubules and binding interactors, or function at IQD cellular locations such as microtubules, would be extremely useful in understanding their function.

1.3.1.1 Calcium links to IQD function

Co-expression assays in planta have shown recruitment of CM2 to IQD1 from free cytoplasmic and nuclear localisation to microtubules and the nucleolus. Further co-expression assays demonstrated IQD1,21,23 and 31 also recruited CM1 and IQD31 showed interaction with CML13 (Burstenbinder, K., 2013). Later studies involving reporters showed RFP-CM2 delocalised to microtubule and membrane locations of GFP-tagged IQD members; 8,13,16,25 and 33 (Burstenbinder, K., 2017). Separate experimentation involving immunoprecipitation of IQD15, 17 and 18 in both roots and siliques resulted in detection of CML13, CML14 and calmodulin family proteins. Yeast two hybrids were carried out to confirm direct calmodulin interactions with CM1,2 and 3 (Wendrich, J. R. et. al., 2018). Bimolecular Fluorescence Complementation (BiFC) assays have also been used to confirm IQD18 interaction with CM1 (Wendrich, J. R. et. al., 2018) and CM2 with IQD5 along filamentous microtubule like structures (Mitra,D. et al. 2019). This evidence for recruitment of at least three CM and several CML proteins by IQDs supports Ca++ signalling regulation of IQD cellular function at microtubules and the PM.

IQDs' calmodulin binding domains implicate the proteins can bind calmodulin in the presence or absence of calcium at different sites. The predicted alpha helical structure, similar to myosin, also indicates the ability to bind more than one calmodulin at a time (Houdusse et al., 2006, Burstenbinder, K., 2018). Preliminary assays to differentiate between IQDs' binding of CM in high versus low calcium concentration have been carried out by IP-MS, using bead binding assays in both EGTA (ethylene glycol-bis(β-aminoethyl ether)-N,N,N′,N′-tetraacetic acid) and raised calcium conditions. The IP-MS experiment showed variation in IQD binding of CM and other interacting proteins. Importantly, IQD18 had a stronger

CM interaction in raised calcium (Wendrich, J. R. et. al., 2018). This indicated calcium signalling may have the ability to modulate whether calmodulin relocalises to interact with IQDs, subsequently affecting other protein interactions. Differential protein interactions may be one means Ca++ signalling moderates IQD function, for example at microtubules, thus transducing calcium signals to changes in microtubule behaviour. Little work however has come close to deciphering calcium's role in modulating IQD function.

Further studies are required into variation in CM and CML partners, the form in which the proteins interact with IQDs and what effect this may have on IQDs' cellular function. With calcium signals being used by plants to help regulate a diverse range of functions in development, defence responses, stress responses and transcriptional regulation, this leaves the potential role for IQD proteins in plants wide open.

1.3.2 Microtubule orientation and IQDs

Building cellulose for cell wall growth requires delivery of the cellulose synthase complex (CSCs) to the plasma membrane, and this is coordinated by microtubule arrays (Liu et al., 2015). The way in which the CSC interacts with microtubules, and how the microtubules in turn organise and interact with the plasma membrane for site specific delivery, is not well understood. Association of IQDs with Kinesin Light Chain-related protein 1(KLCR1) / Cellulose-microtubule-uncoupling protein 1 (CMU1) (Burstenbinder et al., 2013, Liu et al., 2016) has suggested a role for IQDs in CSC delivery during cell expansion. CMU proteins function in preventing the CSC from dragging microtubules with it as it moves along the cell wall. Mutants of CMU proteins have twisted organs similar to mutants in which microtubule orientation is disrupted (Liu et al., 2016). IQDs' association at the PM and with the CMT array potentially confers the ability to act as a tether, linking cortical microtubules to the PM. This could indicate a role for IQDs in facilitating directional cellulose deposition by the CSC as well as to ensure the microtubules aren't disrupted by the CSC, through recruitment of CMUs (Kölling, M. et al. 2019). Calmodulin recruitment by IQDs could implicate relay of a cytoplasmic calcium signal to alterations of cortical microtubule distribution at the plasma membrane/cell wall.

The first *iqd* mutant to be characterised in plant growth was subfamily 2 *sun12* in tomato. A transposon insertion which disrupted the *SUN12* locus,

increasing gene expression, resulted in elongated tomato fruit (Xiao et al., 2008; Wu et al., 2011). The phenotype of this mutant, which included altered cell shape and twisted stems, indirectly strengthened the link between IQDs and microtubule stability/organisation, due to the similarity to the phenotype of plants with mutations in tubulin subunits (Ishida et al., 2007) and in MAPs (Buschmann et al., 2004; Sedbrook et al., 2004). Interesting and varied phenotypes in over expression (OE) lines of *IQD* subfamily members in Arabidopsis also supported functions involving microtubules. Overexpression lines of *IQD11* and *16* also caused elongated cells and aerial organs as well as twisting, while *IQD14* lines resulted in twisted, if not elongated, organs. Overexpression of *IQD25* contrastingly led to shortened, more rounded leaves (Burstenbinder et al., 2017). The variation in pavement cell and organ shape between the different *IQD* overexpressing lines has been linked to their different cellular localisation patterns. IQD25 localises in specific membrane domains and IQD11, 14 and 16 decorate CMTs. Despite the majority of IQD proteins observed along microtubule like structures, the pattern of MT decoration varied. The pattern of CMT decoration of IQD11 and 16, members linked to elongated aerial organs, is distinct out of all 33 members in Arabidopsis, which could explain variation in ectopic lines' shoot growth (Burstenbinder et al. 2017).

The previously cited IP-MS assays of IQD15, 17 and 18 pulled down several interactor proteins other than calmodulin, notably microtubule subunits and other microtubule associated proteins: TUBULIN A, TUBULIN B, SPIRAL2, 14-3-3 GF14, ANGUSTIFOLIA, ACTIN (family) and the BIG Auxin transporter (Wendrich, J. R. et. al., 2018). Of these, SPIRAL2 was particularly interesting, due to the mutant phenotype being similar to that of the IQD OE lines (Nakamura et al., 2018; Leong et al., 2018). SPIRAL2 showed direct interaction with IQD18 in yeast two hybrid and BIFC (Bimolecular fluorescence complementation) assays (Wendrich, J. R. et. al., 2018). The interaction was also affected by calcium levels, leading to the proposal that in higher calcium IQDs interact more strongly with CM, displacing SPIRAL2, which re-localises to minus ends of microtubules, increasing microtubule dynamics through katanin (Leong et al., 2018; Yang et al., 2018). In rice, *OsIQD14* is representative of the *IQD15-18* clade in Arabidopsis. A mutation in this gene resulted in deformed rice grain shape as a result of defects in the seed hull, which constrains the rice grain as it grows. Microtubules are hard to observe in this tissue type, but due to the conservation between *OsIQD14* and *IQD18* in Arabidopsis, microtubule defects are highly likely to be the cause, potentially

through the SPIRAL2 interaction as seen in Arabidopsis (Wendrich, J. R. et. al., 2018, Yang et al., 2018).

Further to these links to microtubule behaviour and growth, IQDs are associated with cell wall deposition in xylem secondary cell wall pits and pavement cells. It had been postulated that the cellulose deposition to secondary wall pits must be modulated by a protein able to bind to microtubules and the plasma-membrane. When IQDs were investigated as candidates to fulfil this role, the *iqd13* mutant showed altered cell wall pit shape. Shape regulation was facilitated through IQD13 increasing stability of cortical microtubules bundled around active ROP-GTPase domains, restricting them to oval shapes, which correspond to the shape of the pits that develop in the cell walls. IQD13's microtubule-binding N-terminus domain and PM-tethering C-terminus domain are both required for this function (Sugiyama, Y., et. al., 2017).

Similarly, there was a link to altered cellulose deposition in *iqd5-1* plants with a reduction in lobe length and definition in their pavement cells. A concentration of cortical microtubules in neck regions, coordinating a higher cellulose deposition in these regions, promotes anisotropic cell expansion in WT pavement cells (Sampathkumar A. et. al 2014). This concentration of cortical microtubules at neck regions is lost in the *iqd5-1* mutant (Mitra, D et al., 2018). In both cases IQD13 and IQD5 appear to function in stabilisation of microtubules at specific cellular locations, with lowered cellulose deposition to these sites in mutants resulting in altered cell shape. Further evidence for microtubule stabilisation by IQD5 came from highly sensitised responses to the microtubule-disrupting drug oryzalin in the mutant line.

The link between microtubule association and IQD's role in plant cells is yet to be fully defined. Evidence suggests that individual members have a role in regulating stability or organisation of microtubules that could impact on the deposition of cell wall components. Their function regarding microtubules could be controlled by calcium/calmodulin. Preliminary investigation suggests other protein interactors with roles in microtubule dynamics are important for IQDs' function as MAPs. Divergence in IQD family member CMT decoration, protein-protein interactors and specific cellular expression could therefore impart differential function across the large gene family. Ties to cellular and organ growth phenotypes linked to microtubule dynamics make IQDs interesting novel candidates for regulating cellular processes important in plant growth.

1.3.3 Functional links to plant growth

As well as strong growth phenotypes in over-expression lines of *IQDs* and subtle cellular level phenotypes attributed to single *IQD* family members, further evidence supports important functions for IQDs in the regulation of plant growth.

A study of *IQD10* in Populus showed the gene to be expressed highest in stressed xylem tissues, displaying a similar tissue expression pattern to cell wall associated genes. Promoter binding assays supported a function in secondary cell wall biosynthesis, with target of a master regulator controlling cell wall biosynthesis able to activate *IQD10*. RNAi knockdown of IQD10 in Populus resulted in increased biomass, with taller plants and thicker stems, suggesting pleiotropic effects. This implicated IQD molecular function downstream of master growth regulators (Badmi, R et al. 2018).

IQD22 in Arabidopsis subfamily 1a has been shown to interact with the DELLA protein RGA, being upregulated by the DELLA protein and down regulated by GA (Zentella, R. et al., 2007). Research presented in the previous section linking family 1c members in Arabidopsis, *IQD15,16,17* and *18*, to microtubule behaviour was undertaken due to mis-regulation of all four genes in a MONOPTEROS (MP) mutant transcriptome, implicating IQD function in growth downstream of an auxin response factor. IQDs are therefore again demonstrated to be downstream elements of master growth regulators and could be directly responsible for changes in cellular processes regulating growth.

Aside from the transposon inducing ectopic *SUN12* expression (Xiao et al. 2009), NIL lines of tomato varying at the *SUN12* locus had notable, although less pronounced, effects on shoot organ growth. These include positive association of IQD levels with elongation of organs, including cotyledons, leaflets, ovaries and subsequently fruits. Impacts on leaf complexity in more extreme over expressor lines as well as leaflet outgrowth in NILs led to conclusions linking IQDs to the control of auxin distribution, however only supported by observed phenotypes (Wu, S et al 2011).

Another fruit shape regulator, OVATE, was found to genetically interact with the *sun12* mutation, increasing growth at the distal end of the fruit, resulting in an elongated, pear-shaped fruit (Lazzaro M.D et al. 2018). Auxin application 3 weeks before anthesis increased cell division and size at the proximal versus distal region of the fruit, and ovaries as well as subsequent fruits were elongated and pear-shaped much like *sun ovate* mutants. Further analysis of the link to auxin in these

mutants highlighted SUN as a regulator of auxin-related genes early in ovary growth, indicating this may be a means for the genes' effect on fruit shape. However, levels of auxin in early ovary development did not appear changed in mutants (Wang, Y. et al. 2019). Nonetheless, multiple research papers suggest functional links between IQDs and auxin.

Further research has strengthened *IQD* association with regulation of fruit shape. Phylogenetic analysis of *IQD* genes in the cucurbit family associated with fruit shape control in watermelon (*ClSUN8*), melon (*CmSUN14*), and cucumber (*CsSUN2*) (Pan, Y. et al. 2017; Dou, J. et al 2018), clustered with subfamily 1a *IQD* genes in Arabidopsis. Research on the function of *ClSUN8* in watermelon confirmed an important effect early in ovule development, with highest expression of the gene -4 days after fertilisation, when there was increased cell division in the longitudinal direction. In one instance, different accessions of watermelon with more rounded or elongated shape had similar expression levels of the gene and a non-synonymous SNP was identified as candidate for altered IQD function (Jin, B. et al. 2017). Other literature in watermelon and cucumber cite accessions with deletions in *IQD* genes and altered fruit shape. More rounded fruit in the cucumber line WI7239 was associated with a 161 bp deletion in the first exon and subsequent lower *IQD* expression than in the elongated accession, WI7238 (Pan, Y. et al. 2017). A gene denoted *Cla011257*, analogous to I*QD26* in Arabidopsis, identified in QTL analysis of an elongated watermelon fruit shape line, contained a 159 bp deletion that resulted in almost three-fold higher *IQD* expression than in those with round fruit. Again, expression was highest in the ovary, demonstrating the importance of *IQD* genes in early development (Dou, J et al. 2018).

Whilst a strong association has been established between *IQD*s and fruit shape control in crops, little information is available as to the underlying molecular mechanism. Conversely, advancements in understanding IQD molecular function have begun to be made using tools available in the model plant species *Arabidopsis thaliana*, although still lacking supporting evidence for organ shape control using loss of function lines.

1.4 Research Aims

The introduction highlights that many molecular components which function downstream of master growth regulators to tune cellular processes required for plant growth remain elusive. The *IQD* gene family have been recently identified as such components, linking multiple regulatory elements that may converge on IQD function to modulate cellular processes relevant to growth. The aim of this project was to use tools available in the model plant species Arabidopsis to better understand the function of IQDs in growth regulation at a cellular and molecular level.

Chapter 2 focuses on selection of subfamily 1a, for which research in shoot growth appeared relevant and transferrable to crop species. Characterisation of macroscopic growth phenotypes in loss and gain of function lines in Arabidopsis are presented. The results uncovered genetic redundancy masking substantial impacts of IQD proteins on Arabidopsis growth. Chapter 3 and 4 investigate in more detail growth defects in stem and leaf shape respectively, unveiling cellular processes affected by 1a IQDs to regulate plant growth. Work in Chapter 5 sought to further establish molecular functions underlying the cellular responses to loss of IQD function and touch on calcium regulation. Finally, Chapter 6 separates the growth modification in gain and loss of function *iqd* mutants from interaction with the DELLA-GA signalling pathway, despite evidence for IQDs as DELLA protein targets.

Chapter 2: Loss and gain of function of subfamily 1a *IQD* genes revealed pleiotropic effects on plant growth

2.1 Introduction

In land plants, the strong conservation of *IQD* genes throughout evolution, and the presence of large families of these genes in any given plant species, are highly suggestive of important functions of *IQD* genes. Whilst all members consistently feature a central IQ67 domain, there is a large variation in length and sequence of N and C terminus across any given plant species' family. Conserved N and C terminal modules were identified and used for phylogenetic classification, placing genes with highest match and position of modules together in sub families. For example, in *Arabidopsis thaliana* there are 33 *IQD* genes, which have been divided into subfamilies 1abcd, 2ab, 3ab, 4 and 5 (Abel, S. et al. 2005).

The large diversity in modules and combinations found across IQD members in different subfamilies suggests divergent functions. Conversely, strongly conserved functions are presumed between IQDs within a subfamily. Various research has sought to understand the relevance of IQDs across multiple plant species. These include the model species *Arabidopsis thaliana*, as well as a large proportion of research in fleshy fruit producing crop plants, such as tomato, watermelon and cucumber, in which IQD function has been associated with fruit shape traits, as presented in main introduction (Wu, S. et. al. 2011, Pan, Y. et.al. 2017, Dou, J. et.al.2019). High levels of *IQD* expression have been associated with more elongated and narrow shoot organs in fleshy fruit crop species; similarly, ectopic expression of certain *IQDs* in *Arabidopsis thaliana* and tomato also resulted in elongated and twisted shoot organ phenotypes (Xiao et al., 2008).

IQD function in *Arabidopsis thaliana* has been studied mostly by overexpression, including subfamily members from 1a, 1c, 2a and b. Overexpression phenotypes varied across different subfamily members, with one line resulting in more rounded leaves and another causing twisting with no organ elongation. Subsequent investigation of cellular localisation linked differing gain of function phenotypes to variation in the decoration of cortical microtubule (CMT)

arrays, found in varying degrees for almost all IQDs of *Arabidopsis thaliana* (Burstenbinder, K. et al. 2017). MAP function has been reported for *IQD5* and *IQD13* which stabilise microtubules, associated with control of pavement cell and secondary cell wall pit shape respectively (Mitra,D. et al. 2019; Sugiyama, Y., et. al., 2017).

Further links in the literature between plant growth and the *IQD* gene family lie in ties to phytohormones. Transcriptome data sets of mutants for MONOPTEROS (MP, also named AUXIN RESPONSE FACTOR5, ARF5) revealed reduced expression of all members of 1c, as well as some of 1a, 2a and 3a, placing *IQDs* in auxin signalling pathways downstream of MP/ARF5 (Schlereth, A. et al., 2010; Möller, B.K. 2012) A family 1a *IQD* member, *IQD22*, also featured on the list of highly mis-expressed genes in plants with gain of function of the DELLA protein REPRESSOR OF GAI (RGA), implicating upregulation of the gene by RGA (Zentella, R. et al., 2007). Further work indicated transcripts of GA biosynthesis genes are upregulated in overexpression lines, positioning 1a *IQDs* in the DELLA-GA signalling feedback loop (Zhou, X. and Sun, T., 2011). Such phytohormone pathways are well studied in the control of growth processes throughout shoot development, and IQDs could yet be a further component characterised in part of these molecular networks.

A further link between *IQD* members in subfamily 1 and regulatory genes that control shoot growth emerged from Chromatin Immunoprecipitation - High Throughput sequencing (ChIP-seq) experiments performed in my research group (Bencivenga, S. et al 2016; Serrano-Mislata, A. et al. 2017). The ChIP-seq data for the BELL-type transcription factor REPLUMLESS (RPL) and for the DELLA protein RGA showed several 1a family members were good candidates for regulation, and therefore could be positioned in growth responses downstream of these regulatory genes.

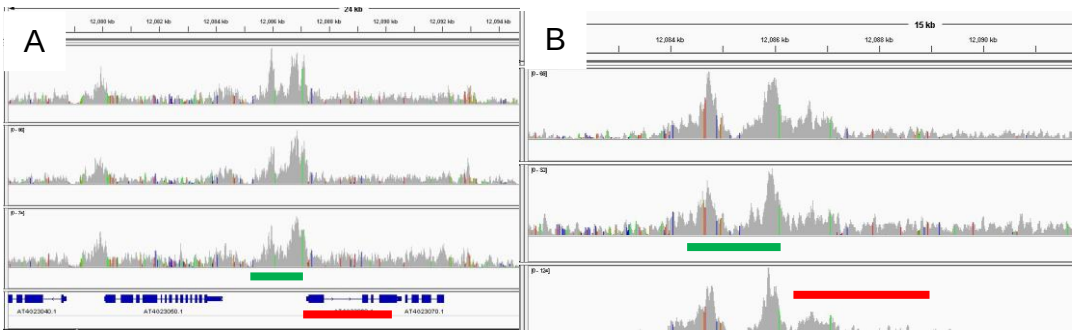

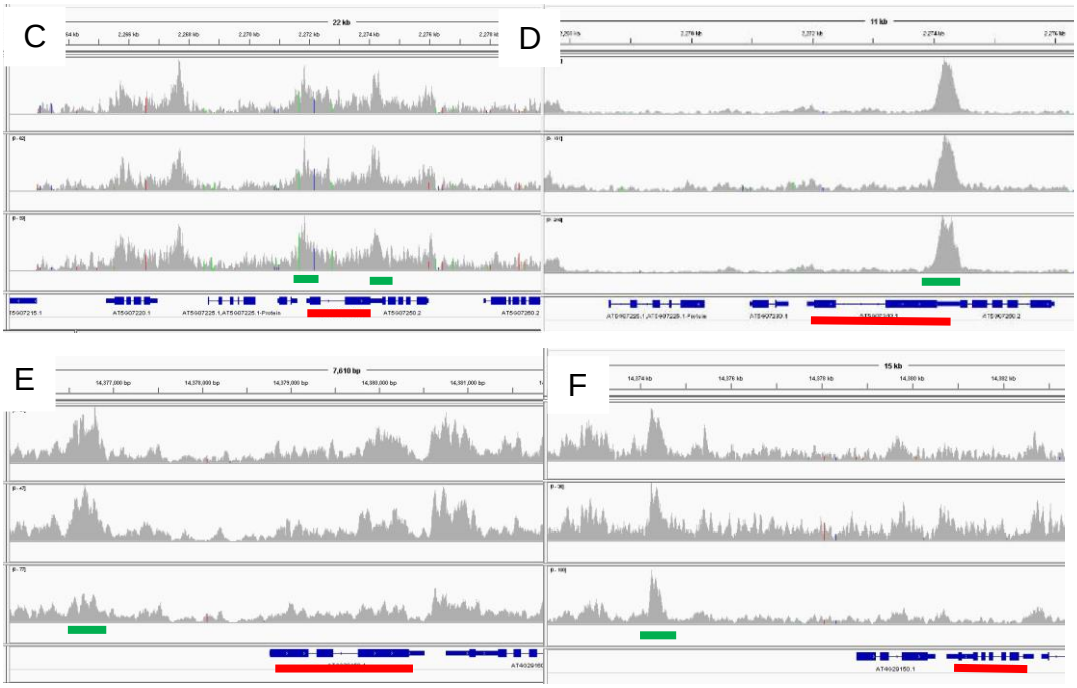

Figure 2. 1: ChIP-seq peaks across several TFs regulating growth processes indicate DNA binding sites close to family 1a *IQD* gene loci. A, B: *IQD22* binding peaks for RGA (A) and RPL (B). C, D: *IQD24* binding of RGA (C) and RPL (D). E, F: *IQD25* bound by RGA (E) and RPL (F). Red underlines genes of interest and green bars show peak regionswith strong statistical support in all three biological replicates.

2.1.1 Aims of this Chapter

Based on links to fruit shape in multiple crop species, ties to phytohormone pathways and to regulatory genes implicated in shoot growth in *Arabidopsis thaliana,* subfamily 1a was selected to study IQD function in shoot organ growth. To establish whether subfamily 1a does indeed impact on shoot organ growth, I used loss and gain of gene function. For this, it was first necessary to overcome the hurdle of genetic redundancy, as family 1a has 6 members in Arabidopsis. This chapter focuses on the production of a sextuple mutant and a transgenic line with inducible gain of function of family 1a *IQD22*, and on the initial characterisation of their developmental phenotypes. This research unveiled effects on the growth of multiple shoot organs, indicating that subfamily 1a genes affect cellular/molecular processes with wide roles in plant growth. Common features of the loss of function phenotypes in different organs direct further research in the following chapters, focusing on uncovering IQD function at the cellular level.

2.2 Results

2.2.1 Generation of novel loss of function mutants in IQD subfamily 1a

As the six genes in subfamily 1a have highly similar module composition, I presumed that functional redundancy was likely an obstacle to studying loss of function. Through collaboration with Dr Katherina Burstenbinder, Institute for Plant Biochemistry, Halle, I received a triple T-DNA mutant line for *iqd25,26* and *27* (*iqd25-1*; SALK_058876.25.70.x, *iqd26-3*; GK-728F02 and *iqd27-2*; SALK_103602.28.55.X). Gene editing by the CRISPR-cas9 system was well established by the start time of my PhD and appeared a promising tool for quickly establishing the sextuple mutant through targeting of the three remaining genes, *IQD22,23* and *24*, all at once.

To target multiple genes simultaneously, pairs of RNA guides within 100 bp of one another and adjacent to PAM Cas9 target sites were designed in required 1a *IQD* gene regions and assembled in GreenGate pUC19-based entry vectors (Lampropoulos, A. et al., 2013). To provide Cas9 activity, ICU2p:cas9 and Ubi10:cas9 modules were also assembled. The Ubiquitin 10 promoter (Ubi10p) is a constitutive promoter commonly used in CRISPR constructs (Castel, B. et al. 2019), whilst the INCURVATA 2 promoter (ICU2p) is highly expressed in meristems and has been used successfully to produce high frequencies of inheritable gene editing (Hyun, Y. et al., 2014). A total of six entry vector slots could be introduced into final GreenGate destination vectors (Lampropoulos, A. et al. 2013 **)**, allowing for the three modules with double guide targets for *IQD* genes, the promoter Cas9 and a selection marker. However, despite sequencing confirming that all overhangs for the cut and paste step into the final vector were correct, the final combination reactions were never successful.

The modules containing promoter, guide, RNA scaffold duos were therefore converted to be compatible with the GoldenGate assembly system (Engler, C et al. 2008) via introduction of *Bpi*I restriction sites and overhangs. The PCR products were carried forward directly into the final reaction with level 1 promoter cas9 reverse orientation and fast red resistance vectors, into destination vector pICSL4723 (provided by SynBio TSL, NRP, protocol followed GoldenGate TSL SynBio; synbio.tsl.ac.uk**).** Guide target modules for *IQD*22,23 and *24* were

successfully combined in the GoldenGate final destination vector and the constructs used to transform *iqd25,26,27* T-DNA mutant line using the established *Agrobacterium tumefaciens* protocol for transforming Arabidopsis (Zhang, X. et al. 2006).

Numerous transformed seeds were selected for red fluorescent seed coat, however, only guides targeting *IQD24* resulted in successful editing. A second-generation plant with Cas9 segregated out was selected with a stable 62 base pair (bp) deletion near the start of *IQD24*. The first 30 amino acids (aa) from the genes' start codon were readable, followed by deletion of codons for 20 amino acids, as well as two bases of the subsequent codon. This induced a frame shift that predicted translation of a further 16 incorrect amino acids before a premature stop codon. Thus, the *iqd24* mutant allele is likely a loss of function allele.

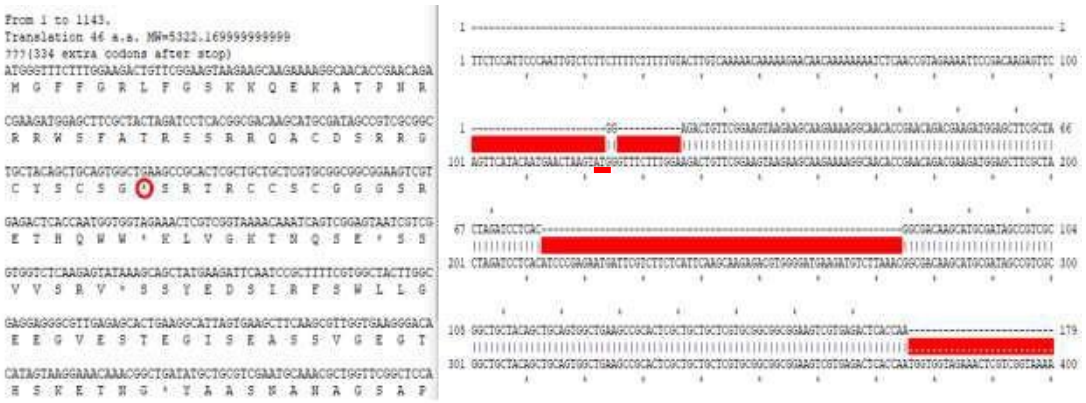

Figure 2. 2: Sequence analysis of selected CRISPR-edited *iqd24* loss of function mutation. Out of frame deletion was found close to the start of the coding sequence (right panel, start codon underlined in red). This resulted in the premature stop codon circled in red (left panel).

To obtain mutant alleles for *IQD*22 and *IQD*23, a further round of CRISPR mutagenesis was attempted, using the GoldenGate system with new pairs of guides designed targeting different gene regions. Again, no mutations were found, either through notable band shifts in PCR products spanning the target region identifying deletions, or as point mutations after sequencing multiple PCR products from successful transformants. Whilst in many cases the CRISPR system is highly efficient and provides opportunities to investigate simulataneous loss of function of multiple genes (Hang, Y and Showalter, A. M. 2020), there is still lots to be understood about guide efficiency and any local gene environment that may restrict Cas9 targeting or editing. Following delays in generating a higher order

sextuple mutant, further T-DNA lines (*iqd22-1* SALK_ 103903.55.75.x and *iqd23-2* SALK_073090) were combined by crossing to obtain the full sextuple mutant.

2.2.2 Establishment of the sextuple *1aiqd* line

Redundancy between gene family members is often partial (Willige, B. C., et al. 2007), so while constructing the sextuple *1aiqd* mutant, I searched for phenotypic changes that could facilitate the selection of increasingly high-order mutants. Growth phenotypes became initially apparent in the triple TDNA line *iqd25,26,27.* The strongest difference between WT grown plants appeared to be in sturdiness of stem and slight increase in lateral branch number. Stem diameter was therefore measured versus WT Col-0 background and trait monitored as subsequent mutations were added to the triple mutant background. To standardise the quantification of stem diameter growth, measurements were taken at the base of the stem when plants had 4 elongated siliques, for large sample sizes in each mutant background. In line with the enhanced stem diameter being caused by loss of 1a *IQD* function, the subtle trait in triple mutant plants was enhanced upon introduction of additional *iqd*24 mutation and then further still upon establishment of full subfamily mutant line (Figure 2.3).

The *iqd25,26,27* line stems' averaged 0.15 mm greater in diameter than WT, which was significant given the small diameter of WT stems in this experiment. A larger increase in stem diameter of 0.31mm occurred in quadruple mutant loss of function line *iqd24,25,26,27*. This increase would be predicted to results in a 35% larger stem cross section area in mutants**.** An even more pronounced 0.7mm increase in diameter occurred in full subfamily mutant line, referred as *1aiqd* in text. This result was reproducible over two experiments with high biological replications, giving strong statistical significance. Highly similar stem diameter increases of 0.714 mmm and 0.712 mm accounted for a very large increase in stem section area, projected to almost double in size with an 88% increase (Figure 2.3)**.** As can be seen in Figure 2.4, the stems of the full 1a subfamily mutant were visibly wider, whilst final plant height did not seem to change (Figure 2.14). This was the first indication that family 1a IQDs may have a role in controlling organ shape, as seen in crop species.

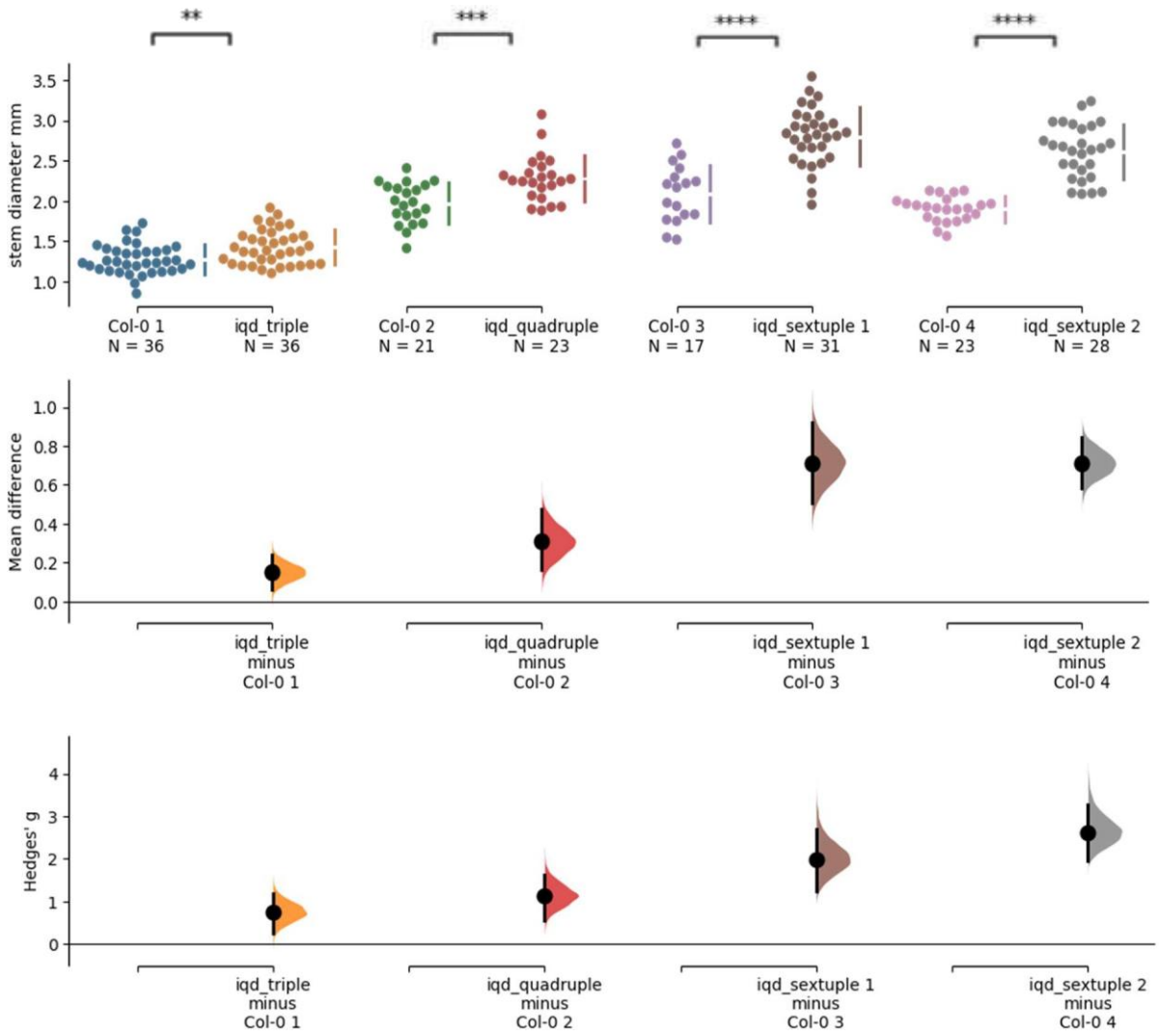

Figure 2. 3 Increasing severity of stem diameter phenotype in successively higher order family1a mutant lines representing unveiling of redundant 1a *IQD* function in plant growth: WT triple data set; WT 1.2733 mm(n=36), triple 1.4248 mm (n=36), diff 0.151444, *p* = 4.457948e-03, Hedge's g value of 0.747. WT quadruple data set; WT 1.921433 mm(n=21), quad 2.280565217 mm(n=23), diff 0.310375, *p* = 6.023607e-04, Hedge's g value of 1.12. WT sextuple data set 1; WT 2.086823529 mm(n=17), sextup 1 2.800741935 mm(n=31), diff 0.713918, *p* = 1.530593e-06, Hedge's g value of 1.98. WT sextuple data set 2; WT 1.898522 mm(n=23), sextup 2 2.610571 mm(n=28), diff 0.712050, *p* = 5.820483e-09, Hedge's g value of 2.61. All *p* values Mann-Whitney test. ** *p*<0.01 *** *p*<0.001 ****p*<0.0001.

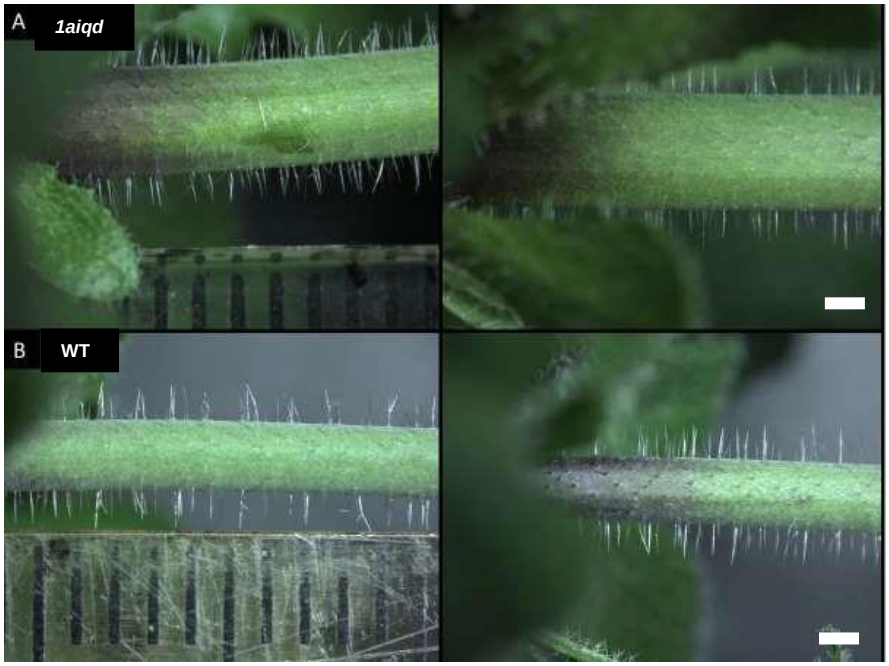

Figure 2. 4 Visible difference between stem thickness of full sextuple mutant line and WT Col-0. Images of representative inflorescence stems of two *1aiqd* mutant plants (A) and WT (B) taken under a light microscope and used to quantify stem diameter as shown in Figure 2.3. Note the striking difference in stem thickness. (scale bar 0.5 mm).

Reproducible growth phenotypes were suggestive of successful disruption of 1a *IQD* function. To confirm that this was the case at the molecular level, expression of the *IQD* genes disrupted by T-DNA insertions was assessed by RT-qPCR. The primers used were designed to detect transcripts downstream of the insertion site, to take into account the possibility that expression in the mutants could still be driven by T-DNA sequences. Tissue samples were collected from shoot apices with flowers and older buds removed to enrich for developing organs, based on evidence that *IQDs* are frequently expressed in rapidly dividing tissues such as meristems (Burstenbinder, K. et al. 2017; Wendrich, J. 2018). Also, expression of *IQDs* during fruit growth peaked in very early stage of ovary development where rapid division occurs (Dou, J. et.al. 2018). Furthermore, imaging of a native translational YFP fusion of the 1a *IQD* gene *IQD24* confirmed strong expression in the SAM, as presented in a subsequent Chapter 5.

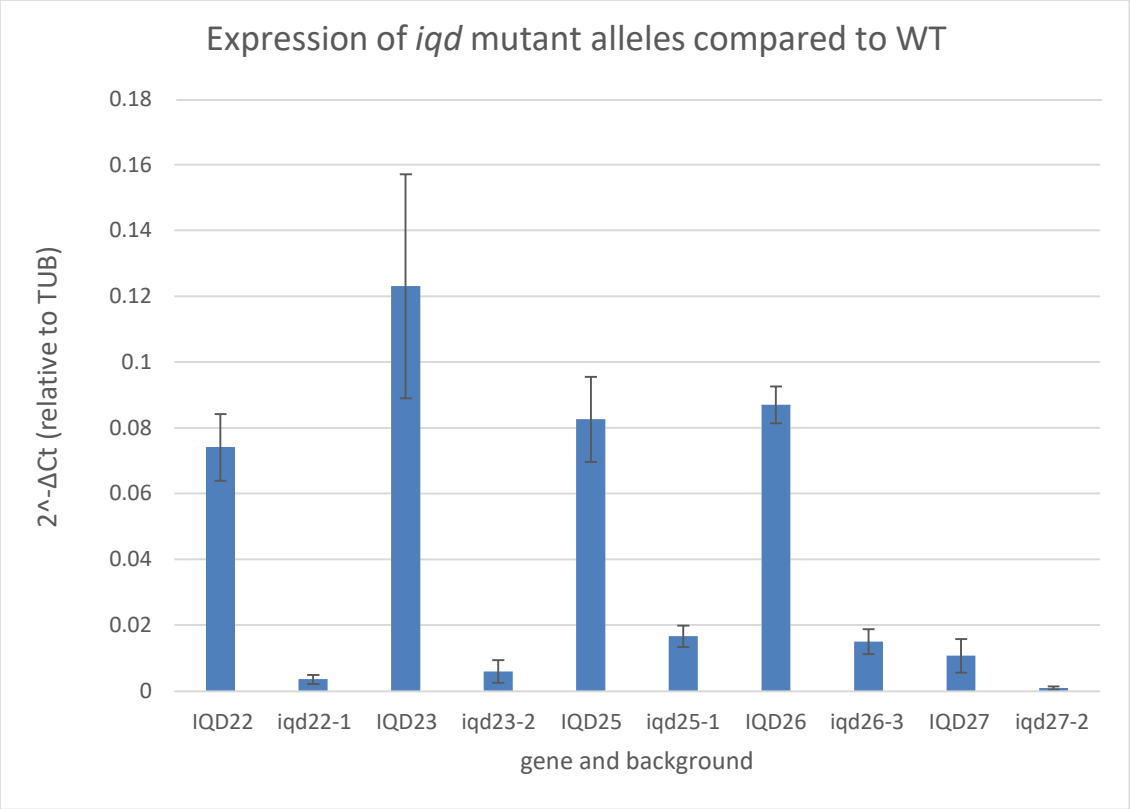

Figure 2. 3: Reduction in 1a *IQD* gene expression observed in the *1aiqd* line.

qPCR analysis of expression of 1a *IQD* genes with T-DNA inserts in shoot apices of WT and *1aiqd* backgrounds. ΔCt values were calculated relative to TUB expression in each sample. Average taken of three technical replicates for each of four biological replicates. The average value of four biological replicates was used to calculate 2^-ΔCt. Error bars represent standard deviation across the biological replicates.

Expression of transcripts downstream of T-DNA insertion sites were greatly reduced in the *1aiqd* line (Figure 2.3), indicating at a minimum greatly reduced function. Transcription starting from within the T-DNA, however, might still result in mRNA encoding a truncated protein. To test whether this could be the case, I verified the position of the T-DNA insertion sites in each *iqd* mutant used to generate the *1aiqd* line. Sequencing was carried out on PCR products from reactions using a reverse primer in the *IQD* gene body and left T-DNA border primer from a genomic DNA template of the *1aiqd* line. The resulting alignments with TAIR database sequences are detailed below for each mutant with position of entry into T-DNA sequence marked.

iqd22-1 SALK 103903.55.75.x: Annotation of the T-DNA insert for *iqd22-1* in T-DNA Express (http://signal.salk.edu/cgi-bin/tdnaexpress) placed the insertion in

the first exon, close to the start codon. Sequence alignment of the PCR fragment revealed that in fact the insertion site was upstream of the start codon, in the five prime UTR region. This could indeed result in lower expression due to disruption of the promoter region, however a normal transcript might still be promoted from native start codon, resulting in incomplete loss of function.

Figure 2. 4: PCR product mapped to TAIR gDNA sequence of *IQD22* The PCR sequence matching TAIR genomic sequence of *IQD22* is highlight in yellow, matching from the first intron into the five prime UTR region, while sequences further upstream has poor match to PCR product, suggesting that they correspond to the T-DNA insert. T-DNA position indicated by green star**.**

iqd23-2 SALK_073090: Annotation of T-DNA insert for *iqd23-2* placed it in an intron close to the end of the first exon. Sequence alignment of the PCR fragment confirmed this, however, showed some discrepancies with the intronic region annotated in TAIR. PCR sequencing from the RP in second exon read from the second exon directly into the intronic region highlighted, with large piece missing. Read ceased to match prior to first exon, confirming annotated T-DNA site.

Figure 2. 5. PCR product mapped to TAIR gDNA sequence of *IQD23*. PCR sequence matching TAIR genomic sequence of *IQD2*3 is highlight in yellow, reading from second exon into highlighted region of intron, further read has no match and implicates T-DNA sequence at start of first intron**,** T-DNA position indicated by green star**.**

iqd25-1; SALK_058876.25.70.x: Annotation of the T-DNA insert for *iqd25-1* placed it near the start of the first exon. Sequencing of the PCR product subsequently confirmed this as sequence matched through the first exon up to bp 72 before nearly 200 bp read with poor match, indicating entry point to the T-DNA.

Figure 2. 6 PCR product mapped to TAIR gDNA sequence of *IQD25* PCR sequence matching TAIR genomic sequence of *IQD25* is highlight in yellow, T-DNA position indicated by green star**.**

iqd26-3 GK-728F02: Annotation of the T-DNA insert *iqd26-3* placed it in the second exon of the gene. The genomic region for which sequence from the PCR product matched is highlighted bellow, confirming the annotated insertion site for.

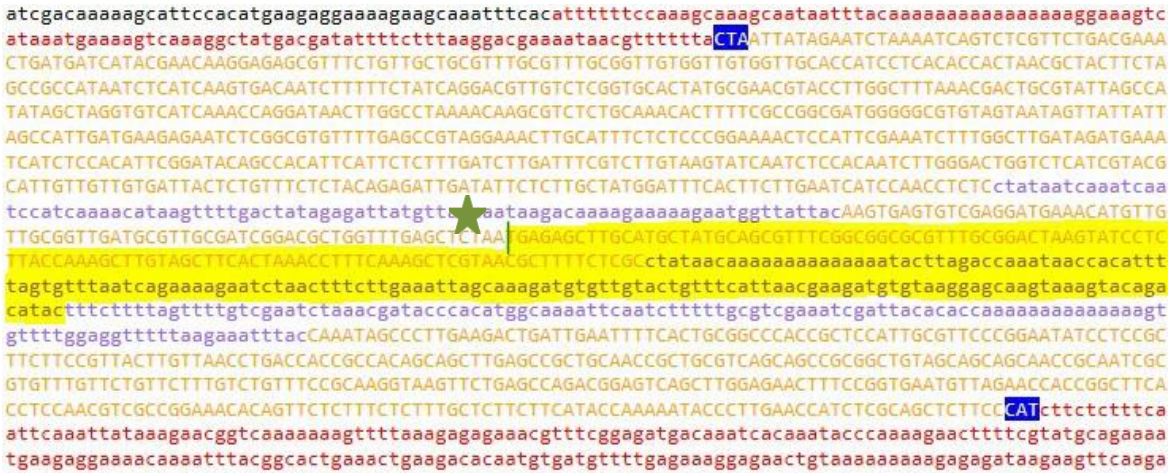

Figure 2. 7: PCR product mapped to TAIR gDNA sequence of *IQD26*. The PCR sequence matching TAIR genomic sequence of *IQD26* is highlight in yellow, reading from first intron to middle of second exon, before subsequent mis-matched sequences, indicating a T-DNA insert in centre of the second exon as annotated. T-DNA position indicated by green star.

iqd27-2 SALK_103602.28.55.X: Annotation of the T-DNA insert for *iqd27-2* placed it at the end of the first exon. The PCR product using RP for genotyping and left border T-DNA primer matched gDNA sequence from second exon through into

first intron before further sequence no longer matched, positioning site of T-DNA insert. Subsequent PCR product using FP in first exon and SALK border primer aligned through first exon to similar intron point before no longer matching. This pinpoints T-DNA insertion in intron between first and second exon, rather than at the very end of the first exon as reported in the public databases.

Figure 2. 8 PCR product mapped to TAIR gDNA sequence of *IQD27*. The PCR sequence matching TAIR genomic sequence of *IQD27* from both forward and reverse primer reactions is highlight in yellow. FP for genotyping matched from first exon to middle of first intron. RP for genotyping matched from second exon into similar middle region of first intron, before sequences no longer matched, indicating T-DNA site in first intron rather than at the end of the first exon. T-DNA position indicated by green star**.**

In summary, the T-DNA mutant lines had confirmed insertions within introns or exons of coding sequences, except for the *iqd22-1* mutant, which had an insertion in the 5' UTR region. This often results in lowered levels of gene expression, as confirmed by RT-qPCR for *iqd22-1*, but the product would be potentially still functional. For the genes where the T-DNA was found within the gene body, the transcripts detected downstream of the insertion site by RT-qPCR would likely be non-functional, due to premature stop codons or out of frame translation form T-DNA sequences. In the unlikely case that the truncated transcripts were correctly translated, the *iqd23-2, 26-3* and *27-2* mutants would still all lack the first exon, and *iqd25-1* would contain a severely disrupted first exon. Both N and C terminal regions have been identified as required for function of *IQD13* in secondary cell wall pit shape control (Sugiyama, Y., et. al., 2017), so the N-terminally truncated IQDs would be expected to have severely impaired function.

To verify whether the transcripts still detected in the mutants might produce truncated IQD proteins, I attempted to amplify cDNA fragments using a T-DNA border primer and the reverse primer used in qPCR reactions, however no product was amplified. As it is not known where expression from the T-DNA might start,

the border primer might not be present in the mutant transcripts. To identify the exact transcripts produced in the mutants, in future I could design primers at the very end of T-DNA fragments based on genomic DNA sequences.

To further assess the contribution of individual mutations to the phenotype seen in the *1aiqd* line, stem thickness was selected as a strong and easily quantifiable phenotype. Study of *iqd26-3* T-DNA line's phenotypic contribution was performed in a population segregating 1:2:1 WT, heterozygous, homozygous for *iqd26-3* T-DNA mutant (Figure 2.9).

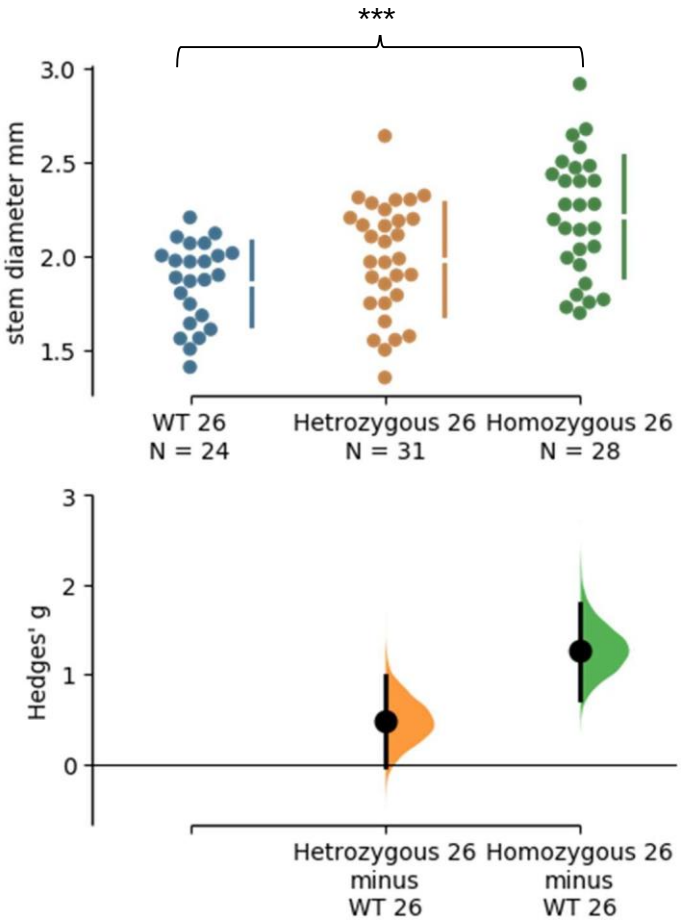

Figure 2. 9: Strong contribution of *iqd26-3* mutant to stem diameter.

Average stem thickness of plants WT for *IQD26* gene locus, 1.8533 mm (n=24). heterozygous at *IQD26* locus 1.9825 mm (n=31). homozygous for T-DNA mutant 2.2110 mm (n=28). stem diameter increases from WT had Mann Whitney *p* values of 0.0819 and 0.000162 respectively. *** $p<0.001$

Heterozygous plants for *iqd26-3* had on average 0.12916 mm larger stem diameters than WT, although this difference was not statistically significant. Homozygous mutant plants had a significant average increase of 0.35760 mm compared to WT. Thus, single loss of function already resulted in detectable changes in stem thickness, supporting the idea that family 1a *IQD* genes function additively in plant growth.

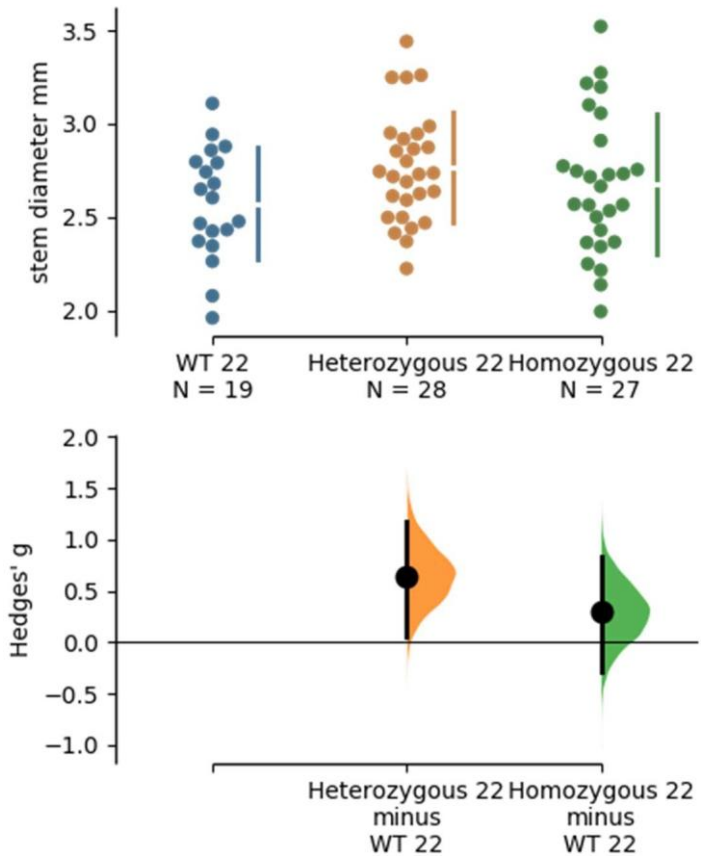

Figure 2. 10: **Weak contribution of *iqd22-1* mutant to stem diameter.**

Average stem thickness of plants WT for *IQD22* locus 2.5721 mm (n=19), heterozygous at *IQD22* locus 2.7634 mm, (n=28). homozygous mutant for *IQD22* 2.6748 mm (n=27). Increases in stem diameter from WT had Mann Whitney *p* values of 0.060761 and 0.546943 for heterozygous and homozygous lines respectively.

The contribution of the *iqd22-1* mutation to the stem phenotype was also assessed (Figure 2.10). Both heterozygous and homozygous mutant lines had only statistically insignificant increases in stem diameter compared to WT plants, suggesting that the *iqd22-1* mutation gene was fully redundant with other family 1a members, or that the allele used indeed was weak, in line with the molecular characterisation described above.

Overall, considering the analysis of gene expression, positioning of T-DNA inserts and contribution to phenotype of the *1aiqd* line, I concluded that the *1aiqd* mutant line has loss of function for at least five of the six genes in subfamily 1a. The possible exception was *IQD22*, for which a strong knock-down of expression was seen, however some functionality likely remains. Therefore, the subsequent phenotypic characterisation may have revealed alterations in growth slightly more moderate than would be observed with fully null mutant line. Nevertheless, the

1aiqd line was the best available tool to give insight into the redundant roles of family1a *IQDs*.

2.2.3 Overall characterisation of macroscopic shoot organ growth phenotypes in the *1aiqd* mutant

As previously discussed, a pronounced increase in stem diameter occurred in the full *1aiqd* mutant and was used to link T-DNA lines in 1a *IQDs* to shoot growth function, as well as revealing redundancy of function within the subfamily. As mentioned, measurements were taken at a uniform developmental stage, when four siliques had elongated. Along with stem pictures for measurements, whole plant pictures were also taken. A trend that emerged was reduced height of mutant plants at same developmental stage as WT (Figure 2.11). Whilst average stem elongation was only 6.5 cm at the set developmental stage in *1aiqd* plants, WT stems reached on average 11.8 cm. This could implicate increased stem diameter at a cost to stem elongation in the *1aiqd* line. Testing this idea would require an analysis of the stem growth dynamics, as detailed later in Chapter 3. Despite this initial reduction in stem elongation, total height reached of mature mutant plants did not appear to differ between mutant and WT lines (Figure 2.13), suggesting that the difference in height was due specifically to variation in early stages of stem growth.

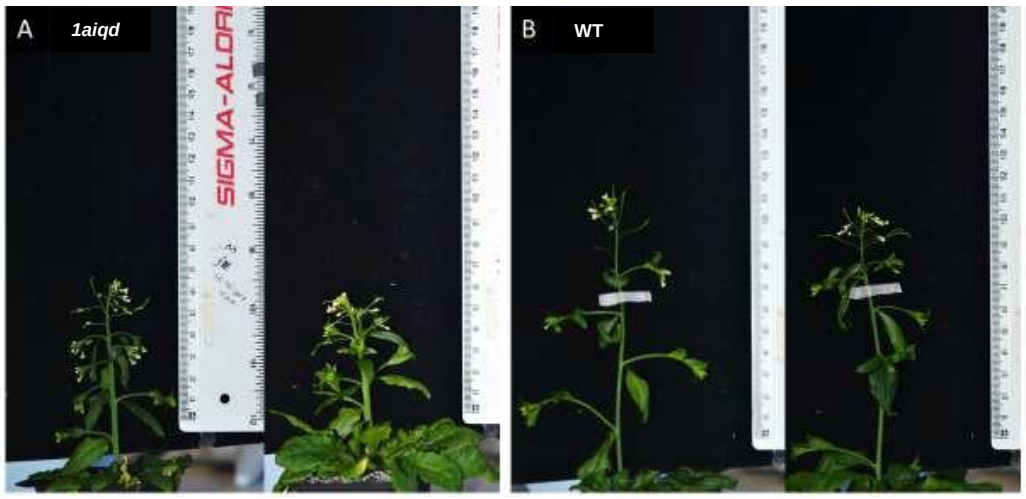

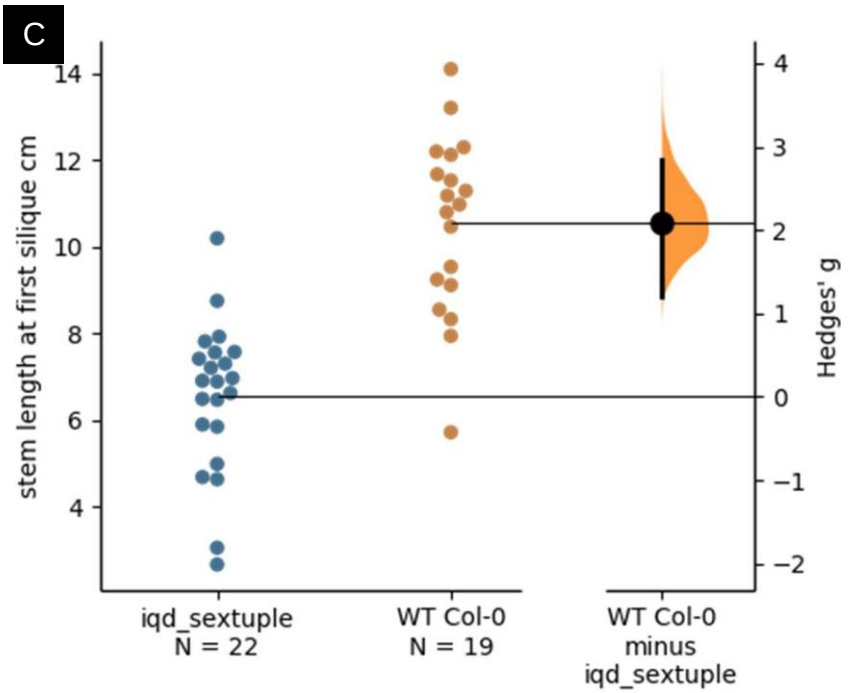

Figure 2. 11: Reduced plant height in *1aiqd* lines compared to at the developmental stage where 4 siliques were elongated. Average stem length from the rosette to first silique. Mutant n=20, 6.481 cm. WT n=23, 11.82 cm. Mean difference from WT to mutant is -4.01 cm, with *p* value= 0.000002 (Mann-Whitney test). **** $p < 0.0001$. Hedge's g is -2.08, showing strong power in this analysis.

As well as potential impact on radial and vertical stem growth, lateral side branches were more numerous, as visible in Figure 2.11A. In *1aiqd* plants the number of side branches ranged from five to nine, whereas in WT plants side branches ranged from three to six, with an overall increase of 30.77% in side branch number (Figure 2.12).

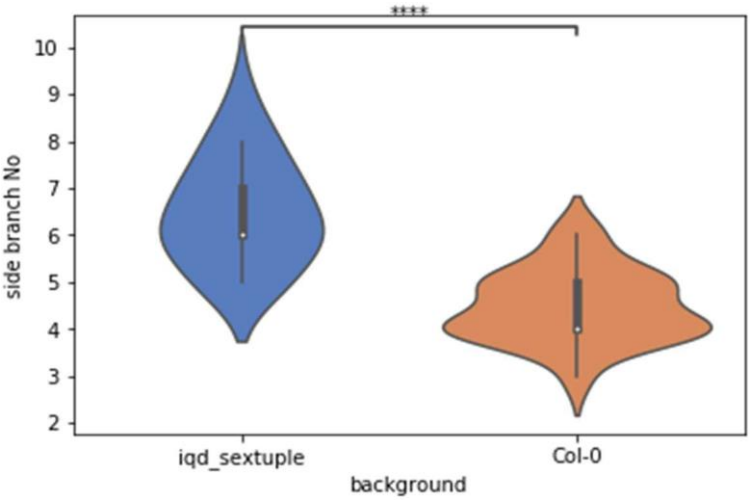

Figure 2. 12: Increase in lateral side branch number in the *1aiqd* line. On average WT had 4.5 side branches and mutant plants 6.5 (both n=20), with an average increase of 2 side branches highly significant, *p* = 2.235e-06. (Mann-Whitney test, **** $p < 0.0001$)

To test whether the increased number of inflorescence branches could increase fruit yield in the mutant, the number of siliques on the main shoot and two side branches was counted in both WT and mutant plants, then multiplied by the average number of side branches in each genotype. On average, mutant plants had a non-significant greater number of siliques on both the main shoot and on individual side branches. The number of seeds per silique was also very similar however there was a very slight increase in number of seeds in WT siliques.

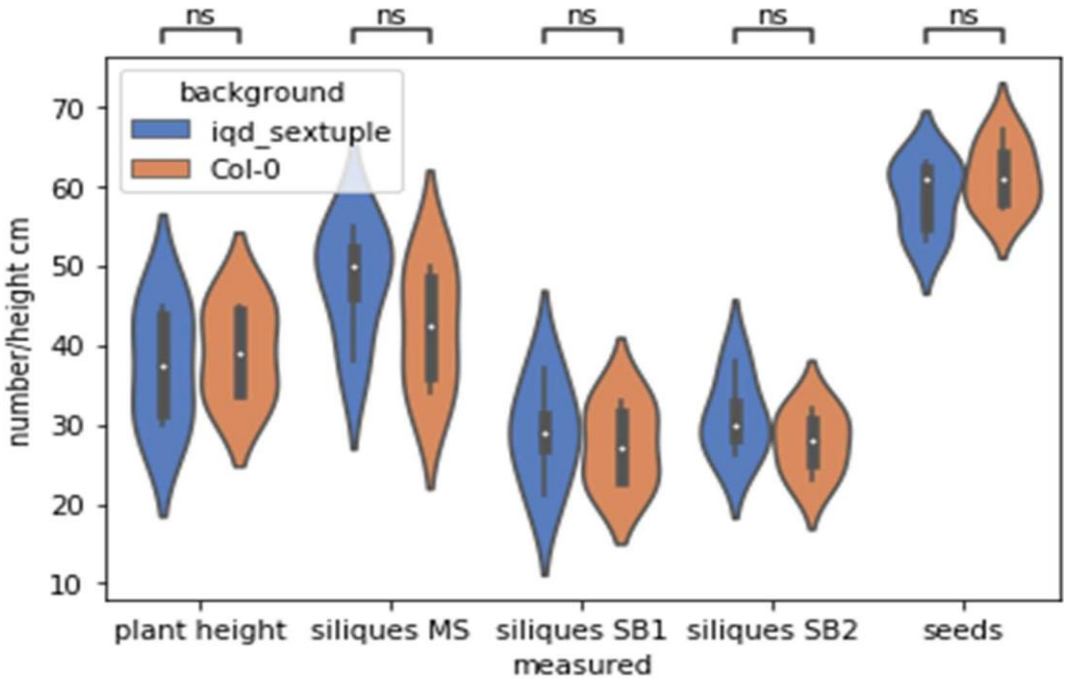

Figure 2. 13: Largely similar final plant height, number of siliques on the main shoot and upper side branches and similar number of seeds per silique in the *1aiqd* mutant indicates that the increase in lateral branch number confers a proportional increase in silique and seed number per plant. MS= main shoot, SB= side branch 1 and 2 respectively. n=4 in measurements of plant height and number of siliques and n=5 for measurement of seeds per silique. Average height: 37.5cm for the mutant, 39.25 cm for the WT. Average siliques on main shoot 48.25 for the mutant and 42.25 for the WT. Silique number on side branch 1: 29 for the mutant and 27.5 for the WT. Silique number on side branch 2: 31 for the mutant and 27.5 for the WT. Average seed number per silique: 58.8 for the mutant and 61.4 for WT. All NS, two-sided Mann-Whitney test with Bonferroni correction

Importantly, the comparable number of siliques on each branch and of seeds in each silique indicates that the mutant had an increase in yield per plant proportional to the increase in branching. In the samples analysed, the average

number of side branches in the mutant plants was 6.25 and in WT only 2.75, so the average number of siliques produced per plant in the mutant and WT can be projected to 235.75 siliques and 117.88 respectively, and the respective numbers of seeds would be 13 862 and only 7 238. Thus, the changes in inflorescence architecture in the mutant plants can be estimated to almost double the seed yield per plant, a feature that could be useful if reproduced in crop species.

The impact of IQD function on fruit shape in crop species was a strong driver for seeking to understand a molecular mechanism by which these proteins affect shoot organ growth. Given the evidence in the literature for fruit shape control, the fruit shape was also monitored in the *1aiqd* mutant. No deviation was noted in fruit length or in the ratio of width to length in the mutant at the ovary stage (Figure 2.14), for which a significant shape change was already apparent in Cucurbitaceae fruits of varying *IQD* expression (Dou, J et al.2018).

Figure 2. 14: Similar width and length of gynoecia in mutant and WT lines prior to fertilisation. A mutant, B WT. scale bar 1mm.

The ratio of gynoecium width versus length was 5.325 for the WT and 5.16 for the mutant, confirming similar shape of ovary before fertilisation. In line with the similar ovary shape, mature siliques in the mutant line appeared very similar to those in WT (Figure 2.15). Whilst mutant siliques were on average marginally longer and narrower, with mild significance for the increased width of WT siliques.

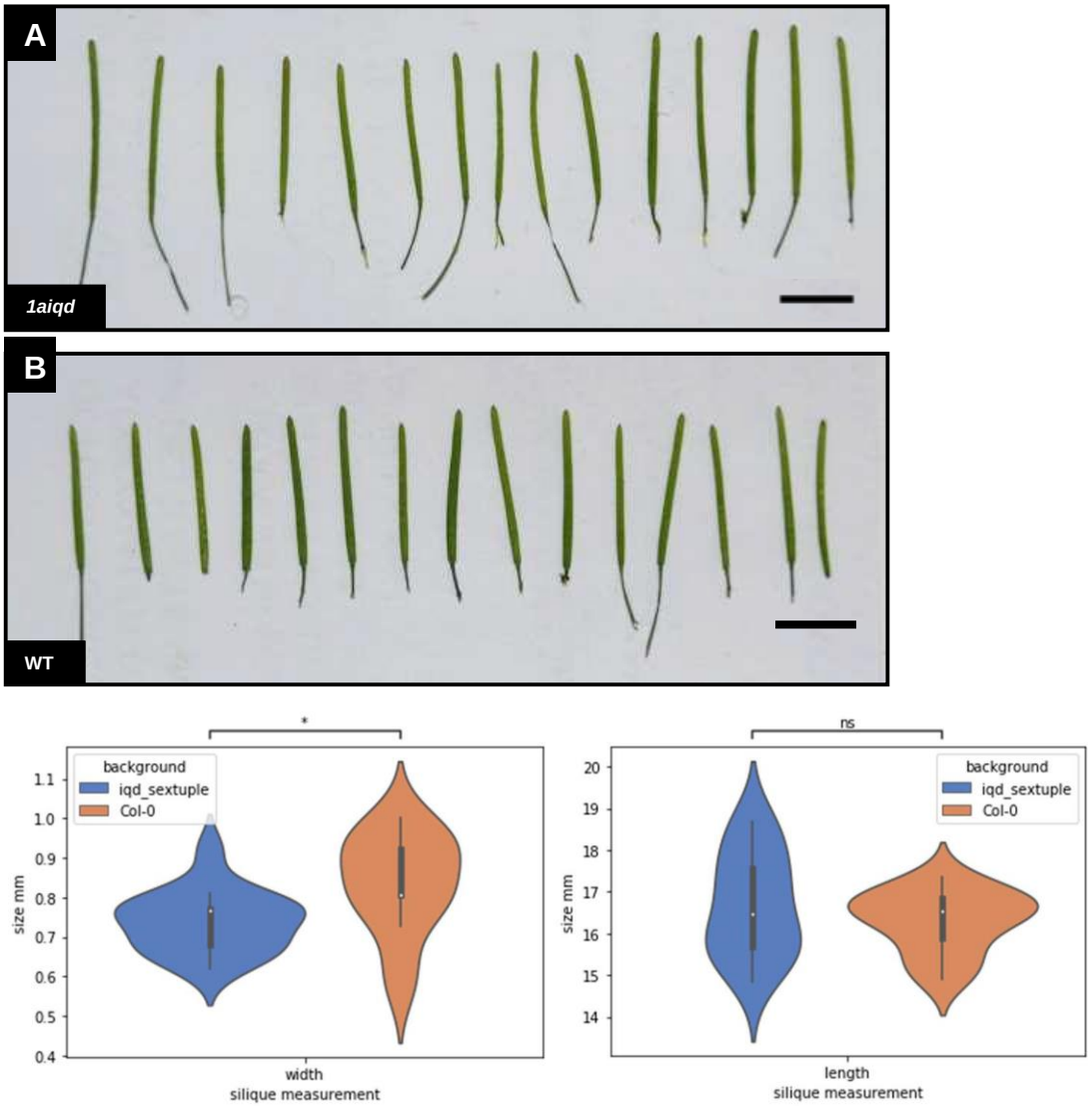

Figure 2. 15: Similar width and length of mature siliques in the *1aiqd* mutant and WT lines. A mutant, B WT. Scale bar 1cm. No significant difference was seen in silique length of mutant (average 16.7mm) and WT (average 16.31mm). Low significance (p =1.057e-02) for an increase in silique width of WT (average 0.837mm) compared to the mutant (average 0.74mm). n=15; $p < 0.05$ *, two-sided Mann-Whitney test with Bonferroni correction.

Whilst having similar fruit shapes and yield of seeds per silique, the *1aiqd* mutant line did have altered seed shape. Seeds lost their oval shape and expanded radially, taking on a more spherical shape in the *1aiqd* line. A significant increase in seed width resulted in an increase in seed area of mutant seeds with

average area of 14 mutant seeds measuring 1.886 mm2 vs 1.64 mm2 WT, a 13% increase in area (Figure 2.16 A,B). A separate comparison of 30 seeds in mutant and WT background confirmed that mutant seeds were 10% larger in area (Figure 2.16 C,D).

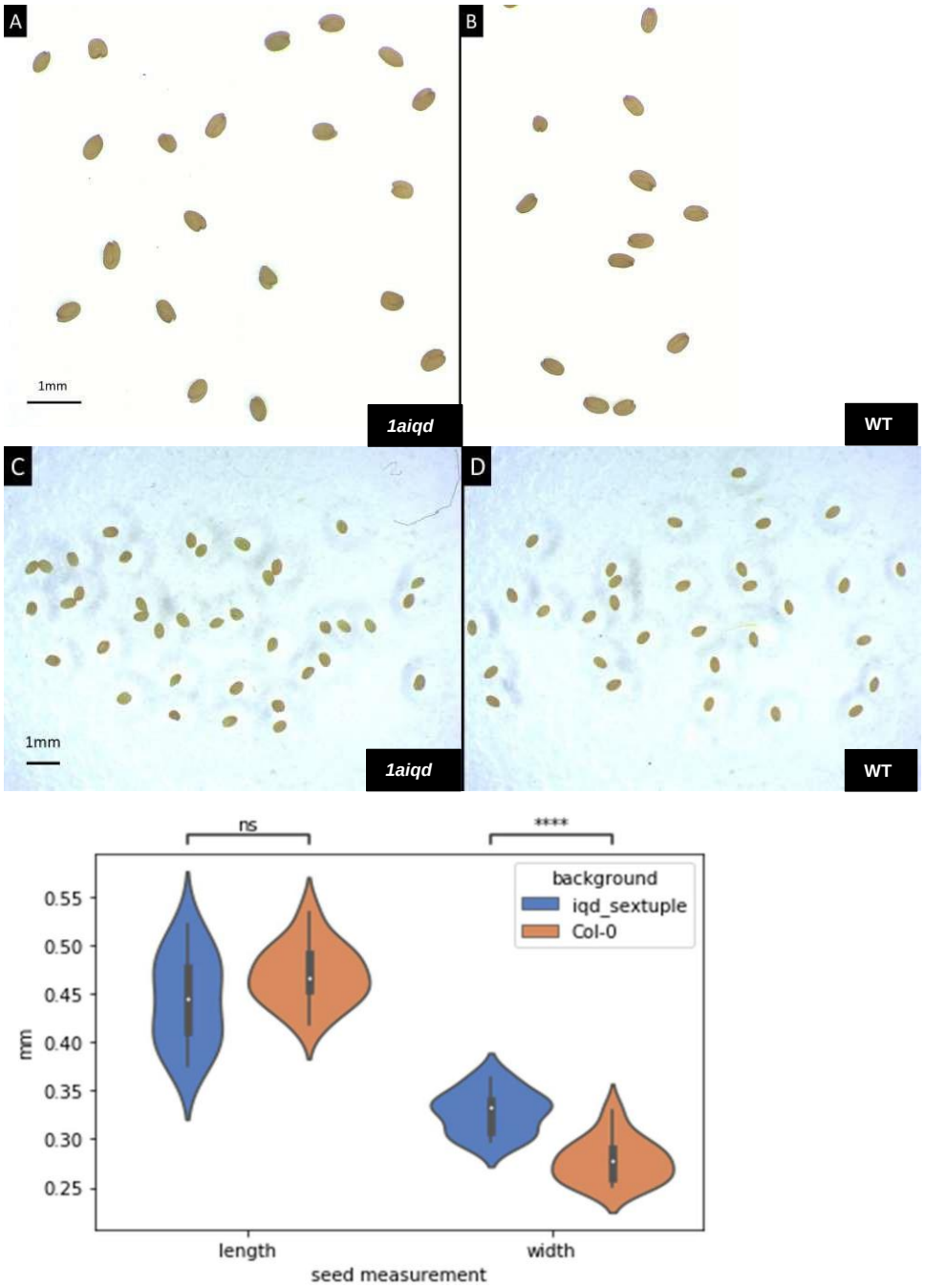

Figure 2. 16 Increased width in *1aiqd* mutant seeds led to more rounded rather than oval shape. Greater width of seed observable in mutant seeds (A,C) versus WT (B,D). E shows Quantification of seed shape in mutant(A) and WT(B). The average seed length was 0.444 mm in the mutant line and 0.470 mm in the WT. The average width was 0.329 mm in mutant versus 0.278 mm in WT, p =9.550e-05. (two-sided Mann-Whitney test with Bonferroni correction, **** p<0.0001, n = 14).

The inflorescence phenotypes described above (thicker stems, increased branching, larger seeds) all indicate a de-restriction on growth with loss of sufamily1a function. Enhancement of growth was similarly identifiable in the vegetative growth phase in the *1aiqd* plant line. Rosettes of mutant plants appeared to cover a greater area and their leaves appeared individually different from WT leaves, with a flatter, fuller appearance, which is discussed in detail in Chapter 4. As well as differences in individual leaves, the rosettes appeared to develop a greater number of leaves whilst in the vegetative phase. Quantification of leaf number per rosette of trays imaged in Figure 2.17, planted at the same time and grown for same length of time in identical CER conditions, confirmed that more leaves were initiated following extended vegetative growth in the mutant line.

Figure 2. 17: Rosettes appeared fuller in the *1aiqd* mutant, with more leaf surface area exposed for light capture. Images of WT (A) and mutant (B) rosettes grown under identical conditions of continuous light, 16ºC for 30 days

By the time WT plants bolted, rosettes had 15.3 leaves but mutant plants had 20.9 just prior to bolting (Figure 2.18). The final number of leaves at bolting is a function of the rate of leaf initiation and period of vegetative growth, making it a standard phenotype used to assess flowering time. To assess flowering time, I measured the number of days from germination to first white flower and time of bolting (Figure 2.19). Photographs of trays in Figure 2.17 were taken the same number of days after germination, demonstrating a delay in transition to bolting in the *1aiqd* line affirmed in Figure 2.19.

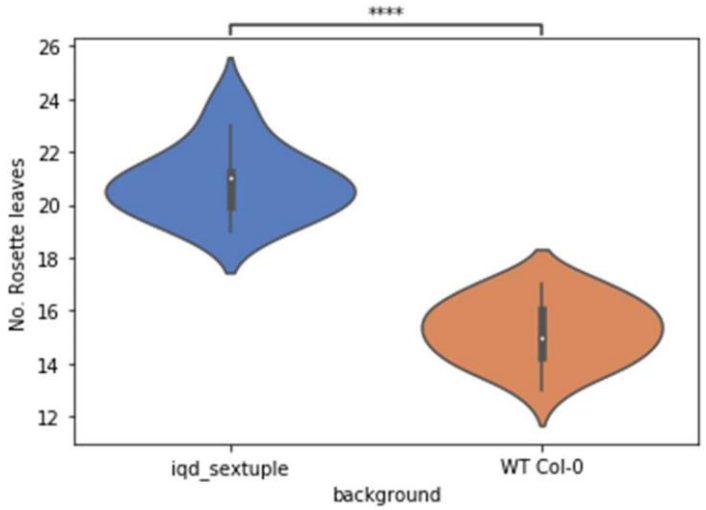

Figure 2. 18: Increase in number of rosette leaves initiated during vegetative growth in mutant line. WT averaged 15.278 leaves whereas mutant rosettes averaged 20.875 (both n=18). A difference of 5.597 leaves, which can be stated with strong significance, *p* = 6.103e-07 (two sided Mann-Whitney test with Bonferroni correction, **** p < 0.0001)

Through assessment of bolting and opening of the first flower in mutant and WT lines it was apparent the delay in number of days between bolting of mutant and WT lines was greater than that of delay in the appearance of the first open flower. Indeed, the vast majority of 25 mutant plants in two studies had flowered by day 37 after germination, just one day later than the time point when all WT plants had flowered. This implicated mutant plant lines had a prolonged vegetative growth phase but upon bolting accelerated the development of flowers.

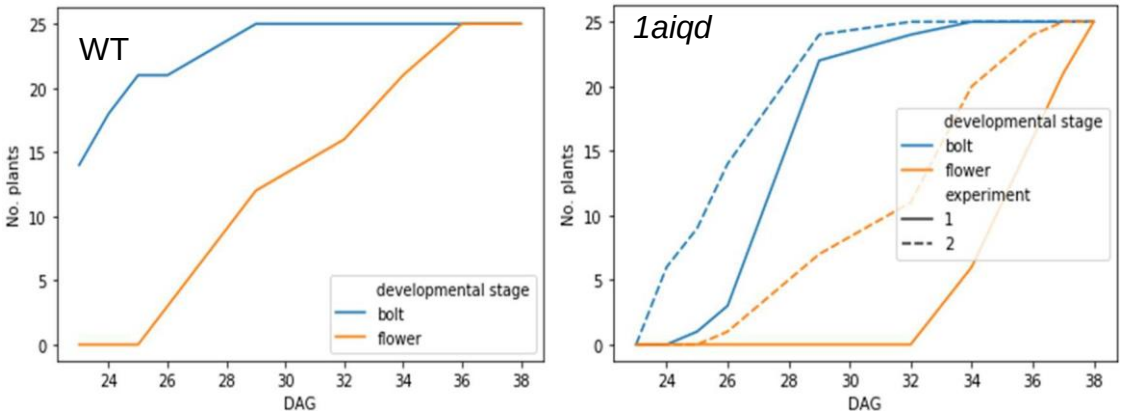

Figure 2. 19: Difference in the delay to bolting and flowering in the *1aiqd* mutant. Blue lines show the cumulative number of plants (out of 25) that had bolted in WT (left panel) and mutant (right panel) plant lines. Orange line corresponds to plants with their first open flower. Whilst an initial lag in bolting and flowering is observed, mutant plants appear to bolt more uniformly with majority bolting between 24 and 28 DAG.

As reported earlier in this thesis, the mutant plants had reduced stem elongation at the stage when the 4th silique had elongated (Figure 2.11). The data would also indicate that mutant plants spent fewer days between bolting and initiation of the first flower, which may have contributed to the reduction in height, rather than a reduction in the rate of stem elongation. Further experimentation to quantify rate of stem elongation growth in *1aiqd* and WT lines was required to test whether enhanced radial stem growth in *1aiqd* line occurred at a cost to stem elongation rate, as detailed in Chapter 3.

Other than enhanced rosette size, a further distinctive rosette phenotype was seen at a lower frequency in *1aiqd* mutant plants: a striking change from spiral to bijugate phyllotaxy was apparent in 4-6% of the plants (Figure 2.20). Following the floral transition, the same plants had side branches arranged in a decussate pattern (Figure 2.21), and flowers were also arranged in opposite pairs (Figure 2.22). Although this phenotype appeared at a low frequency, it was consistently seen in the sextuple mutant line and not apparent in any quintuple mutant plants. The phyllotactic change seen at low frequency, but stable within the plants that showed it, was consistent with model predictions that different phyllotactic patterns, once established, are stably perpetuated (Smith R.S. et al. 2006).

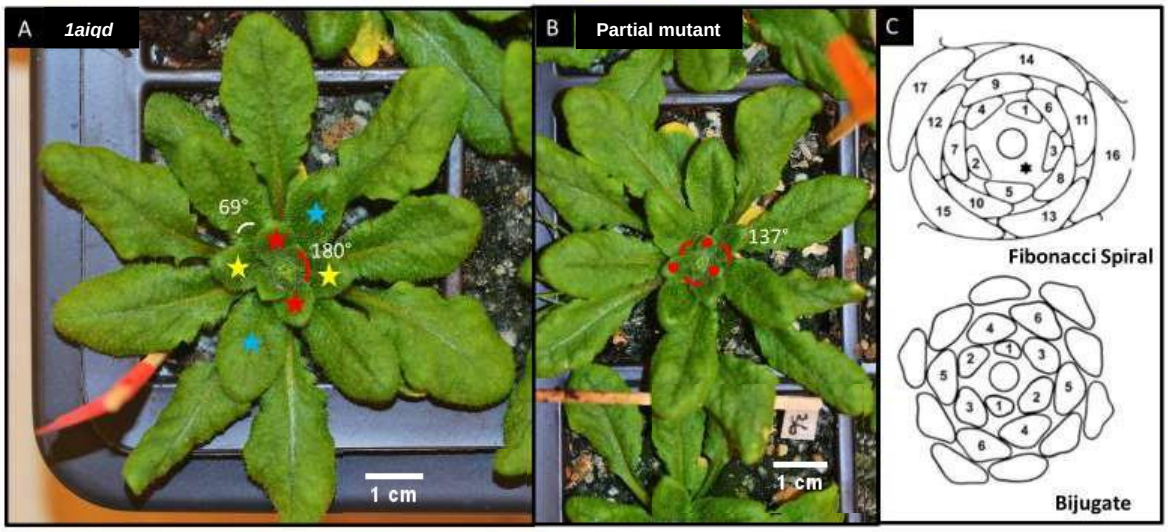

Figure 2. 20: Stable change in the phyllotactic pattern from spiral to bijugate occurred seen in *1aiqd* plants. Phyllotaxy of a sextuple (A) and quintuple plant heterozygous for *iqd23-2* (B) from the same segregating population. C represents different phyllotaxy patterns: at the top, the classic Fibonacci spiral as seen in panel B, and below the bijugate (paired spiral) pattern shown by the plant in panel A (images in C taken from Reinhardt, Didier, 2005, Regulation of phyllotaxis, The International journal of developmental biology 49: 539-46. 10.1387/ijdb.041922dr).

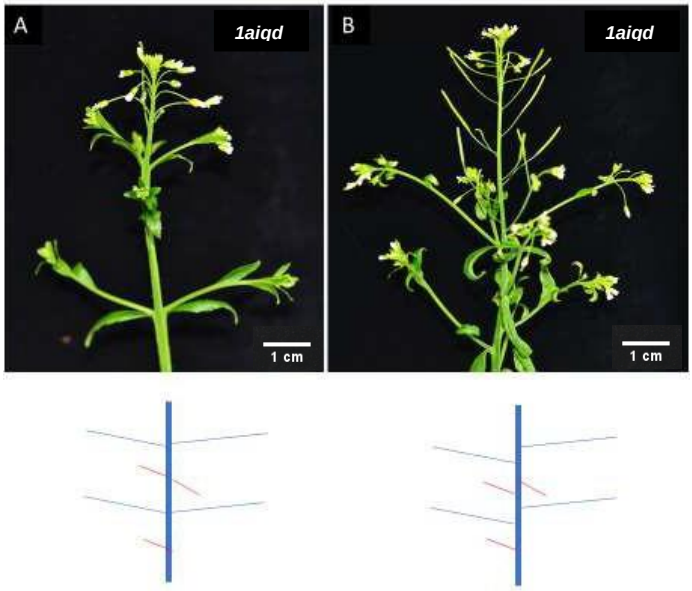

Figure 2. 21: Upon the floral transition, plants with rosettes showing bijugate phyllotaxis produced inflorescences with opposite side branches. Side branch pattern in two sextuple mutant plants from population segregating *1aiqd.* Whilst both showed a decussate phyllotaxis, the initiation time of side branches varied. Sextuple plant A initiated side branch pairs at identical times resulting in no separation by stem internode elongation, whereas sextuple B had a slight delay in initiation of the second branch in each pair, resulting in a slight separation on the stem.

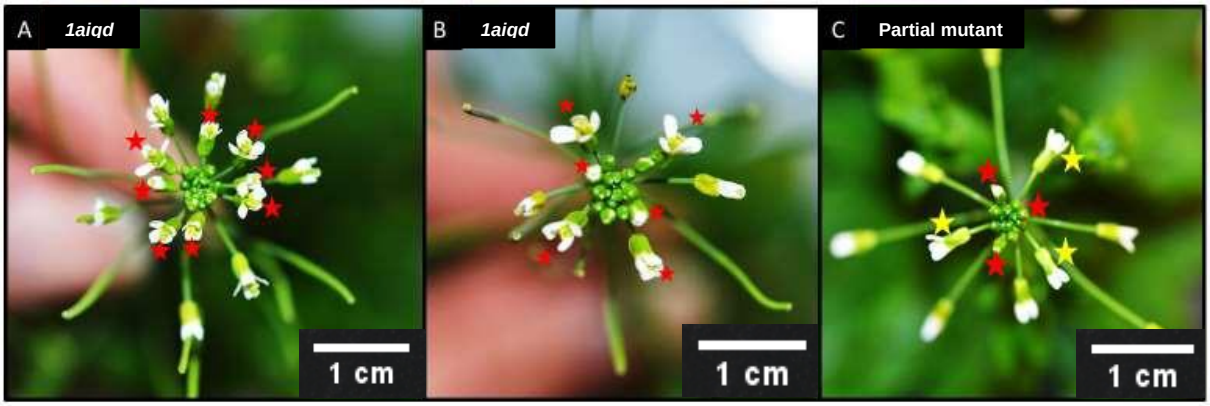

Figure 2. 22: Flowers were also paired in *1aiqd* plants with paired leaves and side branches. Top view of the shoot apex of two sextuple mutants (A,B) and a quintuple mutant plant (C) from a population segregating *1aiqd.* Consistently, quintuple mutants displayed a classic Fibonacci spiral pattern found in *Arabidopsis thaliana* as observed in C. Mutant plants presented flowers in pairs opposite one another, consistent with the paired pattern of organs in the whole shoot, however, differences again arose, this time in the number of flowers initiated. The sextuple plant pictured in A appeared to generate double the flowers than in B whilst maintaining the same cross pattern.

One of the variables that could potentially lead to a shift in phyllotactic pattern is meristem size, as detailed in modelling investigating impact of meristem size and shape as well as primordia size and shape on patterning (Douady, S., Couder, Y. 1996) and in modelling generating all patterns observed in nature (Smith R.S. et al. 2006). is strongly affected by environmental conditions such as increased nitrogen availability, a treatment shown to increase meristem size and organ numbers through modulation of cytokinin signaling (Landrein, B, Jönsson, H. et al. 2018). To test this idea, I measured the frequency of bijugate phyllotaxis in populations of the *1aiqd* line grown under conditions that increase shoot meristem size, including growth in short days, lower temperature (16ºC) and increased nitrogen fertilisation (watering with Miracle Grow fertiliser). None of these conditions increased the frequency of phyllotactic changes. The only exception was growth in larger pots (9 x 9 cm, rather than trays with 4.5 x 4.5cm wells), which increased the frequency to 20%.

Figure 2. 23 More frequent paired leaf pattern of *1aiqd* line rosettes when grown in larger pots. Plants grown in long days at 20 °C in 9 x 9 cm pots, those with leaf pairing denoted by red stars. Scale bars 1cm.

Imaging of inflorescence meristems also failed to show consistent differences in meristem size between the WT and *1aiqd* mutant (Figure 2.24). I concluded that the change in phyllotactic pattern in the *1aiqd* line is unlikely to reflect changes in meristem size.

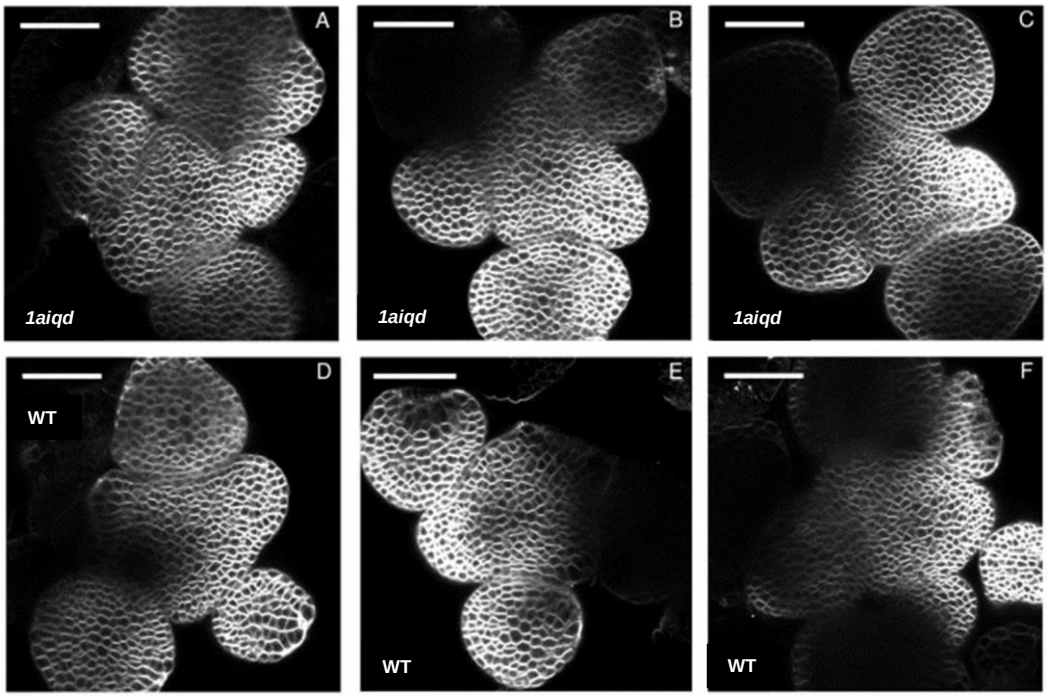

Figure 2. 24: Comparable meristem size in *1aiqd* line plants and WT Col-0.

FM4-64 stained meristems of *1aiqd* (A, B, C) and WT (D,E,F) plants grown under SD conditions at twenty degrees. Scale bars 50 µm.

In summary, multiple shoot growth phenotypes were present in the *1aiqd* line, with a strong trend of increased growth through both organ initiation (e.g. lateral branches, increased leaf initiation) and subsequent organ growth (e.g. stem thickness). Increased meristem size was unlikely to be an underlying factor that may confer growth changes.

2.2.4 Shoot growth defects following ectopic induction of family1a *IQD22*

Generation of inducible gain of function lines provided another platform to investigate the proposed restrictive growth function of subfamily 1a IQDs. In Figure 2.25A, following a treatment course of dexamethasone to the main shoot apex to induce ectopic *IQD22* expression driven by the constitutive RPS5a promoter, shoot organs growth was extremely restricted. Stem internode elongation was reduced, and stems bent in different directions, perhaps caused by local differences in growth rates upon treatment. Sepals and petals were extremely reduced in size, failing to cover the stigma and siliques failed to elongate.

Figure 2. 25: Ectopic induction of family1a *IQD22* in the shoot apex dramatically repressed organ growth. Inflorescence apices of *RPS5a:LhGR Op:IQD22* plant treated with 10 µM dexamethasone (A) and control (B). In both cases, solutions contained 0.1% ethanol and 0.01% Silwet-L77 and were applied directly to the shoot apex using a paintbrush every two days, four times. Images captured a week after the last treatment. Scale side on 1cm above 0.25cm.

In control treated plants (Figure 2.25B) it must be noted that the treatment (containing Silwet L-77 and ethanol at the same concentration as the dexamethasone solution) did inhibit silique elongation as observed in top left picture of the figure. The inhibitory effect of the control treatment, however, was brief, as normal silique growth returned as soon as the treatment ceased, and the shoot apices of control plants one week after treatment appeared similar to the WT. In contrast, restricted growth persisted in the dexamethasone-treated plants.

The impact of ectopic IQD22 on early plant growth, particularly of leaves, was investigated through induction from germination on plates. Again, leaves exhibited repressed growth, appearing less expanded with almost absent petioles. As well as repression of leaf area, leaf shape appeared altered as highlighted in Figure 2.26C, transitioning from a flat round shape to containing a defined bend at the midvein with a heart-like shape. This was consistent with twisting in leaves of reported ectopic IQD lines in Arabidopsis thaliana (Burstenbinder, K. 2017), however, the change in leaf shape and the severe repression in petiole and leaf expansion appeared distinctive to *IQD22* overexpression.

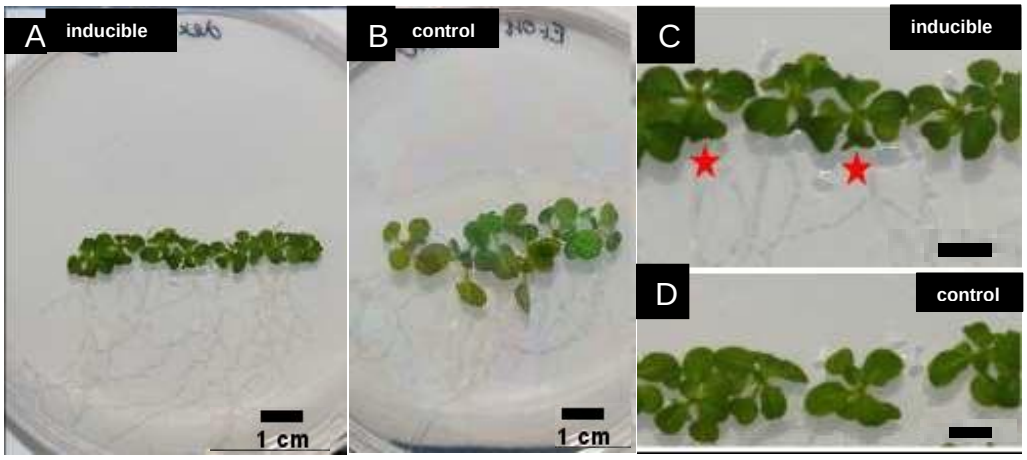

Figure 2. 26: Ectopic *IQD22* expression from germination resulted in repressed leaf and petiole expansion as well as defective leaf shape. RPS5a *IQD22* line was germinated on 10 µM dexamethasone plates,0.01% ethanol, for induction (A) and growth compared to control RPS5a driver plants grown with same concentration of ethanol(B). Closer images of dexamethasone treated inducible *IQD22* line and dexamethasone treated control line, C and D respectively, highlight change in petiole elongation and leaf shape. Red starsdenote heart shaped leaves in seed line with ectopic IQD22 protein. scale bars A,B: 1 cm. C,D: 0.5 cm.

The results of gain of *IQD*22 function therefore support a growth restrictive mode of action for 1a IQD proteins and, together with the loss of function *1aiqd* line, established important tools to study the cellular and molecular basis for IQD function, as described in the following chapters.

2.3 Discussion

One of the motivations to study the function of subfamily 1a *IQD* genes in Arabidopsis was the effect of related genes on fruit shape in Cucurbitaceae species, in which reduced *IQD* 1a function/expression increased radial growth, resulting in rounder fruits. In contrast, no observable change in fruit shape occurredin the Arabidopsis *1aiqd* mutant. However, the markedly increased stem diameter in the Arabidopsis *1aiqd* line implicated a similarly reduced ability to restrict outward radial growth of the stem. The increased fruit diameter following reduced IQD function in the Cucurbitaceae family was linked to greater number of divisionsoccurring in radial planes, which can now be investigated in more detail in the *1aiqd* lines during stem development (Pan, Y. et al. 2017).

The phytohormones auxin and GA are closely involved in the control of fruit growth. While GA’s role is reported following fertilisation, research highlights auxin

as a key element in ovary growth. No detailed mechanism is established however in crop species (Shirley, N.J. et al. 2018). Ovary growth is also controlled by *IQD* genes in the Cucurbitaceae family, with *IQD* expression peaking four days prior to fertilisation (Dou, J. et al. 2018). Studies such as exogenous application of auxin in fleshy fruit crops several weeks before anthesis caused elongation of ovary and fruits, in line with phenotypes of fruits with high IQD levels. This also ties auxin function in shape control of fleshy fruits to that of IQDs (Yang, Y. et.al. 2019). Thus, *IQD* genes might provide a link between auxin function and radial growth to determine fruit shape.

Whilst the literature supports a functional role for auxin in ovary growth across species, the mechanism is largely just presumed to be similar in crop species and Arabidopsis, particularly early stages of development which are cited to undergo similar regulation. In Arabidopsis the role of auxin has been studied in gynoecium patterning, rather than in ovary growth and fruit shape. Uncharacterised divergence between species may account for *IQD* functions' contribution to fruit shape in fleshy fruit producing species, but not in the seed pod producing Arabidopsis. Expression analysis of 1a *IQDs* in the ovary of Arabidopsis have not been carried out and this could also vary between plant species. The peak of *IQD* expression in the ovary prior to fertilisation, as seen in Cucurbitaceae, may be absent in Arabidopsis.

In spite of the possible divergence in the control of fruit shape, the effect of loss of 1a IQD function in Arabidopsis stem development suggests that common mechanisms may be operating to regulate radial growth across organ types. As previously discussed, understanding 1a *IQDs* function in restriction of organ width, such as in the stem of *1aiqd* line, could provide valuable insight into mode of IQD growth control across shoot organs and species. In support of this idea, loss of restricted radial expansion in seeds of *1aiqd* line was analogous to the observed effect of loss function of a rice IQD ortholog equating to whole subfamily 1c in Arabidopsis. In the developing grains of the rice mutant *iqd14-c* (loss of *OsIQD14*), loss of radial growth restriction was proposed to be through defective microtubule organisation in the seed husk, resulting in reduction of pressure normally promoting oval grain shape (Wendrich, J. R. et. al., 2018, Yang et al., 2018). A similar discovery was made in shape control at a cellular level in secondary cell wall pits, for which loss of *IQD13* function conferred a loss of oval shape and more rounded shape, associated with lowered microtubule localisation, presumed to restrict radial growth (Sugiyama, Y., et. al., 2017). This perhaps indicates similar

function of 1a *IQDs* in Arabidopsis seed coat and prompts further investigation into microtubule behaviour in *1aiqd* line.

As well as increased biomass production in the *1aiqd* line through greater stem diameter and larger seeds, the plants also displayed an increase in the number of lateral branches and resulted in a dramatic increase in fruit and concurrently seed numbers per plant compared to WT. Both increased stem diameter and initiation of lateral branching are considered important agronomic traits that affect the resilience of plants to adverse weather conditions and impact the yield potential of crops. This highlights the practical relevance of understanding the mechanisms by which IQD function impacts organ growth and shape.

Once again, the effect of *IQD* genes in lateral branching may be linked to phytohormones. Increases of auxin and cytokinin and reduction in GA levels are well known to promote lateral branch initiation (Martinez-Bello et al. 2015; Müller D and Leyser O. 2011). Cytokinin levels appear linked to auxin's role in initiation, with a function in stabilising high levels of PIN3,4 and 7 in xylem cells at the plasma membrane, therefore proposed to enhance auxin transport in the stem, and consequently induce branching (Waldie, T. and Leyser, O. 2018). DELLA proteins have been shown to induce expression of the *LAS* boundary gene, promoting branch initiation by disrupting the protein SPL9, which represses *LAS*. Therefore, low levels of GA and high levels of DELLA are required for branching (Zhang, Q. Q et al. 2020). This raises the question whether the branching phenotype of the *1aiqd* mutant could reflect functional interplay between 1a *IQDs* and phytohormones such as auxin and GA, to which they are linked in transcriptome data sets (Zentella, R. et al.2007; Schlereth, A. et al., 2010; Möller, B.K. 2012).

Changes in phyllotaxis pattern of all shoot organs were a particularly striking phenotype, albeit with low penetrance. Combined with infrequent occurrence of family 1a loss of function plants displaying individual events of primordia initiating at around 180 ° angle to one another, rather than a stable phyllotaxy change, including those in quadruple mutant populations, indicates the phenotype likely is a direct impact of mutations introduced. Most mutants described to affect phyllotaxis do not result in stable patterns (Lee, B. H. et al. 2009), and this can be taken as an indication of how complex the trait is. The few mutations that generate stable phyllotaxy changes either increase meristem size, such as *abphyl1* (Giulini, A. et al., 2004), or impact PIN distribution in the SAM, as seen following disruption

of PLETHORA (PLT) transcription factors (Prasad, Scheres et al. 2011). Even in those instances, however, the alterations are not stable throughout vegetative and reproductive growth. As discussed in the introduction, key factors in modelling for phyllotaxis are the starting shape and size of the meristem and subsequent inhibition fields generated between newly initiated organs, proposed to be via auxin availability (Smith, R.S. et al.2006, Douady, S. Couder, Y. 1996). Mutants impacting meristem size and PIN1 patterning that result in stable phyllotaxis changes support these as contributing factors. The hypothesis of increased meristem size in the *1aiqd* line was attractive, because it could potentially account for phyllotactic changes as wellas phenotypes such as increased number of organs and thickened stems. A simple increase in meristem size in the *1aiqd* mutant, however, was ruled out. An alternative hypothesis is that 1a IQDs interact with either PIN1 patterning, or function in an unknown mechanism to pre-pattern the observable PIN response. Due to low penetrance of the phyllotaxis phenotype in the *1aiqd* line, function of other *IQD* genes, such as those in family 1c or subfamily two, linked to auxin signalling, could be investigated.

In contrast to the overall increase in growth in the sextuple loss of function mutant, ectopic expression of the family 1a gene *IQD22* driven by the RPS5a promoter, therefore expressed in every cell, seemed to impede growth throughout the shoot, suggesting an inhibitory role in key growth processes such as cell division and expansion. Phenotypes of *IQD* overexpression in early leaves have been reported in a tomato line and for the family 1c member *IQD16* in *Arabidopsis thaliana,* which displayed highly elongated and twisted leaves. The effect of *IQD22* overexpression, however, was more similar to the more compressed twisted leaves caused by ectopic *IQD14* expression and the compressed, rounded leaves observed in ectopic family1a *IQD25* lines in Arabidopsis (Burstenbinder, K. et al. 2017), although with more severely impacted petiole and a distinctive leaf shape. The loss of petiole elongation may be akin to the extreme reduction in stem internode elongation. The divergent growth phenotypes caused by ectopic expression of different *IQD* genes have been linked to differences in cellular localisation, particularly in the decoration of the CMT arrays (Burstenbinder, K. et al., 2017). This prompted me to look more closely at the relation between family 1a IQDs and CMT arrays, as described in Chapter 5. The drastic reduction in stem elongation, leaf expansion and strong impact on flower development also had a strong resemblance to gain of DELLA function phenotypes (Dill, A et al. 2004),

further strengthening the potential link to DELLA regulation, as mentioned above. The bulkier growth of the *1aiqd* mutant was also seen in the vegetative phase due to increases in both leaf number and leaf area. Induced ectopic expression of I*QD22* from germination also impacted leaf shape and size. The details of how 1a *IQD* genes affect leaf growth are presented in Chapter 4, whilst the potential links to DELLA proteins are studied in more detail in Chapter 6.

Such wide-ranging shoot growth effects in the *1aiqd* mutant are not so surprising, considering the links between *IQDs* and phytohormones, calcium signalling and multiple TFs linked to plant growth regulation. Whilst it could seem counterintuitive for plants to evolve mechanisms for growth repression, many growth processes need to be tightly regulated to produce the complex varied structures of shoot organs that allow plants, as immobile organisms, to inhabit a vast proportion of earth. Therefore, well-established precedents exist for a prominent role of growth repressors in shaping plants and in adjusting their growth to environmental conditions, including examples with practical importance such as crop improvement involving repression of stem elongation by DELLA proteins (Serrano-Mislata, A. et al. 2017). The prospect of IQDs being a large family of proteins that restrict growth across land plant species opens opportunities for moderation of their function to partially alleviate growth restrictions without severely disrupting plant development, as is observed after loss of six out of thirty three members in Arabidopsis.

Investigating relationships with hormones known to be important for organ initiation and growth, such as auxin and gibberellin, which are loosely associated with the *IQD* gene family in the literature, could be key to understand by what means IQD proteins fine tune organ growth. The combination of phenotypes and reported cellular localisation of IQD proteins in the literature suggests that IQDs impact fundamental cellular process important for growth. Moving forward from macroscopic phenotypes, the next chapters aimed to unveil the effects of 1a *IQD* genes at a cellular and molecular level, through focused study of specific aspects out of the wide array of phenotypes presented in this chapter.

Chapter 3: Control of stem growth by family 1a *IQD* genes

3.1 Introduction

The stem is a central organ of the plant shoot, contributing to the plant's ability to harness power from sunlight, distribute water and nutrients from the soil to all shoot organs and position flowers for air borne pollinators. In supporting shoot organs such as leaves for optimal capture of light, the stem also must provide resilience to adverse weather conditions such as strong wind. Thus, a finely-tuned stem structure is likely to have been a pillar of plant's evolutionary success.

The stem is composed of multiple, concentric cell regions patterned within an elongated cylindrical structure. Each cell region therefore must coordinately expand and divide in a manner that maintains the patterning while generating much more growth vertically than radially. The cell layers of the Arabidopsis stem can be divided into outer rings of the epidermis and cortex that enclose vascular bundles composed of xylem and phloem, which extend into the central pith. A cluster of cells positioned directly below the SAM initiates stem growth through rounds of orientated cell divisions. This cell region is named the rib zone (RZ) and can be divided into a central region from which the pith is generated and a peripheral cell region, forming concentric rings of the outer stem layers. These outer layers sandwich vascular bundles that differentiate in a highly ordered manner around the pith in response to auxin signalling, which pair organ patterning with vascular development (R.M. Sachs. 1965).

Unlike in dicotyledons, such as Arabidopsis, monocotyledon plant species possess multiple intercalary meristems, which are located at junctions called internodes and promote elongated growth of each section of the stem. Intercalary meristems act much like the rib zone as a source of cells, which divide to pattern the stem and elongate it, and evidence suggests elements regulating stem growth act similarly on RZ and intercalary meristems (Serrano-Mislata, A. Sablowski, R. 2018). However, unlike the concentric cell layers and patterned vasculature bundles found in dicotyledon stems, monocotyledon stems possess one outer layer the epidermis, which surrounds an inner ground tissue with vascular bundles

dispersed throughout. The stem structure itself can still however be divided into inner and outer tissues (K. Tsuda, K. et. al. 2017).

Ordered cell divisions are required both to establish the patterned cylindrical stem structure in the RZ and for subsequent organ growth. In the case of the stem, much of the later growth is aligned with the stem's main axis, requiring cells to have transverse planes of division. In the RZ, whilst the central zone generating the pith contains strong preference for transverse planes, cells in the peripheral RZ show more frequent radially oriented divisions, which generate the cell layers that encase the pith. These cell divisions occur mostly near the growing shoot apex. In germinating seedlings, most growth occurs in the apical hook region and much faster proliferation is observed in epidermal layers compared to central regions such as the pith (Kutschera, U. and Niklas, K.J. 2013). In later stem growth, active divisions have been shown to typically extend 1cm or up to 2 cms below the meristem (Sachs R.M. 1965).

Although indeterminate stem growth depends on the supply of new stem cells from the SAM into the RZ, the overall rate of growth due to cell proliferation alone is modest; a large fraction of stem growth is due to cell expansion, which continues beyond the proliferative phase. Cell division is intrinsically coupled to cell expansion during growth, determining final organ size and shape. Much of our understanding of stem growth has been extrapolated from studies of cell expansion in the hypocotyl, which is considered an embryonic stem, with cell elongation strongly implicated as a driving force for stem elongation. In Arabidopsis, studies investigating the contribution of cell expansion to stem growth indicate cells undergo rapid elongation with increase of up to three times in cell length. The elongation process is complete a few centimetres below the meristem (Hall, H. and Ellis, B. 2012)**.** In-fitting with elongation growth of a thin cylindrical organ, cell expansion is highly anisotropic in stem tissues, with cells extending far more in parallel with the main axis of the growing stem rather than transversely. Combined, the processes of cell division and cell elongation contribute to stem internode elongation. Over the plant maturation period, a stem section's contribution to total stem growth rapidly drops off the further from the meristem it is positioned, having lost a fresh supply of cells and completed any cell elongation.

As previously mentioned, co-ordination between different patterned cell regions is required for uniform extension of the cylindrical stem structure. Therefore, apart from being regulated along the stem's main axis, cell proliferation and expansion need to be coordinated across the concentric tissues of the stem.

Any one cell region could be rate-limiting to whole organ growth. Research has shown the epidermal cell layer has much thicker cell walls than inner stem tissues, particularly in newly growing organs, where the vasculature is yet to establish thick secondary walls. As a result, the epidermis is perceived as less extensible and experimental evidence demonstrated the epidermis exerts a restrictive force on inner stem tissue elongation. For example, when peeled away to reveal inner stem tissue, which is subsequently supplied with water, cells instantly elongated (Peter WS. Tomos AD. 2000). To this end it is suggested the epidermis is under high tension stress and central stem under axial compression stress exerted by the epidermis.

Whilst the epidermis may be a restricting factor on growth, integration with growth of inner stem tissues is likely key for generation of forces driving axial growth in stems. Evidence for this comes from the patterns of cellulose microfibril deposition in epidermal cells of the stem. The stress patterns in a tissue are often considered to be in line with the direction of cellulose microfibrils in the cell walls. The orientation of microfibrils is directed by microtubule tracks and the orientation of these microtubule tracks is influenced by tissue stress (Landrein, B., et al. 2013). Interestingly, in stem epidermal cells, longitudinally arranged fibrils were predominantly observed (Baskin TI. 2005). This is in contrast with the expected orientation of microfibrils given longitudinal cell expansion, if the epidermal cells were under uniform vacuole pressure. In this case, the expected stress pattern in the epidermis, and consequently the orientation of microfibrils, would be transverse. The arrangement of microfibrils on the stem epidermis suggests that the stress pattern in the epidermis is actually longitudinal. The required conditions of axial stress being a number fold higher than radial stress in the epidermis was concluded from two separate studies in sunflower hypocotyl and hollow dandelion immature and mature stems (Hejnowicz Z., Sievers A. 1995b). The underlying cause of this stress pattern is yet to be established, with various hypotheses including differential growth, differential moduli, or growth stress. Regardless of the origin of the stress patterns in the stem, the microfibril deposition and cell geometry implicated a requirement for anisotropic stress in directing cell expansion and stem elongation.

As well as contributing to directionality of cell elongation, stress may well interlink with the other key element directing growth, division. As mentioned above, orientation of cell divisions in the RZ is important for stem organ patterning and directing axial growth. Stress patterns themselves appear to play a strong role in

directing stem growth and microtubules, which are key players not only in cell expansion, but also in positioning the plane of cell division. Early in cell division, the cortical microtubule array (CMT) rearranges to form a pre-prophase band, which marks the future plane of division. Subsequently, microtubule arrays also generate the phragmoplast, which assembles in a pre-decided plane of division to lay down the cell plate for division to occur.

It is largely accepted that cell geometry contributes to directing the plane in which a cell will divide. This rule pertains that where great differences in area between planes of division are present, division will occur in the plane with the smallest area, but where large differences are not present, either plane is almost equally likely. A microtubule mechanism stemming from nuclear positioning may underlie this theory. Radiation of microtubules from off-centre nuclei during interphase occurs and the force generated from these microtubules has been proposed to re-position the nuclei centrally. If the PPB were formed by microtubules spanning the shortest distance between the nucleus and the cell wall, presumed to exert force for repositioning, this could explain why cell division tends to occur along the plane with the smallest area (S. Besson, S. Dumais, J. 2011). The geometry rule of smallest area upholds a strong preference for division planes positioned in transverse planes of cells undergoing marked elongation, as occurs in central pith stem tissues.

Orientating planes of division may not be so simple, however. For a long period, evidence has implicated that mechanical stress also contributes to a cell's decision on division plane orientation (Mirabet, V. Jas, P. et.al. 2011). Models that align division planes along the planes of maximum stress correctly place the divisions observed in SAM boundary regions, a cell region under high stress. These cell division planes are unable to be correctly placed using the smallest area rule. Division along the plane of maximum tension also correctly placed planes in more isotropic growth situations (Louveaux, M. Hamant, O. et.al. 2016). Furthermore, a large change in planes of division in growing roots is required for initiation of lateral roots. In this instance, the initial positioning appears selected by stress, with the first response being directed by changes in polar PIN proteins. Generated auxin gradients then direct, presumably through microtubule reorganisation, periclinal and anticlinal divisions that initiate lateral roots (Lucas, M., Swarup, K. et al.2013). In line with an important role for auxin signalling in orienting cell divisions, auxin transport mutants display distinct incorrect division planes in embryogenesis with only symmetrical and no asymmetric divisions

(Yoshida S, Prusinkiewicz P, et al. 2014). Thus, multiple lines of research implicate stress, microtubule behaviour and auxin gradients in the control of division planes. With multiple contributors, it seems likely that interplay between all factors occurs. In different tissues, under different conditions, one contributor may weigh more heavily than another. It has not yet been established how these signalling elements affect cell division planes, or what may be most important factors orienting divisions in the stem.

A further consideration to take when looking at stem growth is the contribution of each cell region to growth itself. Despite the greater proliferation in epidermis versus pith in the upper region near the shoot meristem, the central pith region accounts for by far the largest area of a cross section through the mature stem. Differences in stem diameter are strongly correlated with pith diameter, for example in tuber mustard. In this species, high ploidy levels were seen in the central pith region (Shi, H. et. al. 2012). Endoreduplication is often associated with larger cells and could be means by which the pith region contributes so greatly to stem area without so frequently dividing (Bourdon M., et. al. 2010). Growth through cell enlargement following endoreduplication, as occurs in pith cells, is also highly important for fast growing fleshy fruits such as Solanaceae and Cucurbitaceae (Bourdon M. et.al. 2010.) Genes involved in cell wall loosening and expansion such as tubulins, expansins and pectin modifiers have been shown to be highly expressed in the later phase of fruit growth associated with endoreduplication in cucumber as well as melon, tomato, grape and apple (Ando, K. and Grumet, R. 2010; Wechter, W.P. et. al. 2008). Of relevance to this thesis, multiple *IQD* genes have been linked to the control of fruit growth and shape in Solanaceae and Curcubitaceae.

To date, several mutants affecting stem growth have been characterised. A prominent example are mutations of *DELLA* genes. Stunting of stem growth, important for crops' resistance to damage by adverse weather, is caused by increased levels of DELLA proteins. DELLA proteins have been shown to impact cell proliferation both through inhibiting transcription factors that control genes important for cell cycle progression, and by directly upregulating genes such as KRP2, a cell cycle progression inhibitor (Serrano-Mislata, A. et. al. 2017). Another mutation with reduction in stem elongation is that of *REPLUMLESS (RPL*), whose function in the RZ has been implicated in the control of cell division planes, which likely accounts in part for the reduction in stem elongation in the mutant. The TF is

also linked to repression of boundary gene expression, known to inhibit hormone signalling inductive of proliferation (Bencivenga, S. et. al. 2016).

Some mutations reveal specific roles of inner tissues in stem growth. One example is a mutation in DEFECTIVE IN CELL EXPANSION (*det3-1*) gene. When combined with the meristem size mutant *clv3*, *det3*-1 increased stem diameter through increased proliferation and cell size in the pith, resulting in axial tears of the stem epidermis. These tears, in line with stress patterns in the epidermis, indicated that an inner increase of volume exerted an outward mechanical stress which the mutant, *defective in cell expansion*, was unable to counter (Maeda, S. 2014). Recently, a QTL associated with stem diameter in tomato was identified as a kinase-interacting family protein (KIP) for which artificially altered levels directly impacted stem diameter. This increase was attributed to increased cell size and number in parenchyma cells. Whilst the stem phenotype was also associated with an increase in fruit size, no assessment of impact on stem elongation was performed (Ye, J. et al. 2020).

3.1.1 Aims of this Chapter

As detailed in Chapter 2, I have obtained a mutant line with substantial loss of function in family 1a *IQD* genes in Arabidopsis. One of the consistent phenotypes in this line was a thicker inflorescence stem, without any obvious change in mature plants' stem height. This phenotype is unusual, in contrast with the much more frequent changes in stem elongation seen in the stem development mutants. In this chapter, I characterised in more detail the cellular basis for the increased stem thickness of the *1aiqd* line.

An additional motivation to study in detail how family 1a *IQD* genes affect stem growth was that the *1aiqd* stem phenotype was analogous to correlations between *IQD* function and fruit shape in other species. Specifically, an accession line with reduced *IQD* levels in cucumber had increased width and more spherical fruit (Pan, Y. et al.2017), whereas increased expression of family 1a *IQD* genes were associated with elongated, more narrow fruits in a watermelon accession line (Dou, J. et al. 2018). Therefore, studying the cellular functions accountable for the *1aiqd* stem growth phenotype in the model species *Arabidopsis thaliana* may have an overarching cross-over with understanding how IQDs function to control organ shape in crop species.

The results presented here highlighted the role of cell division in the pith as causative of a large stem cross section area in the mutant. The increased stem radius also prompted experimentation probing IQD's role in planes of division. Due to increased proliferation paired with cell size differences between WT and *1aiqd* pith cells, and the cell type's link to endoreduplication, possible roles for IQD function in termination of cell cycle and entry into endoreduplication were studied.

3.2 Results

3.2.1 Contribution of different cell types to increased stem diameter in the *1aiqd* line

To get better insight into what may be occurring within the stem tissue to result in increased diameter, I began by analysing cross sections. The stem tissue is composed of multiple cell types from the epidermis and cortex to vasculature bundles and the central pith region. Hand stem sections were cut from fixed samples taken at the base of the stem and position where the first silique elongated at growth stage where 4 siliques had elongated. Cell walls were stained following a modified pseudo-Schiff propidium iodide staining protocol and sections were analysed for the changes in the amount of different tissues and to assess for impact on cell number or size, elements fundamental in controlling organ shape and size and impacted in other stem mutants discussed in the introduction.

Light microscope images of stained sections cut at the base of the stem (Figure 3.1) unveiled the size of vascular bundles was unchanged, but bundle number was increased from around 8 in WT to 12 or more in the mutant line. The increase in bundle number corresponds to the increased stem circumference and could promote increased transport of water, ions and sugars supporting enhanced shoot growth of the mutant line. However, by far the most striking observation was a massive increase in cell numbers in the central pith region, which accounts for most of the increase in stem cross sectional area. The cells also appeared smaller in size than those in WT samples.

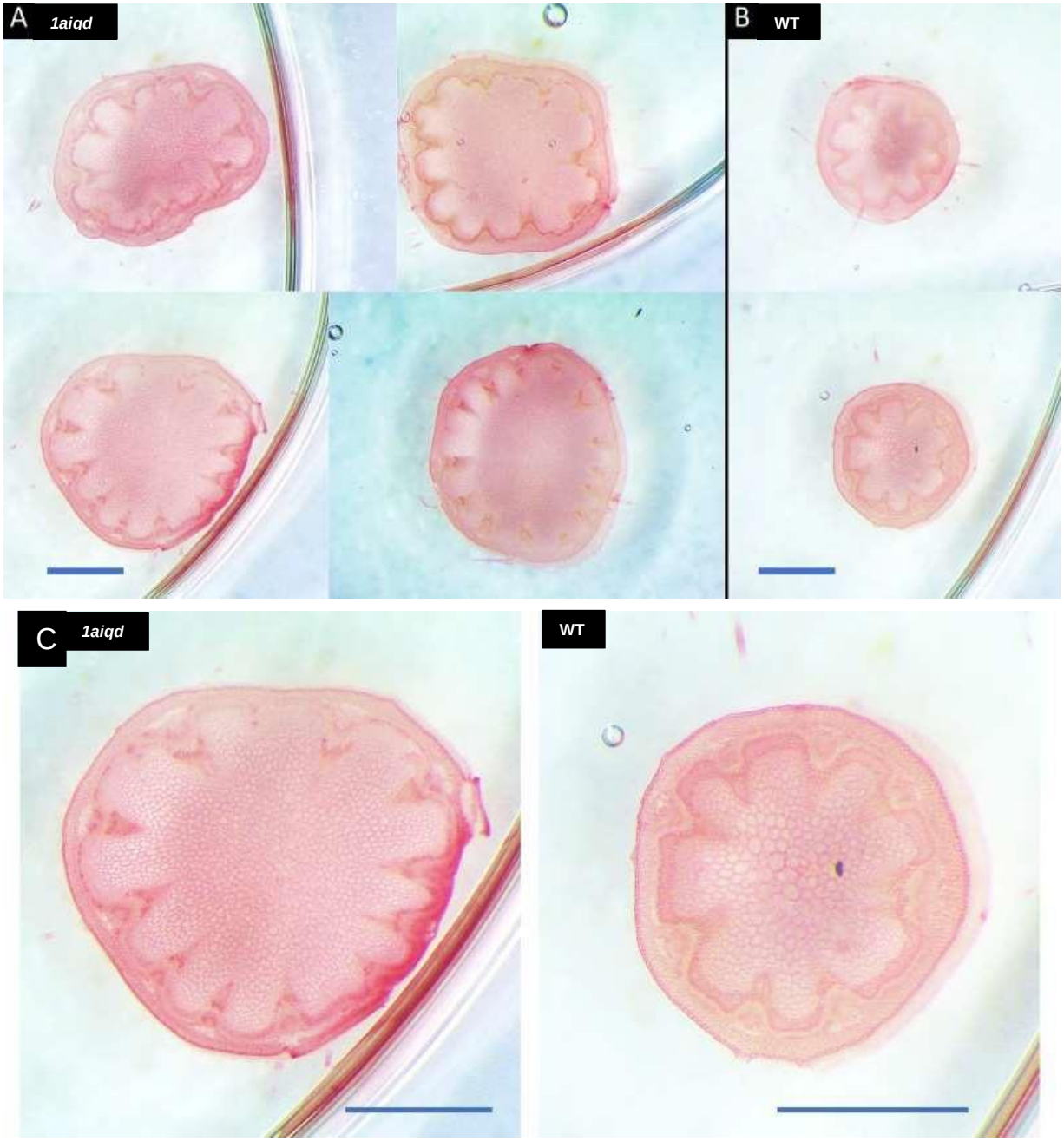

Figure 3. 1: The increased cross-sectional area of stem in *1aiqd* line can be mainly attributed to changes in the central pith region, with a large increase in cell numbers. Representative light microscope images of mPS-PI stained stem slices taken from the base of the stem of mutant plants (A) and WT Col-0 (B). C depicts higher magnification images of one mutant stem section (LHS) and one WT (RHS), where detail of changes in the number and size of pith cells is clearer. Scale bars: 1mm.

Confocal microscopy was used for a closer inspection of any differences in outer cell layers and vasculature bundles between WT and mutant samples. To allow a larger fraction of the stem to be contained in the images, smaller stem sections were taken at the position of first silique elongation. These sections

showed similar growth defects as the hand sections of the stem base, and allowed a comparison of cell sizes in different tissues.

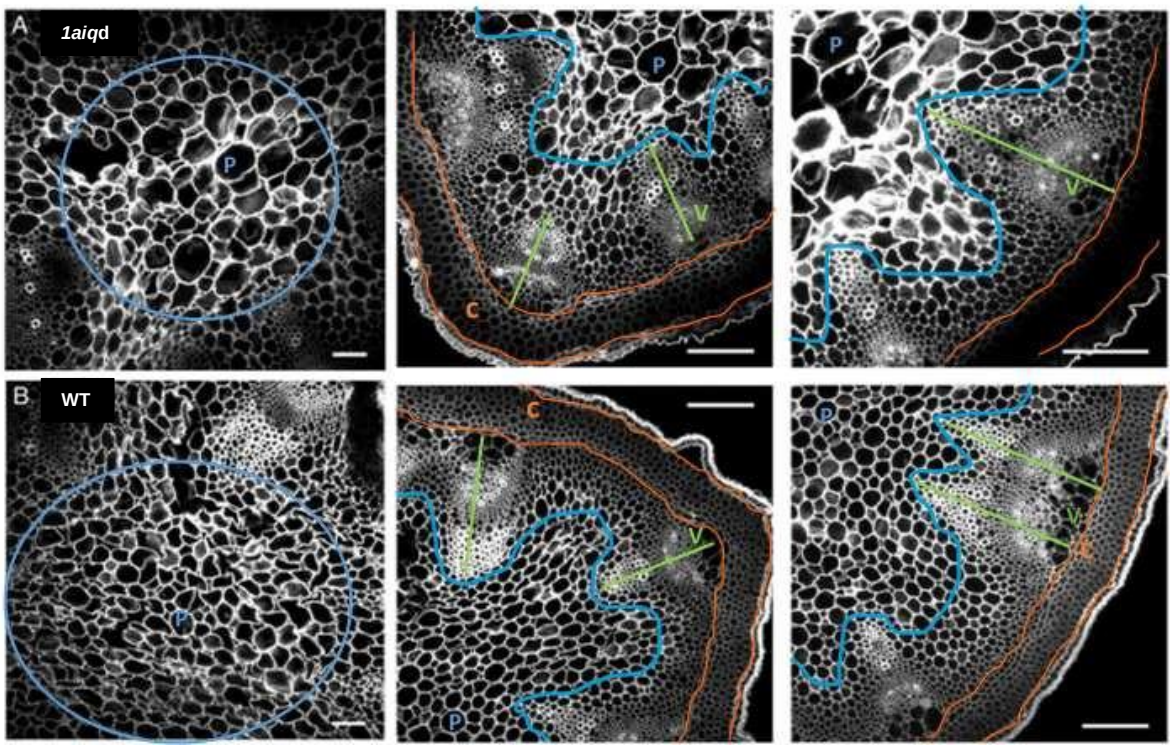

Figure 3. 2: Confocal images of Propidium Iodide stained stem sections highlight increased cell numbers and decreased cell size in the *1aiqd* line.

Stem sections imaged at ×25 magnification were taken from the point in the stem next to the 1st elongated silique of mutant (B) and WT Col-0 (A). (c), (v) and (p) indicate cortex, vascular bundles and pith, respectively. Note that in spite of the thicker stems, the mutant line generally had smaller cells, seen more clearly in the cortex and pith. Scale bars: 50 µm in pith images (left panels) and 100 uM in the middle and right panels**.**

The confocal sections first confirmed the increase in uniformly smaller cells in *1aiqd* pith compared to fewer cells exhibiting large variety of sizes, including much larger cells, in the WT pith. In contrast, individual vascular bundles in mutant stem sections appeared similar in size to those of WT samples (length from outer phloem to inner xylem:220.85 µm in the mutant and 210.77 µm in WT, n=12). Apparently fused bundles appeared more frequent in mutant samples than in WT. The thickness of outer cell layers, including epidermis and cortex, also appeared comparable in mutant and WT samples. In fact, there was a slight decrease in average depth of the outer stem layer in mutant lines across the 6 samples (81 µm in the mutant versus 99.73 µm in WT, n = 6). Thus, the increase in stem diameter predominantly corresponded to a larger pith region in mutant (pith diameter 565 µm compared to 407.9 µm in WT; n= 6).

Whilst slightly reduced in depth, the cortex appeared to have more numerous cell layers, implicating an increase in proliferation, with decrease in cell size accounting for the reduction in tissue depth (Figure 3.2). As with pith cells, individual epidermis and cortex cells were smaller in the mutant (Figure 3.3): mutant epidermal cells averaged 15.06 µm in length compared to 19.09 µm in WT samples, and cortex cells 13.78 µm compared to larger 15.7 µm in WT, n=15 . The large increase in stem circumference implied that many more epidermal and cortex cells were in any given concentric ring, with fruther requirement for increased cell number due to reduced cell size. There was also a non-significant reduction in vascular bundle xylem cell diameter. Violin plots further showed that the size of pith cells in the WT was much more variable while mutant pith cells had a more consistent size, and the majority were smaller in size than in WT pith. Average cells measured 30.67 µm versus 50.96 µm in WT, with strong significance in reduction of size in the *1aiqd* line. Overall, the combination of increased stem diameter and smaller cell sizes across tissues implicated that family 1a *IQD* genes inhibit cell proliferation during stem growth.

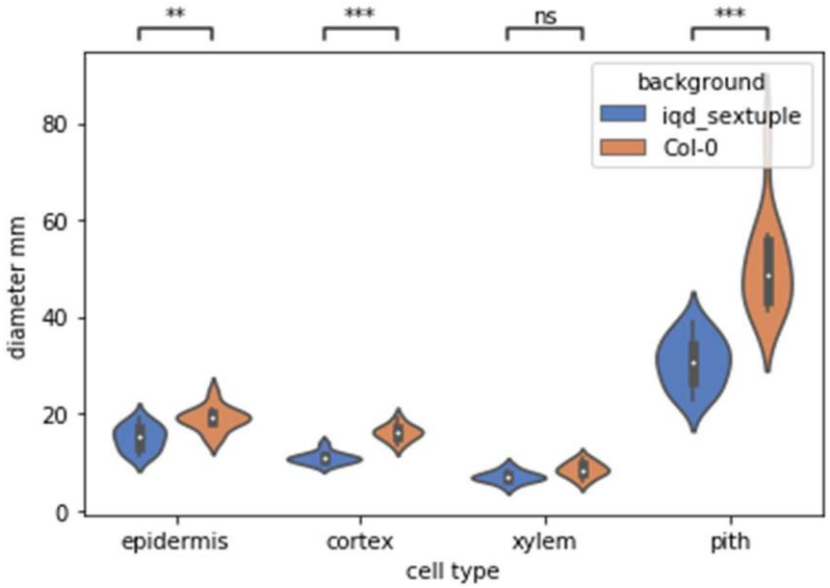

Figure 3. 3: Cells in every stem region were smaller in the loss of family 1a IQD function line than Wt Col-0. Cell diameters were measured in 15 cells across three WT and mutant stem sections in the epidermis, cortex, xylem and pith. Epidermal cells: 15.06 µm in the mutant, 19.09 µm in WT, p = 4.052e-03. Cortex cells: 11.00 µm in the mutant, 16.20 µm in WT, p =1.382e-04. Xylem cells: 7.07 µm in the mutant, 8.53 µm in WT, NS p =7.739e-02. Pith cells: a consistent average cell diameter of 30.67 µm was measured in mutant lines, however in WT samples a larger average of 50.96 µm was calculated with more heterogenous cell sizes in the sample region, p =1.098e-04. ** p < 0.01, *** p <0.001 (two-sided Mann-Whitney test with Bonferroni correction, n=15).

3.2.2 Expression of a family 1a IQD protein in the stem is consistent with a function in the pith early in stem growth

The spatial distribution of the family 1a IQD24 protein in the developing stem in WT Col-0 was analysed to test how the cellular phenotypes correlated with IQD expression. A native translational protein fusion was constructed with a C-terminally attached YFP tag. IQD24 could be observed weakly outlining cells in the epidermis and strongly in central pith region, in line with a potential function in cell proliferation and size control in this region (Figure 3. 4). As reported for other members of the *IQD* gene family, IQD24-YFP showed sporadic localisation in the nucleus, in addition to expression along the cell outlines. In cells displaying nuclear signal, the cell outline appeared weaker, similar to research in the root that implicated nuclear re-localisation of IQD18 (Wendrich, J. et.al. 2018).

To test whether IQD24-YFP was expressed preferentially in regions of cell proliferation, I imaged IQD24-YFP in longitudinal stem sections. Images captured with identical microscope settings along the top 1cm of the stem revealed strongest expression of the protein closest to the tip of the stem, with signal intensity reducing dramatically within 1cm of the meristem (Figure 3. 5). This again is in-fitting with reports of *IQD* expression in young, rapidly dividing tissues (Burstenbinder, K. et.al 2017; Wendrich, J. et.al. 2018; Dou, J. et. al. 2018), and supports the idea that family 1a IQDs function very early in stem growth to control cell proliferation, particularly in the pith region.

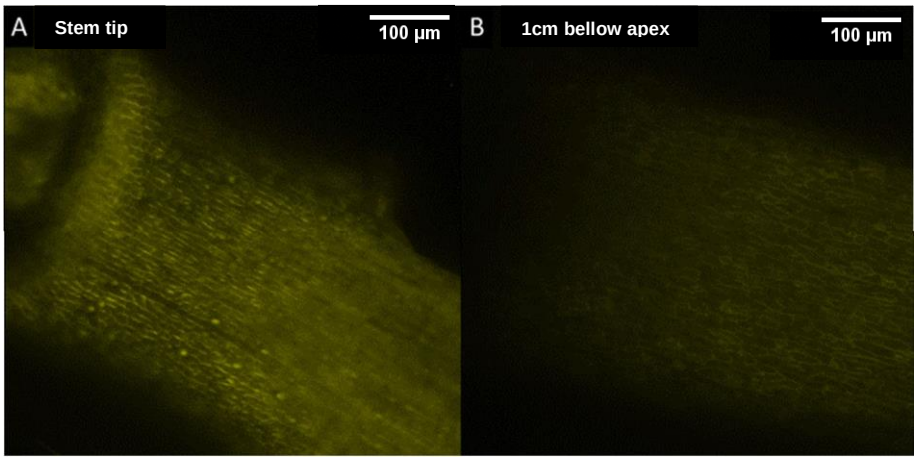

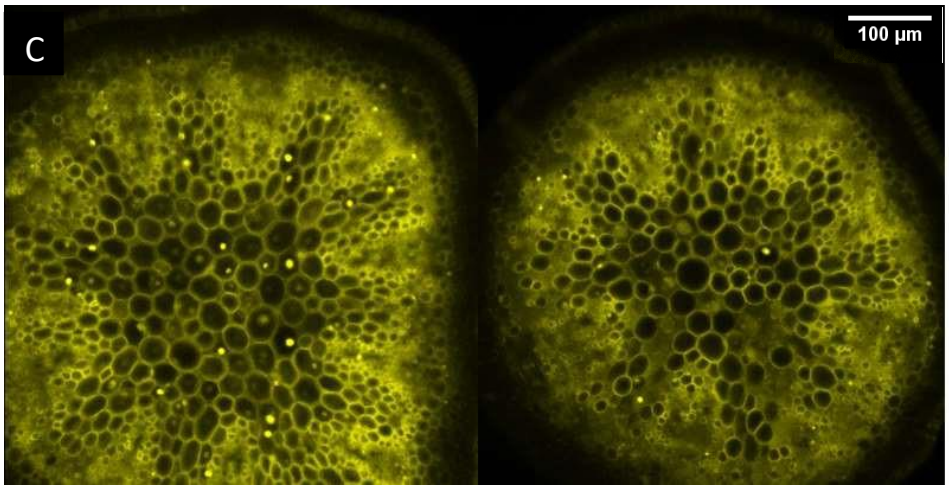

Figure 3. 4: Abundance of IQD24 protein is localised in stem central pith cells and concentration is highest in the region just below the SAM. IQD24-YFP construct expressed in WT Col-0, in longitudinal sections of the stem close to the meristem (A) and 1cm below the meristem (B). C depicts stem cross-sections taken within top 1cm region of the stem. Spatial distribution of the protein indicates potential function in the epidermal cell layer, absence in cortex cell layer, presence in vasculature bundles and high expression in the pith.

3.2.3 Over-expression of 1a IQDs impact on cell proliferation and size in the stem

The results of the loss of *IQD* 1a function line indicated the increased stem diameter could be attributed to increased cell proliferation, particularly in the pith, accompanied by a reduction of cell size. To further explore the effects of 1a IQDs on cell proliferation and tissue growth in the stem, I used a transgenic line in which expression of *IQD22* could be induced by dexamethasone. As presented in the previous chapter, ectopic induction of IQD22 severely repressed stem internode elongation, in contrast to the increased stem growth in the loss of function line. The impacts of gain of *IQD22* function on cell proliferation and size in given regions were therefore investigated in stem sections following dexamethasone induction.

In the highly compressed dex-treated plants, stem sections appeared marginally greater in diameter than control treated lines, however, different cell types were affected disproportionally. Cells in the epidermis and cortex appeared enlarged, while the number of cells seemed unaltered in the gain of function plants. In contrast, pith cells did not show marked changes (Figure 3.5). The preferential effect on the outer stem tissues could reflect the external application of dexamethasone, but also correlated with the observation that these cells showed

lower expression of an IQD 1a marker (IQD24-YFP), so the cortex and epidermis would be the tissues with more marked mis-expression.

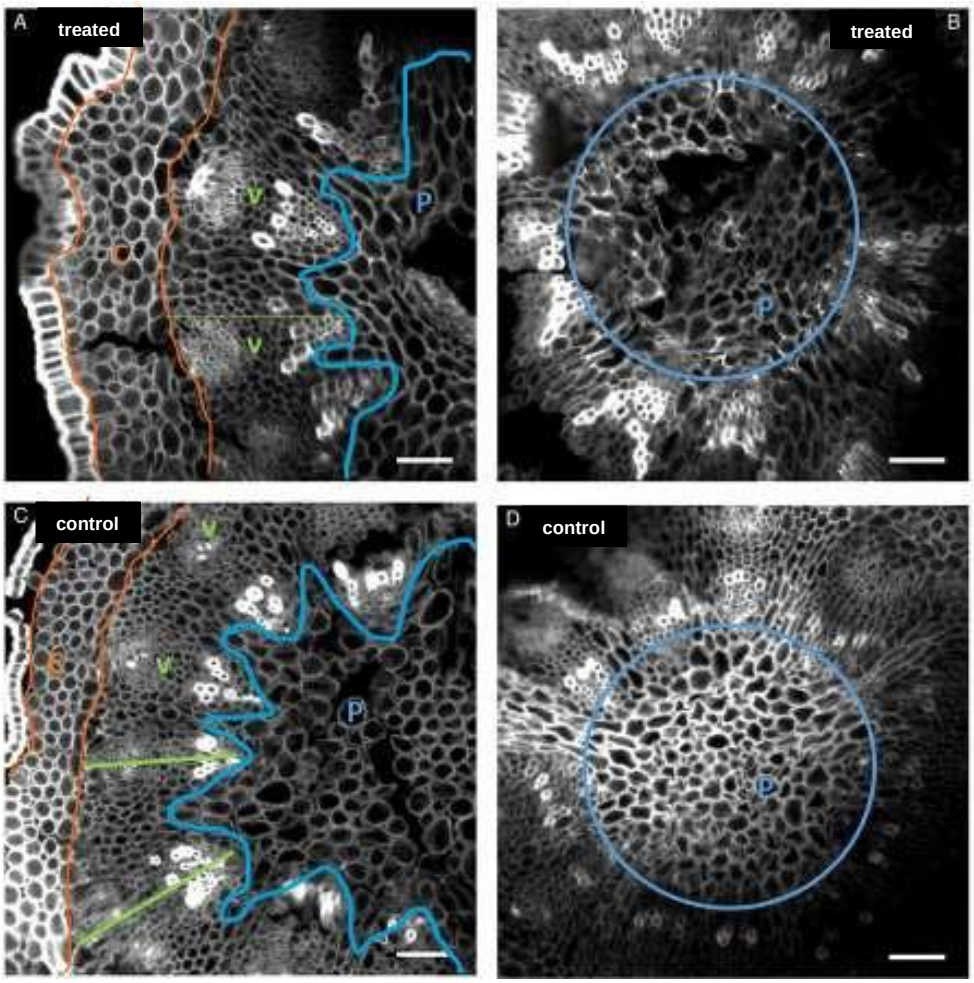

Figure 3. 5: Increased cell sizes in outer stem tissues caused by ectopic IQD22. Propidium Iodide-stained stem sections taken from inducible ectopic *IQD22* plant lines just beneath the SAM, treated with dexamethasone to induce ectopic IQD22 (A,B) and in control (0.1% ethanol, 0.015% silwet) treated plants (C,D). Scale bar: 50 µm. A and C depict greater epidermal, cortex and vascular bundle cell size in treated versus control samples, contributing to increased area in stem cross section. B and D show similar total area of the pith region in treated and control stem sections. (c), (v) and (p) indicate cortex, vascular bundes and pith, respectively

The average depth of the cortex was 82.5 µM and 141.4 µm in sections of control and dexamethasone-treated stems respectively (n=4). This accounted for a 41.7% increase and therefore cortex cells were the cell type with largest contribution to overall increase in stem cross-section diameter of ectopic *IQD22* lines. The length of vascular bundles was also increased in the induced ectopic *IQD22* line, paired with observation of larger cell sizes. Bundles measured 167.5 µm after induction of IQD22, versus 136.1 µm in the control (n=8). Diameter of the

pith, however, was very similar: 242.4 µm in induced plants, compared to 235 µm in the untreated controls. The pith accounted for only 18.95% of the total cross section area in the induced IQD22 plants, but 26.15% in controls. The gain-of-function results therefore showed a stark contrast to the loss of function mutant, where a high proportion of cross section area was encompassed by the pith.

Analysis of cell size across three treated and control replicates confirmed statistically significant differences in epidermal, cortex and xylem cell in stem sections with induced ectopic IQD22, whilst pith cells were not significantly different in size. Both epidermal and cortex cells of induced lines were significantly larger than those in control samples and notable increase in cell size was also apparent in xylem cells of stems with ectopic IQD22 protein levels (Figure 3.6). This therefore can account for outer cell layers increase in cross-sectional area.

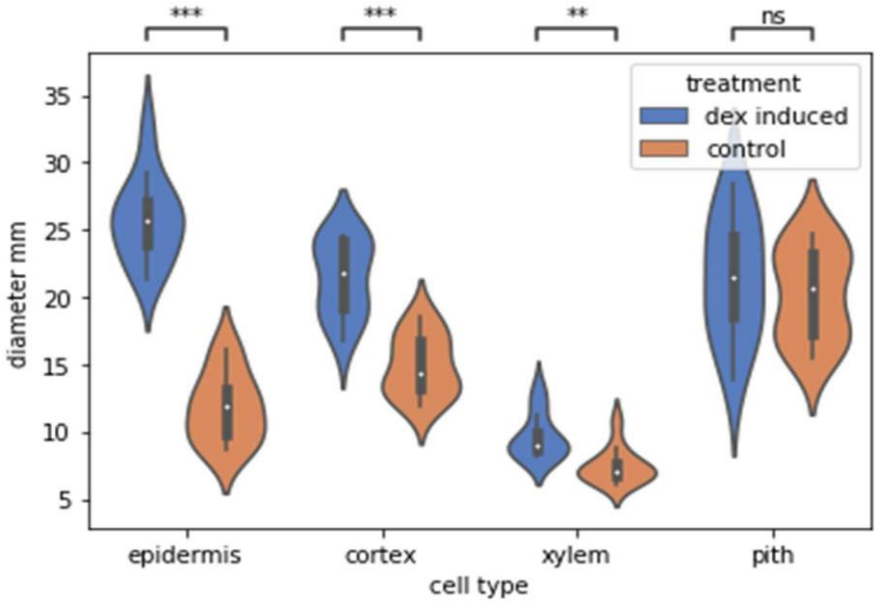

Figure 3. 6: Cell diameter was significantly increased in epidermal, cortex and xylem cells following induction of high levels of 1a IQD22. Diameter measurements of 12 cells across three control and dexamethasone-induced stem sections taken close to the SAM. Measurements in epidermal, cortex, xylem and pith cells showed increase in diameter in all but pith cells. Induced lines epidermal cells averaged 25.82 µm vs 11.83 µm in control treated sections, *p*=1.463e-04. In the cortex cell layer of induced lines cells averages 21.49 µm vs 14.94 µm in control treated, *p*=4.917e-04. Xylem cells in induced lines averaged 9.65 µm vs 7.47 µm in control treated, *p*=5.299e-03. In pith cells of induced lines average cell diameter was 21.55 µm and in control treated samples a similar average of 20.28 µm was calculated, NS *p*=1.0. ** $p < 0.01$ and *** $p < 0.001$ (n=12, two-sided Mann-Whitney test with Bonferroni correction)

In summary, consistent with decreased cell diameter in the loss of function mutant, gain of 1a IQD appeared to increase cell diameter. No marked reduction in cell numbers was present in cross-sections, which is in line with actual slight increase in cross-section area. In the gain of IQD function line, however, the most dramatic phenotype was not on stem diameter but stem elongation. Whilst cross-sections confer cell diameter size differences, total cell size could not be calculated due to limited depth of imaging through stem sections. Reduced stem elongation could be caused by decreased cell proliferation or reduction in cell elongation along the stem main axis. It is possible that severe restriction of division following induction of IQD22 resulted in the majority of stem elongation in induced lines occurring through cell elongation, in line with the enlarged cell diameters. This would be reminiscent of many reports in mutants where impaired cell proliferation is accompanied by increased cell expansion, or where reduced expansion is compensated by increased proliferation, resulting in similar whole organ sizes (Ferjani, A. et al. 2013; Tsukaya H. 2002; Fujikura, U. et al. 2020). In the IQDs instance, proliferation could be impacted, with knock-on effects of reduced and enlarge cell sizes in loss and gain of function lines, respectively.

3.2.4. IQD function in endoreduplication

Extensive plant cell enlargement is often associated with endoreduplication (Ando, K. and Grumet, R. 2010; Wechter, W.P. et. al. 2008). Accordingly, the large cells of the pith have been reported to undergo extensive endoreduplication. For example, in tuber mustard, the greatest degree of endoreduplication occurs in the central pith region, which is the region with the largest cells in WT stem sections (Shi, H. et. al. 2012). Considering that loss of 1a *IQD* function resulted in many more, but smaller pith cells, and that gain of *IQD22* function generally increased cell sizes, I hypothesised 1a IQD proteins could promote the switch from mitotic cell cycles to endoreduplication.

Polyploid nuclei are generally larger (Sugimoto-Shirasu, K. and Roberts, K. 2003), so the first approach taken to test whether endoreduplication was impacted in the *1aiqd* line was to use DAPI staining of stem sections to investigate any differences in nuclear size between the *1aiqd* mutant and WT cells. DAPI staining, however showed similar size nuclei in pith cells of mutant versus WT (Figure 3.7). Further to this, no clear divergent nuclear size was apparent within heterogenous cells of WT pith, where large central pith cells did not possess dramatically larger

nuclei. These results called into question whether 1a *IQD* genes control the transition to endocycles in the pith, and indeed whether endoreduplication has a significant role in the enlargement of pith cells in the Arabidopsis stem.

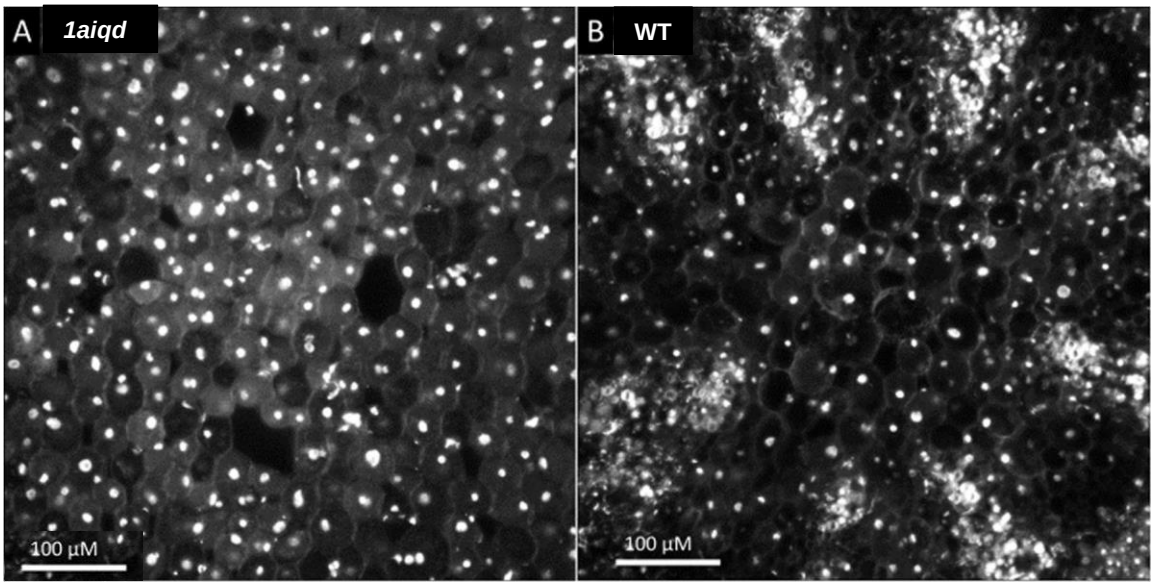

Figure 3. 7 Comparable nuclei size in mutant and WT pith cells. DAPI staining of nuclei in *1aiqd* mutant (A) and WT Col-0 (B) stem sections, showing the central pith region. The numerous small cells in the mutant did not show smaller nuclei than in WT pith cells.

To further establish whether endoreduplication is associated with cell size variation in mutant and WT pith, I next used flow cytometry to measure DNA contents in DAPI stained nuclei. Because endoreduplication also occurs in leaves, for which the method is better established, cell sorting was performed on early leaves as well as stem sections. First, I performed a cell sorting experiment using DAPI staining with leaves from 3 week-old plants grown on GM plates. The results confirmed the presence of cell types of different ploidy in leaves, with most frequently 4N cells, however some 2N and some 8N (Figure 3.8). The frequency of cells in each category did not vary between mutant and WT lines, indicating no impact of 1a IQD function on endoreduplication in leaves. In stem sections, an additional 16N cell population was present, confirming higher levels of endoreduplication in stem tissue than early leaves. Again however, the frequency of cells in both low and high ploidy states were similar between mutant and WT lines (Figure 3.9). Combined, the experimental results indicated that reduced pith cell size in the mutant line is not associated with reduced endoreduplication.

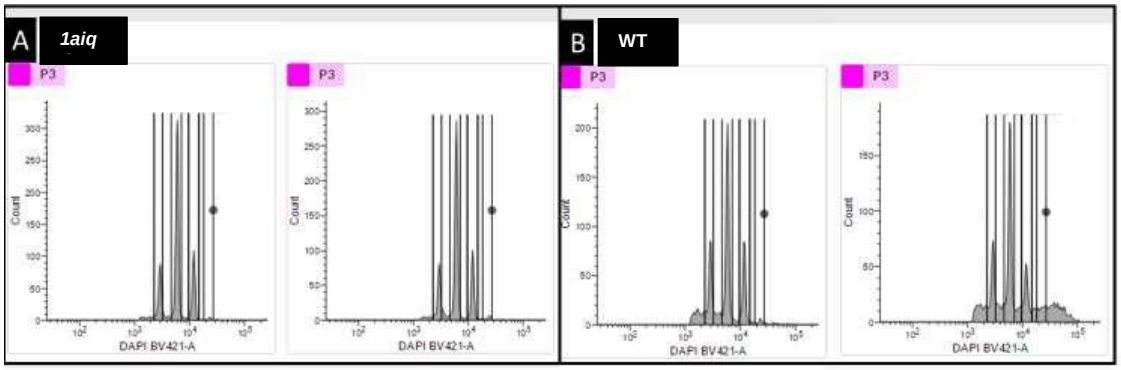

Figure 3. 8: Similar levels of polyploidy in leaf epidermal cells of *1aiqd* and WT plants. Frequency of the 2000 cells sorted with 2N, 4N and 8N nuclei in young leaves of mutant (A) and WT (B) rosette leaves showing very similar occurrence of endoreduplication in mutant and WT lines in the leaf.

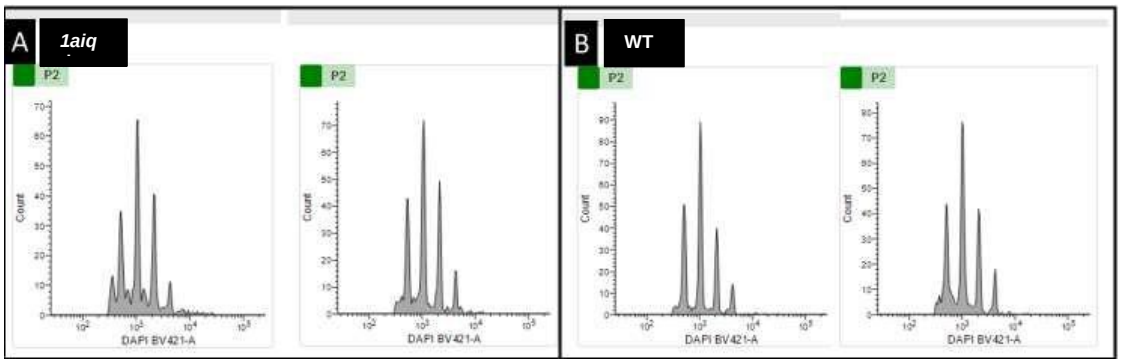

Figure 3. 9: Stem cross sections showed more frequent endoreduplication than early leaves but comparable levels in WT and *1aiqd* plants. Frequency of 1000 cells sorted with 2N, 4N, 8N and 16N nuclei in stem sections of mutant (A) and WT (B) lines again show similar frequency of endoreduplication events between both genotypes.

3.2.5. IQD function in cell division orientation

The results shown in this chapter so far have focused on changes in stem thickness seen in transverse sections, which showed a clear effect of 1a *IQD* genes on radial growth of the stem. These experiments could not show, however, how IQD function affects stem growth in three dimensions. To address this question, I initially performed detailed measurements of longitudinal stem growth.

In Chapter 2 it is presented that the *1aiqd* mutant was shorter than the WT at the stage when four siliques have elongated. This suggested that stem thickening in the mutant could occur at the expense of stem elongation, however, the difference in height might also be attributed to a delay in bolting and faster transition to flowering (Figure 2.19), with subsequent stem elongation occurring at a similar rate to WT. To establish which was the case, the rate of internode

elongation was measured in mutant and WT plant lines, using ink dots as landmarks to track growth. This revealed that stem elongation occurred at a similar rate in the *1aiqd* line, therefore showing propensity to increase stem diameter at no cost to elongation rate (Figure 3.10). Overall, whilst *1aiqd* stem growth was de-restricted outwardly, it remained similar to WT in the vertical direction, which is consistent with leaf shape phenotypes presented in Chapter 4.

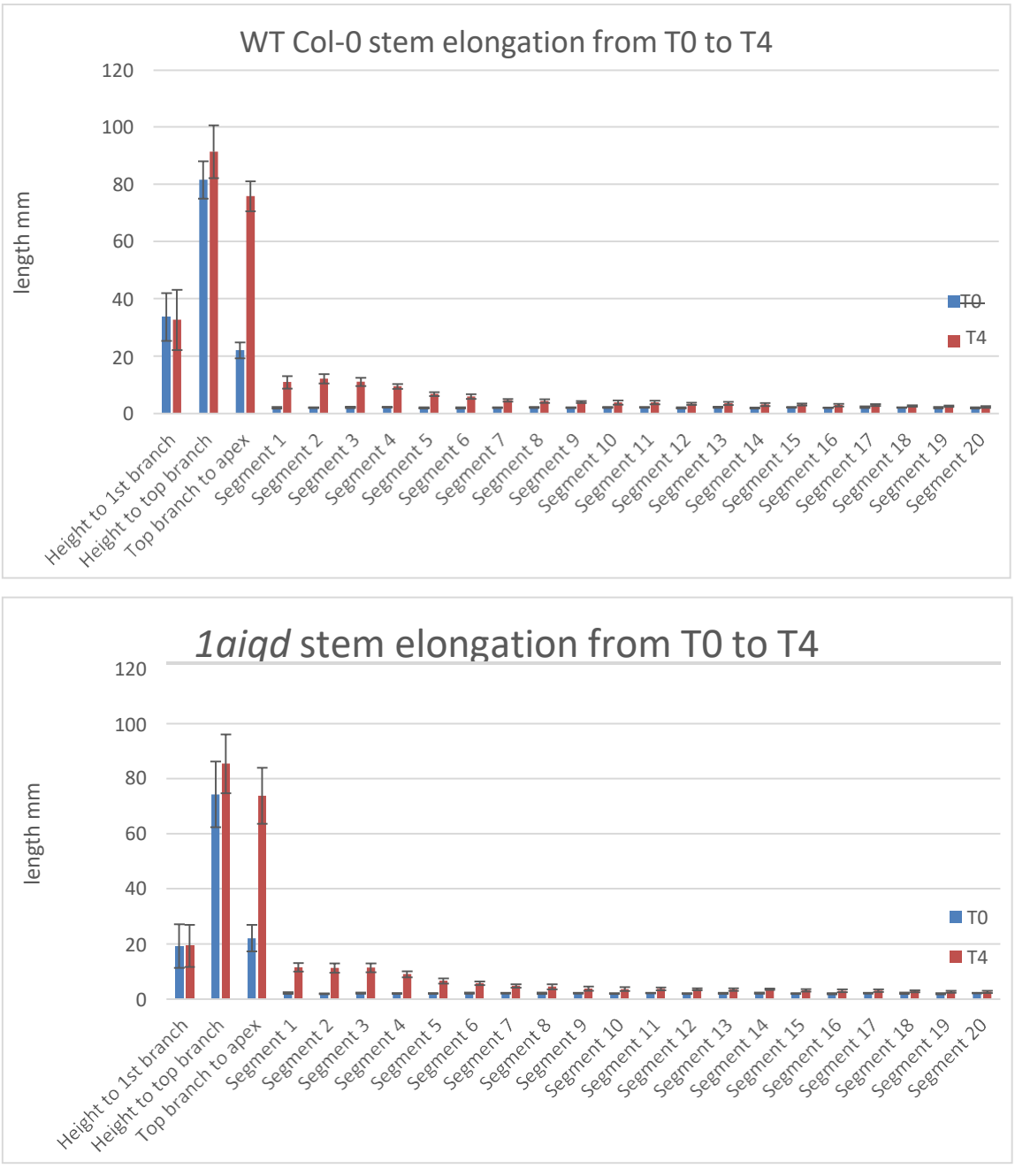

Figure 3. 10: Comparable rate of stem elongation between WT and mutant lines over a 4 day period of growth. Mean length was measured over four days in specified regions following landmarking at 2 mm intervals (with segment 1 starting 2 mm bellow the meristem). The bars show the average length and standard deviation for 10 biological replicates per genotype. WT and mutant lines showed similar growth rate, largely contributed to by the region near the meristem.

As mentioned in the introduction, the strongly oriented growth of the stem results from oriented cell divisions and cell elongation, with a strong preference for transverse divisions and longitudinal elongation. The results presented in Figure 3.10 indicate that stems of the *1aiqd* line elongated at the same rate as the WT, whilst growing thicker. This suggested a potential increased frequency of radial divisions in the mutant. To test this, I focused on the rib zone, where stem growth is initiated. This further investigated proposal that function of 1a *IQD* genes is established early in stem growth, based on expression in the stem presented in Figure 3.4.

The planes of recent cell divisions in the RZ were identified as newly placed cell walls, which appear thinner in mPS-PI images and whose orientation can be measured in 3D as described (Bencivenga, S. et al. 2016). Just through visualisation of cross sections of early pith cells in the RZ in *1aiqd* lines and WT, deviations in division plane were already apparent. Whilst in WT samples clear outlines of pith cells were visible, with no intersection by new cell walls, thin walls crossing the imaging plane were frequently seen in the RZ of *1aiqd* stems (Figure 3.11A). This supports the presence of mostly transverse planes of division occurring in WT pith cells, and more frequent oblique or radial planes in the mutant. The change in division planes was also visible in orthogonal views, with newly formed cell walls highlighted (Figure 3.11C,D), with uniform planes of division directing elongation growth of the WT stem and far less regular patterning of new division planes in the *1aiqd* line's RZ, which showed increased frequency of angles that would contribute to outward growth of the stem.

Quantitative analysis of the angles of new division showed that WT and the mutant clearly diverged in angles to the main axis (defined as the angle between the main stem axis and a line normal to the plane of cell division, Figure 3.12). Whilst the WT showed a predominance of low angles (closer to transverse divisions), the mutant possessed a greater frequency of division planes at high angles of 60-75 degrees to the main axis. This matches the qualitative observation that fewer cells divided transversely in the mutant. Applying the Kolmogorov–Smirnov test to compare the distribution of both data sets gave a *p* value=0.000264 for the null hypothesis that the data sets have the same distribution, and a D value of 0.153. This value was higher than the critical D value of 0.142 for the data set size under a stringent alpha value of 0.001. Thus, the *1aiqd* mutant had a statistically significant change in the of angles of cell division in the RZ. Investigation of radial angles (Figure 3.13) which could be presumed to be

favoured over transverse divisions in *1aiqd* line showed a more similar angle distribution between mutant and WT lines. Same analysis gave *p*=0.16660 and D value of 0.08053, which does not surpass critical D of 0.119 for alpha value set to 0.001, suggesting less significant difference in distribution. This affirmed that rather than changing from directed transverse to directed radial plane of division, more random orientations occurred.

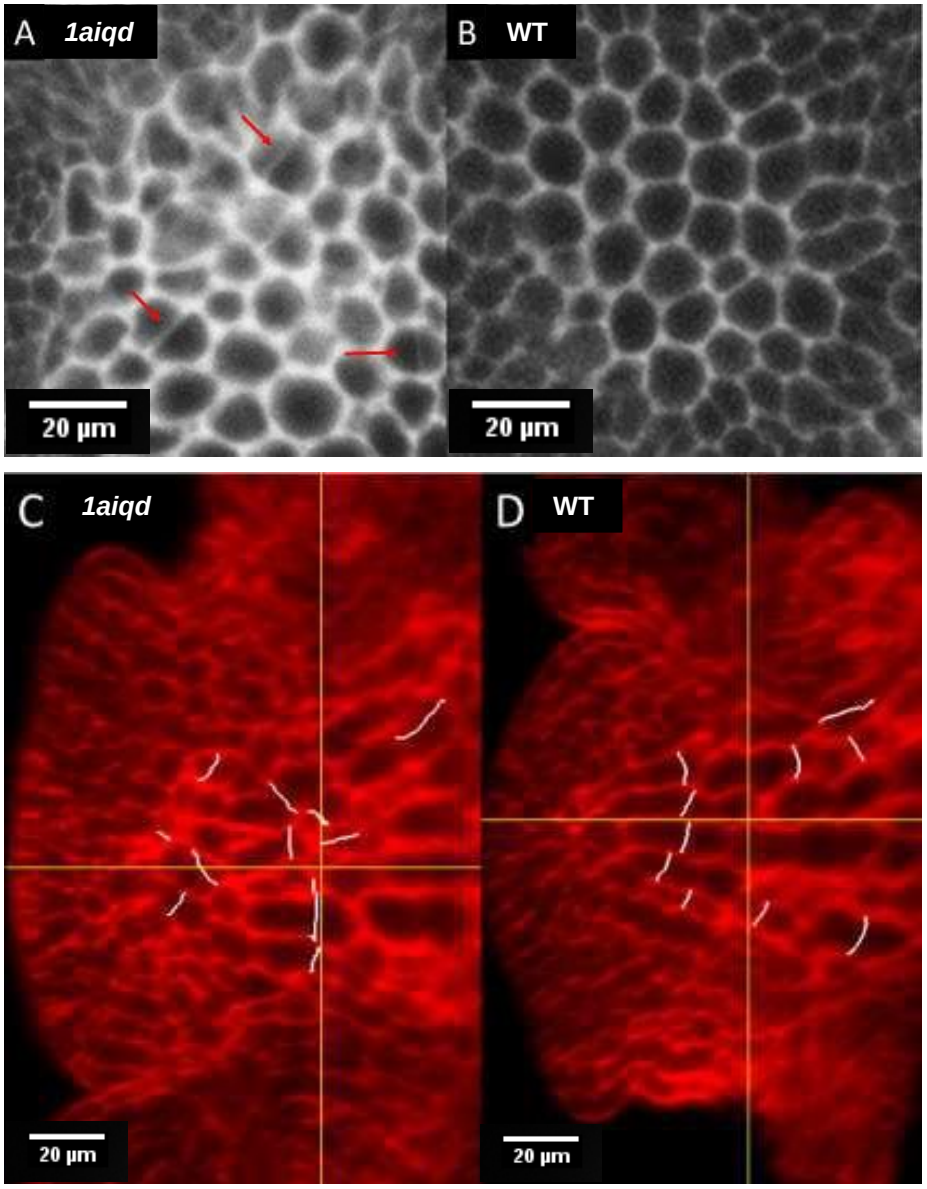

Figure 3. 11: Clear disruption to division plane orientation of central pith cells in the RZ was present in *1aiqd* stems. Transverse cross section through the early pith of *1aiqd* mutant (A) and WT Col-0 (B) showing new cell walls intersecting the imaging plane in the mutant (indicated by red arrows), not seen in WT pith cells, in which new divisions are mostly parallel to the imaging plane. Longitudinal cross sections of the RZ in mutant (C) and WT (D) with newly formed walls detected by signal intensity and cell wall thickness highlighted in white. Transverse planes of division are clearly seen in the WT (D) versus more varied planes of division in the mutant samples (D). scale bar 20 µm.

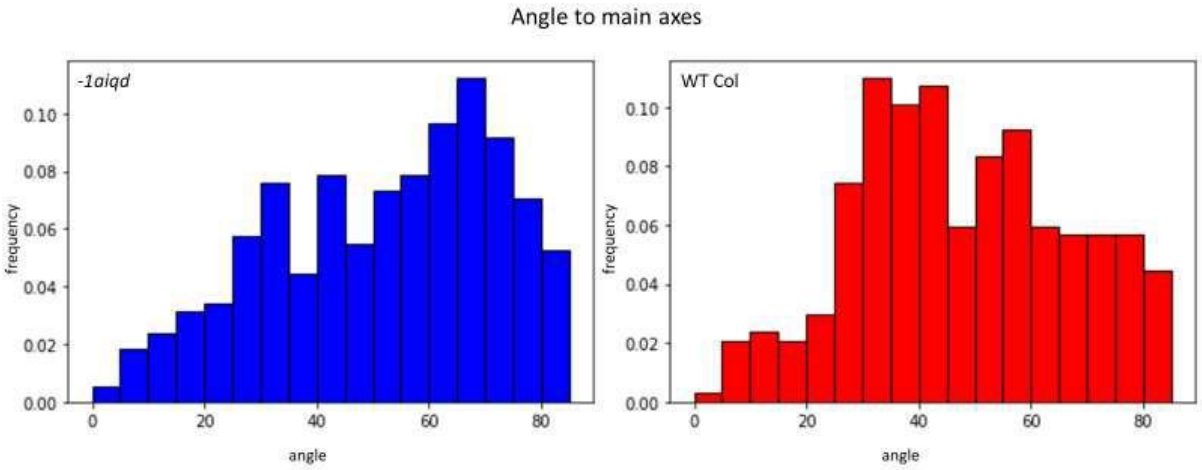

Figure 3. 14: Distribution of the orientation of new divisions of pith cells in the RZ show a higher frequency of mutant cells dividing at high angles relative to the main stem axis compared to WT cells. Relatively frequency of new cell walls formed in RZ cells at given angles to main axis of the stem in WT and mutant are reported. Low angles to the main axis indicate a more transverse plane of division, which occurs more frequently in WT (RHS) than mutant pith cells (LHS). Mutant RZ cells demonstrated a greater propensity to divide at a high angle to the main axis. Newly placed cell walls were detected via signal intensity after mPS-PI staining. The analysis ran on 351 newly placed cell walls in WT RZ and 405 newly placed cell walls in mutant RZ, taken from 4 WT and 4 mutant samples.

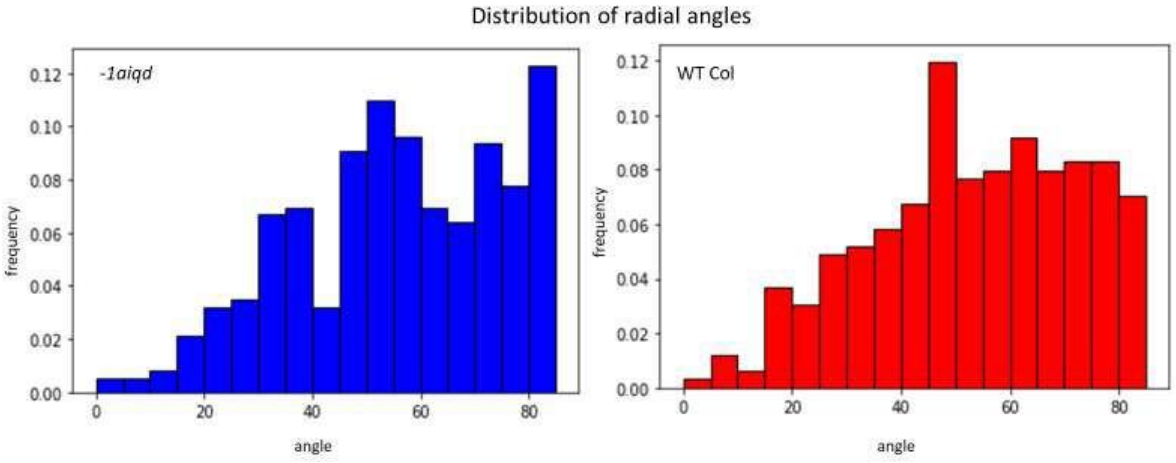

Figure 3. 15: Distribution of radial division planes does not diverge significantly between the *1aiqd* mutant and WT. Relative frequency of angles between the line normal to the wall plane and the line running from the centre of the stem through the centre of the wall are reported low angles correspond to radially oriented divisions. A similar distribution is observed between *1aiqd* line (LHS) and WT (RHS). Newly placed cell walls were detected in RZ cells based on the signal intensity after mPS-PI staining. The analysis ran on 351 newly placed cell walls in WT RZ and 405 newly placed cell walls in mutant RZ, taken from 4 WT and 4 mutant samples.

3.2.6. Effects of 1a *IQD* genes on cell geometry in the rib zone

As seen above, ordered transverse planes of division occurred to a lower frequency in the line with loss of 1a IQD function, resulting in more random orientation of division planes. This suggested that *IQD* genes participate in the mechanism directing planes of cell division in the stem. As introduced, one of the key contributors to control of division plane position is cell geometry, through the smallest area rule. To test whether the division planes in the mutant could reflect altered cell geometry, segmentation of cells in the RZ was used to compare cell size and shape in the *1aiqd* mutant and WT.

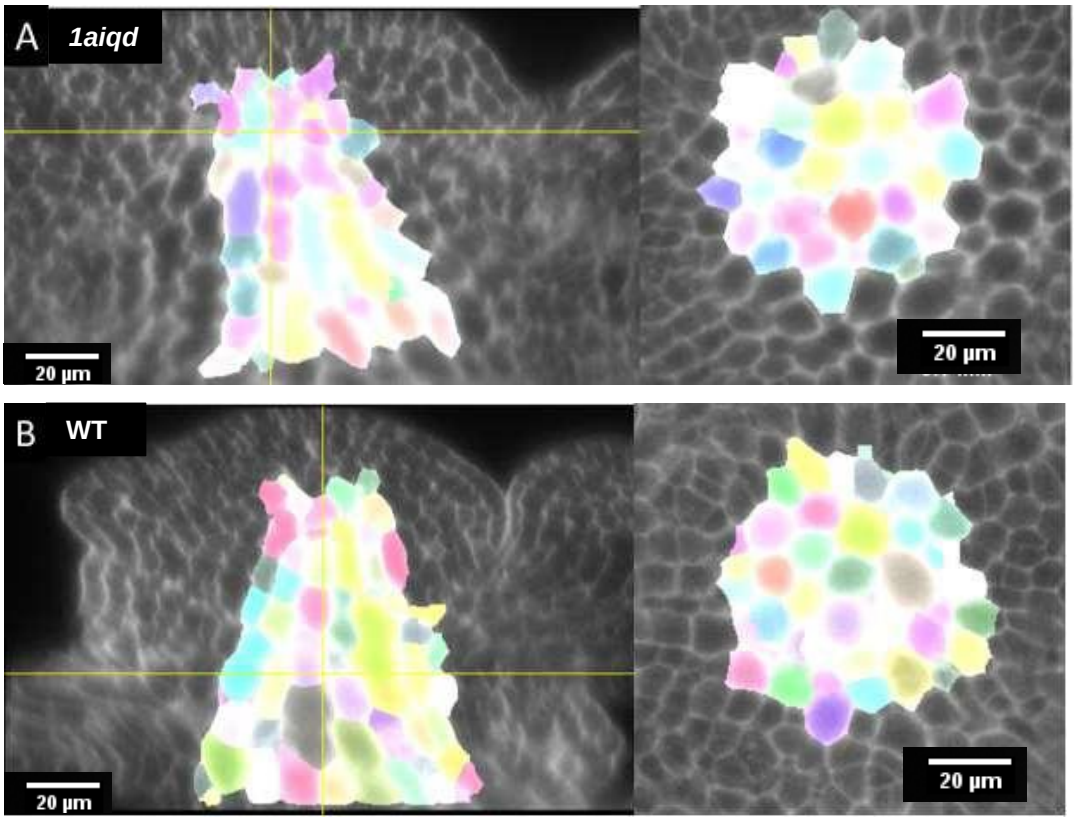

Figure 3. 16: Cell size and shape appear similar in the RZ of *1aiqd* and WT plants. The images show longitudinal and transverse sections of the RZ in mutant (A) and WT (B), with random colours indicating segmented cells selected within the RZ. In both WT and mutant. Distribution of more rounded and more elongated cells in RZ appear similar by eye, with no striking differences in size or shape. Scale bares 20 µm.

Appearance of cell shapes by eye in mutant and WT RZ cells (Figure 3.14) did not indicate obvious differences. To test this impression quantitatively, I compared the geometry of cells in the RZ (which was defined as a region between 25 and 150 µm of the meristem summit, contained within a radius from the main

stem axis that increased linearly from 10 µm near the summit to 30 µm at the bottom). To detect differences in cell elongation, I used the coefficient of variation of cell radii (measured from the cell's centre of mass to each voxel on the cell surface) and comparison of cells total volume.

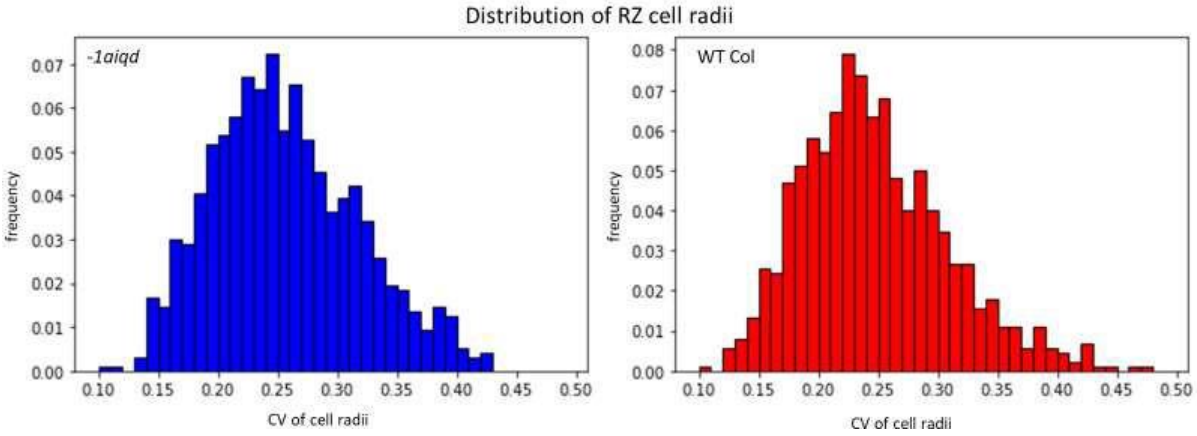

Figure 3. 17: **Similar distribution of coefficient of variation (CV) of cell radii in mutant and WT RZ.** Frequency distribution of the CV of cell radii in the RZ, showing similar distribution in WT (B) and mutant (A) samples. The analysis ran on 887 cells in WT RZ and 966 cells in mutant RZ taken from 4 WT and 4 mutant apices.

Comparing the distribution of the CV of cell radii (CVr) using the Kolmogorov–Smirnov test gave a statistic D = 0.0846 and a *p*-value of 0.00247. For this data set size, the critical D value would be 0.090026 for an alpha value of 0.001 and 0.07525 for an alpha value of 0.01. Therefore, the distribution of CVr differed between mutant and WT, but to a lesser degree than the clear differences seen between angles of division planes. Overall, mutant cell populations had slightly fewer cells with low CVr (between 0.18 and 0.25) and slightly greater number of cells possessed a larger CVr over 0.3, indicating some decrease in cell sphericity in the mutant.

The distribution of cell volumes also appeared similar between WT and mutant cell populations (Figure 3.16). However, the mutant RZ possessed a slightly higher proportion of smaller cell volumes (400-600 µm^3), around 24% of mutant cells vs 19.5% of WT. Whilst the WT RZ possessed a higher proportion of cells with volume 600-1100 µm^3, the mutant RZ had slightly higher proportion of cells 1100-2000 µm^3. The Kolmogorov–Smirnov test gave D=0.0831, *p*=0.0031 meaning again that distributions could be considered different with an alpha value of 0.01 but not 0.001.

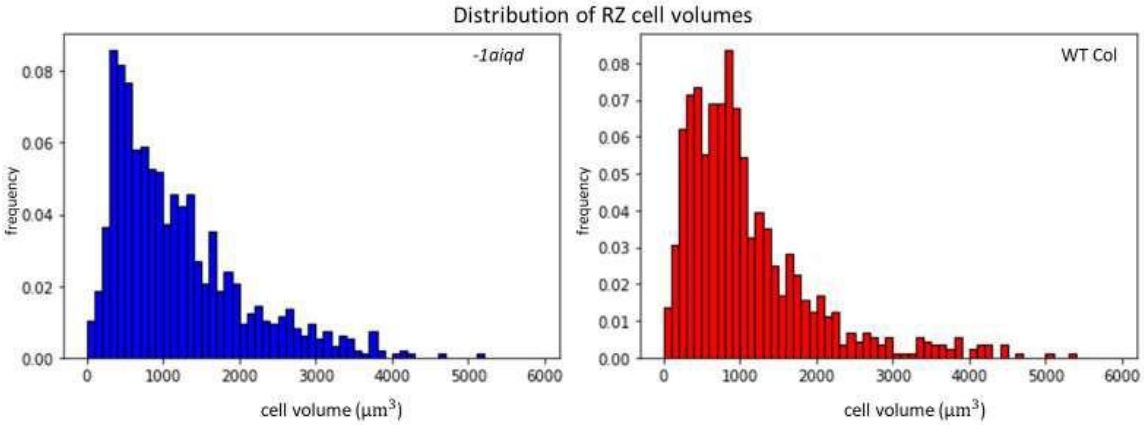

Figure 3. 18: Distribution of cell volumes in the RZ of the 1aiqd mutant and WT varied only slightly. Figure displays frequency distribution of cell volumes of RZ cells segmented in WT (RHS) and mutant (LHS) samples across a range of detected values. The analysis ran on 887 cells in WT RZ and 966 cells in mutant RZ taken from 4 WT and 4 mutant samples.

In summary, the distribution of both cell volumes and of the CVr showed minor differences between the RZ of the mutant and WT, in contrast with the much more obvious changes in the orientation of cell divisions. This suggests that changes in the orientation of cell division were not a consequence of gross changes in cell geometry. The changes in the orientation of cell divisions preceded any large changes in cell geometry or in cell size, indicating that the eventual impact on cell size in sections of more mature stems may be a knock-on effect of changes in cell proliferation in mutant, perhaps reflecting organ-wide control of its final size and shape.

3.2.7. Possible role of *IQD 1a* genes in regulating the duration of the proliferative phase of growth

As well as number of cells in any given region undergoing division and rate at which division cycle is completed, an important parameter in the control of organ growth is the duration of the phase during which cell proliferation contributes to growth. It could therefore be the case that loss of *IQD* function results in extending the proliferative phase occurring in stem growth, which would also result in the far greater cell population seen in mature stem sections of the *1aiqd* line.

Whilst the difference in cell numbers appeared more pronounced in mature tissues such as base of the stem *versus* close to the meristem, the measurements at different stages of development suggest that the effect on stem

diameter is similar between early stages (at the point where the first silique elongated) and late time points (at the base of the stem). The diameter of WT sections at the first elongated silique were 70% that of the *1aiqd* mutant, compared to 67% at the base. Furthermore, the measurements of internode elongation showed that the region of active growth (within 2 cm of the meristem, coincident with the proliferative region of the stem; Serrano-Mislata, A. et al., 2017) was the same in WT and the *1aiqd* mutant (Figure 3.10). Based on these results, I conclude that family 1a IQDs do not regulate stem growth by modulating the duration of the proliferative phase. Further thoughts about the mechanism involving IQD function and how it might restrict proliferation are explored in the subsequent chapters.

3.3 Discussion

The stem seems structurally simple being, in a simplified sense, an elongating cylinder. However, divergence in microfibril deposition from that predicted for a pressurised cylinder, and detected stress patterns that are yet to be explained experimentally or through modelling indicate a hidden complexity. The literature on stem growth in fact highlights how further work is required to explain plants' control mechanisms in shoot organ growth. The phenotype of aberrant growth driving increased stem radius following loss of 1a *IQD* function could be a useful system to gain understanding of the mechanism pushing the narrow cylindrical structure of the stem upwards during growth, whilst restricting outward expansion. A subset of the *IQD* family could be identified as new molecular components aiding restriction of organ growth, specifically impacting outward growth of organs rather than elongation growth.

The macroscopic characterisation presented in Chapter 2 clearly demonstrated thicker stems in the mutant line. Shorter plant height at stage where four siliques elongated potentially suggested that increased stem width was at a cost of stem elongation (Chapter 2, Figure 2.11), but investigation of stem elongation rates indicated increased radial growth at no loss to elongation growth (Figure 3.10). The increased diameter of the stem could be seen as analogous to increase in diameter of fruit organ growth in cucumber and melon accessions in which QTL analysis points to reduced expression level/ functionality of family 1a *IQD* genes (Jin, B. et al. 2017; Pan, Y. et al.2017). Similar changes with more spherical shapes were seen in rice grains of family 1c *iqd* mutant (Yang et al.,

2018), the seeds of the *1aiqd* line (Chapter 2), and in changes in leaf shape to be present in the subsequent Chapter 4. In the context of increases in whole organ width, the increase in stem diameter of *1aiqd* line can be used as a model to investigate effect of IQD protein level on planes of cell division orientation, known to impact final organ shape. From studies on IQD function in Cucurbitaceae fruit development, conclusions insinuated a change in the preference of plane of division.

Further analysis of the stem phenotype in this chapter and correlation with IQD expression implicated function early in organ growth. Therefore, the impact on division planes was investigated in the RZ using fixed PI-stained meristems. Identification of new cell walls showed that the ordered transverse division planes in WT were disrupted following loss of 1a IQD function. Whilst transverse divisions still occurred in the mutant, a high proportion appeared aberrant, dividing with high angles from the main axis of the stem. Overall, this would account for greater growth in diameter of mutant stems and demonstrate a function for IQD proteins in determining planes of cell division. However, no clear direction of radial planes of division occurred in central pith of the *1aiqd* line, as could be assumed from the fruit shape literature. It can be inferred from this research that more random division planes may also be occurring in other instances of changed organ shape associated with IQDs.

The huge increase in the number of pith cell files a few centimetres below the meristem in sections taken at the position of first silique elongation might be directly attributed to sustained defects in division plane orientation stemming from the RZ (or ovary in the context of fruit growth). Consistent stem elongation rates between *1aiqd* and WT lines implied that the rate of divisions that promote stem elongation is independent of IQD function, however, divisions that increased the number of cells radially were increased. Whilst small initial differences of populations of cells in radial plane may be observed in the RZ, persistence of aberrant divisions could lead to a large increase over the centimetres of proliferative region bellow the apex. Thus, the driving force for the stem growth phenotype in the *1aiqd* line could be an increase in the number of cell files along the radius of the stem, caused by an shift in the orientation of cell divisions. If the rate of transversal cell divisions remained the same, then the additional cell files would lead to an increase in the overall rate of cell proliferation, explaining the larger number of cells in the mutant stems, while the rate of stem elongation remained the same.

Alternatively, to explain such a vastly increased number of cells populating the pith, 1a IQDs might impact both planes of division and the frequency of divisions. Whilst completing the mitotic cell cycle and entering endoreduplication did not appear to be impacted by *IQD* expression, it still remains that proliferation rate is a key factor contributing to organ growth and could be implicated in the large size of *1aiqd* plants, with increased surface area of leaves, increased stem thickness and increased number of side branches and floral organs. Further investigation into whether IQD function may yet be involved in the rate of progression through the cell cycle is therefore of interest.

One means by which IQDs could increase the number of cells could be through the gene families' association with phytohormones such as GA and auxin, both linked to induction of cell proliferation as well as cell expansion (Braun, N. et al. 2008; Xu, Q et al. 2016). These links therefore could be a key avenue to investigate for enhanced growth phenotypes caused by increased cell divisions. In the future, once plant lines are established, imaging of a triple cell cycle reporter spanning G1,S and G2 (Desvoyes, B. and Gutierrez, C. 2020) in pith and other shoot regions such as leaves, with prominent growth phenotypes in loss of function mutant, could be carried out, looking for patterns suggesting differential behaviour in proliferation. Also, establishment of the CycB1;1:GUS reporter (Colón-Carmona A. et al. 1999**)** in the loss of function background could be used to study whether proliferation is impacted in various growth processes affected in the *1aiqd* line.

Specifically in relation to the confirmed function of 1a IQDs in the orientation of division planes, it remains to be investigated how IQDs particpate in this process. One theory of orientating division planes is that of favoured division along plane of smallest area. This is in-fitting with mainly transverse divisions in highly elongated WT central pith cells. Investigating geometry of pith cells in the mutant line through segmentation, where the preference for transverse planes of division appeared impaired, revealed however that cell geometry was largely unchanged between WT and mutant lines. A slight deviation in the distribution of sphericity or volumes between WT and mutant plants seemed unlikely to be the driving factor for such a clear change in division plane orientation. This raises the question as to whether other factors impacting planes of division, such as mechanical stress, for which strong role in direction of vertical stem growth is implicated in literature, are altered. As discussed, there is potential for increased proliferation in the pith zone as well as altered planes of division in the mutant line. This might alter stress

within the growing stem, as outer stem layers adjust to increased growth of the internal pith (Maeda, S. 2014). Therefore, change in stress patterns may result in differing division planes directed by microtubule orientation, cited in the literature as a way cells transduce stress patterns into the choice of division plane orientation (Landrein, B., Hamant, O. 2013). This hypothesis, however, would not easily explain the early changes in in division planes in the RZ, before noticeable changes in pith size were established.

Alternatively, IQDs could have a more direct effect on microtubule dynamics in the RZ. As highlighted in the introductory chapter, IQD proteins are MAPs with proposed functions in microtubule dynamics (Sugiyama, Y., et. al., 2017; Mitra,D. et al. 2019). Loss of MAP function could impact the selection of division planes due to changes in microtubule behaviour. Furthermore, auxin gradients may also have a role in microtubule array orientation and division plane orientation in growing stems yet to be annotated. This highlights multiple avenues of further investigation into IQD function and the means by which the proteins impact orientated divisions and restrict stem radial growth. Research presented in the subsequent chapters aimed to address these unknowns in hope to not only better understand IQD functions' impact not only on growth in the stem but also other shoot organs for which phenotypes were observed in the loss of function mutant.

In contrast to increased stem growth in loss of *IQD* function lines, stem elongation was severely impeded following induction of the subfamily 1a *IQD22*. The effects on the stem's cell layers highlighted, in contrast to loss of function lines, that cell diameter was markedly increased by 1a IQD gain of function. The hypothesis that 1a IQDs functioned in promoting entry into endoreduplication, which could explain cell size phenotypes, was discarded experimentally. The question remains of why loss of function resulted in small and uniformly sized pith cells, whilst gain of function increased the size of outer stem layer cells. As well as the pith cells, both epidermal and cortex cells were smaller in the *1aiqd* line, despite low or undetectable *IQD24* expression. The smaller cell size further amplified the increased level of proliferation required to generate concentric outer stem layers surrounding a much larger pith. Due to requirement for coordinated growth in outer and inner stem regions, change in growth of the inner layer may direct outer layer growth. Thus, reduced cell size in all stem cell layers might be an indirect response to aberrant organ growth. Detection of the expanding pith could result in downregulation of cell expansion machinery, particularly activated during

endoreduplication. This would account for endoreduplication still occurring without eliciting changes in cell size associated with the process in mutant lines.

Cellular changes associated with overall organ growth are often attributed by a phenomenon named compensation, where changes in proliferation are balanced by cell expansion to maintain overall organ size and shape. This idea is supported by cell enlargement in mutant backgrounds where proliferation is reduced (Ferjani, A. et al. 2013; Tsukaya H. 2002; Fujikura U, et al. 2020). This would be consistent with loss of stem elongation in the ectopic *IQD22* line being caused by severe reduction in cell division and subsequently feeding into enhanced expansion in an attempt to restore organ growth. It must be noted however, that changes in cell size in the gain of function line could instead be linked to altered microtubule behaviour, as is cited in the literature for other Arabidopsis lines with ectopic *IQD* expression, which showed defects in cell size and shape (Burstenbinder, K. et al. 2017). Restricted cell expansion in the loss of function line may be through a mechanical feedback mechanism following increasing tension stress exerted on the epidermis.

Other phenotypes not to be ignored in the loss of function line were the increased number of vasculature bundles, matching the larger stem circumference, extra rosette leaves and more numerous side branches (Chapter 2). These phenotypes might be interconnected. The literature highlights how primary vascular pattern and phyllotaxis are highly coordinated, with vascular sympodia corresponding to phyllotactic parastichies in rosette leaves, side branches and floral pattern in the inflorescence. It is presumed that through expression of *ATHB8*, a known procambium marker, the vasculature pattern reflects the pattern of organ initiation, with high expression at the sites of established primordia (Kang, J. Dendler, N. et. al. 2003). Establishment of both organ initiation sites and vascular differentiation are linked to auxin transport and establishment of auxin maxima (Fàbregas, N. et. al. 2015). Although auxin distribution may be accountable for differential organ initiation and vascular bundles in *1aiqd* line, it may not necessarily be via changes in auxin transport. The *1aiqd* mutant has a larger stem radius, and the number of maxima produced by auxin transport is greatly affected by the initial shape/size of tissues. However, due to auxins' link to vasculature differentiation and organ patterning, paired with phenotypes occurring in the *1aiqd* mutant, auxin gradients themselves may be affected in the mutant, even if this could be an indirect downstream response to changes in growth patterns.

Concluding, high levels of *IQD* expression early in stem growth appear to restrict outward stem growth through minimizing divisions in planes divergent from directed transverse orientation in the central pith zone. Loss of IQD function appears to have no impact on proportion of cells dividing along the longitudinal axis of the stem, important for elongation stem growth, however it increased divisions in planes contributing to radial expansion. The change in division plane orientation early in central RZ cells was not paired with obvious changes in cell geometry implicating that IQDs do not affect the choice of cell division by changingcell shape. Considering the literature on both stem growth and division plane orientation, altered responses to tissue stress patterns involving microtubule orientation could be accountable. This directed further work aiming to better understand the cellular function of IQDs, including links to microtubule arrays. Increased proliferation rates contributing to the stem growth phenotype in the *1aiqd* line could also reflect functional interplay with phytohormones. Altered auxin patterns which could account for further phenotypes in the *1aiqd* line are investigated in the following chapter.

Chapter 4 Control of leaf shape and margin complexity by family 1a IQDs

4.1 Introduction

The focus of the preceding chapter, stem development, remains one of the least studied aspects of plant growth, which introduces limitations when interpreting observed cellular defects and thinking about the cellular functions of IQDs. In this chapter, I focused on the growth changes in leaves caused by loss of subfamily 1a IQD function, with a particular focus on leaf serrations, which have been intensively studied and offered additional opportunities to connect IQD function to well-characterised processes in plant organ growth, especially auxin transport and responses. Characterisation of cellular and molecular elements contributing to leaf growth phenotypes in the *1aiqd* line could further the understanding of what underlies growth changes in the stem as well as other phenotypic variations from WT plants, such as organ initiation and patterning, for which auxin transport and gradients are also well characterised.

The leaf has a highly adapted shape, which is in part driven by light capture. Therefore, in most plant species leaves develop as a flat structure with expansive surface area. Leaf structures vary in complexity across plant species, with Arabidopsis possessing simple leaves with serrated margins at the leaf base. Leaf edges can vary from serrated such as in Arabidopsis to smooth or lobed. Leaves classified as compound, such as in tomato, generate leaflets with full separation from the mainleaf body.

As well as light capture multiple factors drive diversity in leaf shape including external environmental conditions. Leaf structure can sensitise immobile plants to changeable environmental factors such as temperature, water availability and consumption by insect pests (Nicotra, A. B. et al. 2011). Other than flat shape,leaf adaptations for light capture include evolving tropism to position leaves towards light, with leaf angle and positioning moderated daily with changing sun position, a mechanism attributed to polar auxin transport by PIN3 (Ding, Z. et al. 2011). Establishment of phyllotactic patterns, for example the fibonacci spiral patterns of Arabidopsis rosettes, is thought to aid optimal exposure of leaves to light (Strauss, S. et al. 2020), exemplifying how the adaptation of leaves to capture light energy has been a great driving factor in the evolution of plants.

Research has studied factors important for growth of flat leaves, an attribute adapted by many plant species, including Arabidopsis. Leaves are initiated as rod-like primordia, far from the eventual shape of the mature organ. Establishment of dorso-ventral polarity leads to the differentiation of upper (adaxial), and lower (abaxial) leaf surfaces and has been purposed as a mechanism for formation of a flat structure, as well as the establishment of tissue types required for efficient photosynthesis. To this end, the adaxial layer contains closely packed cells with high levels of chloroplasts for light capture, while the adaxial layer consists of more loosely spaced cells for gas exchange of photosynthetic input and byproducts.

Specific gene expression patterns early in leaf primordia have been shown to define adaxial and abaxial identity. Gene classes with a strong contribution to leaf surface identity include class III HOMEODOMAIN LEUCINE ZIPPER (HD-ZIP) transcription factors and class II HD-ZIP proteins in complex with ASYMMETRIC LEAVES (AS)1/AS2, expressed in cell types that form the upper adaxial leaf surface. In cell types forming the lower abaxial layer, expression of the GARP (Golden2, ARR-B and Psr1) family transcription factors, KANADI 1-4 (KAN1-4) and auxin response factors ARF2, ARF3 and ARF4 are key. Many genetic factors are polarised before primordium outgrowth, emphasising the importance of organisation in the vegetative meristem, both for patterning of organ initiation and polarity of growth in leaves.

Auxin gradients are also imposed in establishment of polarity in leaf growth. A mechanism of transport appears to drain auxin in the adaxial region to reinforce leaf polarity, with ARFs also positioned in the abaxial leaf layer, implicating auxin function in abaxial determination. High proliferation at the leaf margins is paired with increased auxin biosynthesis, again highlighting the importance of auxin gradients in leaf growth.

Interactions between the adaxial/abaxial domains during growth result in generation of a third middle domain important for leaf lamina growth. Modelling studies and experimental manipulations of the pectin methyl-esterification status further showed that partitioning of the leaf primordium into a middle domain with low cell wall elasticity, surrounded by two domains with a higher elasticity is sufficient for asymmetric growth of the primordium and lamina initiation (Maugarny-Calès, A. and Patrick Laufs**,** P. 2018).

Research into biomechanical signals and plant growth have advanced, with recent literature linking biomechanics to establishment of the flat leaf structure through microtubule orientation. Whilst microtubule organisation along external

surfaces of the leaf epidermis did not appear to reflect stress patterns in the tissue, those along walls in the adaxial-abaxial direction in inner leaf tissue appeared more highly organised, and this matched the direction of greatest stress. Modelling further highlighted how anisotropic wall tension, as directed by microtubule orientation, would help maintain, and amplify further, growth patterns established by adaxial-abaxial polarity, driving generation of a flat structure. Reasons for failure to organise CMTs at the leaf surface according to predicted stress were proposed to be either the increased thickness and potentially stiffness of the cell wall in the outer epidermis, thus responding to stress differently, or that models cannot yet correctly predict stress felt in this cell layer, demonstrating there is still much to understand in the field of biomechanics and tissue growth (Zhao, F. et al. 2020).

Genetic factors have also been identified in the control of leaf margin complexity, as well as a very strong link to auxin distribution by PIN1. One of the best studied examples of feedback between auxin transport and gradients with other factors that control shoot organ growth is that of leaf serration initiation. In this process, the transcription factor CUP-SHAPED COTYLEDON (CUC) 2 interacts synergistically with PIN1 in generating auxin gradients that position serration outgrowths; accordingly, *cuc2* and *pin1* mutants present a totally smooth leaf edge (Nikovics, K. et al. 2006). CUC2 is expressed in the leaf margin and is required for PIN1 expression in specific foci where serrations are initiated. Auxin maxima produced by PIN1 activity in turn negatively regulate CUC2 by increasing miR164, which degrades CUC2. As auxin increases at serration initiation foci, increasing cell division and outgrowth, CUC2 levels decrease, reducing PIN1 recruitment. This negative feedback limits size of serrations formed. This is affirmed by the increase of CUC2 levels through use of auxin transport mutants, excluding the essential *PIN1*, which have lowered miR164 levels and result in increased outgrowth of serrations (Bilsborough, G. D. et al. 2011).

Processes implemented in primary leaf serrations and processes required for compound leaf formation are reported to have largely overlapping gene regulatory networks. *CLASS I KNOTTED1-LIKE HOMEOBOX* (*KNOX*) genes, which are normally expressed in the shoot meristem and inhibited during development of simple leaves, are re-activated during compound leaf formation in the majority of species that evolved more complex leaf structures (Bharathan et al. 2002). Repression of genes such as *SHOOT MERISTEMLESS* (*STM*) and *BREVIPEDICELLUS* (*BP*) or equivalent, has been shown to extend the

developmental period of indeterminate growth, generating the more complex compound leaf shapes. Mutants in the aptly named *SAWTOOTH1* and *2* (*SAW1-2*), regulatory genes of the KNOX1 family, also have increased serration phenotypes. Mutation in the *SAW1-2* tomato ortholog *BIPINNATE* (*BIP*) increases leaf complexity, highlighting similarity in genetic regulation. In some legume species, a separately evolved mechanism reliant on *LEAFY* (*LFY*) / *UNIFOLIATA* (*UNI*) gene facilitates compound leaf growth, with this being the primary divergence from conserved gene regulatory networks (Nicotra, A. B. et al. 2011; Townsley, B. and Sinha, A. 2012).

As previously introduced, Arabidopsis possesses primary leaves with serrated leaf margins, with serrations concentrated on the margin region close to the base of the leaf. Various alterations could occur in the accepted model involving CUC2 and auxin gradients for restriction of the sites where serrations are initiated. One such is that the leaf margin develops a reduced response to maxima of auxin concentration over time, with this affecting the leaf tip first. Another is for the leaf margin to lose the ability to generate auxin peaks over time. Alternatively, the mechanism generating maxima and the ability to initiate serrations is not impacted, however the shift in relative growth rate along the proximal/distal axis over time accounts for the restriction of serrations to the base of the leaf, where proliferation continues for longest (Kasprzewska, A. et al. 2015).

A further adaptation integrating leaf function with plant growth is the vascular system, primarily for distribution of sugars produced in photosynthesis to shoot and root organs for cell metabolism and growth. Vascular pattern formation is reported as a self-organizing process, in which auxin plays a central role. Diffusion of auxin maxima in the tip of early leaves, paired with PIN1 function, is reported to induce MP expression in a broad region in the leaf mid zone. PIN1 transport in this broader area of MP expression is proposed to concentrate auxin in a narrower cell file, through a feedback loop that involves upregulation of PIN proteins by auxin and PIN-mediated auxin transport towards neighbouring cells of highest auxin content (Jonsson, H. et al. 2006). Subsequently, high enough auxin concentrations are reached for activation of genes involved in vascular vein differentiation, such as *ATHB-8*. Inhibition of polar auxin transport or induction of incorrectly high auxin concentrations shortens the distance between leaf primordia initiation sites and between lateral veins along the mid vein, supporting the idea that both processes employ similar mechanisms, involving epidermal convergence points of PIN1 and auxin maxima. However, multiple mutants impairing auxin

transport have only slightly disrupted vasculature patterning, resulting in some concluding that whilst auxin remains a primary player in patterning, divergent mechanisms have evolved with partially redundant functions (Biedroń, M. and Banasiak, A. 2018).

4.1.1 Aims of this Chapter

As has already been presented in Chapter 2, rosettes of *1aiqd* mutant plants appeared fuller than those of WT, with a greater number of leaves initiating over a longer growth period. This chapter will zoom in on changes in individual leaves between the *1aiqd* mutant and the WT. The results presented include differences in leaf shape and area between WT and mutant plants, which combined with a flatter leaf surface, give a fuller appearance to the *1aiqd* rosettes.

The increased width of leaves in the mutant, like the stem diameter increase, strengthened the link between 1a IQD function and restriction of growth parallel to the main axis of growth. The generation of flatter-laying leaves in the mutant potentially placed 1a IQDs in the process of blade outgrowth, as explored in the discussion.

The initial characterisation of changes in leaf shape also highlighted prominent differences in leaf serration number and outgrowth, together with a broadening of the upper leaf blade in the *1aiqd* line. The main focus of experimentation sought to uncover the cellular and molecular processes underlying the distinctive differences in number and final area of serrations along the leaf perimeter in the *1aiqd* line. This phenotype strongly implicated 1a *IQD* genes as regulators of leaf complexity and directed investigation of interplay between auxin maxima and IQDs and vice versa.

4.2 Results

4.2.1 Leaf Shape Analysis

Figure 4. 1: Comparison of rosette growth in short day conditions highlighted more pronounced leaf margin serrations in the *1aiqd* line, also visible after growth in constant light. A,B show *1aiqd* sextuple mutant plants grown under short day (SD) at 20ºC or under constant light (CL) at 16ºC, respectively. C and D represent WT Col-0 controls grown in same conditions.

A consistent growth phenotype was present in rosettes of sextuple mutant plants *versus* WT Col-0 plants grown at sixteen degrees in constant light (CL). Leaves of the mutant appeared wider and more spread out with less curling (Figure 4.1B). They were also more numerous, allowing the rosette to appear fuller (Chapter 2, Figure 2.18). When grown under short day (SD) conditions, another striking difference between mutant and WT leaves stood out, with more pronounced serrations spanning a greater proportion of the mutant leaves' perimeter (Figure 4.1A). Inspection of individual leaves from four-week-old mature rosettes grown under both growth conditions confirmed the differences in serration formation and outgrowth (Figure 4.2).

Figure 4. 2: abaxial view of mature CL and SD-grown leaves highlighted the flatter shape of the leaf and increased frequency and depth of serrations in the *1aiqd* line. A: abaxial view of four-week-old rosette leaves, three rosette leaf number 6-7 and three of number 11-12, grown at 20°C under SD. WT (top) and sextuple mutant (bottom). B: leaves of same number from mature rosettes grown at 16°C under CL. Again WT leaves are displayed at the top and sextuple mutant at the bottom.

To quantify the differences between leaves of mutant and WT lines, *morpholeaf* software was used (Biot, E. et al. 2016; Andrey, P. & Maurin, Y. 2005). This software outlines individual leaves and marks the sinuses and peaks of each serration, as well as measuring leaf parameters such as height, width and area. Manual corrections were required for the deep sinuses of the more pronounced mutant serrations and to factor in serrations that curl into the abaxial side of WT leaves, preventing automatic detection by the software (Figure 4.3).

Figure 4.2B depicts leaves of mature rosettes grown in CL conditions under which the mutant leaves, whilst remaining narrow at the base, developed wider than WT leaves towards the distal end. As with increased radial growth in the stem, the change in leaf shape is reminiscent of IQD's role in restricting the radial growth of fleshy fruits. While height of both leaf number 6-7 and 11-12 in the *1aiqd* line was not significantly different to WT leaves, width of leaf 6-7 was 2.61mm greater than WT and 4.82mm wider in leaf 11-12 of the mutant line (Figure 4.5). Larger sample sizes and lower variability of width in WT samples in leaves 11-12 gave strong significance for increased width of mutant leaves, but width was also consistently wider for leaves 6-7. With similar average length leaf blade but greater width, the area of leaves, particularly number 11-12, would be

predicted to be larger in the *1aiqd* line. This metric was also captured through morpholeaf software and presented in Figure 4.6.

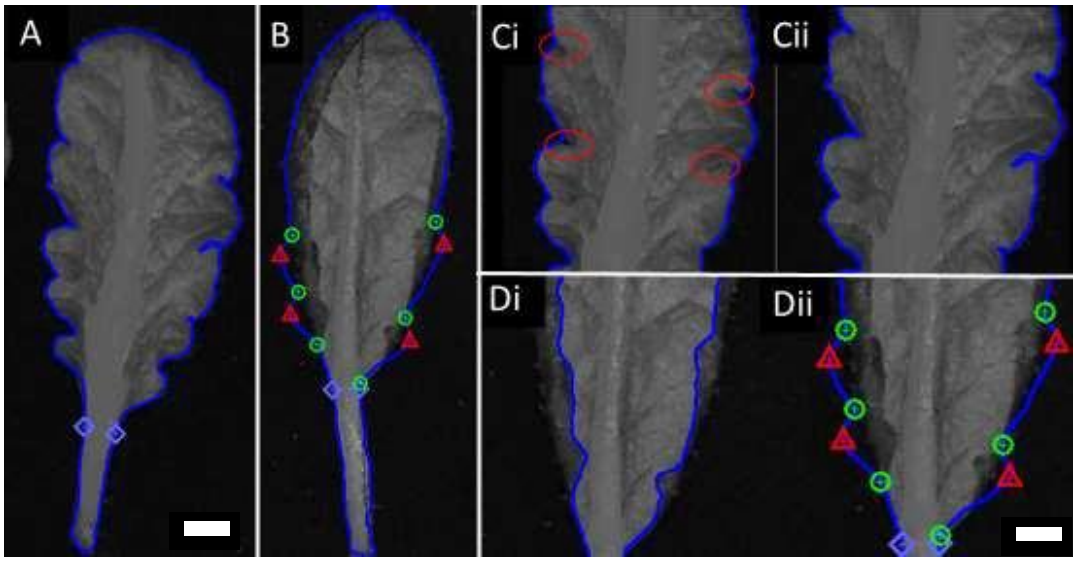

Figure 4. 3: outline of leaves with markings for shape quantification using *morpholeaf*, detailing manual corrections made. A: example of a finished leaf outline; B: addition of sinus points as green circles and peaks as red triangles. Ci: deep sinuses of SD mutant leaves were not correctly traced automatically (circled in red) and had to be corrected, Cii. Di highlights the issues of WT leaves curling inwards towards the abaxial side, preventing the detection of serrations, which were manually added (Dii). Scale bars 0.25cm.

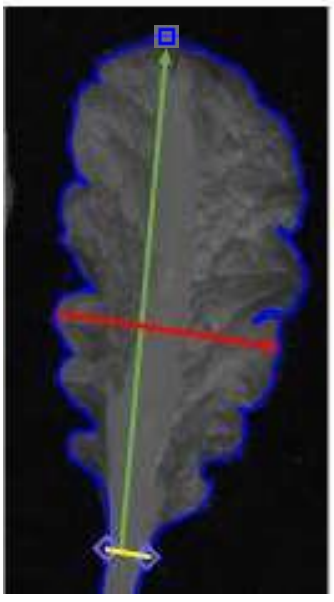

Figure 4. 4: Markings represent leaf measurements taken by *morpholeaf*. The red arrow represents the width of leaf (BB) measurement between serration peaks. Green arrow represents length measurement from upper petiole (blue diamond markers) to blade apex (blue square) and the leaf area of leaf was defined by the outline above the yellow line marking the top of the petiole (Biot et al., Practical Guide for MorphoLeaf).

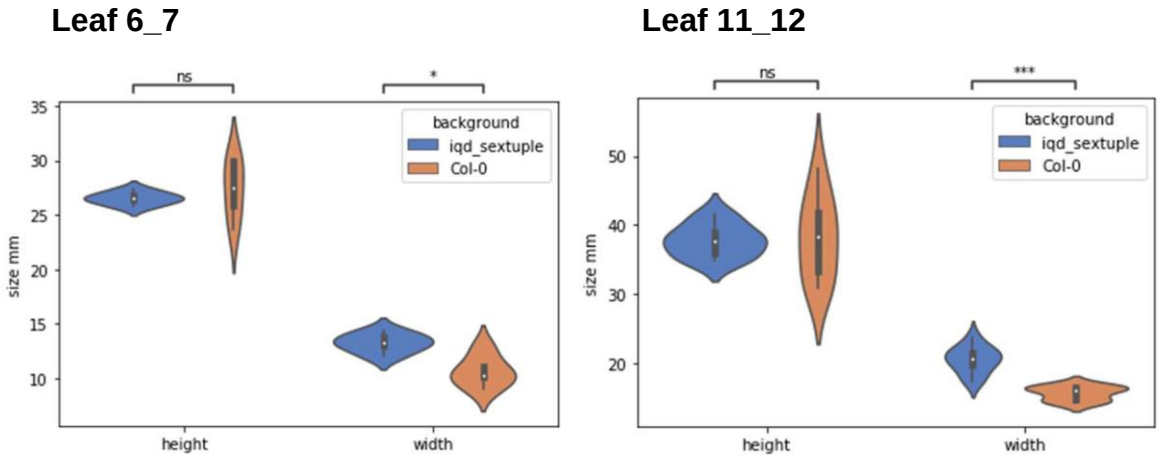

Figure 4. 5: Whilst having similar length, rosette leaves in the *1aiqd* line were broader than WT Col-0, particularly older leaves. Height was similar in mutant and WT leaves 6-7 and 11-12 (6-7 mutant: 26.565 mm, wt: 27.408 mm. 11-12 mutant: 37.8mm, WT: 38.17 mm). A slightly significant 2.61 mm difference in width of leaves was seen in leaf number 6-7 (WT: 10.866 mm, mutant: 13.276 mm, *p*=4.314e-02) and in leaf 11-12, with higher replicates, a highly significant 4.82mm difference in width was present (WT: 15.946 mm, mutant: 20.037 mm, *p*=8.973e-04). *p*-values from two sided Mann-Whitney test with Bonferroni correction; * *p*<0.05 , ***p*<0.01, ****p*<0.001; n=5 for 6-7 leaf number and n=9 for 11-12 leaf number.

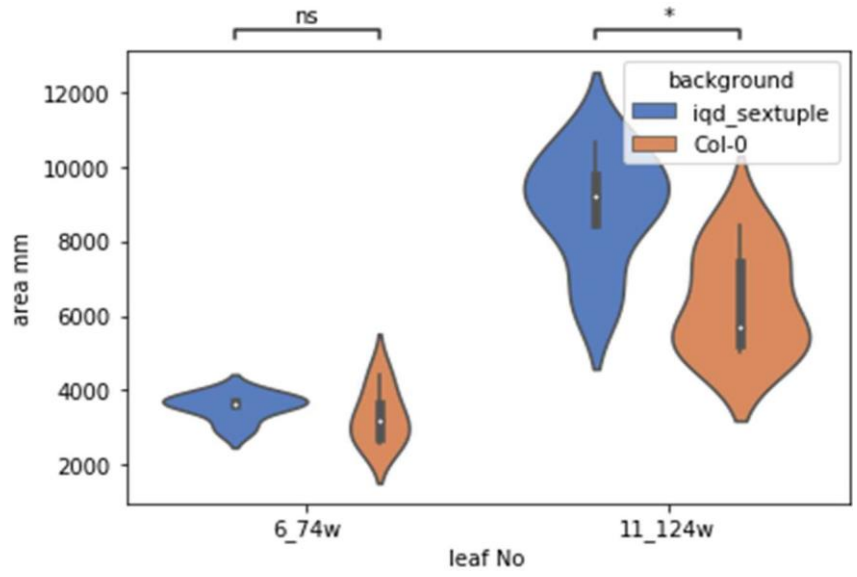

Figure 4. 6: Both rosette leaf number 6-7 and 11-12 of mutant leaves had on average greater surface area than those in WT rosettes, with a most pronounced difference in older leaves. There was only a small difference in the area of leaves 6-7 (mutant: 3576.36 mm^2, WT: 3313.7 mm^2, d 262.66 mm^2), but in leaf 11-12 mutant leaf area was on average 2537.57 mm^2 larger (mutant: 8915.93 mm^2, WT: 6378.36 mm^2, *p* = 1.456e-02). *p*-values from two-sided Mann-Whitney test with Bonferroni correction. * *p*<0.05; n=5 for 6-7 leaf number and n=9 for 11-12 leaf number.

Overall, changes in leaf shape conferred a modest increase in area in the *1aiqd* line, which was most pronounced in older leaves. Combined with the greater number of leaves following changes in vegetative growth period presented in Chapter 2 (Figure 2.11), altered leaf shape and propensity to lay flatter might enhance light capture in the *1aiqd* rosette compared to WT Col-0.

The increase in both number (Figure 4.7) and size (Figure 4.11) of margin serrations in the loss of function mutant was also quantified. Highly significant increases in the number of serrations were seen in both younger and older rosette leaves grown at SD and CL conditions. The serrations did not just appear more numerous in mutant plant leaves, but also much more pronounced. A more detailed analysis of serration width, height and area was performed to show how loss of 1a IQD function affected serration outgrowth (Figure 4. 7). The distance between sinuses, reported as width, did not diverge significantly between WT and mutant lines (Figure 4.9), whereas serration height was clearly different (Figure 4.10); both combined resulted in larger serration areas in the mutant (Figure 4.11).

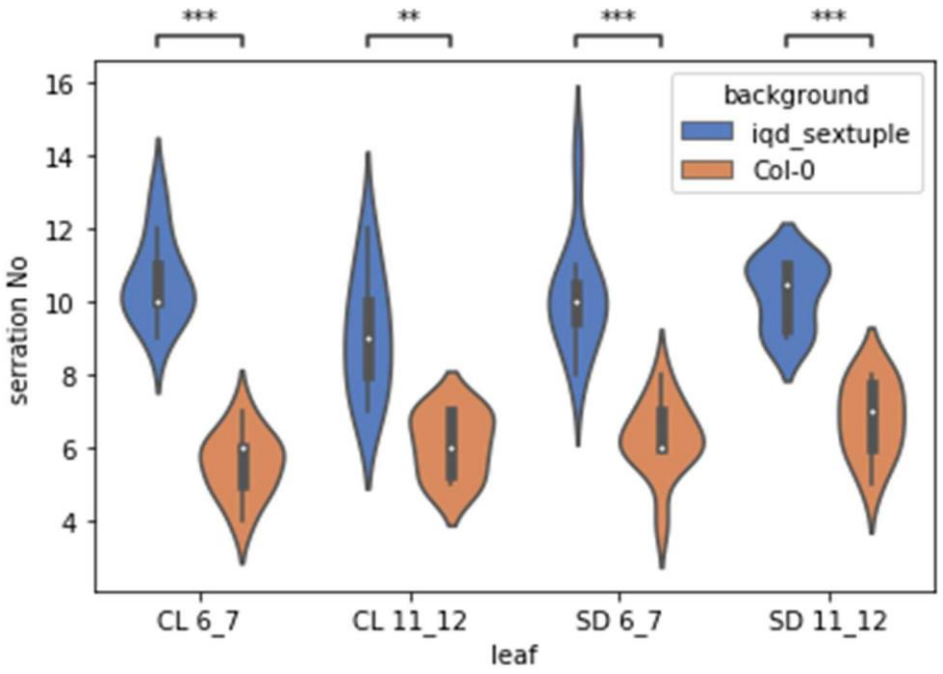

Figure 4. 8: In all leaf conditions significantly more serrations were initiated in the *1aiqd* line. The average number of serration in WT and *1aiqd*, the difference and significance under both growth conditions were:

CL 6-7: Col-0 5.56, mutant 10.6, difference = 5.04, *p* = 1.343e-03;
SD 6-7: Col-0 6.17, mutant 10.18, difference = 4.01, *p* = 4.182e-04;
CL 11-12: Col-0 6.1, mutant 9.1, difference = 3, *p* = 2.786e-03;
SD 11-12: Col-0 6.8, mutant 10.2, difference = 3.4, *p* = 8.858e-04.
p-values were from two sided Mann-Whitney tests with Bonferroni correction; * p < 0.05 , ** p < 0.01, *** p < 0.001; n=10.

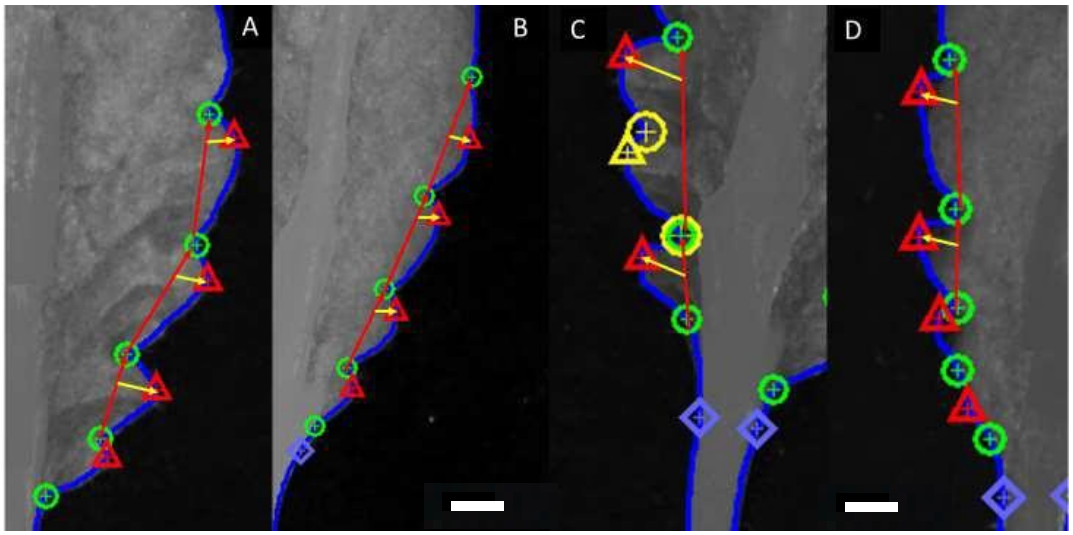

Figure 4.8: Measurement of leaf serrations using *morpholeaf*. From left to right: A, B: mutant (A) and WT (B) leaf 11-12 grown in SD conditions; C, D: mutant (C) and WT (D) leaf 6-7 grown in SD conditions. Serration width was the distance between two consecutive sinuses (green circles) and the height (yellow arrows) measured from the highest point of the serration (red triangles), to the line between sinuses. The area of a serration was defined as the number of pixels contained within the line joining primary sinuses and the blue outline of the leaf. 0.25cm scale.

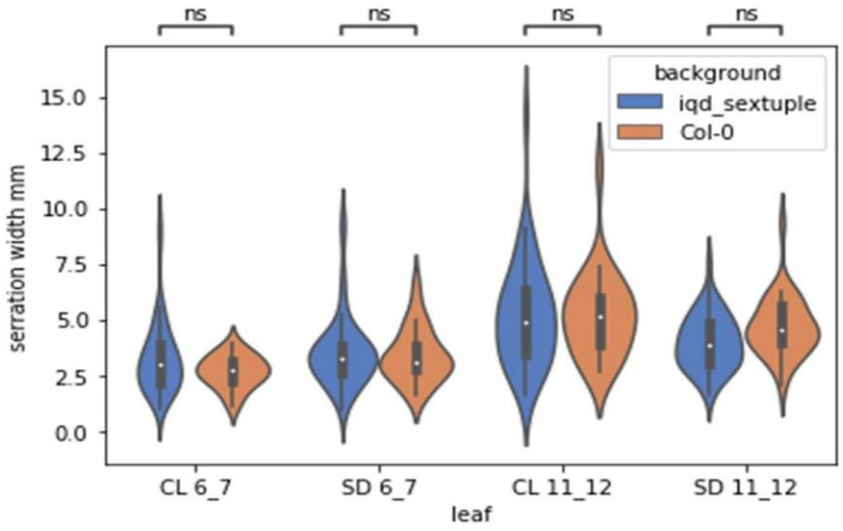

Figure 4. 9: No significant difference in serration width in any leaf number or growth condition. Average serration width is reported in young and old leaves of WT and mutant line rosettes grown under both SD and CL conditions, with difference:
CL 6-7 2.689 mm in WT (n=17) and 3.241 mm in mutant (n=56), d 0.552 mm;
SD 6_7 3.414 mm in WT (n=30) and 3.54 mm in mutant (n=52), d 0.126 mm;
CL 11-12 5.39 mm in WT(n=28) and 5.09 mm in mutant (n=44), d 0.3 mm;
SD 11-12 4.723 mm in WT (n=34) and 3.999 mm in mutant (n=50), d 0.724 mm.
For all differences, *p* values were larger than 0.05 (two sided Mann-Whitney test with Bonferroni correction).

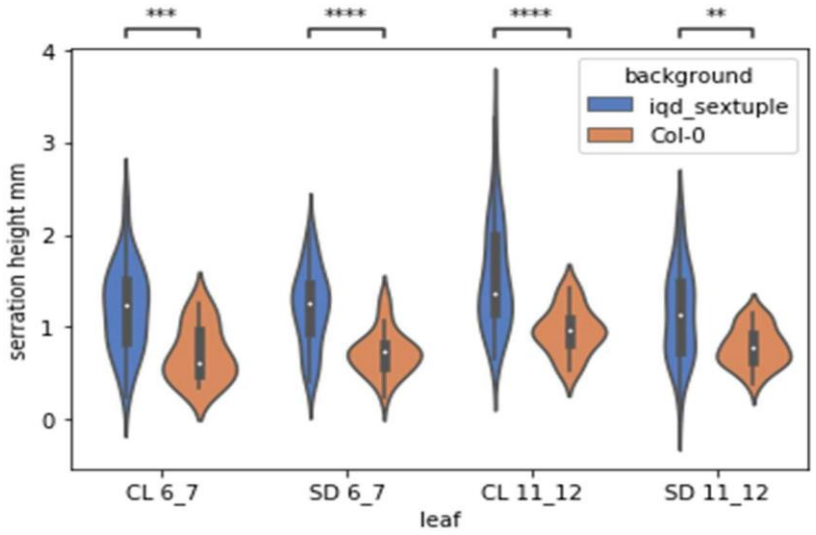

Figure 4. 10: **Mutant serration height was greater, with strong significance in all leaf number and growth conditions.** Average serration height is reported in young and old leaves of WT and mutant rosettes grown under both SD and CL conditions, with difference and *p*-values (two sided Mann-Whitney test with Bonferroni correction):

CL 6-7: 0.711 mm in WT (n=17) and 1.203 mm in mutant (n=56), d 0.492 mm, *p*=4.356e-04;
SD 6-7: 0.724 mm in WT (n=30) and 1.214 mm in mutant (n=52), d 0.49 mm, *p*=4.327e-06;
CL 11-12: 0.963 mm in WT (n=28) and 1.544 mm in mutant (n=44), d 0.581 mm, *p*=2.445e-05;
SD 11-12: 0.783 mm in WT (n=34) and 1.158 mm in mutant (n=50), d 0.375 mm, *p*=1.168e-03.
(* *p*<0.05 , ***p*<0.01, ****p*<0.001)

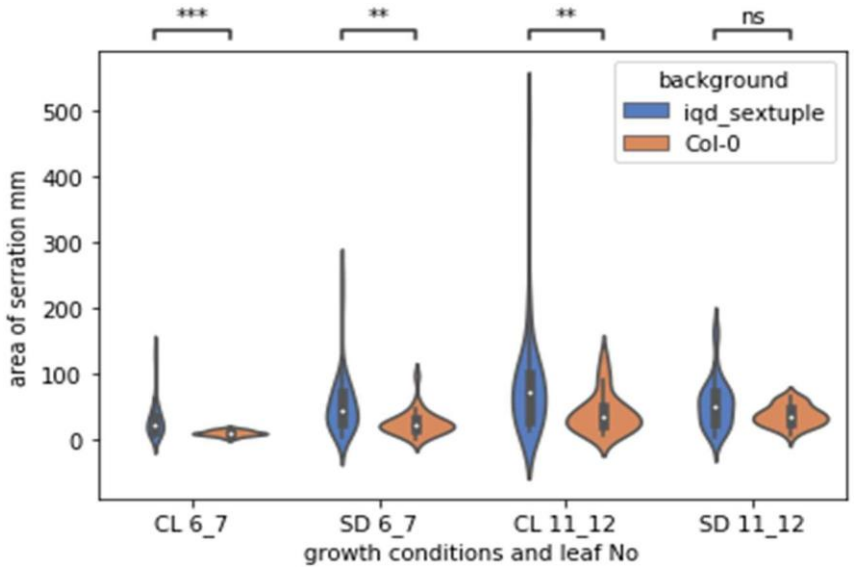

Figure 4. 11: Serrations in mutant plants were larger. Average serration area is reported in young and old leaves of WT and mutant line rosettes grown under both SD and CL conditions with difference and *p*-values (two sided Mann-Whitney test with Bonferroni correction):

CL 6-7 20.756 mm in WT and 29.63 mm in mutant, d= 8.874 mm, *p*=4.979e-04;
SD 6-7 26.267 mm in WT and 53.999 mm in mutant, d= 27.732 mm, *p*=1.499e-03;
CL 11-12 41.706 mm in WT and 81.883 mm in mutant, d= 40.177 mm, *p*=9.165e-03;
SD 11-12 37.784 mm in WT and 56.235 mm in mutant, d= 18.451 mm, *p*=8.352e-02.
The sample sizes (n) were the same as for height and width in Figures 4.10 and 4.11. Percentage area increases in *1aiqd* were: CL 6-7 30% increase, SD 6-7 51.4% increase, CL 11-12 49.1% increase, SD 11-12 32.8% increase.

The increase in serration length in the *1aiqd* mutant would be expected to contribute to at least part of the increase in leaf area shown in Figure 4.6. Combined with the increase in number of serrations distributed along the perimeter of the leaf edge, the total proportion of the leaf that is serration would therefore be larger in the mutant lines as confirmed in Figure 4.12. The proportion of leaf found in serrations was higher in leaf number 6-7 than that of older leaves 11-12 in both growth conditions, whereas the overall increase in leaf area was more pronounced in the older leaves (Figure 4.6) supporting 1a IQDs restriction of growth both at serrations and in lateral growth of the whole the leaf blade. Indeed, excluding larger serration area in leaf 11-12 the area of leaf blade in *1aiqd* plants was still larger as reported in Figure 4.6 (Figure 4.13).

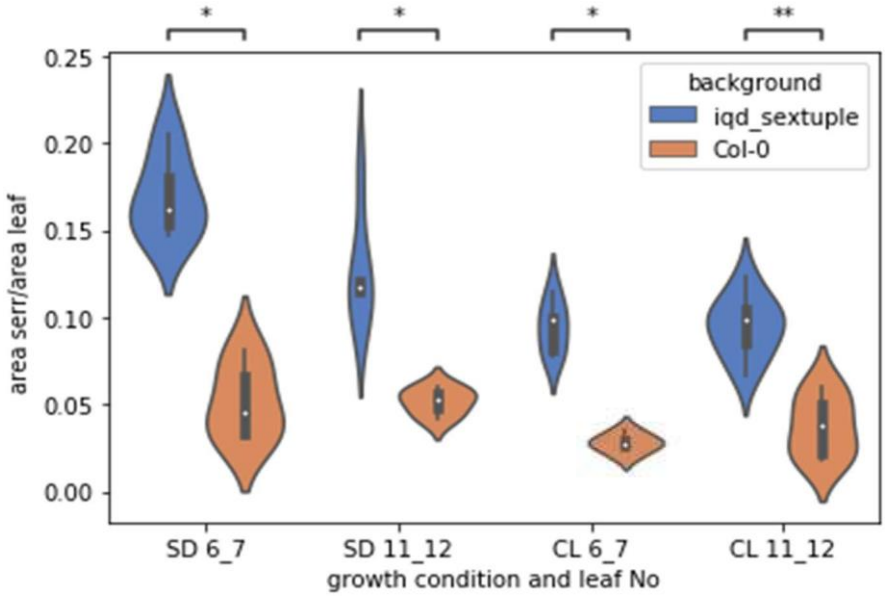

Figure 4. 12 proportion of total leaf area composed by serrations was greater in *1aiqd* leaves. The average value of combined serration area relative to the total leaf area, the difference between mutant and WT, sample sizes and *p*-values (two sided Mann-Whitney test with Bonferroni correction. * $p<0.05$, ** $p<0.01$) were:

SD 6-7: WT 0.052, mutant: 0.17, difference = 0.118, n = 5, p = 2.437e-02;
SD 11-12: WT 0.052, mutant 0.128, difference = 0.076, n = 5, p =2.437e-02;
CL 6-7: WT 0.033, mutant 0.0947, difference = 0.0617, n = 5, p = 2.437e-02;
CL 11-12 WT 0.041, n = 7, mutant 0.0865, n = 9, difference = 0.0455, p=2.066e-03.
The percentage increase in the mutant compared to WT was: SD 6-7 69.4%, SD 11-12 59.4%, CL 6-7 65.2%, CL 11-12 61.9%.

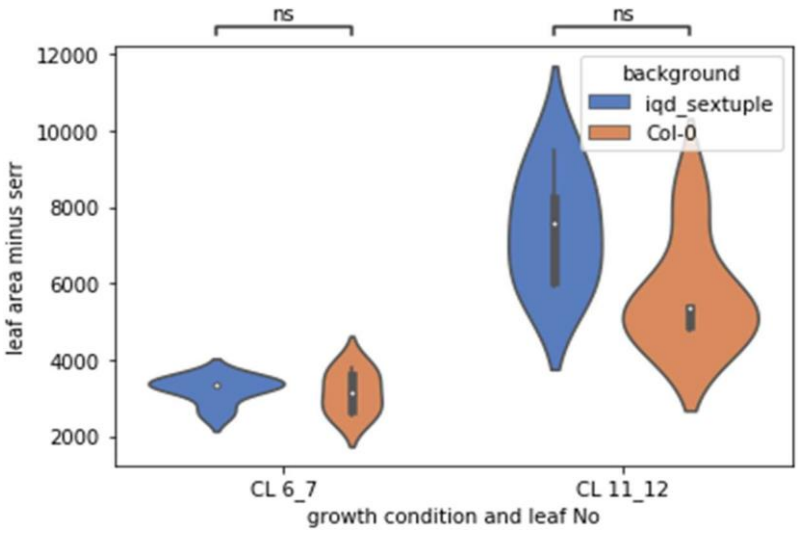

Figure 4. 13 Area of rosette leaf 11-12 is larger in the mutant with serration area subtracted. There was only a small difference in the area of leaves 6-7 (mutant: 3240 mm^2, WT: 3158.37 mm^2, d 81.7 mm^2), but in leaf 11-12 mutant leaf blade area was on average 1738.62 mm larger, a 23.3% increase, despite removal of larger serrations (mutant: 7457.80 mm^2, WT: 5719.16 mm^2). NS in sample size n=5

A defining feature of serrations in Arabidopsis is restriction of their initiation to the base of the leaf perimeter. The increase in the number of serrations, together with the fact that serration width and leaf length were similar in the *1aiqd* mutant and WT plants, would imply that loss of *1a IQD* function extends the ability of initiating serrations towards the upper region of the leaf. This was confirmed as presented in Figure 4.14. In WT Col-0, the height at which serrations reach along the leaf was very similar between leaf number 6-7 and 11-12 in any given condition however, as was already visible in Figure 4.2, the serrations reached further up the leaf when grown in SD conditions compared to CL. This indicated a relatively fixed position under which serrations can form from the leaf base, which is extended in slower growth conditions.

The increased proportion of the leaf margin showing serrations in the mutant was consistent in different growth conditions. The apparent exception was rosette leaves 11-12 grown in CL conditions. However, this could be accounted for the fact that the highest serrations in the *1aiqd* leaves had low curvature and only slightly indented sinuses, and consequently they were not detected by morpholeaf as primary teeth (Figure 4.15D). Manual inspection confirmed that leaves 11-12 grown in CL also had serrations higher up from the base of the leaf in the *1aiqd* line (Figure 4.15).

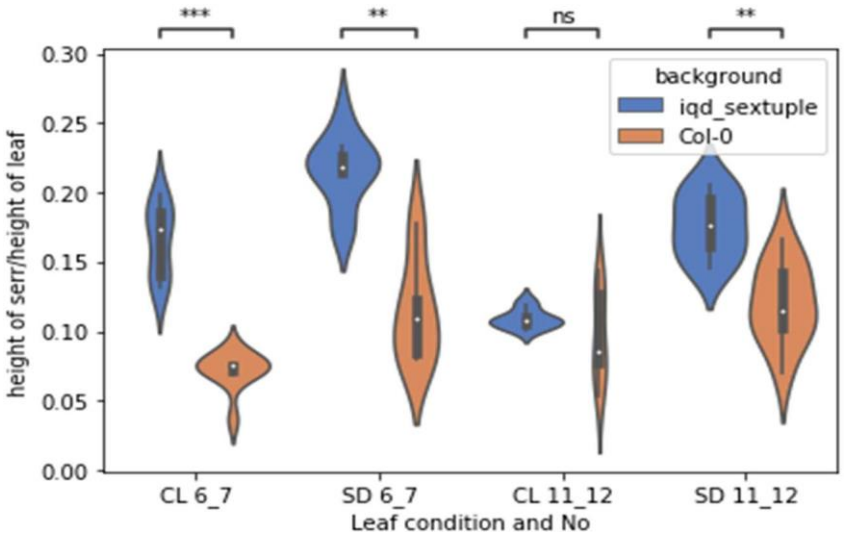

Figure 4. 14 In *1aiqd* lines serrations extend higher up the length of the leaf perimeter. The position of the highest two serrations was taken in each of the 5 leaves in any condition giving n=10. All mutant leaves had serrations significantly higher up the leaf blade, except for leaf 11-12 grown in CL. The average ratios of serration height to leaf length in the WT and mutant, the difference and *p*-values (two sided Mann-Whitney test with Bonferroni correction. * $p<0.05$, ** $p<0.01$, *** $p<0.001$) were:
CL 6-7: WT 0.072, mutant: 0.166, difference = 0.094, p = 7.307e-04;
CL 11-12: WT 0.097, mutant: 0.109, difference = 0.012, not significant;
SD 6-7: WT 0.115, mutant 0.216, difference = 0.101, p = 2.331e-03;
11-12: WT 0.120, mutant: 0.176, difference = 0.056, p = 2.331e-03.

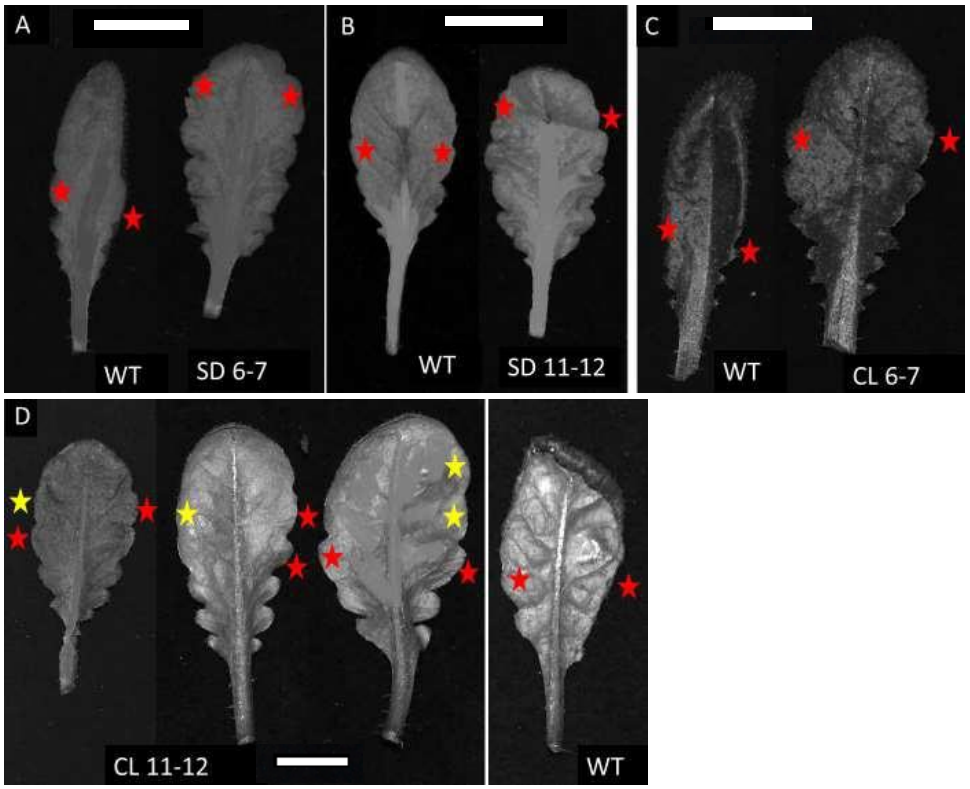

Figure 4. 15 Outgrowth of serrations higher up the length of *1aiqd* leaves can be seen even when not detected in the *morpholeaf* analysis. Red stars depict highest serrations accounted for in analysis in each growth condition and leaf number. Yellow stars indicate shallow serrations not counted in the analysis, which decreased significance of CL 11-12 data in Figure 4.14. Scale bars 1cm.

The higher number of serrations in the *1aiqd* mutant, extending further into the upper regions of the leaf, raised the question of how 1a IQDs affect the initiation of serrations. One hypothesis was the serrations could be initiated at a slower rate in WT leaves compared to the mutant in a given time period. Alternatively, serrations could arise at a comparable rate, but over an extended period in the mutant. A third possibility would be that serrations are initiated in similar numbers in *1aiqd* leaves and WT, but distal serrations only become visible in the mutant because of their enhanced growth. This was supported by greatest serration height found in SD conditions compared to CL, and in smaller leaf 6-7 than 11-12, intriguing a factor of rate of growth in leaves (Figure 4.14).

To explore these possibilities, I turned my attention to earlier stages of leaf development. Comparison of young leaves between the *1aiqd* line and WT every 3 days from 10 DAG till 30 DAG suggested that serration initiation rate and pattern were similar between WT and mutant lines. Serration outgrowth, however, appeared enhanced in mutant leaves from early stages (Figure 4.16). Differential growth could be sufficient to gain serration definition in the upper leaf blade of the mutant. Thus the differences in serration number may not reflect changes in their initiation.

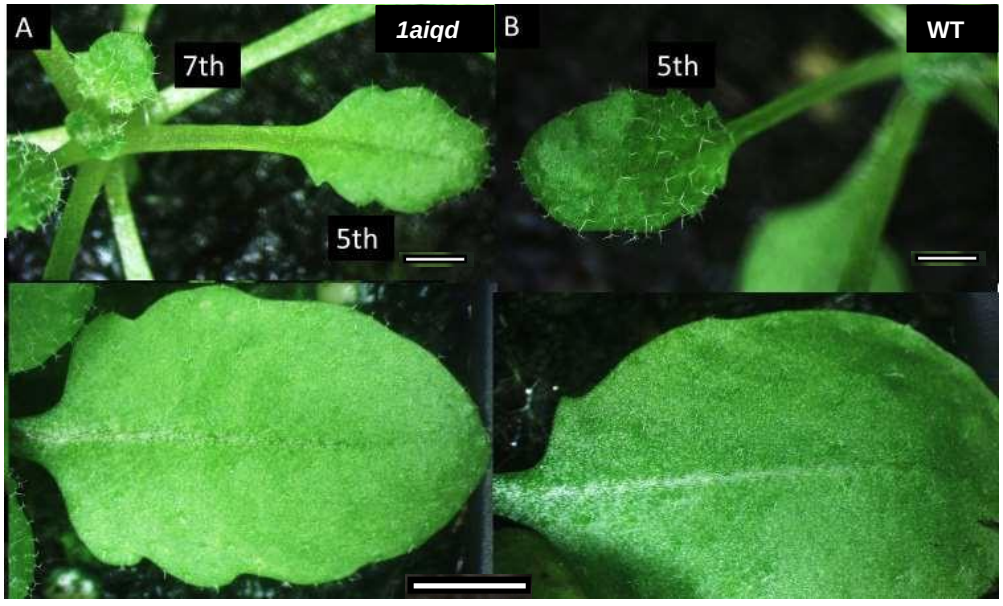

Figure 4. 16: Comparable initiation but greater serration outgrowth is observed over time. Images of 5th initiated leaf of both mutant(A) and WT(B) lines grown under CL for 17 days (top panel) and 30 days (bottom panel). At 17 days growth, similar number of serrations are initiated in identical pattern however those in mutant plants (A, top panel) appear larger and more rounded than in WT (B,top panel). Scale 0.1 cm. At 30 days growth serrations appear more numerous and notably larger in the *1aiqd* line. Serrations initiated higher up the leaf blade in WT may already be smoothed out through rapid upper leaf blade growth. Scale 0.2 cm.

4.2.2 Link between subfamily 1a IQDs and auxin maxima in serration outgrowth

Both the initiation and outgrowth of serrations rely on PIN patterning to generate auxin maxima. The larger serrations extending further up the length of the leaf in the mutant suggested that 1a IQDs could be molecular components moderating this process to limit serration outgrowth. A similar enhancement of serrations was seen in mutant lines with impaired downregulation of *CUC2* by auxin, leading to extended PIN localisation and delivery of auxin to the initiated serrations (Bilsborough, G. D. et al. 2011). As described above, the *1aiqd* mutant showed enhanced serration outgrowth as soon as serrations became visible in developing leaves indicating *1a IQDs* may function in limiting the concentration of, or sensitivity to, auxin maxima, although duration may also be impacted. One factor could be a greater auxin supply, which was investigated further.

As a first step to test whether 1a IQD function could be linked to auxin transport or responses during the development of leaf serrations, the localisation of a 1a protein IQD24 was probed in early leaves. Figure 4.17 clearly demonstrates a high expression of IQD24-YFP in newly initiated leaf serrations. In the early stages of leaf development (second leaf, Figure 4.17A), IQD24-YFP was highly expressed in the leaf tip and in regions of vasculature, with expression at the periphery of the leaf base already noticeable. In the more mature 1st leaf, in which first serrations are initiated at base of the leaf, the strong IQD24-YFP expression in the leaf tip was lost and new protein maxima appeared in the tip of initiated serrations, whilst expression in the vasculature became better defined.

The localisation of IQD24-YFP in early leaves not only supported a function in serration outgrowth but also showed a strong overlap with regions of intense auxin flux, supporting a functional interplay between 1a IQDs and auxin in the development of leaf serrations. Indeed, at even earlier stages (Figure 4.17B), IQD24-YFP localisation started highest at the leaf periphery, where auxin is cited as being involved in leaf growth through promotion of cell division. Slighty later, maxima of IQD24-YFP appeared at the leaf tip, along with a prominent and broad expression down the central region of the leaf, mirroring the known pattern of auxin distribution early in vascular development (Biedroń, M., and Banasiak, A. 2018).

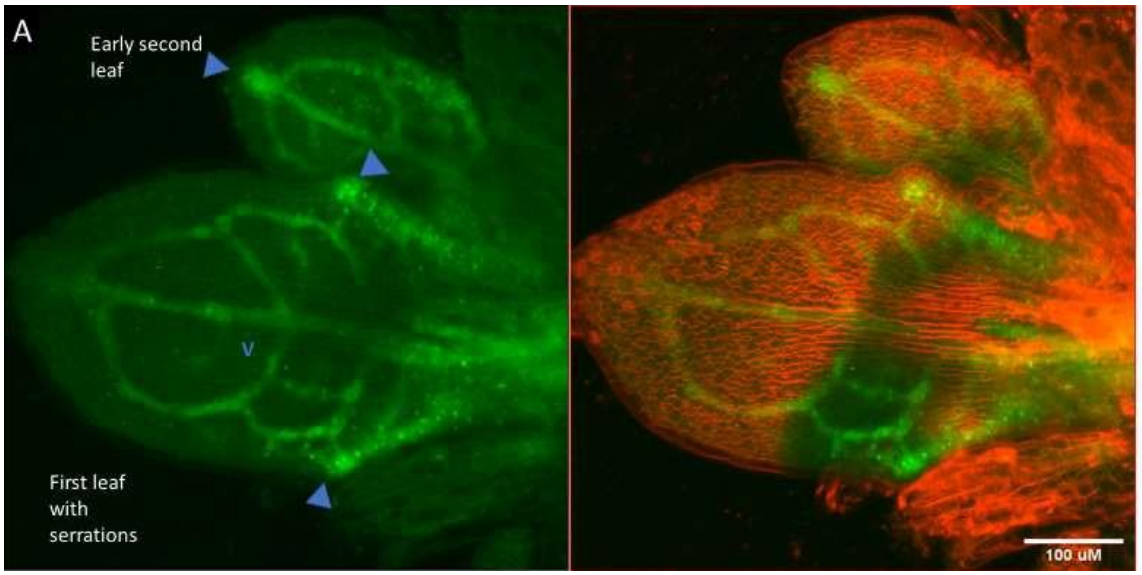

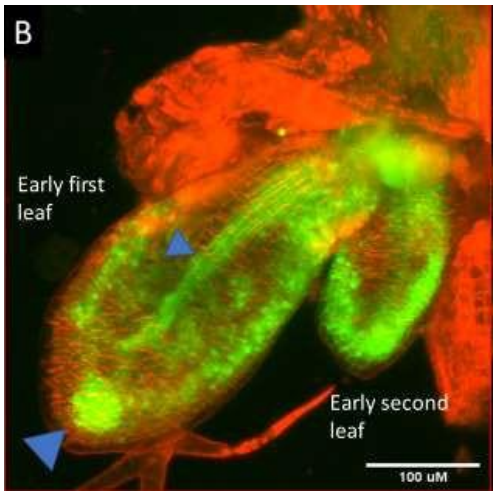

Figure 4. 17 IQD24-YFP expression in developing leaf serrations supports function in growth. A. 2nd leaf and 1st leaf with serrations initiated imaged 14 DAG expressing the IQD24-YFP construct. The left panel shows a z-stack projection of the GFP signal, while the right panel is combined with the FM4-64 membrane stain. B. z-stack projection combined with FM4-64 membrane stain detailing 1st and 2nd leaf imaged at earlier stage 9 DAG (IQD24 expression maxima highlighted by blue arrows and vascular pattern by v, scale bars 100 µm)

I next compared the expression of IQD24-YFP with the localisation of reporters for auxin signaling (DR5:GFP) and transport (PIN1-GFP). Figure 4.18 highlights the similarities and differences between the localisaiton of IQD24-YFP and auxin reporters in early leaves of similar developmental stage. Supporting the idea that auxin and 1a IQDs are functionally interlinked, all three markers were strongly expressed in developing serrations, whilst expression of IQD24-YFP and PIN1-GFP also coincided in the vasculature. Thus, the IQD24-YFP pattern mirrored closely those of highest auxin concentration and transport pathways in the leaf. A detailed look, however, showed differential localisation at the tip of serrations. Maximum intensity projections including the FM4-64 membrane stain highlighted that whilst DR5:GFP and PIN1-GFP were expressed mostly in the perimeter epidermal cells at serration tips, IQD24-YFP expression was highest in a more central region of the serration and was lacking in the outer two cell layers outlining the leaf perimeter (Figure 4.18A-C). Orthogonal views confirmed that although IQD24-YFP signal was present in the overlying epidermis, expression

maxima occurred a few cell layers below in the central region of the serration. (Figure 4.18D)

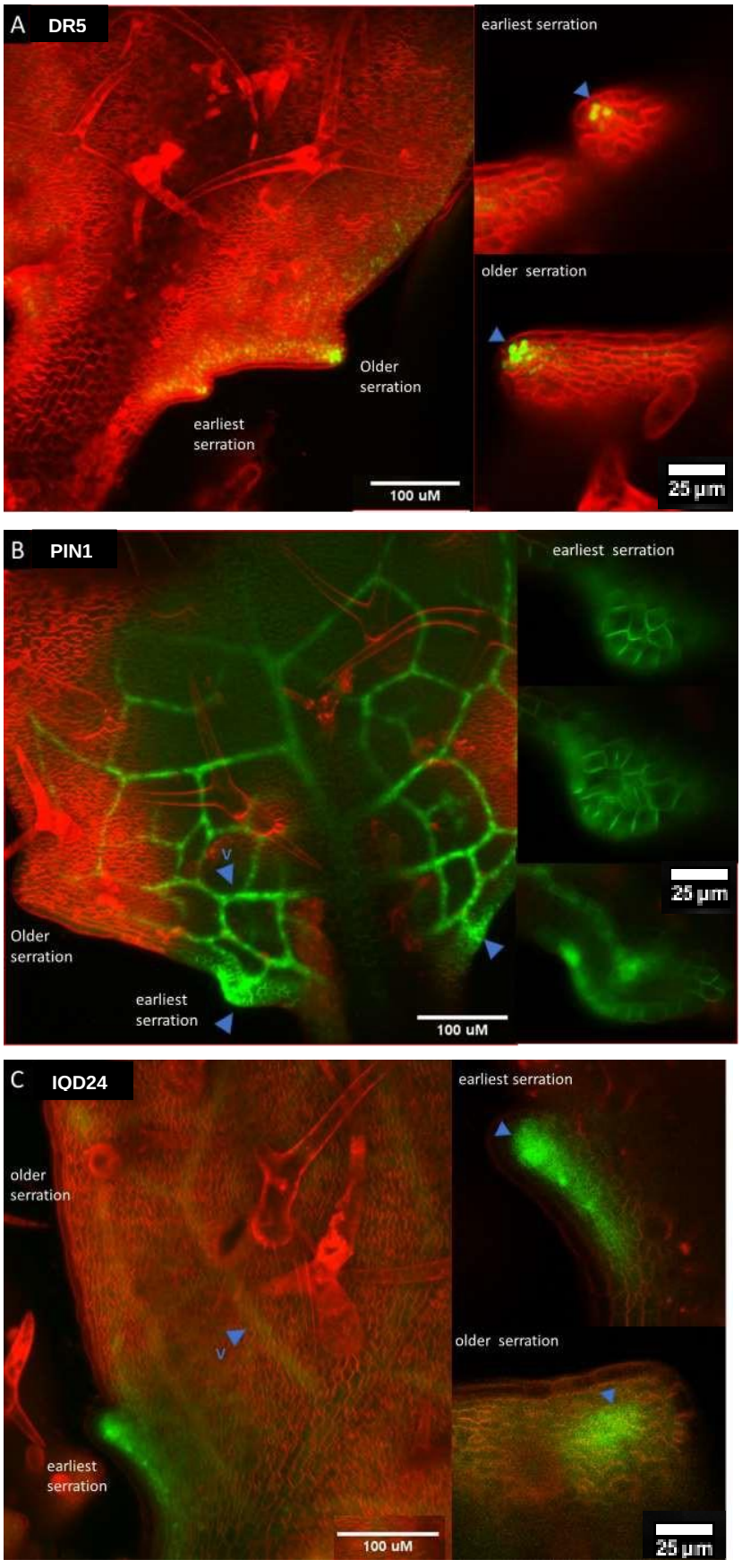

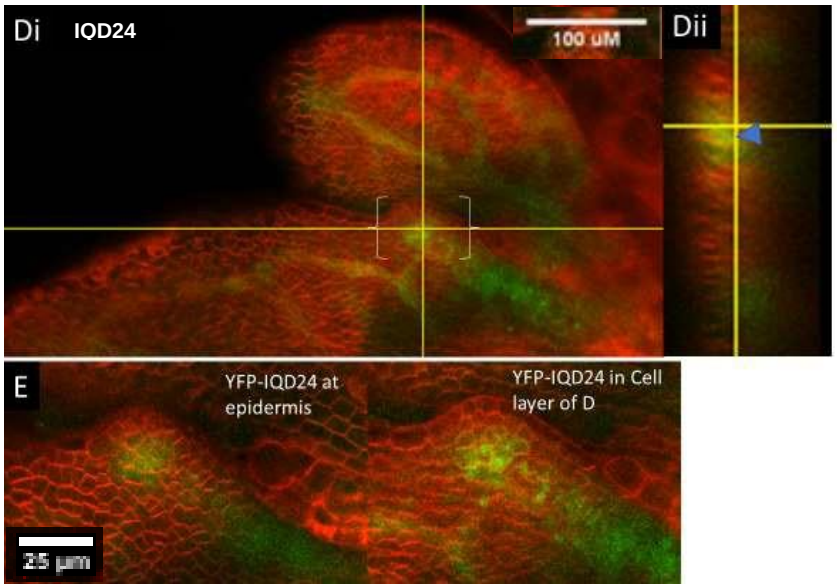

Figure 4. 18: **Comparison of IQD24-YFP expression with auxin reporters in developing leaves**. A: nuclear DR5:GFP reporter in early leaf, with magnification of first and second serrations; arrows point to activation of DR5:GFP in cells at the very tip of serrations. B: PIN1-GFP in similar stage leaf with magnification of first serration showing planes through L1 to deeper cell layers; arrows point to PIN1 expression in L1 cells overlying a developing serration and in the vasculature(v). C: Leaf expressing IQD24-YFP with magnification of first and second serration; arrows indicate highest expression in cells at the centre of developing serrations and in the vasculature. Di shows cell layer where IQD24-YFP expression in serrations was highest, several cell layers bellow the epidermis denoted by orthogonal view Dii with blue arrow. E magnification of serration in D, weaker IQD24-YFP expression visible at epidermis (left panel) and maximum expression in plane shown in D (right panel). (cell outlines FM4-64 memberane stain)

Several *IQDs* of family 1c have been proposed to be regulated by auxin (Wendrich, J. et al. 2018). To verify *IQD24-YFP* is regulated by auxin, I tested the effect of high auxin levels (10 µM 2,4-D for 22 hours). As a positive control, GFP:DR5 was highly induced across the whole leaf (Figure 4.19A). Despite artifically raised auxin levels, particularly in the epidermal layer, the low levels of IQD24 found in the epidermal cells of early leaves were not increased by the 2,4-D treatment (Figure 4.19E,F). As well as this, the specific pattern of IQD expression including at the vascular veins and in central region of outgrowing serrations appeared unchanged. Expression in these regions, unlike epidermal expression, might however be increased, although this could not be quantified because the settings for each image capture had been adjusted for optimal signal without over-exposure (Figure 4.19C,D). As noted previously, protein remained absent in the leaf perimeter and appears to be rapidly reduced as serrations matured, with

diminished maxima in older serrations in Figure 4.18C and 19D (multiple images in older leaves show no protein in mature serrations, these are not shown).

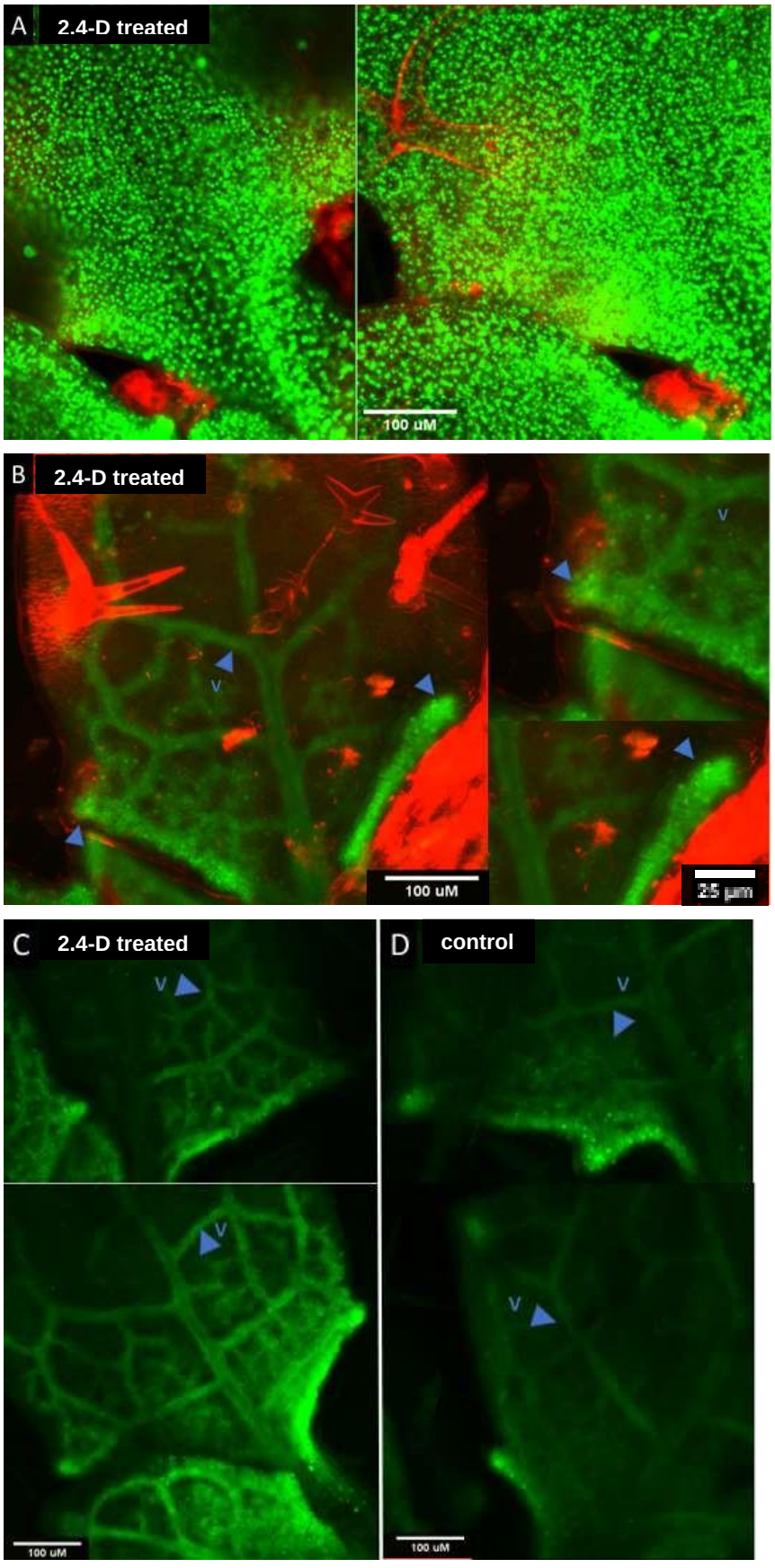

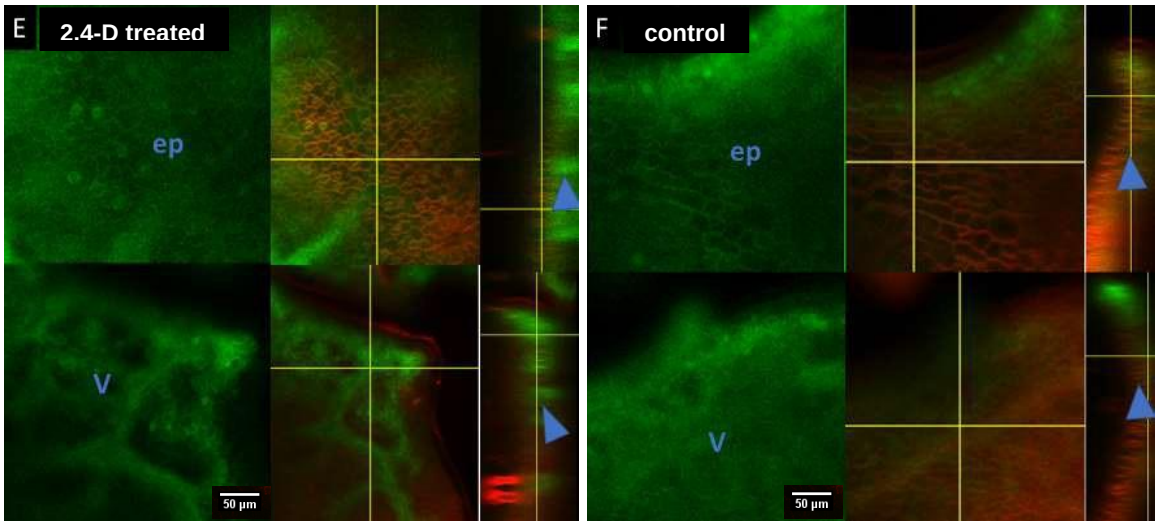

Figure 4.19 : **Response of IQD24-YFP and auxin reporters to auxin treatment.**
Leaves treated with 10 µM 2,4-D for 24 hours, comparable with the controls shown in Figure 18 A-C. A, B: DR5:GFP (A) and IQD24-YFP (B) counterstained with FM4-64; arrows indicate developing serrations, v indicates vascular expression . C,D: IQD24-YFP without FM4-64 staining after 2,4-D treatment or water treated control respectively, arrows highglighting vascular signal difference. E,F: orthogonal views of IQD24-YFP expression in epidermis (denoted ep, top) and vascular veins (denoted v, bottom) following 2,4-D treatment or water-treated control, respectively; arrows show stronger vascular expression in treated sample while epidermal signal remains weak.

Overall, whilst the localisation of IQD24-YFP clearly correlated with sites of high auxin transport and auxin response in leaves, it did not appear that auxin concentration by itself controlled *IQD24-YFP* expression. Simple upregulation of *IQDs* by auxin can be excluded, but auxin might still function to up-regulate IQD protein levels in combination with other factors that are not affected by increased auxin levels. Alternatively, auxin may activate *IQD24*, however other factors could repress *IQD24* in leaf perimeter cells of the serrations, where auxin concentration is high but *IQD* expression absent.

4.2.3 IQD function impacts PIN1 orientation during serration outgrowth

As shown above, the expression of IQD24-YFP closely mirrored that of PIN1 in early leaves, marking the vascular system and the most recently initiated serration (Figure 4.18). Expression was indeed more consistent with PIN1 in this respect than with the DR5-GFP reporter, which showed a stronger response in the older leaf serration, whilst just starting to be expressed in the earliest (Figure 4.18 A). In contrast, both PIN1 and IQD24 were predominantly localised in the earliest serration and were quickly downregulated, suggesting a function in building up the auxin gradient (Figure 4.18 B.C).

To test whether 1a IQD function was important for PIN1 localisation and auxin transport, I crossed the PIN1-GFP reporter into the *1aiqd* mutant background. However, these experiments were disrupted because the reporters became silenced in the sextuple mutant, potentially due to shared sequences with one or more of the T-DNA insertions in the mutant. By looking at lines with different combinations of *iqd* mutations, the mutations in *IQD22* and *IQD26* were identified as problematic. For subsequent experiments, a partial loss of funciton line was used, which segregated the *iqd22-1* and *iqd26-3* T-DNA insertions. Interestingly, whilst in WT samples PIN1 had a clear polar localisation in both the leaf perimeter as well as in epidermal cells across the surface of the serration, PIN1 only appeared to have clear polar localisation in the leaf perimeter in partial loss of function plants heterozygous for *iqd22-1* and *iqd26-3.* PIN1-GFP was less clearly localised in the epidermal cells of regions corresponding to high *IQD* expression. This may indeed imply a function for IQD proteins in controlling auxin transport and concentration at serrations.

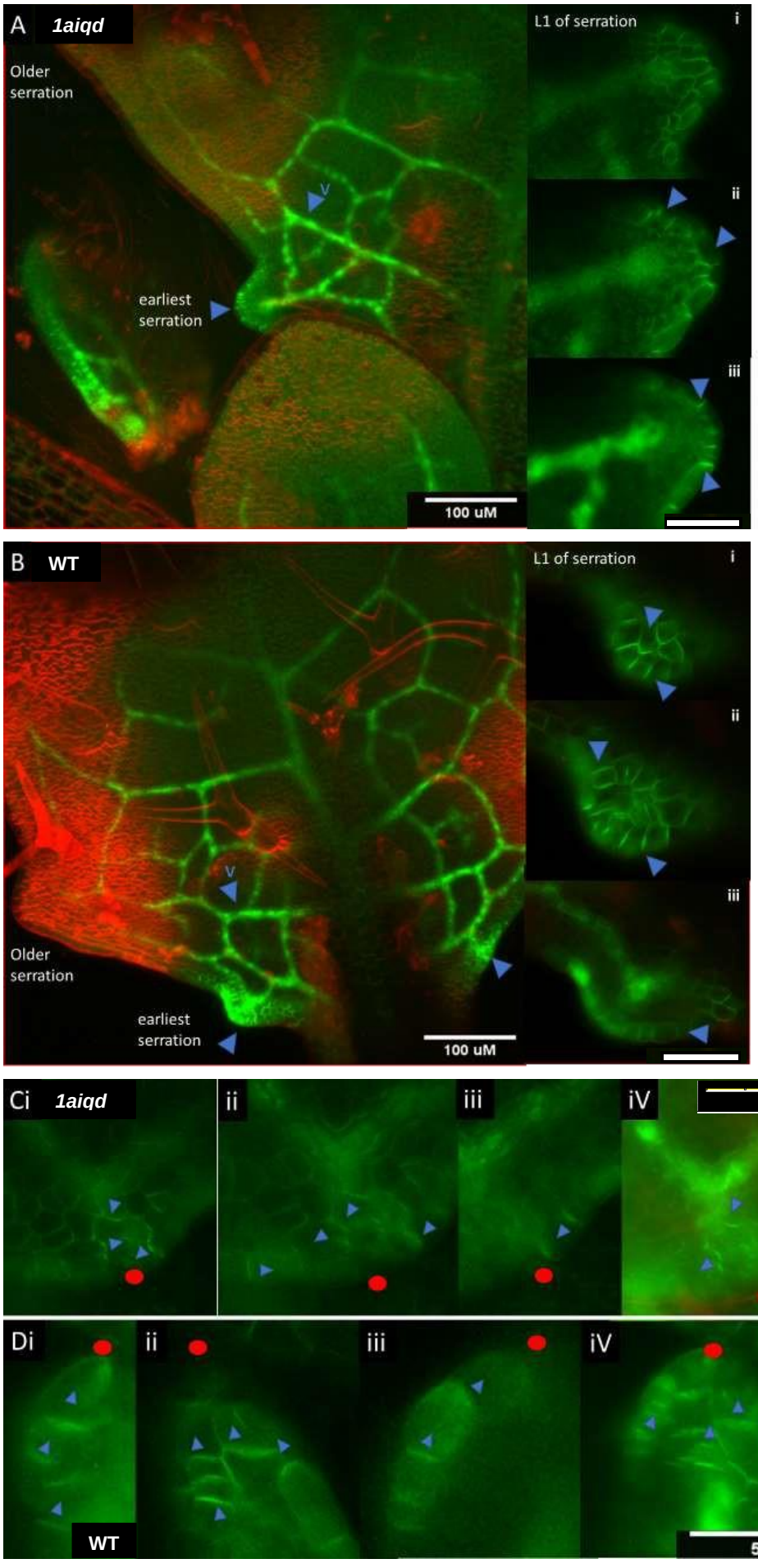
A 1aiqd
Older serration
earliest serration
V
100 uM
L1 of serration
i
ii
iii
B WT
Older serration
earliest serration
V
100 uM
L1 of serration
i
ii
iii
Ci 1aiqd
ii
iii
iV
50 µm
Di
ii
iii
iV
WT
50 uM

Figure 4.20: Reduced *1a IQD* function appears to impair polar PIN localisation in newly initiated leaf serrations. A,B: maximum intensity z-projections of early leaves expressing PIN1-GFP, scale bar 100 µm, with smaller panels showing single consecutive optical sections through the upper cell layers of developing serrations in the mutant background *(heterozygous iqd22-1, iqd26-3)* (A) and in the WT (B), scale bar 30 µm; arrows denote cells where polar localisationoccurs, notably absent in L1 of mutant. C,D: close-ups of developing serrations of a mutant leaf (C)and WT(D), scale bar 50 µm; i-iii show single optical sections from the epidermis to a few cell layers deep and iv shows the corresponding maximum intensity projection. Serration tip is marked by red circle and direction of auxin flow by PIN1 localisation indicated by arrows. Greater directionality towards tip is present across WT serration.

This indicates high expression of 1a IQD proteins in a central serration region from early in initiation is important for patterning of PIN proteins and therefore auxin maxima generation. Disruption to polar patterning, whilst PIN1 proteins still strongly localise to serration region, may be factor contributing to greater serration outgrowth in the mutant line.

4.2.4 Test of subfamily 1a *IQD* function in vascular development

The pattern of IQD24-YFP aligned with the developing leaf veins much like PIN1-GFP (Figure 4.21A, B). As PIN1 is positioned to generate a gradient of auxinconcentration required for vascular differentiation, and family 1a IQDs appeared toaffect PIN1 patterning in serrations, I took a closer look at vascular differentiation in the *1aiqd* line.

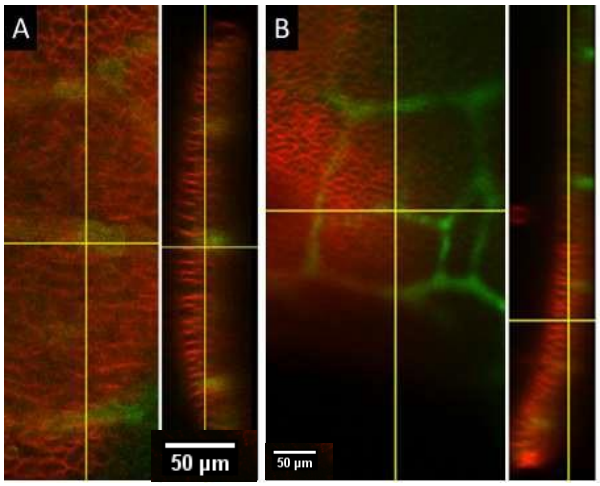

Figure 4. 21 Orthogonal views of IQD24-YFP (A) and PIN1-GFP (B) in vascular vein region shows expression in cell types just below epidermis of the leaf. Scale 50 µm.

Whilst PIN1-GFP had a clear polar pattern during serration outgrowth, the localisation in developing veins was less clear and appeared similar between

between mutant and WT lines (Figure 4.20 A,B). Nonetheless, *IQD24* expression appeared in a broader mid-vein region before more narrowly defined veins developed, suggesting a possible function throughout vein patterning and differentiation. Imaging of early leaves in fixed seedlings, however, did not show any obvious differences between the *1aiqd* line and WT, either in the vascular pattern (Figure 4.22) or in images of differentiated veins in mPS-PI-stained leaves samples (Figure 4.23). These results indicate either that the expression of 1a *IQDs* in developing veins is not functionally relevant, of that a function in vascular development is obscured by further levels of redundancy.

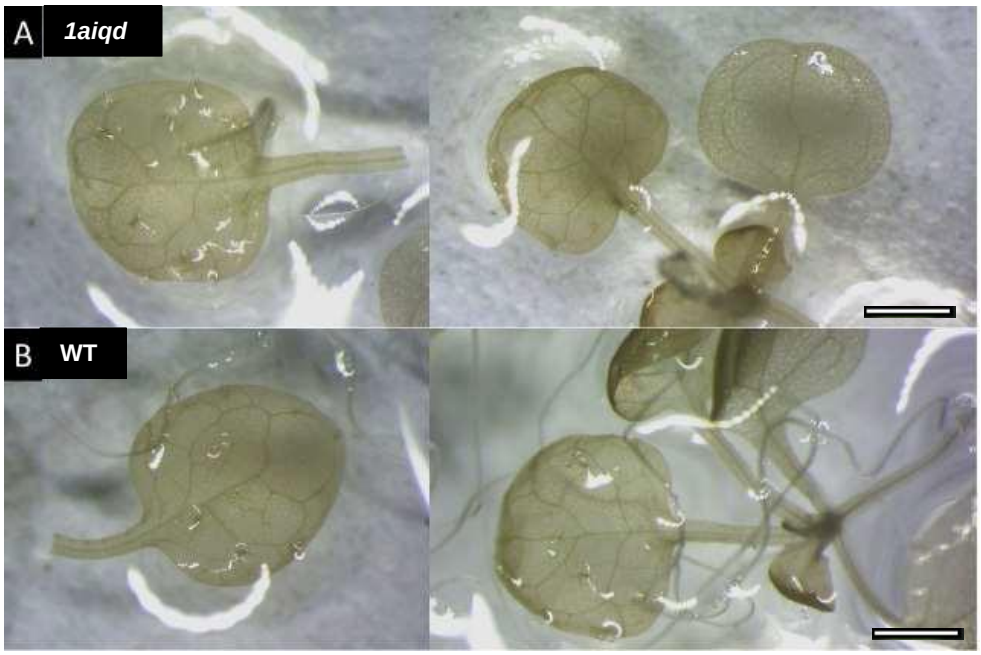

Figure 4. 22: No defects observed in vascular patterning in *1aiqd* mutant leaves. Fixed leaves of mutant (A) and WT (B) seedlings imaged under light microscope. Scale bars 1 mm.

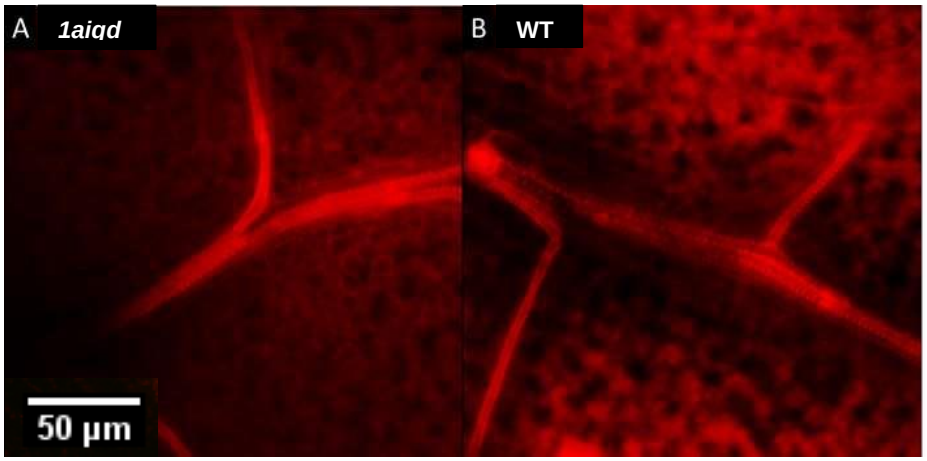

Figure 4. 23: Correct vascular differentiation in the *1aiqd* mutant. Confocal images of veins in PI stained early leaves of the mutant (A) and WT (B)

4.3 Discussion

The initial observation that individual leaves appeared to be of larger surface area from comparing rosette growth (Chapter 2) was confirmed quantitatively in this chapter. As with IQD's modification of stem growth, no impact was apparent in length of the leaf, supporting no functional interaction with elongation growth. Instead, when grown in CL conditions, the *1aiqd* mutant leaves showed greater growth perpendicular to the main leaf elongation axis. Broadening of the leaf appeared to be enhanced mostly in the upper leaf region, bestowing a more pear-like shape to rosette leaves of *1aiqd* line rather than the narrower, oval WT leaves. Whilst not quantified in SD growth conditions, leaf shape was similarly broadened towards the leaf tip, with no reduction in width tapering to a more pointed tip, as seen in WT leaves (Figure 4.2A.B). Increased width in the upper leaf region was most pronounced in the oldest leaves of the rosette and could importantly result in enhanced light capture.

This change in organ shape is analogous to the broader organ shape caused by reduced level of IQDs in crop fruits and the stem phenotype presented in Chapter 3. As well as changes in leaf width, the petioles in mutant lines were visibly more substantial (Figure 4.2) with again the greatest difference in width. A function of 1a IQD proteins in the petiole was also suggested by the almost complete lack of petiole growth in seedlings grown with ectopic *IQD22* expression (Figure 2.26). This again showed similarities to stem growth, with radial growth de-restricted in the *1aiqd* mutant, whilst gain of function inhibited elongation growth. Based on the discovery that changes in cell division planes were associated with increasing radial growth in the stem, it will be important to verify whether a similar mode of IQD action is present in petiole and leaf lamina growth.

Studies of *IQD* genes related to those of Arabidopsis subfamily 1a have been performed in Cucurbitacea species. For example, a study in watermelon strongly associated restricted radial growth of the fruit with increased expression of gene *CsSUN8*, whose closest homolog in Arabidopsis is the family 1a *IQD26* (Dou, J. 2018). The watermelon fruits deviated greatly in diameter, but with a minimal reduction in fruit length associated with the increased radial growth, similar to the stem and leaf shape phenotypes of the *1aiqd* line in Arabidopsis. In cucumber, two major QTL for fruit shape were identified in a study that used genotypes that diverged greatly in both fruit length and width. In this example both

QTL contributed to both radial and elongation growth (Pan, Y. et al. 2017). The strongest QTL, in chromosome 1, was attributed to *CsSUN2* gene, which is phyllogenetically close to *CsSUN8* in watermelon and subfamily 1a in Arabidopsis (Jin, B. et al. 2017). Therefore, divergence exists in literature on whether the main impact of 1a IQD function in Cucurbitaceae is on radial growth or both radial and elongation growth. My own results support that family *1a IQD* genes have a role in restricting radial and lateral growth. This contrasts with the strong effects on longitudinal growth seen after ectopic expression of *IQD* genes of other subfamilies, such as subfamily two in tomato (Wu, S. et al.2011) and members from 2a and 1c in Arabidopsis however, is in parallel with the more rounded leaf phenotype of ectopic 1a member *IQD25*, supporting divergent function in plant growth across subfamilies (Burstenbinder, K. et al. 2017).

Other than leaf shape, IQD function clearly impacted leaf complexity. Generation of auxin maxima is essential for serration growth and has been associated with increased cell proliferation. Faster outgrowth of serrations from initiation could occur through increased proliferation, with establishment of a greater and greater proliferating cell population as serration growth proceededs, enhancing area difference between WT and mutant serrations. The increased outgrowth of leaf serrations of the *1aiqd* line therefore warranted investigation into the functional interaction between *1a IQD* genes and the establishment of auxin maxima. An interaction was supported by the overlapping expression patterns of IQD24 with those of reporters for PIN1 proteins and for auxin response in developing leaves. Furthermore, partial loss of *1a IQD* function caused a visible disruption of the polar localisation of PIN1 in serration regions overlaying regions of maximum IQD24 protein expression. A polar distribution was however still visible in perimeter epidermal cells lacking IQD expression. This disruption of polar PIN orientation, normally found in cell walls pointing in the direction of serration tips, might result in auxin maxima that are more diffuse and less specific to the serration tip, perhaps inducing cell proliferation and growth over a larger area in the serration, which would lead to the observed macroscopic serration phenotype. The DR5 reporter indeed was activated most strongly in epidermal cells at the serration tip in WT background. It would be interesting to test whether the DR5 reporter is expressed in a wider region in developing serrations of the *1aiqd* mutant. To this end, establishment of the GFP-DR5 reporter in a high order mutant background is underway.

The increased growth of leaf serrations in the *1aiqd* mutant could result from a faster proliferation rate over a similar developmental time period, or from an extended proliferative period, as in cited auxin transport mutants where PIN1 localisation remains at serration sites for longer (Bilsborough, G. D. et al. 2011). An extended growth period could occur through altered auxin maxima less effectively degrading CUC2, extending PIN1's localisation and auxin delivery. The results on stem growth in 1*aiqd* suggested an increased proliferation rate over a similar time period (Chapter 3). To investigate whether the same happens in leaf serrations, a cell division marker such as CycB1;1:GUS (Colón-Carmona A. et al. 1999**)** should be used.

The *1aiqd* mutation affected not only the size, but also the shape of leaf serrations, demonstrating more pronounced outgrowth with increased height. Height was however not the only characteristic contributing to the increased area of serrations in mutant lines. Whilst the width at the base of the serrations was similar between *1aiqd* and WT plants, the shape of serrations themselves was different. Serrations continued to grow wider in mutant plants, with a more semi-circular shape, rather than tapering towards a tip, highlighted by Figure 4.2A,B. This was similar to the change of shape in the upper leaf blade. The changes in serration shape could be studied in more detail, not only by looking at the rate and duration of cell proliferation in different regions but also by investigating changes in planes of division, as done for the stem in Chapter 2.

The changes in PIN1-GFP localisation in the leaf serrations of the *1aiqd* mutant raise the question whether altered auxin transport could have contributed to changes in stem growth. Less is known about auxin transport and gradients in the stem. A severe *pin1* mutant show almost full loss of ability to initiate lateral shoot organs, but still grows a stem. In *pin1* plants, DR5-GFP signal was impaired in the meristem L1 layer and in the vascular bundles, where the reporter is normally expressed. Auxin immunolocalisation however showed that auxin was still present in the vascular strands and connected lower region of the meristem but lost in the L1 of the meristem (Banasiak, A. et al. 2019). As cited in association with cytokinin function in lateral branching, PIN3,4 and 7 participate in auxin transport in xylem cells of the stem, and enhancement of this may contribute to main stem growth (Waldie, T. and Leyser, O. 2018). Therefore, questions are posed such as whether IQD function might also impact auxin gradients in the RZ, potentially through changes in other members of the PIN family such as 3,4 and 7, increasing divisions and stem growth.

The changes in PIN1 localisation in the leaf serrations may be an indirect effect of 1a IQD function. This is suggested by the fact that the highest expression of IQD24-YFP occurred in deeper tissue layers underlaying the epidermal layer. IQDs may be directing polar PIN localisation in a non-cell autonomous way. Mechanical stress has been linked to both microtubule dynamics and PIN PM localisation (Heisler, MG. Hamant O. et al. 2010; Li, T. et al.2019), so changes in tissue mechanics would be one interesting candidate to mediate the effect of IQDs across cells. It is plausible that 1a IQDs could alter the distribution of stresses in the growing tissue through changes in microtubule dynamics and potentially through changes in cell division planes, and that altered stress patterns in turn would lead to changes in PIN localisation and auxin dynamics. Alternatively, IQDs could directly influence PIN polar localisation, resulting in altered auxin dynamics and changes in cell proliferation in tissue regions where high IQD expression normally exists, such as serrations and RZ. Further probing of microtubule dynamics and PIN behaviour will be necessary to explore these hypotheses.

A phenotype that was almost as pronounced as increased serrations in leaves of the *1aiqd* line was the ability of leaves to lay flat, rather than curling towards the abaxial leaf surface as in WT Col-0. Whilst this was not tackled experimentally in this chapter, a further understanding of IQD function and the literature on establishment of flat leaf shape can be used to propose several hypotheses. IQDs' proposed function in microtubule dynamics may again be important in this phenotype due to the fact that biomechanical direction of microtubule organisation supports the mode of growth promoting a flat leaf structure (Zhao, F. et al. 2020). Therefore, a change in microtubule behaviour upon loss of *1a IQDs* could be the reason behind enhanced flattening. Alternatively, as presented in this chapter, *IQDs* may also function to establish auxin gradients controlling proliferation. Curling towards the abaxial surface in Arabidopsis leaves could result from increased cell proliferation in the abaxial surface, where auxin accumulates along with ARFs (Maugarny-Calès, A. and Patrick Laufs**,** P**.** 2018). Sub-family *1a IQD* expression has only been assessed in the epidermal layer of the adaxial leaf surface and it could be interesting to investigate whether it is absent in the abaxial surface, revealing a contribution to polarised growth through adaxial-abaxial separation. Finally, it is believed that leaf shapes have evolved to optimise light capture while minimising negative impacts of environmental stressors, such as temperature and water availability. The effects

of IQDs on leaf curling raise the question whether these genes also participate in the detection or response to environmental stresses that affect leaf growth.

Chapter 5 IQD subcellular function

5.1 Introduction

In previous chapters, I described how subfamily 1a IQDs affect cellular processes important for organ growth, including oriented cell divisions and localisation of the PIN1 auxin transporter. In this chapter, I investigated the subcellular basis for the function of family 1a IQDs.

Interactions with the microtubule cytoskeleton was an important focus. Based on studies of other *IQD* genes (Mitra,D. et al. 2019; Sugiyama, Y., et. al., 2017) and on the subcellular localisation of IQD24, I expected family1a IQDs to regulate microtubule dynamics. To test this, I focused on leaf epidermal cells, which have been used as a model system to study the role of microtubule arrays in cell morphology, and whose shape has been shown to be affected by other *IQD* genes (Burstenbinder et al., 2017). As seen later in this chapter, visualisation of the pavement cells in mature leaves of *1aiqd* mutant plants also presented phenotypic variation in lobing on the adaxial surface.

Another important line of study was on PIN patterning. Phenotypes in phyllotactic patterning, lateral branch initiation as well as increased organ growth supported a functional interplay between IQDs and the establishment of auxin maxima. Chapter 4 showed that IQDs may be a molecular component contributing to polar PIN organisation. In this chapter, I further studied the role of IQDs in patterning PIN1 during organ initiation, as well considering whether IQD's molecular contribution is through transduction of a mechanical stress signal.

The strong conservation of calcium dependent and independent calmodulin binding domains in the *IQD* family indicates calmodulin association must also be integrated into any mechanism proposed for IQD cellular functions. So far it remains unclear how Ca++ signalling interacts with IQD function. As available resources were limited for the large part of my PhD, with the *1aiqd* mutant line established with less than a year left of experimental time, only simple questions were proposed and tested. Nevertheless, interesting connections arose more

recently between Ca++ signalling, microtubule dynamics and mechanical sensing, which need to be considered.

5.1.1 Role of microtubule arrays in the development of interdigitated epidermal cells

Monitoring pavement cells throughout leaf growth demonstrated they initially have simple geometry and acquire their interdigitated shape first at the tip of the leaf, then gradually towards the base. Pavement cells vary in how pronounced and spaced out their lobes are across plant species, which is in-fitting with the large degree of variety in leaf shape and size across plant species. Whilst propositions including increasing the contact area with neighbours for faster communication, positioning of other leaf surface cells such as guard cells and stomata and to help leaves resist breakage exist (Glover B. J. 2000, Sotiriou P. et al. 2018), the theory most supported to account for evolution of the interdigitating pattern is to resist mechanical stress on cell walls in this cell layer.

Multiple studies concluded that mechanical stress is a key driver of cell-shape morphogenesis and that PC shape could be an adaptation related to mechanical forces acting on the leaf epidermis. It has already been introduced in previous chapters that the epidermis is under high tension from inner tissues, so adaptation may occur to reduce mechanical stress on epidermal cell walls. A combination of evidence and modelling showed that the pattern of tissue stress depends on growth directions. During anisotropic growth, as seen in stems and roots, elongated cells best resist stress, whereas the interdigitated PC shape reduces the magnitude of force felt on the cell wall in tissues that are growing isotropically, such as the leaf epidermis (Sapala A. et al. 2018).

One reason stress is a key process linked to PC shape development is the study of microtubule re-orientation early in lobe initiation. Microtubules respond to stress, impacting cell shape as expansion takes place due to introduction of cell wall mechanical anisotropy (Landrein, B. Hamant, O. 2013). The concentration of cortical microtubule arrays in the convex neck regions flanking lobes implicated high stress in neck regions. Modelling and studies of cell wall tension in different regions of lobed pavement cells affirmed that neck regions were highly stressed (Sampathkumar A. et. al 2014). Through fortifying these regions by cellulose microfibril deposition, microtubules' orientation is thought to enhance the

anisotropic shape as the cells expand. Whilst this demonstrated stress responses enhance the interdigitated PC shape, it did not place it as an upstream factor initiating lobe outgrowth.

Different mechanisms exist for lobe outgrowth focusing on local outgrowth of lobe regions, restriction at neck regions or a combination of both. Research seeking genetic components important for lobe formation identified Rho GTPase family members, ROP2 and ROP6, which actively repress localisation of one another at the PM, partitioning the PM into different ROP2 and ROP6 occupied regions (Belteton, S. A. et al. 2018). It has been proposed that ROP2 localises in the tip of lobes, degrading a microtubule organiser ROP-INTERACTIVE CRIB MOTIF-CONTAINING PROTEIN 1 (RIC1), relaxing re-enforcement of cell walls by reducing CMT concentration in these regions. ROP2 is also proposed to recruit dynamic actin through RIC4. Synergistically, ROP6 was shown to localise in the neck regions and upregulate RIC1, fortifying these regions. Combined, this generates anisotropic cell wall expansion and PCs' lobed shape. This mechanism implicates microtubule dynamics in both lobe initiation and fortification of the interdigitated shape.

Further research in cell wall heterogeneity during lobe formation identified region-specific pectin modification. Levels of demethylated pectin correlated with cell wall stiffness, with de-esterified pectin increasing stiffness in neck regions and generating differential growth. This is potentially placed upstream of lobe initiation and was shown to precede microtubule re-orientation at the necks (Altartouri, B. et. al. 2019; Amir J. et al. 2019). Loss of cell wall extensibility mediated by expansins following de-esterification further validates a contribution of this process to growth asymmetry in PCs (Wang X. et al. 2020).

Through modelling, including elements such as pectin modification that amplify the cell walls' mechanical heterogeneity, a slight cell wall buckling under high stress was proposed as a mechanism for lobe initiation. A slight buckle, presumed to be in a relaxed cell wall region identified by ROP6 domain and esterified pectin, would generate stress in flanking regions. These would be fortified through microtubule behaviour, becoming necks of a lobe that is further pronounced with cell expansion (Altartouri, B. et.al. 2019). Most recently, a bold hypothesis replaced theories of turgor pressure, wall stress and cellulose reinforcement with simply pectin behaviour. Pectin is formed in nanofibrillar structures. These are closely spaced in necks and widely spaces in lobes, where it was proposed de-esterification caused expansion and this was sufficient for

differential growth (Haas K.T. et.al. 2020) which again would be enforced by microtubule concentration at neck regions. Mutants with defects in microtubule localisation at neck regions indeed still initiate lobes but less defined ones (Mitra,D. et al. 2019).

Microtubules have also been shown to align to stress patterns in growing tissues and to re-organise to differential stress patterns following artificial stress generation. A study of microtubule behaviour postulated this phenomenon may be largely self-organising and initiated by a change in dynamics according to stress felt at the cell wall, along which they closely align in the CMT array (Landrein, B. Hamant, O. 2013). A mechanism involving sensing of stress by microtubules and response to this is yet to be discovered. Here, IQD proteins have emerged as potential players: the MAP mutant *iqd5-1* identified as an interactor protein important for microtubule's ability to pattern according to stress, with requirement of IQD5 localisation for stabilisation of microtubules concentrated in PC neck regions (Mitra,D. et al. 2019).

5.1.2 Links between mechanical stress and auxin transport

Advancements in high resolution imaging detailed PIN1 protein localisation at PMs in parallel with microtubule organisation in the SAM, particularly in boundary cells under high stress, indicating PIN localisation may also be influenced by stress patterns in growing tissues (Heisler, MG. Hamant O. et al. 2010). As well as this, both microtubules and PIN1 reoriented around sites of cell ablation, where severe mechanical stress occurs. Microtubule orientation was however not required for polar PIN1 patterning in the meristem, with persistent organ initiation directed by PIN1 patterning over several days application of the microtubule depolymerising drug, oryzalin. As well, the re-orientation of PIN1 following ablation required a preceding calcium wave, whilst microtubules continued to re-orientate with eradication of the calcium signal (Li. T et. al. 2019). This implicated that whilst stress patterns may contribute to both microtubule organisation and PIN proteins' membrane localisation, they are unlikely to be intrinsically linked and do so perhaps through separate mechanisms.

Postulated mechanisms implicate that mechanical signals are likely transduced through the cell wall, however, may also be detected at the PM of cells. Changing tension at the PM altered PIN1 localisation, with more fluid membranes lowering PM localisation and PM's under tension possessing high

PIN1 concentration. Whilst other membrane-localised proteins requiring cycling also display some element of this behaviour, put down to change in the rates of incorporation and removal from membrane sections by vesicles, PIN proteins appear more sensitive to changes in membrane fluidity and were deemed responsive to stress signals (Nakayama, N. et al. 2012). This supported regulation of PIN PM localisation by mechanical stress and a stress response induced by differential tension on the PM. Disruption of a mechanism allowing PIN proteins to orient in response to stress may impact multiple processes, such as organ initiation and serration outgrowth, as observed in *1aiqd* mutant.

5.1.3 Ca++ and mechanical signalling

Sensing of stress through tension at the PM led to a proposal that calcium signalling, initiated by touch-activated channels, transduces stress signals to downstream elements, such as microtubules and PIN proteins (Braam, J. 2005). Calcium is supported in the literature as a signal that could impact microtubule behaviour, destabilising cortical microtubules in lysed protoplasts. It was proposed that the microtubule-bundling protein pp50 is inactivated by calmodulin binding (Cyr, J. R. 1991). More recently, Wang et al. 2011 established a connection between a calmodulin-like protein (CML24) and the organisation and orientation of CMTs. *cml24-2* and *cml24-4* mutants had reduced root length and altered orientation of MTs in epidermal cells. These observations are not straightforward to interpret though because of the wide range of proteins calmodulins can interact with and regulate.

One calmodulin binding protein (CaMBP) that is also a microtubule-associated protein (MAP), KINESIN-LIKE CaM BINDING PROTEIN (KCBP/ZWI), has a role in plant development (Narasimhulu, S.B and Reddy, A.S.N. 1998). KCBP functions through binding and moving along MTs, particularly those involved in cytokinesis, but its function is disrupted in elevated calcium (Buschmann, H. et al. 2015). A calcium-binding protein associated with the PM in Arabidopsis, renamed MICROTUBULE DEPENDENT PROTEIN 25 (MDP25) (Hamada, T. 2014), also destabilises CMTs in elevated calcium (Li J, et al. 2011). As calmodulins (CMs) are the most likely calcium messenger proteins used by the plant to control microtubule organisation in response to external and internal signals (Hepler, P.K. 2016), it seems likely other CaMB-MAPS have roles in plant growth processes. IQDs are an excellent candidate to investigate in this respect.

Moderation of CM/CML levels through plant development indicates a wide-reaching role for calcium sensors in plant growth, which is yet to be characterised. This could be conferred by regulation of microtubule organisation through calcium signalling following modification of IQD function. As mentioned, PIN1 reorientation following mechanical stress is hypothesised to follow a calcium wave but microtubules still reorientate when this signal is blocked. Whilst calcium interplay with microtubules through MAPs could be important in fine-tuning microtubule behaviour important for plant growth processes, there is no requirement for a calcium signal to transduce altered microtubule behaviour for re-orientation to stress. Microtubule behaviour, PIN1 PM localisation and IQD function may all be regulated by calcium signalling, which is an additional molecular component to be added to hypothesised cellular mechanisms.

5.1.4 Aims of this Chapter

In this chapter, I explored links between IQD function and calcium signalling, microtubule dynamics and PIN1 localisation.

My initial experiments on calcium signaling were performed before my work became focused on subfamily 1a, and used instead translational YFP fusions of IQD17 and 18, which are members of subfamily 1c expressed in the shoot meristem (these reporter lines were obtained near the start of my project from collaborator Professor Dolf Weijers, Wageningen University). Biochemical and genetic experiments were designed to investigate whether perturbation of calcium signalling in the shoot meristem might affect IQD function through disruption of specific cellular and tissue localisation patterns. The same cellular localisations were later confirmed to be seen also in 1a IQD members, as revealed by the IQD24-YFP construct. Change in cellular calcium concentration has been proposed to alter microtubule dynamics, to which IQD function is linked (Sugiyama, Y., et. al., 2017; Mitra,D. et al. 2019). Thus, microtubule organisation was also investigated in the shoot meristem following altered calcium signalling. Finally, as calcium signalling elements often feature feedback on calcium influx (Wakelam, M.J.O. and Berridge, M.J. 2007) downstream effects of 1a and 1c IQDs on calcium signalling itself was investigated.

Following establishment of the *1aiqd* mutant line, the role of subfamily 1a IQDs in MT dynamics was investigated in the process of PC lobing, where

microtubules' ability to re-organise according to stress patterns is important and 1a IQD function appeared to contribute to cell shape.

Experiments to explore links between 1a IQDs and PIN localisation in the shoot meristem were prompted by results in leaf serrations described in the preceding chapter, and by the changes in phyllotaxis in the *1aiqd* mutant, described in Chapter 2. Disruption to PIN1 PM patterning during organ initiation was assessed in the *1aiqd* background. I also tested the hypothesis that IQD function mediates polar PIN patterning by transducing the protein's response to mechanical signals, by probing the sensitivity of PIN1 PM localisation in the meristem after treatments considered to induce mechanical stress, comparing *1aiqd* mutant and WT backgrounds.

5.2 Results

5.2.1 Does altering calcium signalling perturb IQD localisation and/or function

IQD proteins possess distinctive cellular localisation patterns including PM, CMT and nuclear localisation signals, although the nature of CMT decoration may confer unique functionality (Burstenbinder, K. Moller, B. 2017). A particularly puzzling element of IQD localisation is that of sporadic nuclear signal proposed to be cell cycle dependent. IQD nuclear localisation was required for the root's growth response to Ca++ chelation by EGTA (Wendrich, J.et al. 2018) and whether IQD nuclear localisation could be altered by calcium signalling was of interest. A calcium signal may perhaps direct IQD nuclear localisation to promote growth responses. IQDs' microtubule and PM localisations, likely required for cellular processes IQDs control, are directed by positively charged patches on the proteins (Burstenbinder, K. et al. 2017) and binding of CM/CML protein partners might disrupt this.

To test whether Ca++ signalling affects the localisation of IQD proteins in the shoot meristem, I imaged a IQD18-YFP reporter after activating a calcium-mediated response. One elicitor of a rapid calcium signalling response is flg22, a pathogen associated molecular pattern (PAMP)(Ranf, S. et al. 2011). To investigate changes in localisation or regulation of protein levels, the localisation of

IQD18-YFP was monitored immediately after flag22 application as well as at 1,1.5 and 2 hour time points.

A striking localisation change was observed one hour following flg22 treatment with appearance of bright punctate bodies, particularly visible towards the surface of the meristem (Figure 5.1B). The peripheral cellular localisation attributed to cortical microtubule and PM association as well as occasional nuclear signal remained. Planes imaged deeper in the meristem of water control (C) and flg22 treated (D) samples showed a similar pattern, but with lower intensity in treated samples. Further controls, however, showed that the clear change in IQD18 localisation in the outer layers of the meristem was caused by the surfactant used in the flag22 treatment (Silwet L-77), rather than by the elicitor.

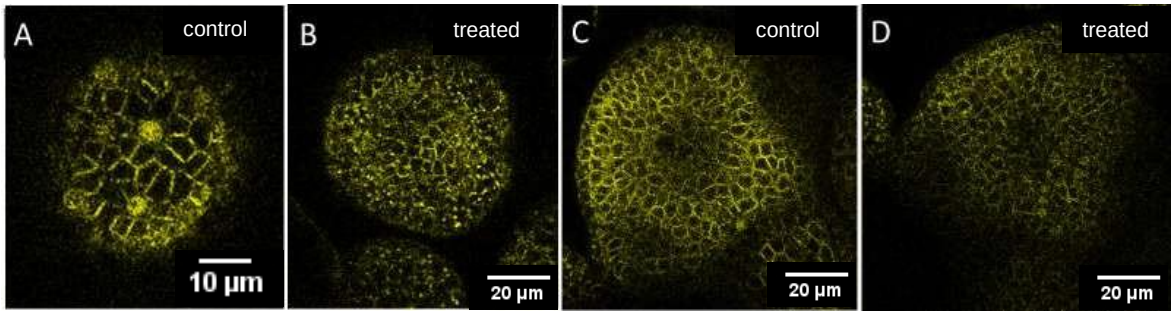

Figure 5. 1: Sequestering of IQD18 protein into punctate bodies following flg22 treatment was caused by Silwet-L77. Apex immersed in 10 mL water (A,C) or treated with 100 nM flg22 and 0.01% Silwet-L77 (B,D). Images one hour following treatment at top of the meristem dome (A,B) and a deeper plane through the meristem (C,D).

Due to the most dramatic localisation effect being attributed to chemical stress in this assay, and no clear alteration in frequency of nuclear localisation or disruption to peripheral localisation, it could be concluded that calcium signalling elicited by flg22 did not perturb YFP-IQD18 localisation. This experiment was also carried out on IQD17-YFP reporter lines, with no disruption of microtubule localisation. However, both 1c IQD reporters appeared to show reduced signal intensity following 1 hour flg22 treatments (Figure 5.1 and 5.2). Samples imaged first in water then immediately after flg22 application (Figure 5.2 C) indicated some reduction in signal was likely through laser bleaching of the fluorophore however a greater degree of signal reduction is apparent following longer treatment with flg22. This did not occur under similar length treatment times with water controls (Figure 5.2 D) indicating the elicitor is responsible. In addition to the reduced intensity of IQD reporters, flg22 treatment also appeared to reduce the levels of the RFP-tubulin microtubule marker at the cell periphery (Figure 5.3).

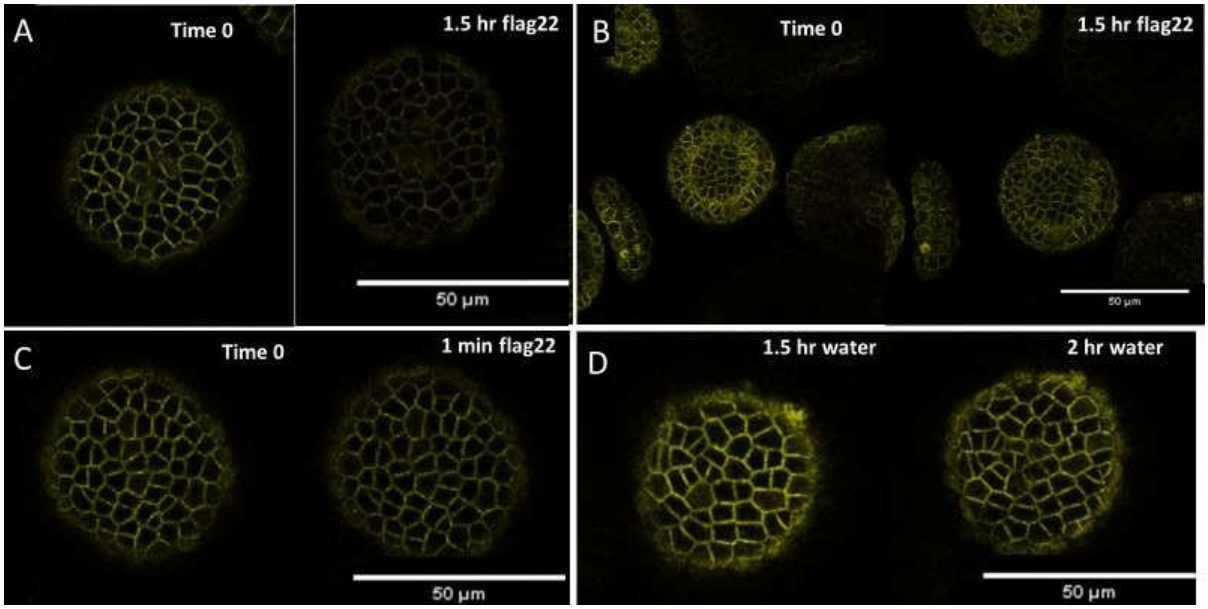

Figure 5. 2: flg22 treatment lowered signal intensity at the periphery of cells indicating reduced PM and CMT protein levels. IQD17-YFP (A) and IQD18-YFP (B) reporters immediately after 10 µM flg22 treatment (time 0, left panel of A,B), and 1.5 hours following treatment (right of panel A,B) imaged under identical laser settings. C shows sample imaged in water at time 0 (left panel) and immediately after addition of flag22 (right panel) and D shows sample images after resting 1.5 hours in water (left of panel) and re-imaged after 2 hour time point (right of panel). 3 biological replicates were collected for 1.5 hr flg22 treated IQD18-YFP and 5 for IQD17-YFP lines.

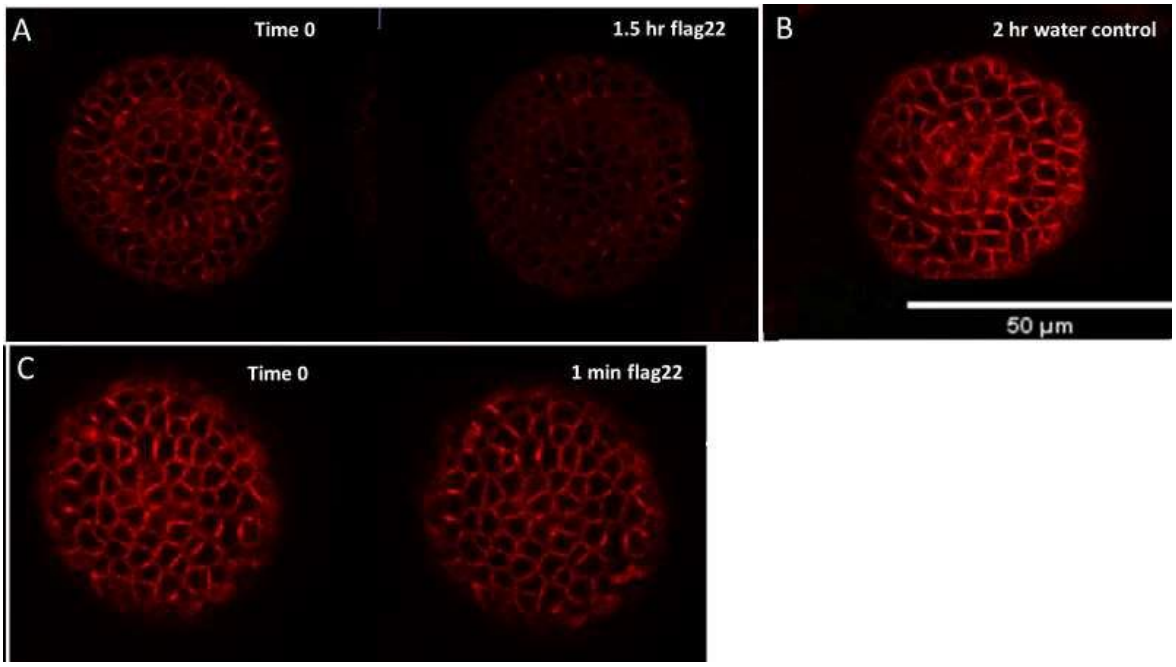

Figure 5. 3: flg22 treatment reduced the intensity of the RFP-tubulin microtubule marker 1.5 hours after treatment. A: microtubule reporter imaged immediately after flg22 application (Time 0, far left panel) then 1.5 hours later (right panel), imaged using identical microscope settings. 3 biological replicates gave identical results. B: control imaged 2 hours after water treatment with no reduction in reporter signal. C; sample imaged in water at Time 0 and immediately after application of flag22 with slight reduction in signal.

As discussed in the introduction, very few microtubule-associated proteins are calcium interactors, even though calcium signalling has been implicated in microtubule stability (Cyr, J. R. 1991). As IQDs interact with calcium sensor proteins and exhibit microtubule association, this makes them good candidates to mediate the effects of calcium signals on microtubules. The reduced intensity of IQD reporters after flg22 treatment would be consistent with the hypothesis that calcium signaling controls association of IQD proteins with MTs, and consequently MT dynamics. However, whilst flg22 is known to elicit a calcium response, it is specifically associated with pathogen response rather than growth processes, and therefore might impact on microtubule density through a pathway not involving IQD function. Therefore, the reduced levels of MT-associated IQDs could be a consequence of changes in microtubule density after flg22 treatment.

In these biochemical studies, different time frames post elicitor induction were monitored, but the effects of calcium signalling on IQD expression levels or the role of calcium throughout different developmental stages could not be assessed. To address these questions, plants with a long-term disruption in calcium signalling were required. Considering that calcium channels play a central role in calcium signaling (Hepler, P.K. 2016), I aimed to test the effect of calcium channel mutants on IQD levels and localisation. To narrow down the number of mutants to use in lengthy crosses and imaging experiments, the available mutants were first pre-screened for shoot growth defects, which would be expected if a pathway linked to IQD function were affected.

Two calcium channel mutants out of 66 phenotyped (detailed in plant materials, section 8.1) had severely affected shoot growth. These were *annat4* (Figure 5.4A) and *cngc4* (Figure 5.4B). The *cngc4* mutant was severely dwarfed in size and *annat4* had defects involving pigmentation, leaf shape and size.

Figure 5. 4: Phenotype of two calcium channel mutants that dramatically impact shoot growth. Ai**:** *annat4* mutant (pot left of image) compared to WT Col-0 (pot right of image); Aii shows a close-up of the mutant leaf shape. B: *cngc4* mutant grown alongside WT.

Due to *IQD* expression early in plant growth in fast dividing tissues such as meristems (Wendrich, J.et al. 2018, Figure 5.1) it was investigated whether growth defects were apparent from early growth in the SAM.

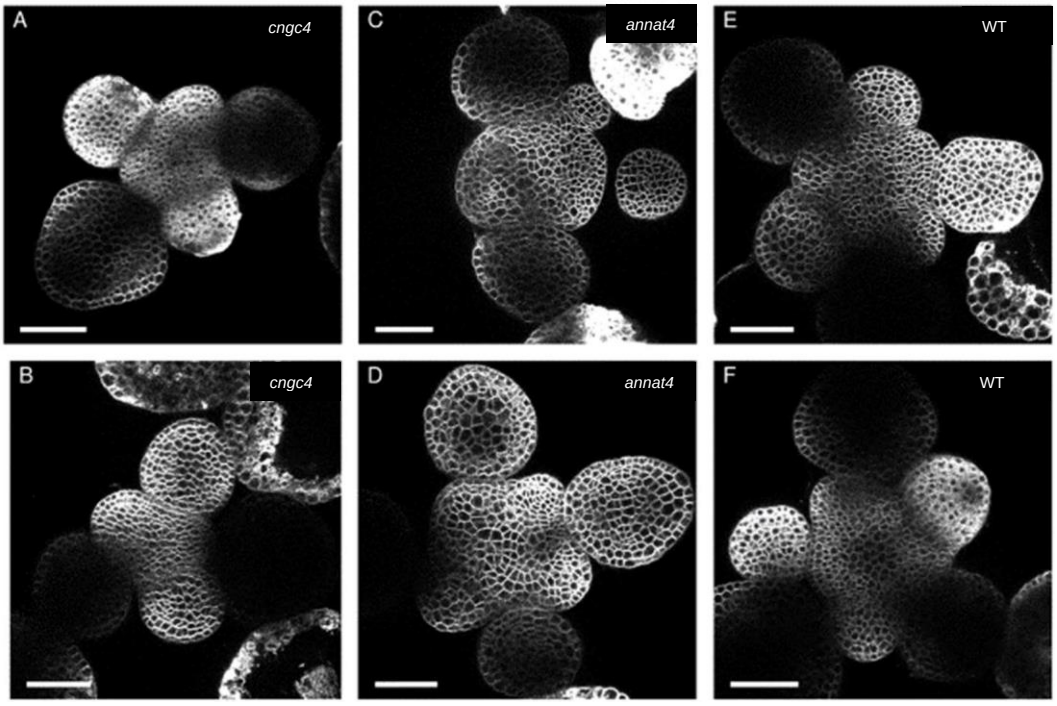

Figure 5. 5: Meristem size and phyllotaxy defects in calcium channel mutants with pleiotropic shoot defects. *cngc4* meristems (A,B), *annat4* meristems (C,D) and WT Col-0 (E,F) all with 50 um scale bar

The meristems of *cngc4* plants were visibly smaller (Figure 5.5A,B), particularly the central region whilst emerging primordia were closer in size to WT. In *annat4* mutants, meristem size was not clearly affected (Figure 5.5C,D), but the phyllotactic pattern was disrupted, with the meristem in Figure 5.5D containing primordia closest in age emerging almost directly opposite one another in a similar fashion to first phyllotaxy defects in 1a IQD mutants (Figure 2.20). The phyllotaxy and leaf shape defects identified *annat4* as an interesting calcium channel mutant to assess disruption to IQD expression, localisation or function.

To test whether the *annat4* mutant affected the levels or localisation of meristem-expressed IQD proteins, the IQD17-YFP and IQD18-YFP reporters were crossed into the mutant background**.** As can be observed in 3D projections (Figure 5.6), IQD17-YFP was most highly localised in meristem boundary regions and found at a lower concentration in the central region and primordia in both WT and *annat4* mutant background. Single plane images clearly captured the YFP signal along filamentous structures, indicating the outline of cells in both WT and mutant background are due to association with CMTs. Figure 5.7 depicts IQD18-YFP expression in *annat4* background (B) in comparison to WT (A). Again, both maximum intensity projections and single virtual sections showed that WT and mutant plants had similar protein concentration, expression pattern across the meristem and cellular localisation, including the frequency of nuclear localisation. Therefore, in an altered calcium mutant that affects shoot growth processes linked to IQD function, IQD tissue and cellular localisation patterns were not affected.

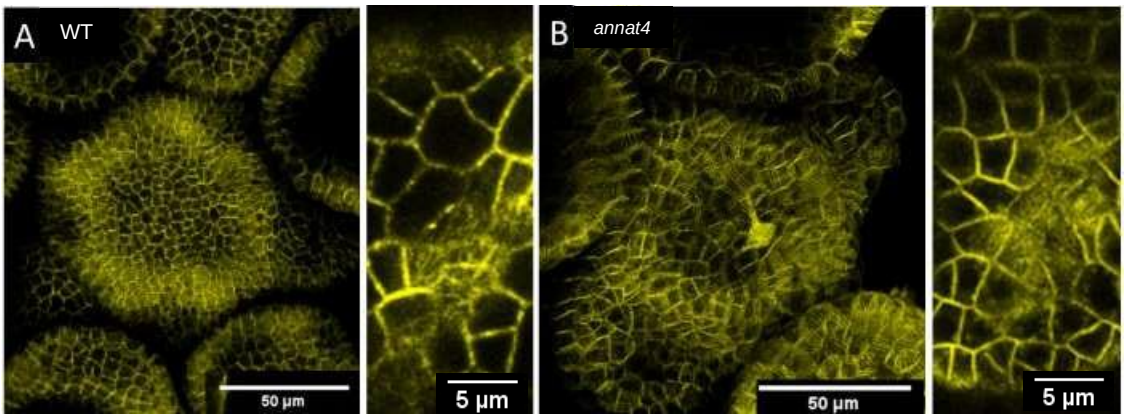

Figure 5. 6: No disruption to IQD17-YFP expression level or localisation in the *annat4* background. A depicts IQD17-YFP localisation in a WT sample and B in *annat4* mutant background. Maximum intensity projections of image stacks through the epidermal layer of the SAM are shown (left panel of A, B) and single plane images highlighting microtubule like filaments (right panel A,B). Scale 50 µm and 5 µm.

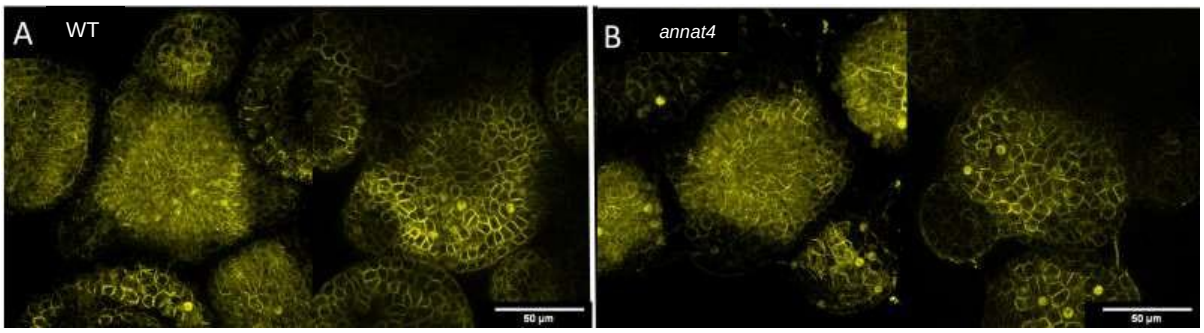

Figure 5. 7: IQD18-YFP localisation was also consistent in *annat4* mutant background. A depicts IQD18-YFP localisation in a WT sample and B in *annat4* mutant background. Maximum intensity projection of z stack images through the epidermal layer of the SAM (left panel of A, B) and single plane images (right panel)**.** Scale bars 50 µm.

To check whether meristem defects of *annat4* were associated with changes in CMT arrays, the RFP-Tubulin reporter was also crossed in to *annat4* background. The RFP-Tubulin reporter showed that microtubule orientation was not notably different in central dome meristem cells of WT (Figure 5.8A) and *annat4* (Figure 5.8B). There was a potentially higher concentration of microtubules on the cell surface in *annat*4, although this could be an artefact of the flatter dome of the meristem. Disruption of *annat4* and calcium transport across membranes impacts whole shoot growth, perhaps in part through altered microtubule behaviour, which might be mediated by MAPs such as IQDs. Nevertheless, altered calcium signalling likely results in disruption of multiple downstream molecular networks, so the potential disruption to microtubule behaviour shown in Figure 5.8 would be unlikely to be solely accountable for the severe growth defects of the *annat4* mutant.

In conclusion, sustained disruption to calcium signalling throughout plant growth did not impair 1c *IQD* expression or protein localisation. It may still stand that 1c IQDs have a functional relationship with a calcium channel not investigated. A functional relationship may exist with 1a IQDs for which similar shoot developmental process are impacted in mutants. Alternatively, cytoplasmic calcium could affect IQD's binding to other proteins without affecting IQD location, and this may modulate their function in processes such as microtubule dynamics.

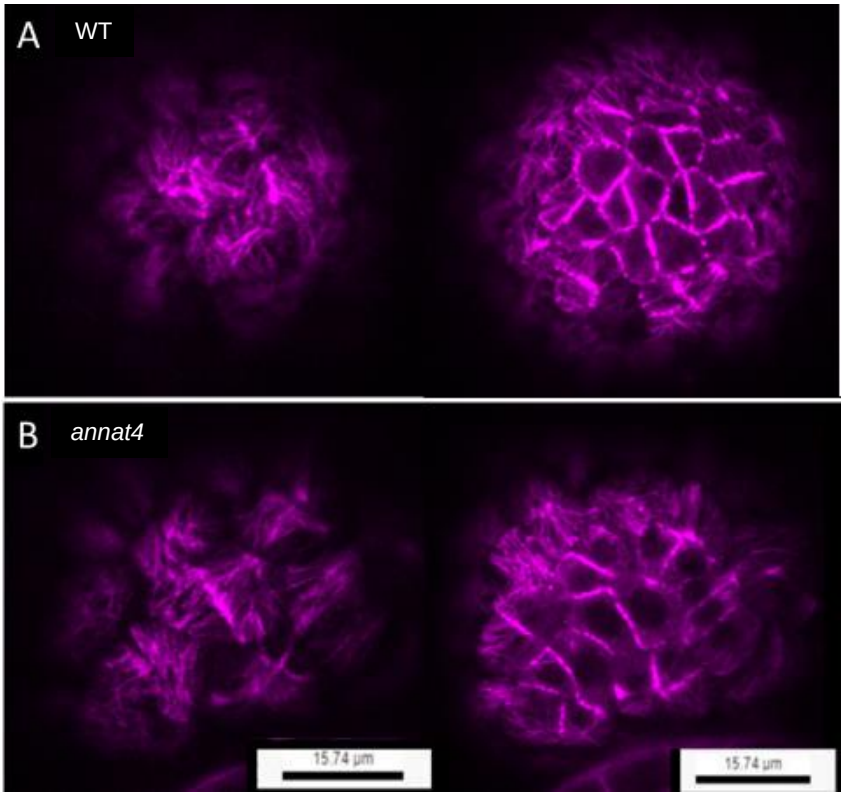

Figure 5. 8: **Similar microtubule organisation in WT and *annat4* meristems but higher concentration in *annat4*.** A: WT; B: *annat4*. In each panel, the images on the left and right show, respectively: maximum intensity projections of confocal image stacks ofRFP-tubulin, showing microtubule organisation in top central cells of the meristem and single confocal sections of top cells. Scale 15.74 µm left and right panel respectively.

5.1.1 Downstream calcium response to ectopic IQD expression

Proteins in calcium signalling networks can often have a feedback function on calcium signalling itself due to the sensitivity of cells to high cytoplasmic concentrations and requirement for oscillations (Wakelam, M.J.O. and Berridge, M.J. 2007). In light of this, a system was established to monitor calcium release events using the R-GECO calcium reporter (Dana, H. et al. 2016) after induction of ectopic levels of both 1a and 1c IQDs. Overexpression of both *IQD17* and *22* in the shoot apex resulted in shoot growth defects, however more severe stunting of shoot organs occurred in the 1a I*QD22* line (Figure 5.9). Shoot growth defects occurred following several days of gene induction via dexamethasone treatment and changes in calcium signalling that precede growth defects were investigated twenty-four hours after induction.

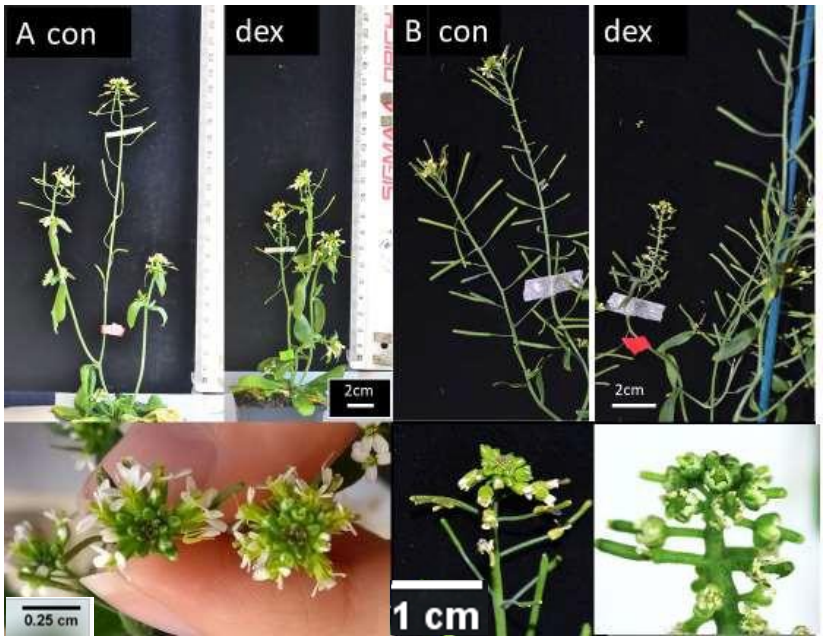

Figure 5. 9: Stunted growth and sepal defects in both ectopic 1c IQD17 line and 1a IQD22 line, with greater severity in 1a line. Inflorescence apices of *RPS5a:LhGR Op:IQD22* (B) *and Op:IQD17* (A) plants treated with 10 µM dexamethasone (A) and control (B). In both cases, solutions contained 0.1 % ethanol and 0.01% Silwet-L77 and were applied directly to the shoot apex using a paintbrush every two days, four times.

Meristems were dissected and incubated in growth media containing 10 µM dexamethasone (dex) for 24 hours prior to imaging. Maximum intensity z -stack projections of images taken every second for 10 minutes (Figure 5.10) were used to visualise cells in which calcium release occurred across the meristem of control and dex-treated samples. Threshold values were set for each sample to only detect brighter intensity than the background signal, highlighting cells with increased cytoplasmic calcium. I attempted to collect images in a single plane of the meristem, however sample growth or movement upwards in the growth medium following liquid submersion resulted in imaging several cell layers deeper than the initial plane. In lines ectopically expressing IQD22 and 17, a far greater number of cells had increased signal intensity above background levels (Figure 5.10).

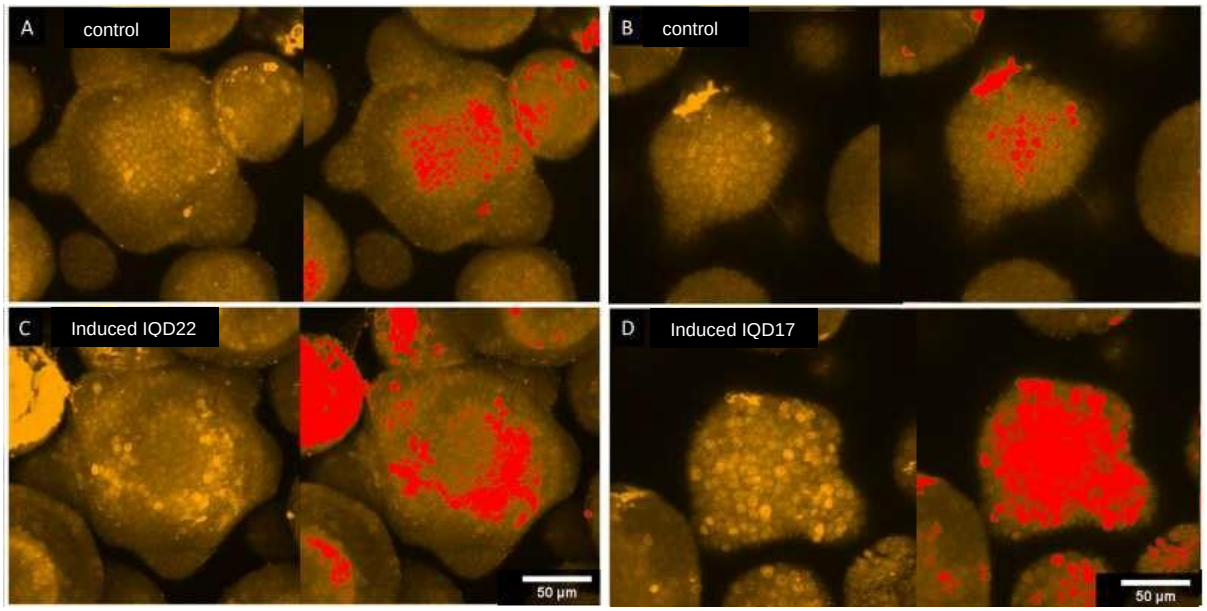

Figure 5. 10: Higher frequency of cells with calcium release events following ectopic IQD expression. Maximum intensity z stack projections of images collected ever second over 10 minutes (left panel in A,B,C,D), with threshold set according to background calcium intensity (right panel). A and B show control treated samples, C dex induced *RPS5a:LhGR Op:IQD22* sample and D induced *Op:IQD17* sample. Solutions contained 0.1% ethanol and 0.01% Silwet-L77**.** 4 biological replicates for each line.

It was important to investigate whether dexamethasone or Silwet-77 induced differences in calcium signalling irrespective of ectopic IQD protein levels. WT (Ler-0) plants expressing the R-GECO calcium reporter were subjected to both dex and control treatments confirming that they did not induce high numbers of cells with calcium release events. In fact, dex-treated controls (Figure 5.11B) appeared to have a lower frequency of calcium release events than Silwet-L77, ethanol controls (Figure 5.11A), confirming that the increased frequency of cells with raised cytoplasmic calcium was due to induction of IQD protein expression.

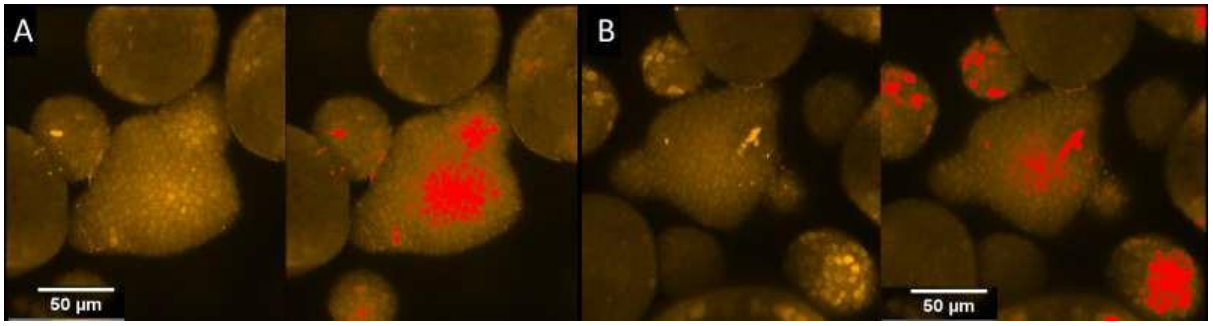

Figure 5. 11 No induction of calcium release events by control treatments. Maximum z-stack projections (left panels) with cells exceeding a threshold above background signal highlighted (right panels), as in Figure 5.10. Ler-0 R-GECO plants treated with control solutions lacking (A) or containing dexamethasone 10 µM (B). 4 biological replicates for both dex and control treatment.

To quantify the frequency of calcium release events in induced and control meristems, 20 cells were randomly selected as ROIs in the central meristem region of samples imaged from the top of the central dome every second over 15 minutes (Figure 5.12). The analysis was performed using the Imagej plugin Time-Series Analyzer, which plots a readout of signal intensity throughout the time period (https://imagej.nih.gov/ij/plugins/time-series.html; Schindelin, J. et al. 2012). As mentioned, whilst single plane of imaging was selected, the sample moves upwards during the imaging time-period, capturing the tip of the meristem dome and 4-5 cell layers beneath. The number of cells undergoing calcium release in each meristem was measured as the number of ROIs for which the Time-Series Analyzer readouts showed a sharp increase and subsequent decrease of signal at any point during the imaging period.

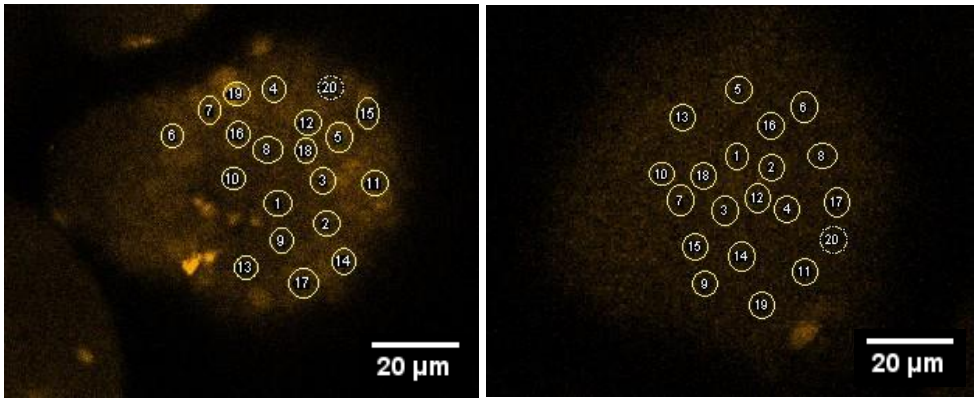

Figure 5. 12: Example of analysis of dex treated meristem (left panel) and control treated meristem (right panel) with selected ROIs displayed across the central zone of the meristem.

Using the criteria described above, the number of cells showing calcium release in each treatment is reported in Figure 5.13 below. This experiment confirmed the elevated frequency of cells in which calcium release events occurred following ectopic induction of IQD17 and IQD22 proteins. Respectively 71.25% and 75% of ROIs selected had at least one sharp increase in signal intensity versus only 26.25% and 23.75% of ROIs in the control-treated or dex-treated Ler-0 controls, indicating three times as many cells with calcium releases.

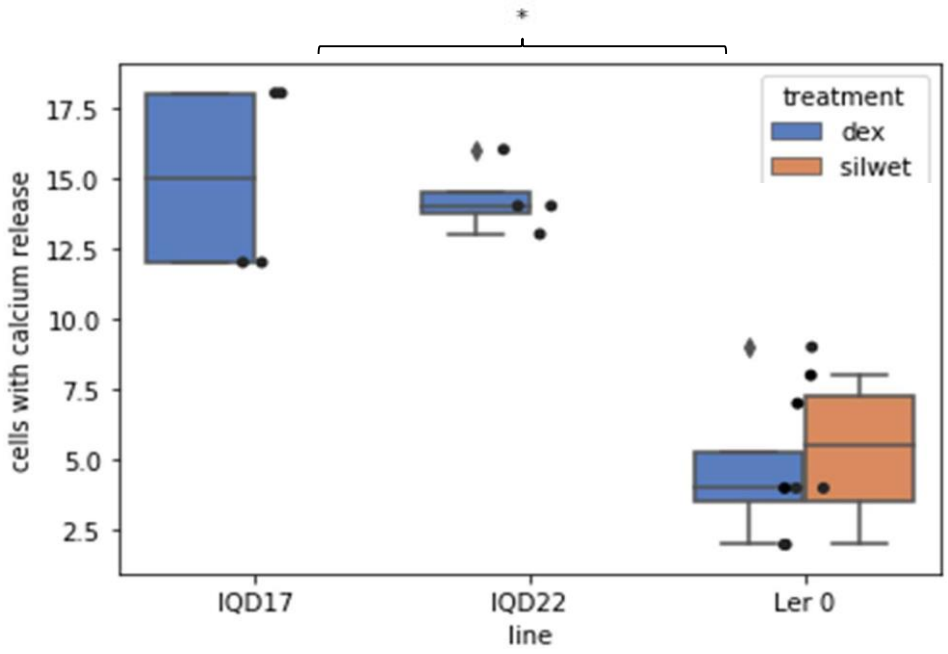

Figure 5. 13: Increased frequency in calcium release events across the central region of the meristem dome in both 1a and 1c ectopic IQD lines. A total 20 regions of interest (ROIs) were selected across the central region of the meristem as shown in Figure 5.12. The calcium release frequency of 4 dex treated inducible *IQD17* and *IQD22* meristems as well as dex and control treatered Ler-0 lines (n=4) (dexamethasone: 10 µM in solution containing Silwet L-77 0.015% and ethanol 0.1%; silwet con: same solution but lacking dexamethasone) are presented. The increase in frequency of ROIs with calcium release in ectopic *IQD17* and *IQD22* lines compared to dexamethasone and control treated Ler-0 line was significant, with p=2.747e-02 and p=2.843e-02 respectively (two-sided Mann-Whitney test with Bonferroni correction). p<0.05 *

As well as quantifying the number of ROIs in which a calcium release event occurred, the frequency of elevation events across the imaging period was calculated. The imaging frame moved through several layers of cells with potential for multiple cells to have calcium release events. Whilst any control sample analysed possessed a single observable calcium release in the time frame, in the inducible IQD17 line 25% of ROIs captured two calcium release events and 25% of ROIs showed three or more events. Ectopic IQD22 lines possessed 18.75% of ROIs with two calcium release events and 17.5% with three or more. Representative signal intensity readouts for individual ROIs are shown in Figure 5.14, illustrating the occurrence of multiple frequency changes across the imaging period in inducible IQD plant lines versus single calcium release events in control lines.

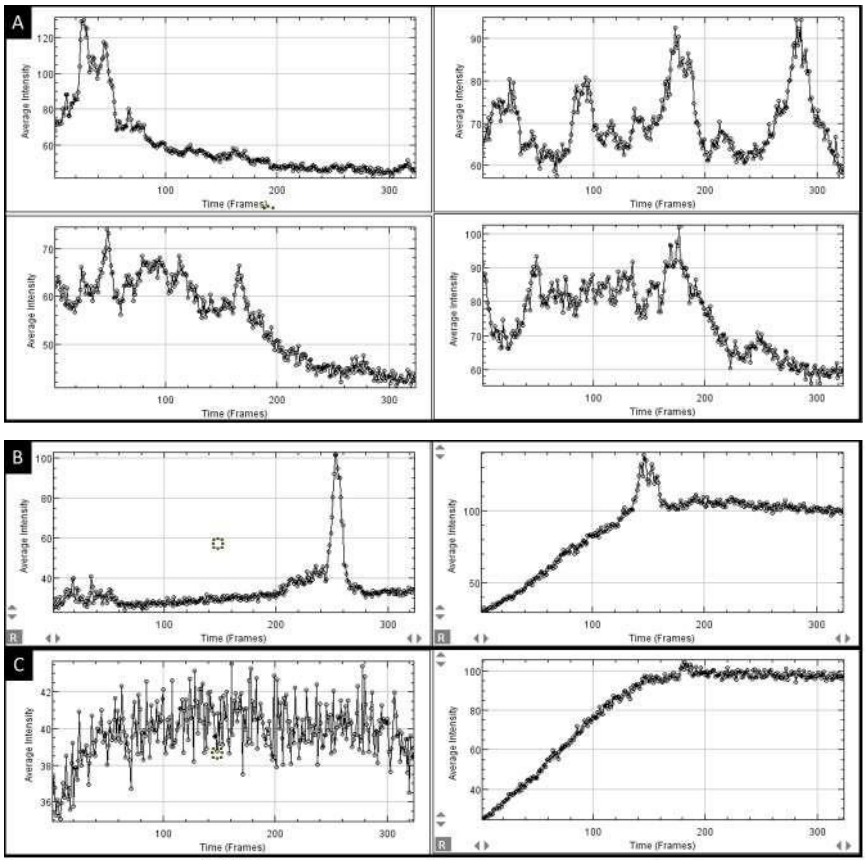

Figure 5. 14 Ectopic IQD meristems exhibit both higher frequency of ROIs with calcium release and a higher frequency of calcium release events across the analysis time frame. Signal intensity readouts demonstrating different calcium release patterns in dex-induced ectopic IQD lines (A) compared to control treated lines (B). Example of readout where no increase in frequency was observed (C). The multiple calcium release events over different cell layers in any given ROI across the 324 s time frame implicated an even greater than 3 fold increase in number of cells undergoing calcium release events shown in Figure 5.13.

In conclusion, ectopic expression of either *IQD17* or *IQD22* caused a robust increase in the frequency of meristem cells showing a pulse of calcium in their cytoplasm, as detected by the R-GECO reporter. Whilst IQD structure implicates a role for calcium in modulating their function, the impact of IQD proteins on calcium signalling itself had yet to be investigated. My preliminary findings indicate that there may be feedback regulation of IQDs on calcium signals in the plant.

1a IQDs function in pavement cell shape involving microtubules

Following establishment of the *1aiqd* line, one of my priorities was to investigate whether 1a IQDs regulate microtubule arrays. As introduced, IQD proteins have been previously linked to microtubule stability during the

development of lobes in epidermal pavement cells (PC), albeit through a very distantly related IQD subfamily 3 member (IQD5). Unlike *iqd5-1*, the *1aiqd* mutant has obvious leaf development defects, with increased leaf width and margin serrations, further prompting the question whether 1a IQDs also have a role in the development of leaf epidermal pavement cells.

To investigate changes in the leaf epidermis, I initially used phase contrast light microscopy to image imprints in 3% agarose of the adaxial and abaxial faces of the leaf base, mid-section and upper region. Three leaves were collected from three plants of each genotype. Interestingly, in contrast to the reduced lobing in the *iqd5-1* mutant, PCs of the *1aiqd* line had increased frequency of smaller and more defined lobes in the adaxial epidermis of leaves grown under both SD and CL conditions (Figures 5.15 and 5.16). The PC phenotype presented most strongly in leaves of SD grown plants (Figure 5.16). The lobing phenotype was consistent in lower, mid and upper leaf sections of all samples so the clearest imprint images were selected for figures.

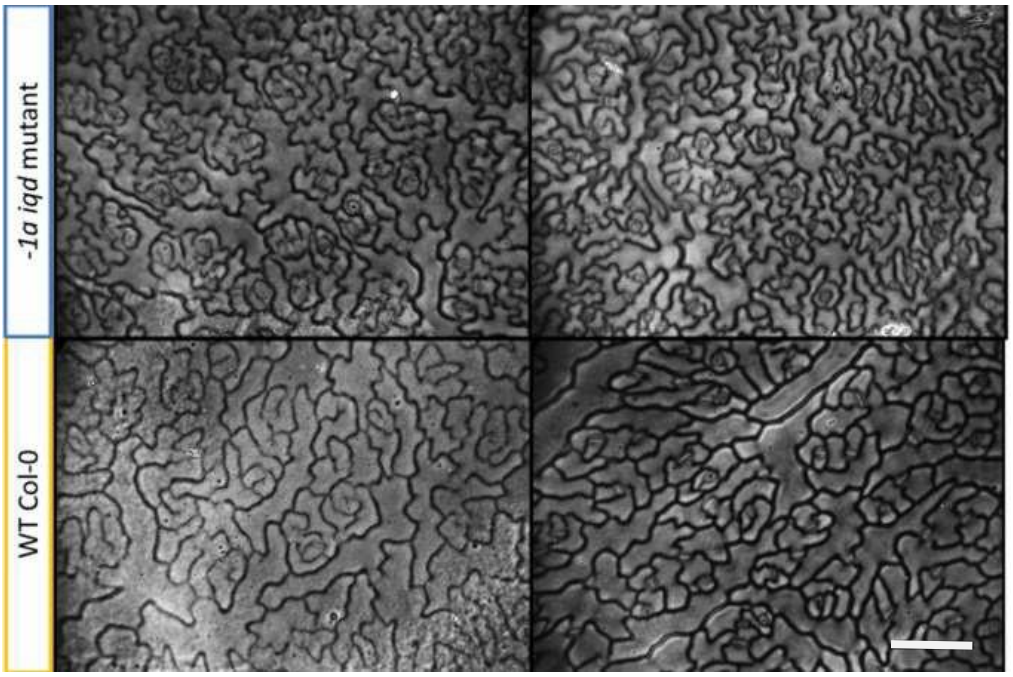

Figure 5. 15**: Increased frequency and definition of lobes in PCs of adaxial leaf surface when grown in CL.** Images acquired from adaxial leaf imprints of mature rosette leaves older than leaf 12 grown for 4 weeks at CL 16°C. Mutant (top) and WT(bottom) (each panel shows a 580 by 410 µm leaf area, scale bar 0.1 mm). Representative images out of 100 images for each genotype, collected from three leaves each from 3 plants.

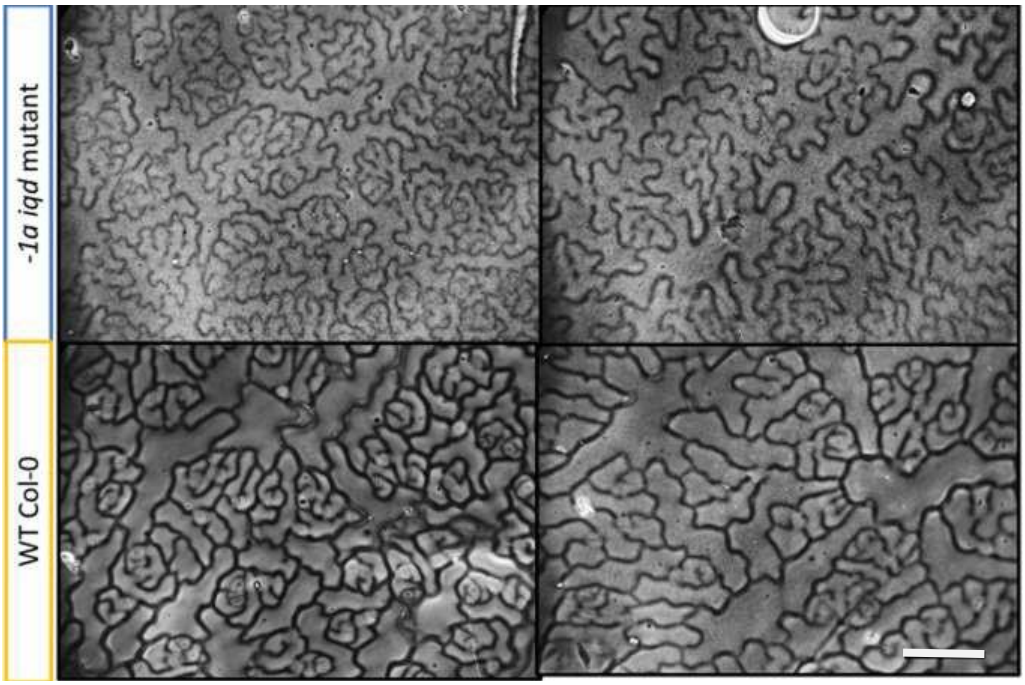

Figure 5. 16: Further pronounced increase in serration frequency and outgrowth on the adaxial surface of mature leaves grown under SD. Images acquired from adaxial leaf imprints of mature rosette leaves older than leaf 12 grown for 4 weeks at SD 20°C. Mutant (top) and WT (bottom) (580 by 410 µm leaf sections, scale bar 0.1 mm). Representative images out of 100 images for each genotype.

Differently from the adaxial side, the abaxial surface of mature leaves did not show an obvious difference in PC lobing between WT and the *1aiqd* mutant (Figure 5.17). The different effects on the two sides of the leaf could reflect the much higher degree of lobing seen on the abaxial surface. Alternatively, *1a IQDs* might be differentially expressed during development of the adaxial and abaxial epidermis.

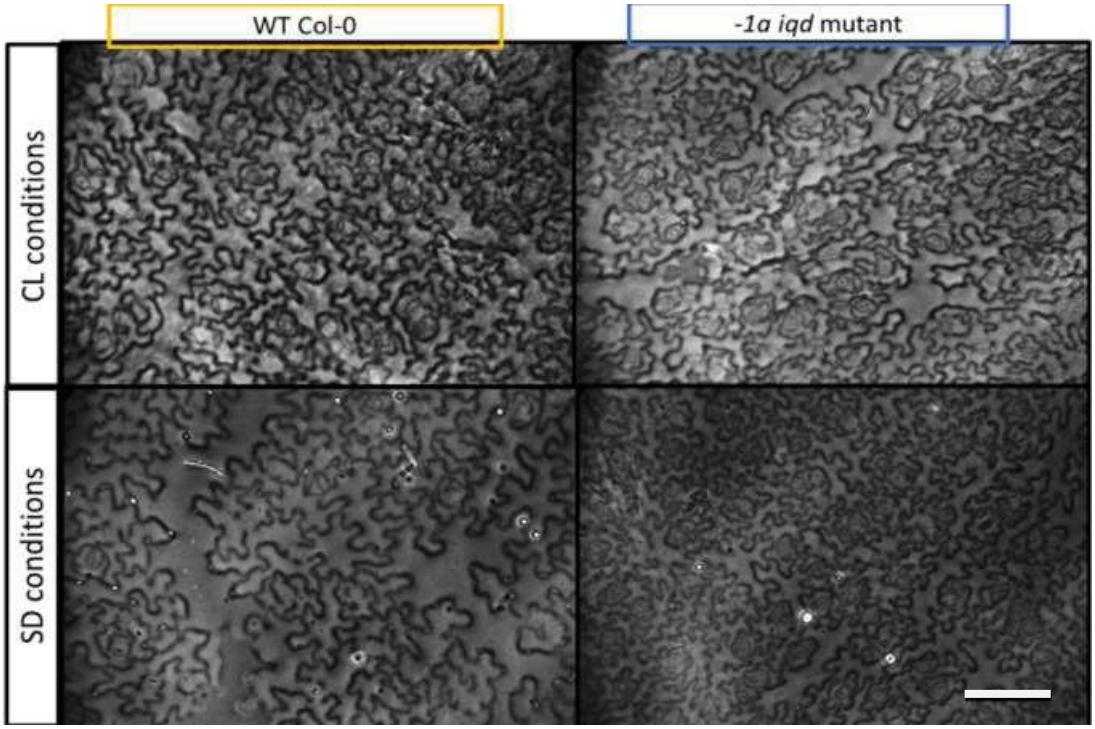

Figure 5. 17 Similar PC appearance in WT and mutant leaves abaxial surface.

Comparison of pavement cell lobe formation in the abaxial (AB) leaf surface of mature leaves older than leaf 12 of WT and *1aiqd* mutant plants grown in CL (top) and SD (bottom) conditions (scale bar 0.1 mm). Representative images out of 40 images for each genotype

To test the effect of increased 1a IQD activity, the leaf imprint experiments were also carried out using leaves of *RPS5a:LhGR Op:IQD22* plants grown on medium with and without 10 µM dexamethasone. Converse to the adaxial PC phenotype in the loss of function mutant, adaxial PCs of early leaves from plants overexpressing IQD22 had reduced definition of lobes (Figure 5.18).

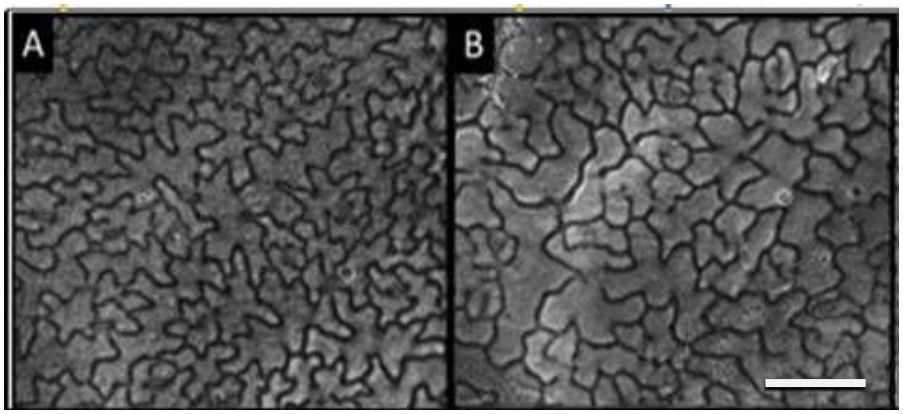

Figure 5. 18: Decreased lobing definition in lines overexpressing IQD22.

Control treated *RPS5a:LhGR Op:IQD22* (A) had pronounced lobes in the PCs of the adaxial leaf surface, but following induction of ectopic IQD22 by dexamethasone (B), lobe definition was much reduced (scale bar 0.1 mm). Representative images of 40 for each growth condition, from one leaf off three young plants.

Microtubule organisation plays an important role in fortifying emerging lobes as the interdigitated PC shape begins to develop, as well as in contributing to mechanical cell wall anisotropy that may be involved in lobe initiation (Sapala A. et al. 2018). Thus the PC lobing phenotype of the *1aiqd* mutant raised the question whether 1a IQDs altered the dynamics of MTs. Furthermore, the previously characterised cellular responses in the *1aiqd* mutant, such as disrupted division plane orientation, might also be explained by a function of family1a IQDs in microtubule dynamics.

To compare CMT dynamics in PCs of the WT and *1aiqd* mutant, the RFP-tubulin reporter was crossed into the sextuple mutant background. Unfortunately, as reported previously in Chapter 4 for auxin reporters, the T-DNA lines for *IQD22* and *IQD26* also appeared to silence the expression of the RFP-tubulin reporter. The patchy expression seen in the mutant made it difficult to find regions with enough cells expressing the reporter for a reliable comparison of microtubule organisation. With this limitation in mind, the results presented in Figure 5.19 showed no clear difference in the behaviour of microtubules in the few images of leaf PC cells in the mutant.

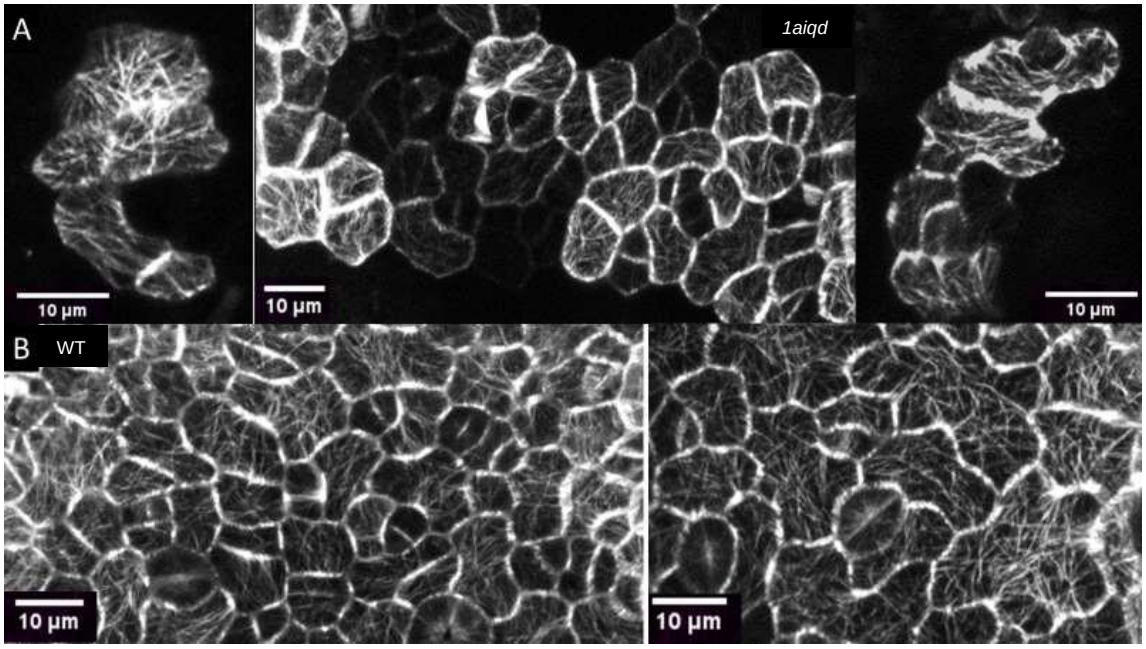

Figure 5. 19: No clear difference in microtubule organisation in limited PCs captured in first leaf of the *1aiqd* line. The RFP-tubulin reporter was imaged for immature PCs of the first leaf at 9 DAG in *1aiqd* mutant (A) and WT (B) lines. In the mutant, expression of the reporter was patchy in early leaves and subsequently absent, indicating that the reporter was silenced.

As an additional test for a role of 1a IQDs in CMT dynamics, I tested whether the *1aiqd* mutant and WT differed in their sensitivity to the MT-depolymerising drug oryzalin, as shown previously for the *iqd5* mutant (add reference). In the few mutant cells that could be imaged, treatment with 2 µM oryzalin caused a disruption of CMTs comparable to that seen in the WT (Figure 5.20).

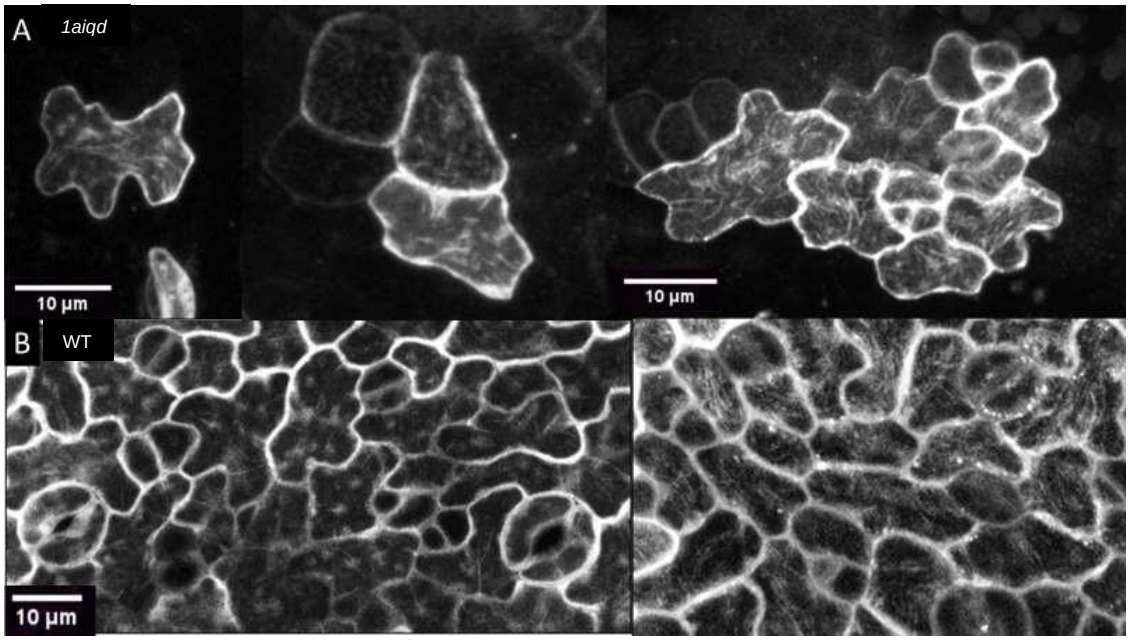

Figure 5. 20: Microtubule organisation was similarly disrupted by 2 uM oryzalin treatment of first leaf in both WT and mutant lines. Microtubule organisation in PCs of first leaf at 9DAG in the *1aiqd* mutant (A) and WT (B) lines following one hour submergence in 2 µM oryzalin solution,0.02% DMSO.

Silencing of the RFP-tubulin reporter in the *1aiqd* line was less severe at earlier stages of development, as seen in cotyledons. Microtubule dynamics is also easier to image in developing PC cells in cotyledons, which are more accessible for imaging at an early developmental stage. This prompted me to repeat the comparison of PC lobing in cotyledons. In contrast to leaves, however, imprints of *1aiqd* and WT cotyledons showed no difference in PC lobing (Figure 5.21), indicating that 1a IQDs' function in PC lobing is specific to leaves. To further investigate whether IQD function differs between cotyledons and leaves, I compared the expression of the IQD24-YFP reporter in leaf and cotyledon pavement cells. Expression was readily seen in root meristems but in cotyledons the signal was the same as the background fluorescence seen in plants lacking the reporter. Subsequent imaging of the epidermal cell layer in early leaves of transplanted seedlings confirmed that IQD24-YFP was expressed in the leaf

epidermis, where the PC lobing phenotype was observed (Figure 5.22). These results add to recent literature reporting a divergence in the mechanism of lobing between cotyledons and leaves (Grones, P. et. al. 2020).

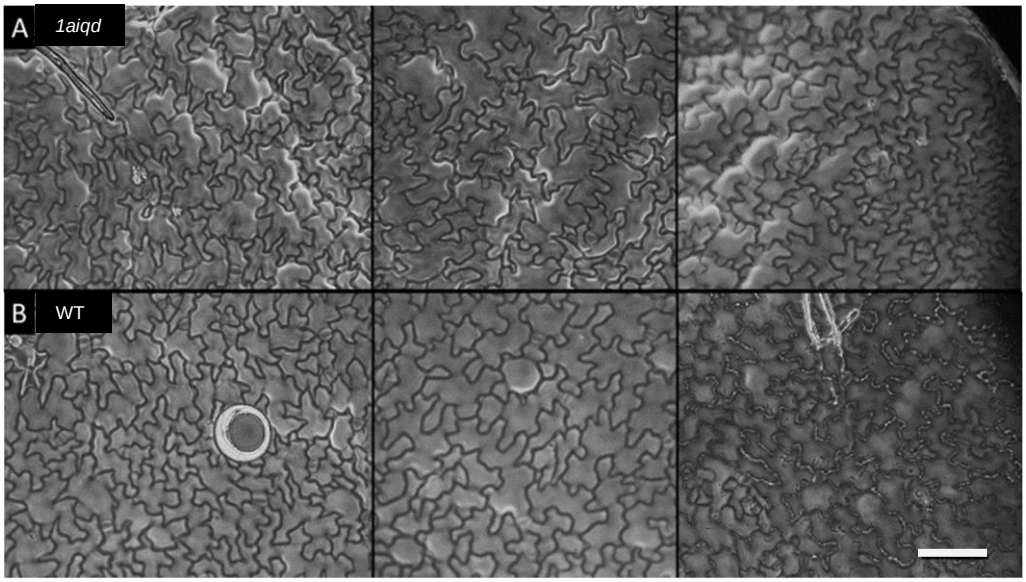

Figure 5. 21. Phase contrast images of three mutant (A) and WT (B) AD cotyledon imprints showing similar degree of lobing. Scale 0.1 mm

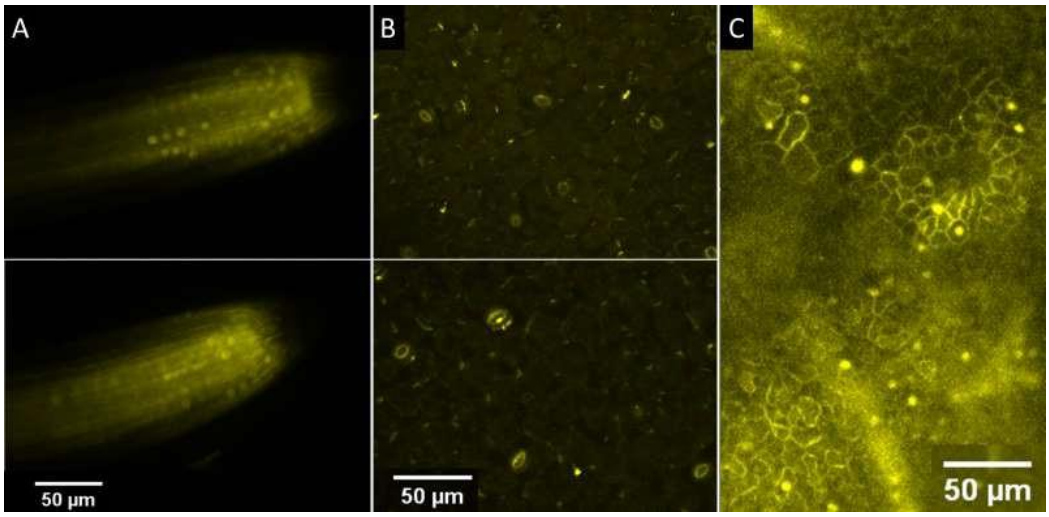

Figure 5. 22: IQD24 is absent in the adaxial epidermal cells of cotyledons but present in leaves. A: IQD24-YFP expression in root tip of seedlings. B top image shows cotyledon surface imaged in seedling positive for IQD24-YFP signal in the root tip and bottom image shows cotyledon epidermis imaged in seedling with no YFP signal in the root, as a negative control. C IQD24-YFP expression in epidermal layer of first leaf. Scale 50 µm.

In conclusion, further work is required to establish if altered microtubule behaviour is present in the *1aiqd* line that could be causal of the PC lobing phenotype in leaves, as well as the altered division planes seen in the stem.

5.1.2 1a IQD function in PIN1 distribution in the shoot meristem

Organ emergence from the SAM is one of the main developmental processes patterned by PIN1-mediated polar auxin transport. Following from the phyllotactic changes seen in the *1aiqd* mutant (Chapter 2), together with the changes in PIN1 localisation during outgrowth of leaf serrations (Chapter 4), I investigated whether 1a IQDs controlled PIN1 localisation in the shoot meristem. Changes in PIN1 patterning during primordia emergence were investigated in the mutant and compared with the defect seen in serration outgrowth. IQD24-YFP was expressed in the meristem central dome but strongly downregulated in emerged primordia (Figure 5.23A,B). This shows disparity to expression in serration outgrowth, where IQD24-YFP was up-regulated from emergence. Orthogonal view showed that whilst expression in the central dome was present in the epidermal cell layer, signal intensity was brighter in the cell layers below. Epidermal cells are where PIN1 reorientation is reported to take place. Maintenance of a high region of expression in the boundary region separating emerging primordia from the main meristem dome may again implicate *IQD* expression adjacent to PIN1 foci, suggesting that effects on PIN localisation might be non-cell autonomous.

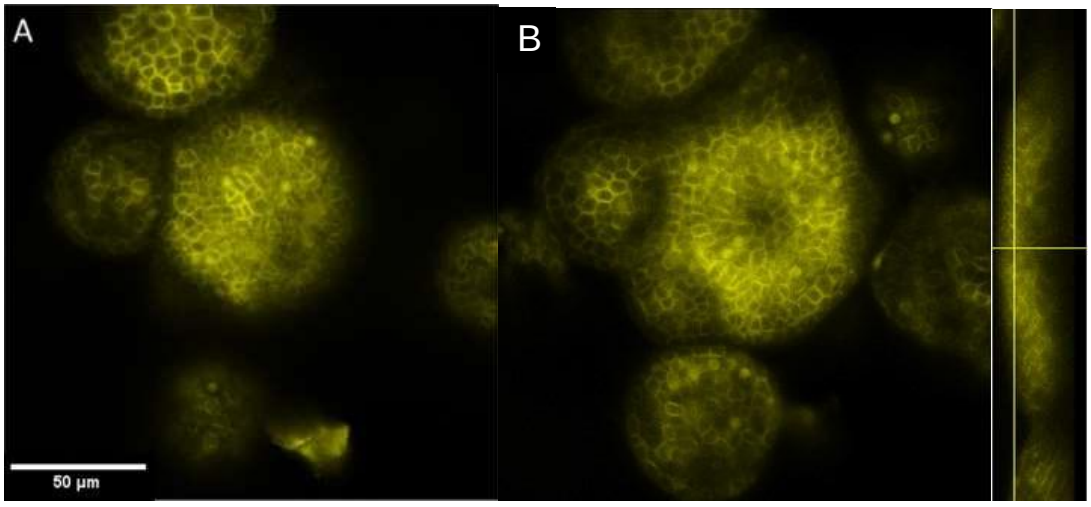

Figure 5. 23: IQD24-YFP expression was high in central region of the meristem, particularly boundary regions, and was downregulated in newly initiated primordia. Single z plane images of the IQD24-YFP reporter imaged in the meristem depicting expression in upper dome (A) and mid-region (B) as well as orthogonal view (far right panel) corresponding to plane of A, showing higher expression in the subepidermal layer of central dome and organ boundaries

To compare PIN1 localisation in the WT and 1a IQD mutant, the PIN1-GFP reporter was crossed to the mutant, but as reported in previous chapters, the reporter became silenced in the sextuple mutant background. For this reason, I compared PIN1-GFP between the WT and a partial loss of function line (heterozygous for *iqd22*-1and *iqd26-3*). The switch to bijugate phyllotactic pattern had low penetrance in full sextuple *1aiqd* mutant, and it appeared a lesser degree of altered patterning occurred in primordia emergence in the line heterozygous for *iqd22-1* and *iqd26-3* (Figure 5.24) While partial loss of function lines never presented universal organ pattern changes, a low frequency of around 20% have occurrence of some primordia initiating opposite one another in the SAM. In this experiment 1 in 4 of the samples had divergence in primordia patterning from WT with this frequency supported by imaging of 10 *iqd24,25,26,27* loss of function line apices (not presented). Given that the partial loss of function line retained PIN1-GFP expression, while still showing some disruption of phyllotaxis, it was used to monitor changes in PIN1-GFP in comparison with the WT.

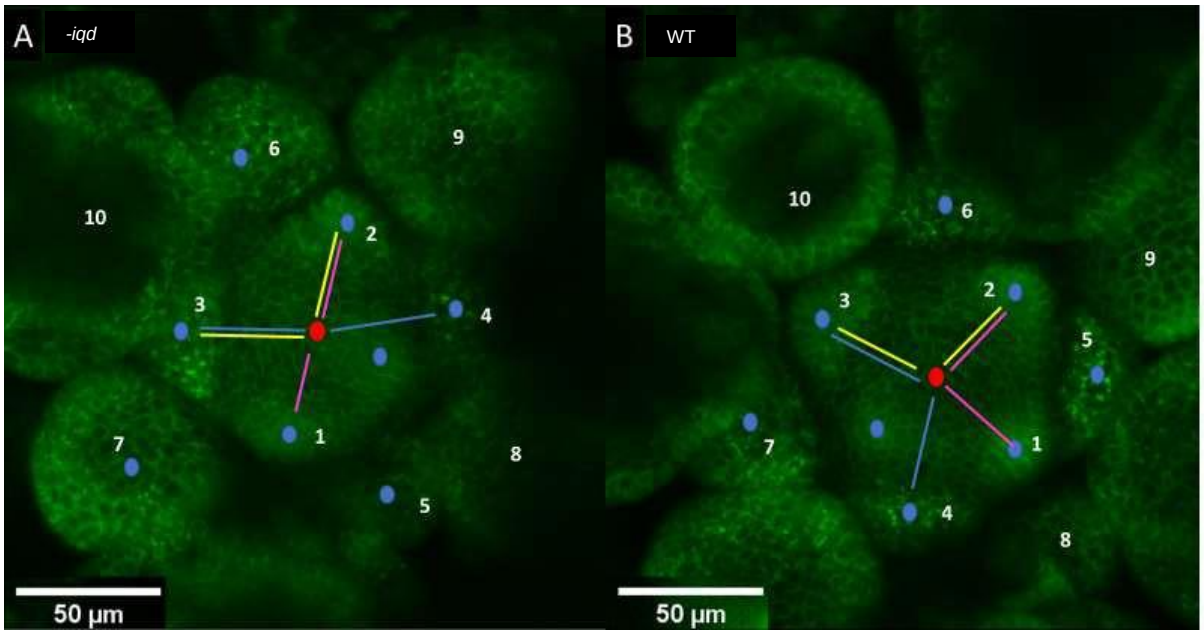

Figure 5. 24: Several primordia emerge at angles close to 180 degrees in the line with partial loss of *1a IQD* function. Mutant A WT B. Divergence from spiral phyllotaxis in the mutant. Angle between first and second primordia marked in purple and between second and third primordia marked in yellow. Angle between third and fourth primordia marked in blue. Successive primordia numbered up to 10.

Figure 5.25 indicates a potentially stronger polar localisation of PIN1-GFP in early primordia of WT meristems than in the partial loss of function line, however the difference in PIN1-GFP localisation was far less clear than in leaf serrations. In sections through early primordia, polar localisation of PIN1 only occurred at the tip

of growing primordia in the mutant (Figure 5.25C) but extended over a broader region in WT primordia (Figure 5.25D). This suggested again that PIN1 polar patterning may be disrupted by loss of 1a *IQD* function, but the relatively subtle and qualitative observations should be tested further using quantitative methods, and with a more severe loss of 1a *IQD* function. The results in the SAM may also differ from leaf serrations due to *IQD* expression, which was clearly upregulated in serrations but downregulated in emerging primordia, indicating differences between IQD function in the two processes.

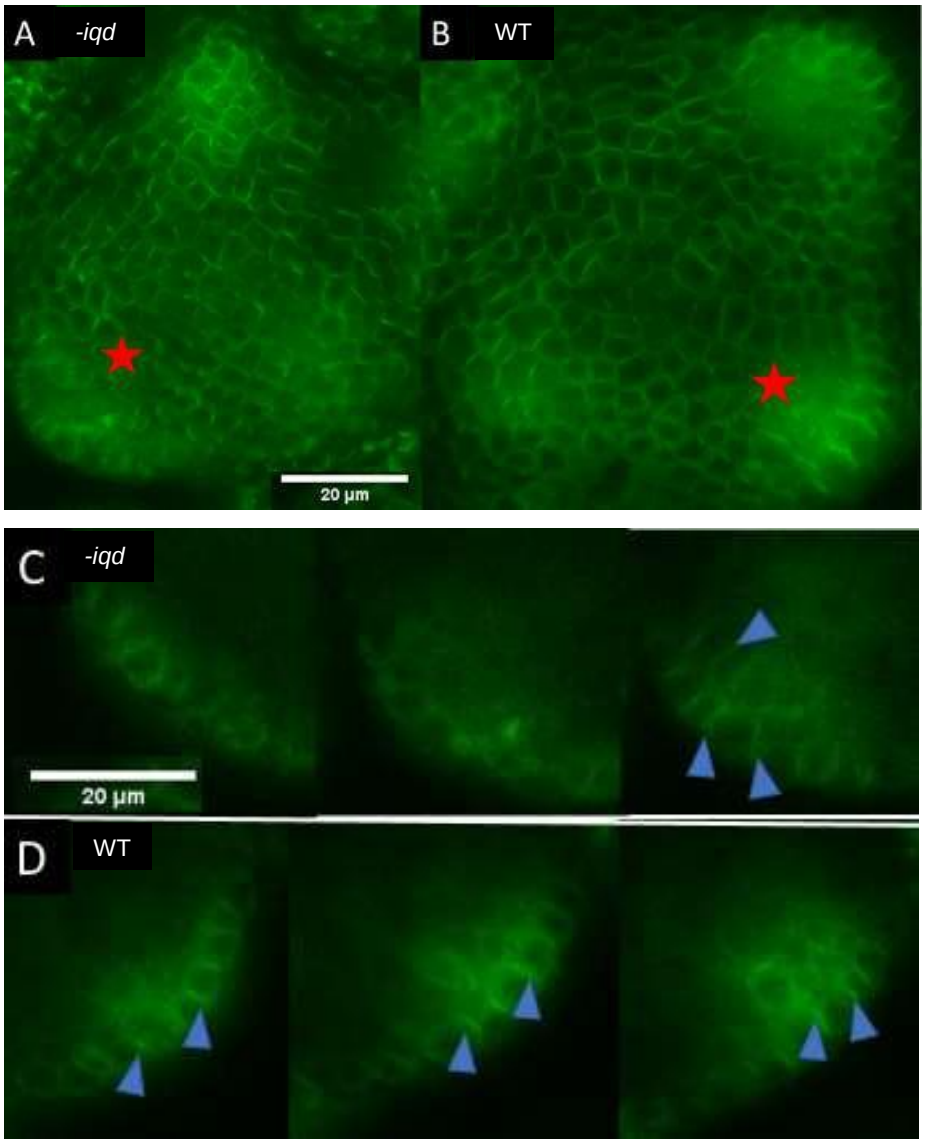

Figure 5. 25: Potentially reduced PIN1 polar localisation in emerging primordia after partial loss of 1a IQD function. A and B show maximum intensity projections of image stacks taken through meristems expressing a PIN1-GFP reporter in a mutant line with partial loss of 1a IQDs (homozygous for *iqd23,24,25,27* and heterozygous for *iqd22*-1and *iqd26-3*) and WT meristems, respectively. Red stars highlight emerging primordia. C and D show vertical sections of the same image stacks as in A and B, respectively; the vertical sections were taken through the earliest visible primordium, starting when increased PIN1-GFP intensity is seen at the perimeter of the central meristem dome. Blue arrows depict cells where polar PIN1 localisation occurs (scale bars 20 µm)

As mentioned above, a non-cell autonomous role for IQDs was suggested by the slight discrepancy between IQD24-YFP expression and the location where PIN1-GFP localisation appeared to be disrupted in the mutant. One hypothesis for this is that 1a IQDs might change how mechanical stress affects PIN1 localisation. As introduced, research in tomato meristems showed that increased pressure on the PM through hypo-osmotic conditions resulted in increased PIN1 protein localisation at the PM. This result was consistent with other membrane tension assays such as DMSO treatment and variation in temperature (Nakayama, N. et al. 2012).

To explore whether 1a IQDs might regulate responses to mechanical stress, I assessed the sensitivity of PIN1 localisation to an increase in pressure induced by hypo-osmotic conditions between the partial loss of function mutant and WT lines. Both lines were treated for one hour in 0.2 M mannitol followed by 1.5 hours in water. PIN1-GFP in mutant plants seemed less sensitive to the transition to hypo-osmotic conditions, compared to the WT (Figure 5.26 vs Figure 5.27). The WT showed a slight increase in localised PIN1 following the hypo-osmotic treatment, although it was much more subtle than observed in the cited paper.

Overall, in all four biological replicates, PIN intensity seemed to be lower in WT background at 0.2M mannitol and then to show a greater increase at the PM upon movement to hypo-osmotic conditions. Signal intensity at the PM appeared to differ less in all mutant samples at varying osmotic pressures, however there was variation in this, as presented in Figure 5.26. Given the subtle differences in PM localisation in WT samples, a firm conclusion could not be made. However, these results encourage investigating further the hypothesis that 1a IQDs promote the response of PIN1 to mechanical signals.

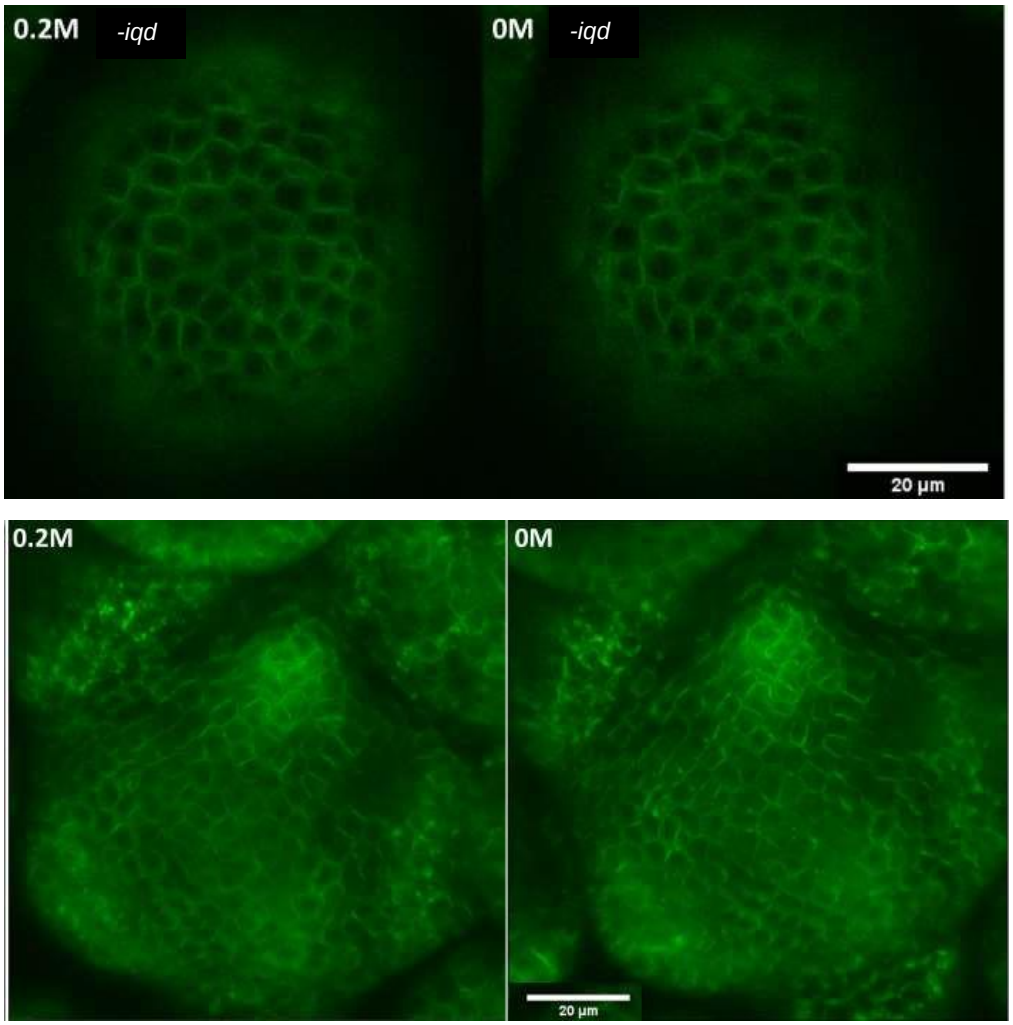

Figure 5. 26 Weak response of PIN1 polar localisation in response to hypo-osmotic treatment in the partial loss of *1a IQD* function line, although subtle differences in the WT controls (Figure 5.27) prevented a strong conclusion being drawn. Mutant meristems heterozygous for *iqd22-1 and iqd26-3* T-DNA mutations expressing the PIN1-GFP reporter. Upper images show PIN1 localisation in a single plane at the top of meristem domes after resting in 0.2M mannitol solution for one hour, then re-imaged after submergence in 0M mannitol solution for 1.5 hours. Bottom images show z-stack maximum intensity projections of a different mutant meristem. A limited increase in PM localisation of PIN1-GFP was more clearly visible in sample B, although this sample has the greatest response of four mutant line biological replicates. (scale 20 µm)

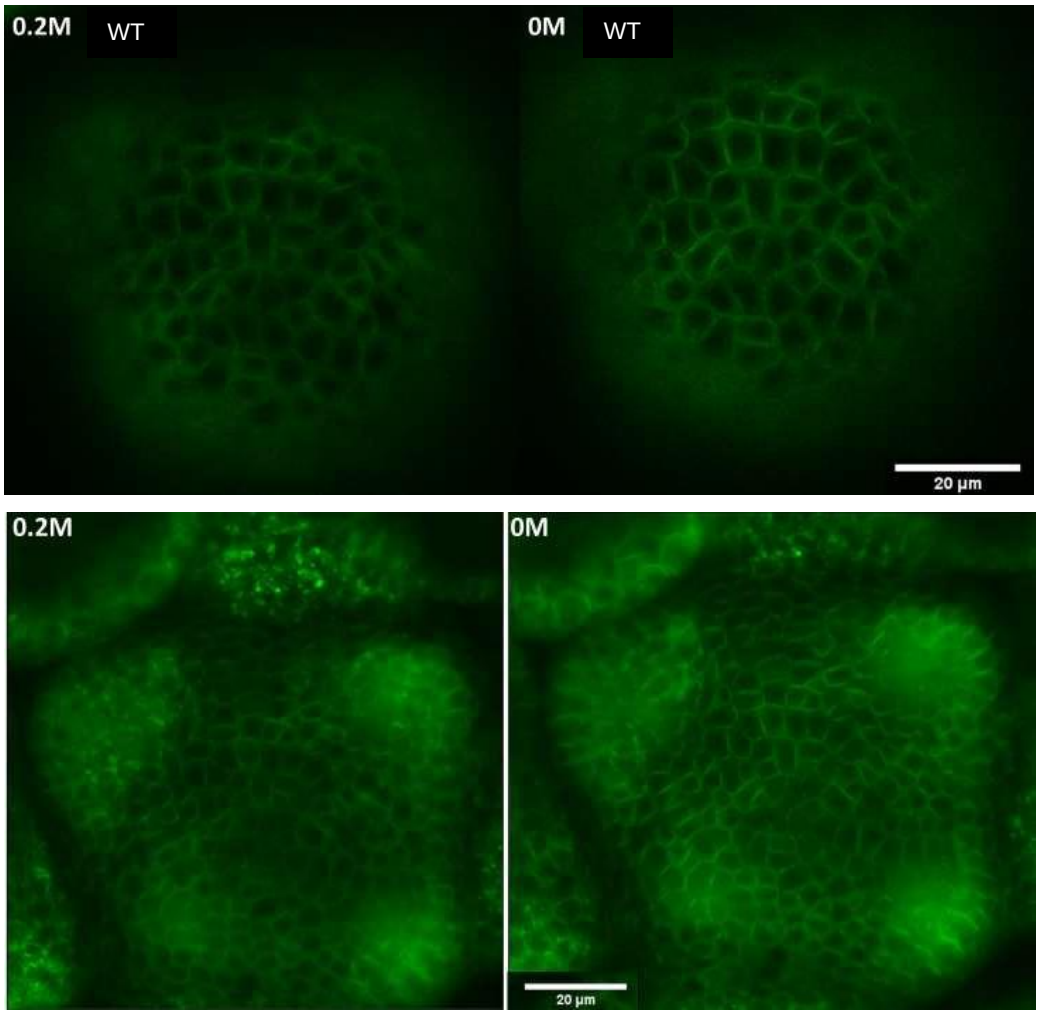

Figure 5. 27 A greater increase in PIN1-GFP PM localisation could be observed in WT samples following hypo-osmotic conditions, although still relatively subtle. Upper images show PIN1-GFP localisation in single plane at top of a WT meristem dome after resting in 0.2M mannitol solution for one hour then re-imaged after submergence in 0M mannitol solution for 1.5 hours. Bottom images show maximum intensity projections of the same meristem. All treated WT samples had similar response, n=4, scale bar 20 µm.

5.3 Discussion

Early experiments were performed to answer the question of whether differing calcium concentrations could perturb CMT and nuclear localisations important for IQD function through altered calmodulin bound states, or whether it was more likely this impacted function without changing IQD localisation. Results indicated that localisation at microtubules and movement to the nucleus is independent of changes in cellular calcium concentration and calmodulin bound state. Subsequently, supporting results were published finding that separate regions of IQD proteins are involved in CM binding and MT binding (Yang et al., 2018). Thus, IQDs likely recruit CM/CML proteins to given cellular localisations, where function is regulated by CM binding. Indeed, since this preliminary experimentation, assays have shown CM re-localisation to IQDs at microtubules in vitro (Burstenbinder,K. et al. 2017; Mitra,D. et al. 2019).

Calmodulins display nucleo-cytoplasmic partitioning and bind membrane-associated proteins, with most of their binding partners being cytosolic or nuclear proteins. Positioning of calcium sensors is important for locally generated calcium concentrations upon release from stores, as well as specific signalling in the nucleus. Required positioning of CMs match those conferred by IQD re-localisation of free CM. Therefore, IQDs could function by localising calcium sensor proteins to sites of calcium signalling. This could be important for correct signal transduction to downstream CM interactors, or indicate IQDs themselves are sensitised through their localisation for modification of function upon calcium concentration changes.

Instances may exist where CM/CML proteins compete for binding with other interactors, or in which they facilitate additional protein-protein interactions allowing assembly of protein complexes with specific function. Calmodulin binding has been inferred in terminating a given function, for example KCBP (Buschmann H et al. 2015) as well as initiating cellular functions (Yang, T. Poovaiah, B. W. 2002). Termination of IQD function by CM binding is supported by the loss of elongated twisted organs, similar to those in *spr2* mutants, in the ectopic *OsIQD14* line following additional ectopic expression of CM1. CM is hypothesised to prevent binding of SPR2 to IQD14, thus SPR2 retains activity altering microtubule behaviour (Yang et al. 2018). This further supports calcium signalling's ability to alter microtubule dynamics through calmodulin binding MAPs, including IQDs, which may interact with other MAPs depending on cellular calcium concentration.

The different growth response of different IQD ectopic lines could not only be based on differential decoration of CMT arrays and direct IQD function as MAPs, but also rendering different binding partners non-functional through excess IQD sequestering them.

A clear increase in the frequency of cells with calcium release events in the meristem occurred well before macroscopic growth defects in ectopic IQD lines. Thus my results indicated that IQDs can also feed back on calcium signalling. Sequestering of CM/CML proteins by excess IQD, reducing the response to calcium signals in the cell, may in turn lead to an indirect increase of calcium release. Future work can determine if cellular calcium release is directly impacted by IQD protein levels by studying R-GECO behaviour in the *1aiqd* line. If a reduced frequency of calcium release events occurs in the loss of function background, direct impact could be inferred, but if there is no impact, this would indicate that increased signalling in ectopic lines is induced following disruption of calcium sensors such as CM/CML. The importance of calmodulin interactions for IQD function itself can be inferred by complementing the array of phenotypes in the *1aiqd* line with 1a IQD proteins featuring inactivated IQ67 domains. Use of IP-MS to pull down YFP in IQD24-YFP plant lines could also reveal any novel protein interactors that could be specific to subfamily 1a.

Further work sought to establish what function 1a IQDs may possess in modulating microtubules. In mature leaves of *1aiqd* plants, PCs had more frequent, narrower and more pronounced lobes than WT. The PC lobing phenotype in the adaxial surface of *1aiqd* mature leaves was opposite to that in the adaxial surface of cotyledons in the *iqd5-1* mutant, where lobes were less pronounced. The literature on ectopic *IQD* expression phenotypes supports family 1a lobing phenotypes in gain of function, with over-expression of 1a *IQD25* reported to have reduced definition of lobes (Burstenbinder, K. et al. 2017), as seen with *IQD22* (Figure 5.19). *IQD5* is a member of subfamily 3a in Arabidopsis, the most divergent from subfamily 1a (Chapter 1, Figure 1.1). It is not impossible that such a large and diverse gene family has evolved different cellular functions through modulation of similar cellular components. In the case of *iqd5,* a function in stabilising the concentrated microtubules at neck regions was proposed (Mitra,D. et al. 2019). Localisation patterns appear conserved to elements such as microtubules across the whole family, and therefore subfamily 1a IQD proteins could also impact microtubule behaviour, however one that modifies PC shape in an opposing way.

Imaging of the IQD24-YFP reporter implied that 1a IQD function in PCs is organ-specific, with a role in developing leaves but not in cotyledon PCs. Attempts to gain insight into microtubule organisation and oryzalin sensitivity in the adaxial surface of early leaves failed due to patchy expression of the reporter, likely due to silencing. The exact functions involving microtubule dynamics and PC shape in leaves are therefore yet to be unveiled in the *1aiqd* line. Based on the literature that links microtubule behaviour to PC lobing, increased frequency may involve a faster or stronger microtubule response to newly detected stress sites at the cell wall. Even small buckles on the cell wall may be re-enforced enough to induce differential growth as the cell expands. Therefore, a sensitised microtubule response to stress could be proposed that could result in faster re-orientation. Alternately, microtubule behaviour could vary in regions controlled by ROP domains, pre-determining the anisotropy of cell wall mechanics. Either microtubules highly sensitised to destabilisation or divergent ROP domains could be proposed, whereby ROP activity would more readily generate cell wall mechanical anisotropy to promote lobe outgrowths.

Further work is required to investigate the hypothesised divergent microtubule behaviour in the *1aiqd* line. To circumvent the difficulties of using the RFP-tubulin reporter in the *1aiqd* background, MT immunolocalisation could be used. The latter could also help in future investigations of MT organisation in the stem pith and leaf serrations, where *IQD* expression is concentrated in deeper cell layers. Overcoming the tendency of the sextuple mutant to silence reporter lines will be important since live imaging will still be required to capture dynamics and shed light on whether family1a IQDs do possess a function in microtubule behaviour during cell and tissue growth.

The result separating 1a IQD PC function in cotyledons and leaves is intriguing in the light of recent literature showing a strong role for PIN proteins in PC lobing in leaves, but not in cotyledons (Grones, P. et al. 2020). The involvement of auxin transport and gradients in pavement cell shape has been questioned after the PIN1-AUXIN BINDING PROTEIN-1(ABP1) ROP activation mechanism was discredited and subsequently normal PC lobing in cotyledons of auxin transport mutant plants (Belteton S.A. et al. 2018). Work in early leaves, however reiterated a role for auxin transport and fluctuating auxin gradients in lobe formation, whilst confirming that cotyledon PCs were not affected (Grones, P. et. al. 2020). This paper observed dynamic changes in auxin concentration as PCs formed lobes, accompanied by dynamic changes in PM localisation of auxin

transporters such as PIN3 and AUX1. Unanimously, papers in both cotyledons and leaves report exogenous auxin application increases PC size and lobe number, indicating that cellular auxin concentration impacts PC growth, including lobing. How intrinsic auxin is for the initiation of lobes remains controversial, but varying auxin concentration at different lobe development stages, including prior to first lobe forming, would place auxin upstream in a mechanism for lobe initiation in PCs of leaves (Grones, P. et al. 2020). Therefore, IQD interplay with PIN localisation, including others not investigated by reporters such as PIN3, PIN4 and PIN7, which are linked to PC and xylem auxin transport, could be causal of increased lobing in *1aiqd*'s PCs. It could also be interesting in future work to use reporters for other PIN family members such as PIN3 to investigate association with PC and stem growth phenotypes involving auxin in the family 1a loss of function mutant line.

Whilst PIN1 distribution according to mechanical stress patterns appears independent of microtubule organisation in growing meristems (Heisler, MG. Hamant O. et al. 2010), altered microtubule dynamics in the *1aiqd* mutant could disrupt cell division planes, for which microtubule organisation features at multiple stages (Dixit, R. and Cyr, R. 2004). Altered mechanical signals across growing tissues would impact other elements directed by stress patterns, such as PINs. This in turn could lead to further shoot growth modification through changes in auxin gradients, which could be associated with cell proliferation in *1aiqd* phenotypes, as well as organ initiation and patterning.

PIN1 localisation is sensitive to stress felt at the PM of cells (Nakayama, N. et al. 2012) and one of the postulated mechanisms for a mechano-sensing mechanism is via touch activated calcium channels positioned at the PM (Braam, J. 2005; Li, T. et al. 2019). IQDs may function in a non-cell autonomous way, featuring as a component in the calcium signalling mechanism directing PIN orientation according to stress patterns. The results presented in this chapter, however, were not strong enough to tie partial loss of IQD function to reduced PIN1 PM localisation directed by mechanical stress. A process inducing strong PIN1 relocalisation according to stress in Arabidopsis meristems is cell ablation (Li. T et. al. 2019), which could be used in mutant and WT backgrounds to investigate whether PIN1 orientation around ablation sites is impaired in the mutant line.

In conclusion, in contrast to the progress in understanding the cellular defects that contributed to the shoot growth phenotypes caused by loss of 1a IQD function, identifying the molecular functions underlying these cellular changes was

not as successful. Future work aiming to achieve this is detailed and expanded further in the final discussion.

Chapter 6 Subfamily 1a IQDs' regulation of plant growth in relation to the DELLA pathway

6.1 Introduction

In Chapter 4 I explored links between subfamily 1a IQDs and auxin signalling, directed both by literature and the leaf serration phenotype in the *1aiqd* mutant. In this chapter I studied links to another hormone with important roles in organ growth, gibberellin.

DELLA proteins function to repress the gibberellin signalling pathway, which is important for processes such as seed germination, flowering and elongation growth. A total of five DELLA proteins have been identified in *Arabidopsis thaliana* and two, *GA INSENSITIVE (GAI) and REPRESSOR OF ga1-3* (*RGA*), are associated most strongly with the control of elongation growth. Whilst possessing strong gene regulatory activity, DELLA proteins do not possess DNA binding domains. Instead, they interact with other transcription factors, which target them to DNA sites to alter gene expression, in many cases repressing transcription (Park, J et al. 2013).

DELLA function is in turn inhibited by gibberellin (GA), which promotes DELLA binding to the GIBERELLIN INSENSITIVE DWARF (GID1) receptor, leading to DELLA degradation through a ubiquitin proteasome–dependent mechanism involving the F-box protein SLEEPY1 (SLY1). The DELLA domain is key for degradation, as identified in GA insensitive mutants such as *rga- Δ17*. DELLAs have been shown to positively regulate GA synthesis, showing that a feedback loop moderates their strong restriction of growth (Yoshida, H. et al. 2014).

In the *rga-Δ17* gain of function mutant, restriction of elongation growth results in severely dwarfed shoot organs, including repressed leaf expansion and reduced stem internode elongation. Further phenotypes include dark leaf pigmentation and delayed flowering time. Research into DELLA function also unveiled promotion of boundary genes in association with initiation of lateral

branching (Martinez-Bello et al. 2015; Müller D and Leyser O. 2011) and association with compound leaf complexity in tomato, where increased expression of KNOX genes downregulate GA biosynthesis (Connie Champagne, C. and Sinha, N. 2004).

Whilst initial research revealed that high GA levels promoted cell expansion driving growth, particularly in stem elongation (Yang T. et al.1996; Ubeda-Tomas S. et al. 2008), it was subsequently shown that levels of DELLA proteins can also moderate cell division (Achard P. et al.2009). Research investigating how GA levels promote leaf expansion found both cell elongation and division contributed to the phytohormones' impact (Xu, Q. et al. 2016). Direct targets of DELLAs regulate division, such as *STUNTED* (STU), which promotes cell proliferation through interaction with cyclin-dependent kinase inhibitors, and is downregulated by RGA (Yen, L. et al. 2012). Such fundamental process in plant growth are often regulated by genes with universal impacts on shoot growth.

As highlighted in Chapter 2 and the general introduction, subfamily 1a *IQD* genes have been reported to be up-regulated by the DELLA protein RGA (Zentella, R. et al., 2007). Further to this, a published abstract implicated that double and triple loss of function mutants (*iqd22,23,24*) in subfamily 1a were hypersensitive to GA treatment, whilst over-expression lines were insensitive (Zhou, X. and Sun, T., 2011), insinuating a function downstream of RGA in reducing GA responses, in turn facilitating growth restriction by DELLA proteins.

Interaction between 1a IQDs and DELLA proteins was also suggested by ChIP-seq experiments performed in my research group for RGA (Serrano-Mislata, A. et al. 2017). Binding peaks occurred close to the *IQD22*, *IQD24, IQD25* and *IQD27* loci, although only weak binding was seen for *IQD23* and *IQD26* (Figure 6.1). Overall, the available evidence at the start of my work supported an interplay between subfamily 1a IQDs and DELLA proteins.

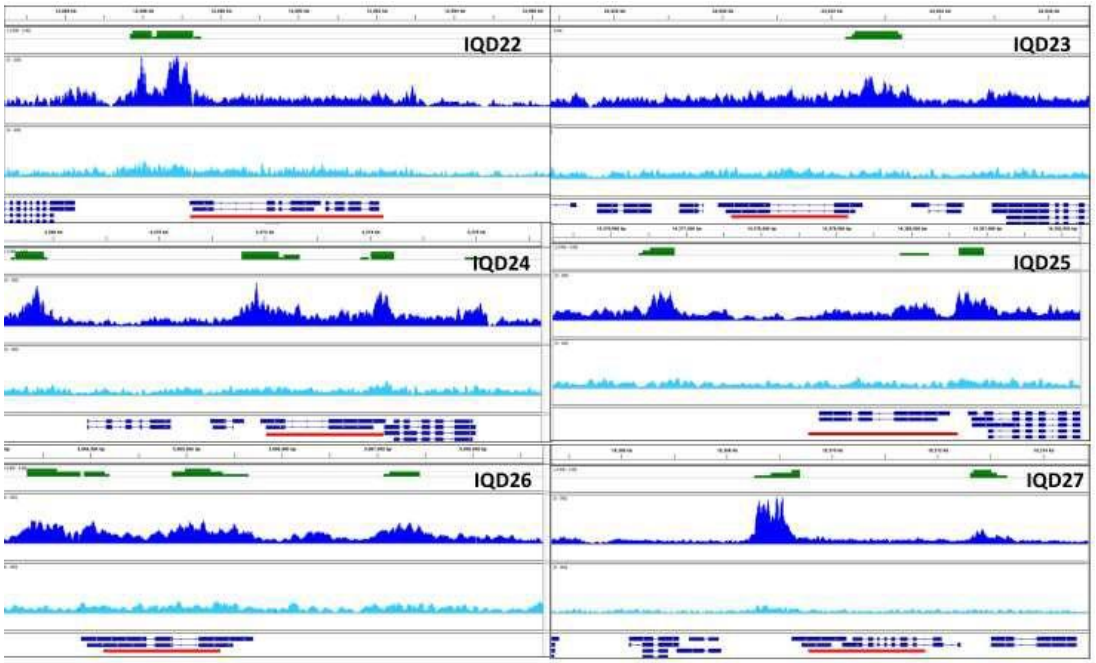

Figure 6. 1. RGA binding peaks were located within or in the vicinity of several 1a *IQD* genes. Binding peaks identified by chromatin precipitation - high throughput sequencing (ChIP-seq) in 1a *IQD* gene regions (Serrano-Mislata, A. et al. 2017) highlighted with green and present in three biological replicates with statistical significance compared to controls, shown for each locus in light blue. *IQD* gene location underlined in red.

6.1.1 Aims of this Chapter

Genes controlling variation in shoot height and growth often function either as transcription factors that regulate cell cycle progression or in phytohormone metabolism and signalling (Busov V. B. et al. 2008). *IQDs* impact whole shoot architecture and have been linked to key growth regulating phytohormones such as auxin and GA. There are similarities between the growth effects of subfamily 1a IQDs and DELLAs: plants with gain of 1a IQD function presented severely repressed elongation of shoot organs, while loss of function resulted in increased leaf and stem growth (Chapter 3 and 4). Enhanced growth in *1aiqd*' shoot organs appeared to be linked to an increase in cell proliferation, which GA has been shown to promote. Based on these data, it could be proposed that RGA upregulates IQDs, which then contribute to the repression of shoot growth by restricting cell division. On the other hand, phenotypes such as increased lateral branching and increased radial rather than elongation growth suggest different functions not associated with GA signalling.

Research in this chapter aimed to investigate a link between IQD function and DELLAs, using both genetic and biochemical analyses. Whether a feedback relationship between IQD proteins on DELLA protein levels contributes to IQDs growth repressive function is investigated, as well as the importance of IQD function for growth repression downstream of DELLAs. Growth responses of *1aiqd* plants to elevated GA were also tested, to assess changes in sensitivity to the phytohormone.

6.2 Results

6.2.1 Do family 1a IQDs positively feedback on DELLA protein levels to restrict growth

The compaction of shoot organs following induction of ectopic IQD22 protein levels showed similarity to phenotypes of gain of DELLA function mutants. As mentioned above, 1a *IQDs* are candidate target genes of at least one of these DELLA proteins, RGA, transcriptionally. A large number of regulators control DELLA protein activity to fine tune growth repression. One function of IQDs downstream of RGA could be positive feedback regulation of the DELLA protein itself, causing the severe shoot growth dwarfing seen in lines with 1a IQD overexpression (Figure 6.2). Alternatively, IQDs could function in processes downstream of DELLA proteins to repress elongation growth.

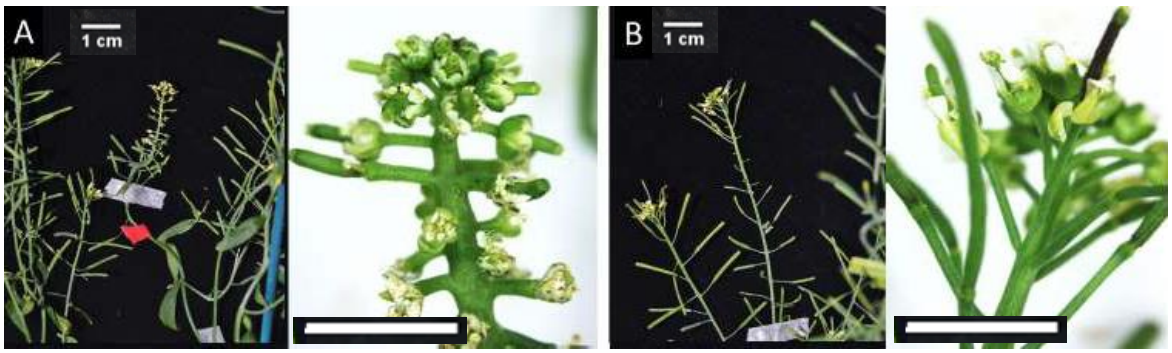

Figure 6. 2: Induction of ectopic IQD22 in the shoot apex caused phenotypes similar to gain of DELLA function. Inflorescence apices of *RPS5a:LhGR Op:IQD22* plants treated with 10 µM dexamethasone (A) and control (B). In both cases, solutions contained 0.1% ethanol and 0.01% Silwet-L77 and were applied directly to the shoot apex using a paintbrush every two days, four times. Images were captured a week following the last treatment. Scale 1cm.

Both 1a IQDs (Chapter 4) and DELLA-GA levels regulate leaf growth. To monitor effects on leaf growth, the ectopic *IQD22* line was germinated on medium containing dexamethasone (dex). Again, ectopic IQD22 protein induced severe, pleiotropic growth restriction (Fig 6.3Biii). To assay whether this could be through IQD22 induction of DELLA activity, the induction of ectopic IQD22 was combined with increased GA levels. Any rescue of growth repression by the GA treatment was subsequently monitored (Figure 6.3 Biv).

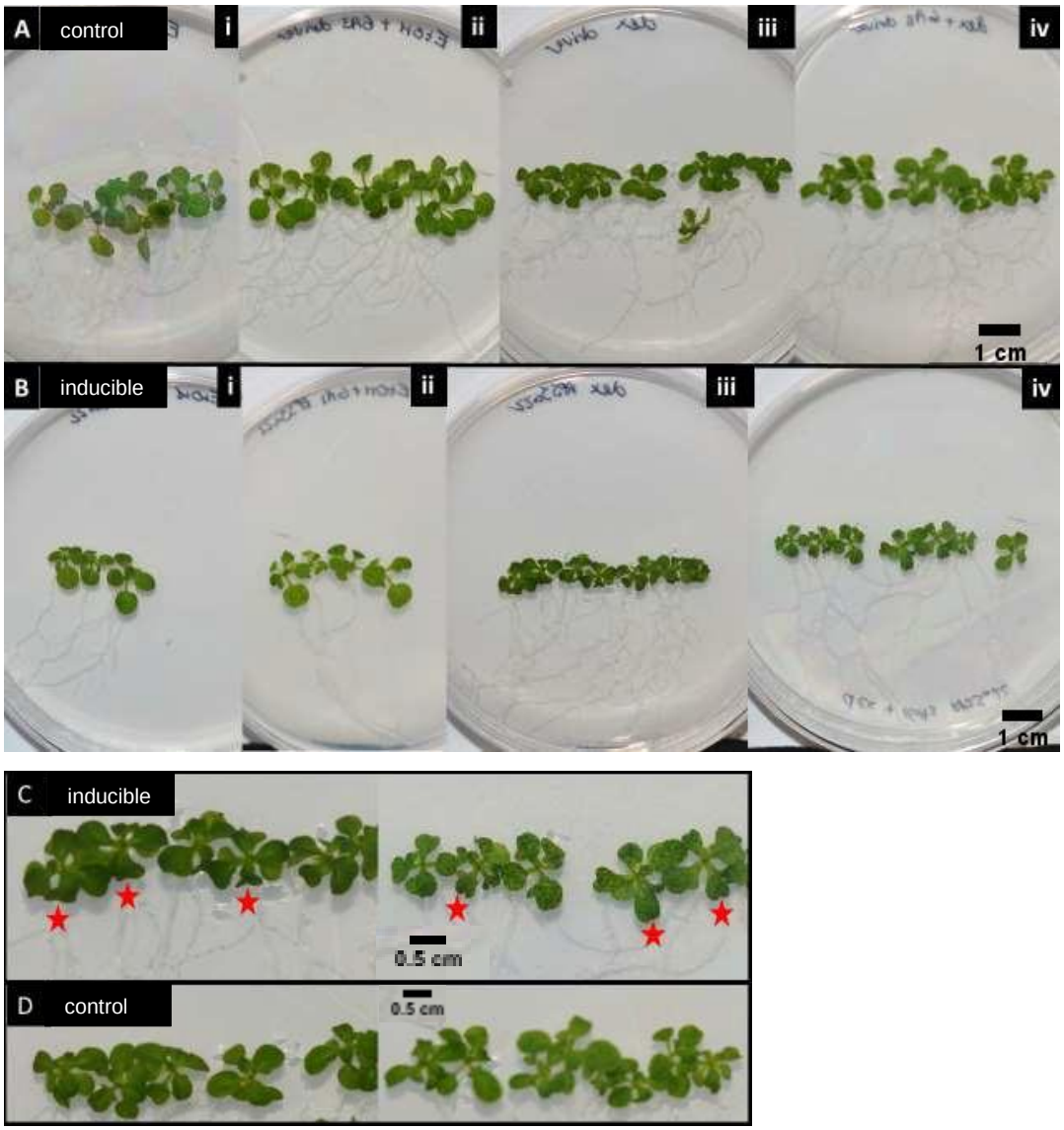

Figure 6. 3: Ectopic *IQD22* induction repressed leaf blade and petiole growth as well as altering leaf shape independently of GA response. *RPS5a:LhGR* driver seedlings and *RPS5a:LhGR Op:IQD22* seedlings grown on 0.1% ethanol control (Ai,Bi), 10 µM GA3 (Aii,Bii), 10 µM dexamethasone (Aiiii, Biii) and 10 µM dexamethasone + 10 µM GA3 (Aiv, Biv). C and D highlight differences between dex and dex+GA treated seedlings of the RPS5a *IQD22* line and RPS5a empty driver plants, respectively. Red stars highlight altered upper leaf blade shape in both dex and dex+GA treated inducible plant lines.

The inducible *IQD22* line did not appear to exhibit leaky overexpression of IQD22, as seedlings developed identical to controls (Figure 6.3Ai,Bi). *RPS5a:LhGR Op:IQD22* seedlings germinated on dex induction plates exhibited pronounced repression of growth paired with severe defects in petiole formation and leaf shape (Figure 6.3C, Chapter 2). Dex-treated control empty driver lines had slightly reduced growth (Figure 6.3Aiii), however GA treatment fully rescued this (Figure 6.3AiV, D). GA treatment, however, was not sufficient to rescue the growth defects following dex treatment of inducible *IQD22* lines. The severe petiole and leaf shape phenotype remained and whilst leaves appear slightly more elongated they were still compressed compared to controls (Figure 6.3C). This indicates the developmental defects in the *IQD22* ectopic line are not the result of enhanced expression of DELLA proteins. The additive effects of IQD22 induction and GA treatment suggest that the effect of IQD22 on leaf elongation was largely independent of DELLA function.

Loss and gain of function 1a *IQD* lines both impact leaf shape and adaxial epidermal PC shape (Chapter 4, Chapter 5). A prominent reduction in lobing was seen in RPS5a *IQD22* lines treated with dex, regardless of GA treatment (Figure 6.4F). Epidermal cells in dex treated control plants lacking the inducible *IQD22* construct appeared similarly lobed to 0.1% ethanol control treated lines (C,D and G,H) affirming high levels of IQD22 protein were causative. Thus, as seen for inflorescence growth, the PC shape phenotype caused by IQD22 induction could not be attributed to a positive feedback on DELLA expression.

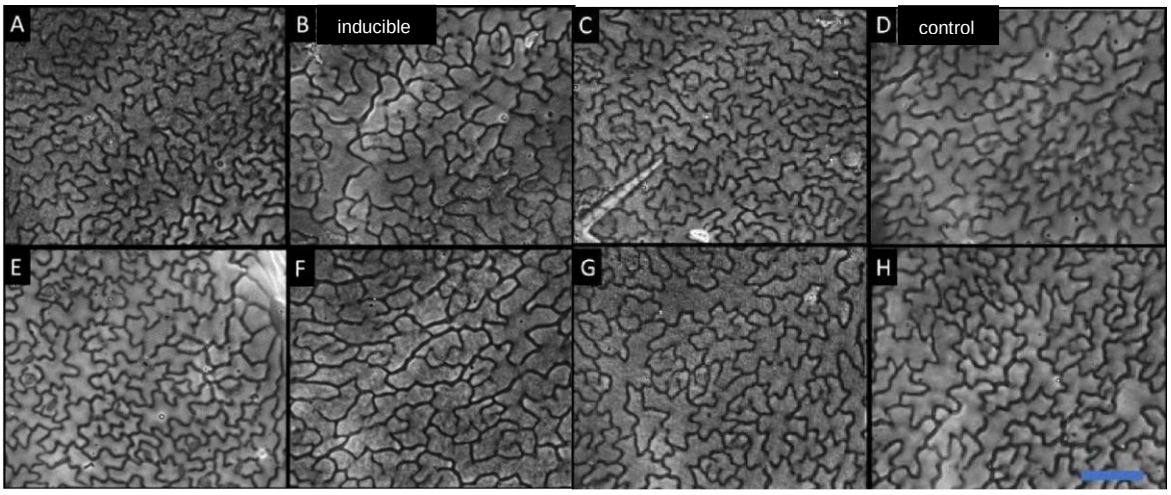

Figure 6. 4: Reduced PC lobing by ectopic IQD22 was not reverted by GA treatment. Adaxial surface PCs of RPS5a *IQD2*2 seedlings grown on 0.1% ethanol control (A) and 10 µM dexamethasone (B). RPS5a driver seedling grown on 0.1% ethanol control (C) and dexamethasone (D). Respective treatments + 10 µM GA3 (E-H) Scale bar in H representative for all sections, 0.1 mm in length.

The hypothesis that IQDs function in growth repression irrespective of DELLA activity was further tested genetically through introduction of the inducible ectopic *IQD22* construct into a pentuple *DELLA* loss of function background. As in the Ler-0 background with functional DELLAs (Figure 6.2), phenotypes such as reduced internode elongation and inhibited growth of floral organs followed induction of high levels of IQD22 protein in the absence of DELLA proteins (Figure 6.5).

Figure 6. 5: Ectopic IQD22 still repressed shoot growth when induced in a *DELLA* loss of function background. *RPS5a:LhGR Op:IQD22* line in a pentuple DELLA loss of function background following dexamethasone (A) and control (B) treatment. Both solutions contained 0.1% ethanol and 0.01% Silwet-L77 and were applied directly to the shoot apex using a paintbrush every two days, four times. Upper panel show effects on stem elongation, with treated shoot denoted by red star, and lower panels show effects on floral bud growth. In lower panels of A a treated shoot apex, left of panel, is imaged next to a totally untreated apex, right of panel.

Whilst a quantitative conclusion cannot be made that growth restriction was as pronounced as in plants with wild-type *DELLA* function (Figure 6.2), given that *IQD22* ectopic expression still dwarfed shoot growth in the pentuple *DELLA* mutant background, feedback regulation on *DELLAs* can be excluded as causal to 1a IQDs' function in growth repression. 1a IQDs must restrict growth independently of DELLAs.

6.2.2 Sensitivity of the *1aiqd* line to GA

It has been implicated that IQD function could restrict growth by decreasing sensitivity to the growth-promoting hormone GA (Zhou, X. and Sun, T., 2011). This would be consistent with restricted growth in ectopic *IQD22* lines despite GA treatment, however, the continued growth restriction following removal of DELLA proteins supported an independent means of growth restriction. Loss of 1a *IQD* function was in turn proposed to sensitise a plants' response to GA, which could explain increased growth in the *1aiqd* line. Sensitivity to GA was investigated through spray application of 10 µM GA3 twice a week from seedling to mature plant stage.

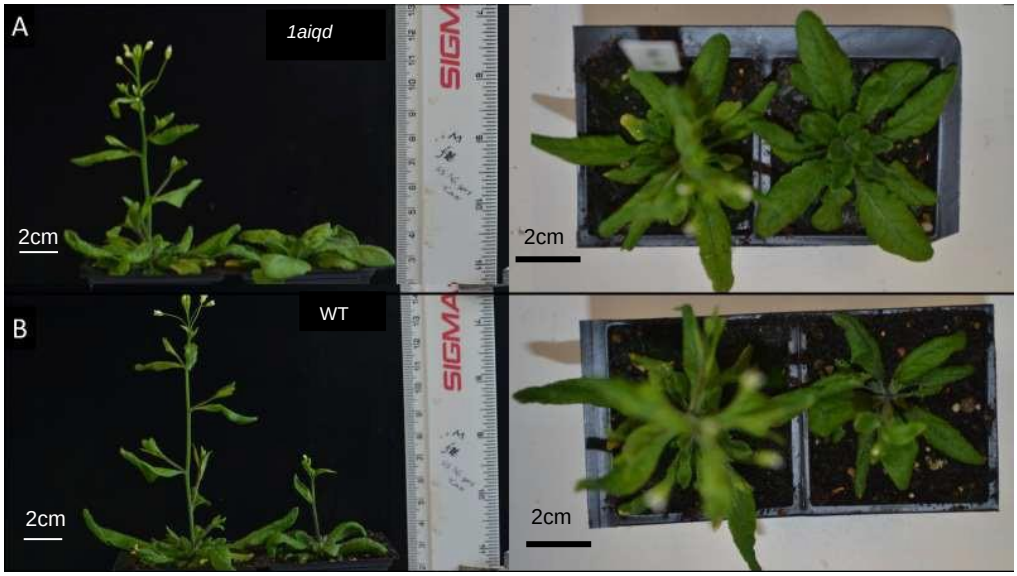

Figure 6. 6: Overall growth of WT and *1aiqd* plants appeared equally sensitive to externally applied GA. A *1aiqd* mutant line and B WT Col-0. On each panel, the plant on the left was sprayed twice a week from seedling stage with 10 µM GA3 and the corresponding water-treated control is shown on the right.

GA3 treatment induced premature floral transition in both mutant and WT lines. At the point of imaging in Figure 6.6, 2 of 6 control treated WT plants had bolted, however none of control mutant plants, supporting the *1aiqd* lines' tendency to delay floral transition as presented in Chapter 2. Measurements of vertical growth of stems in treated WT and *1aiqd* lines versus the control lines indicated GA sprayed WT lines were on average 6.17 cm taller than their controls and *1aiqd* treated lines 8.33 cm taller (n=6).

As detailed in Chapter 3, rosettes of the untreated *1aiqd* line were bulkier, with wider leaves that laid flatter (left of panel Figure 6.7A vs B). GA3 treatment induced a narrower elongated leaf shape and increased abaxial curling in both WT and *1aiqd* plants (Figure 6.6, 6.7). Whilst the area of mutant leaves still appeared larger than that of WT, the effect of GA treatment in elongation growth and leaf curling appeared equal in both lines.

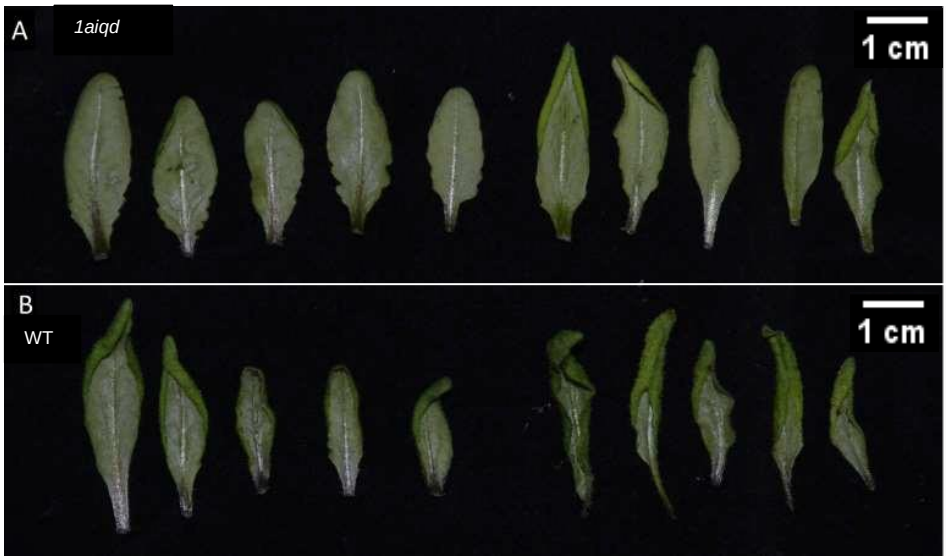

Figure 6. 7 GA treatment increased leaf curling in both WT and *1aiqd* plants.
5 leaves from control treated plants (left of panel) and 5 from treated plants (right of panel) from *1aiqd* line (A) and WT Col-0 (B).

Stem thickness was greater in the *1aiqd* plants in both control and GA treatment conditions, however the average stem thickness increased in treated WT plants, compared to only a slight increase in mutant plants following treatment. Therefore, in the mutant stem elongation growth seemed more impacted by GA3 treatment than radial growth, whereas growth in both dimensions was enhanced in WT. This suggests that GA and 1a IQDs affect stem thickness through similar processes, which are already closer to their maximum effect in the *1aiqd* line. Overall, the treated *1aiqd* and WT lines appeared more similar to each other than to their respective controls (Figure 6.9). Thus, GA treatment had similar impacts onWT and *1aiqd* line growth, indicating DELLA proteins have similar functionality in both backgrounds. No increased sensitivity of *1aiqd* plants to GA3 treatment was clear in the results presented.

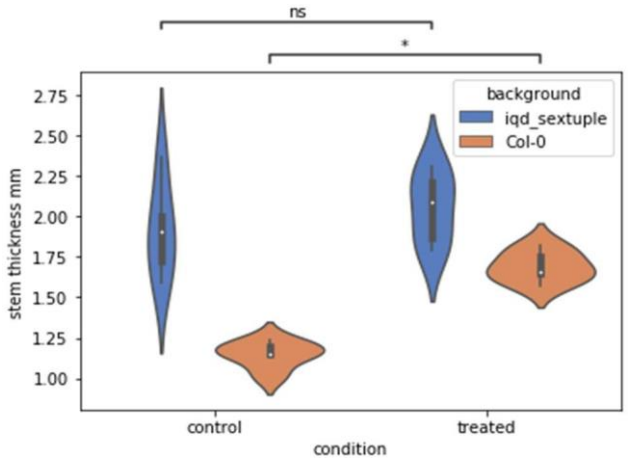

Figure 6. 8: Only WT lines treated with GA3 displayed notable increase in stem thickness. In the mutant stem diameter increased on average 6.8 %, NS. In WT plants the average increase was 27.3% increase. (n=5) *p*= 2.437e-02. two sided Mann-Whitney tests with Bonferroni correction; * $p < 0.05$.

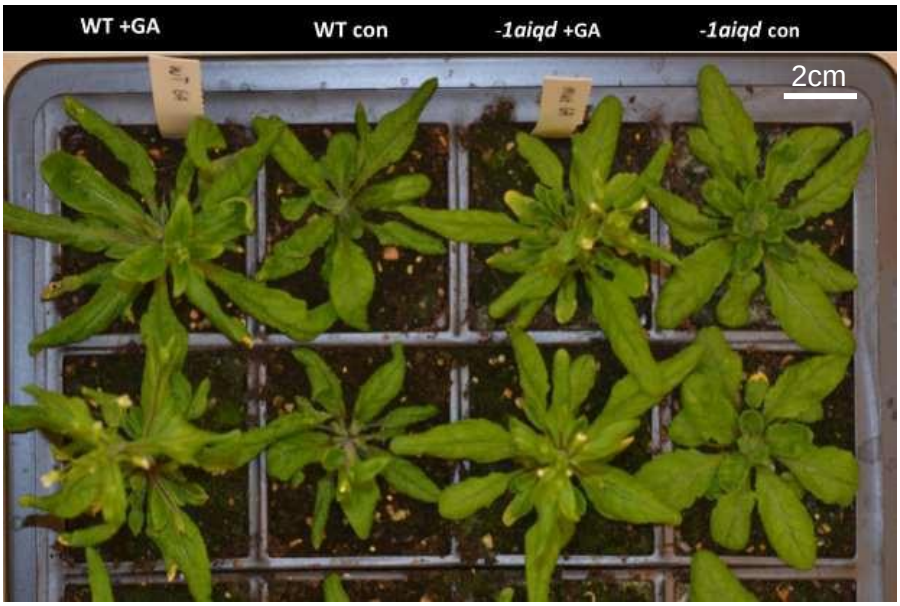

Figure 6. 9 While WT and *1aiqd* plants appeared very different, those treated with GA appeared similar. Rows marked +GA were sprayed twice a week from seedling stage with 10 µM GA3, versus water sprayed control plants. WT and *1aiqd* genotypes are also indicated above each row.

6.2.3 IQD function in growth restriction downstream of RGA

To assess the contribution of 1a IQD function to growth repression by RGA, I also investigated the growth response of the *1aiqd* line in the presence of artificially high RGA protein levels, using the GA biosynthesis inhibitor paclobutrazol (PAC) and the gain of function line *rga-Δ17*.

A common assay for sensitivity to PAC treatment is measuring hypocotyl elongation, so I tested whether the *1aiqd* mutant was less sensitive than WT to hypocotyl repression induced by PAC treatment. Results in Figure 6.10, however, showed a similar response in both WT and *1aiqd* mutant seedlings treated with PAC, with severely dwarfed growth and darker green cotyledons.

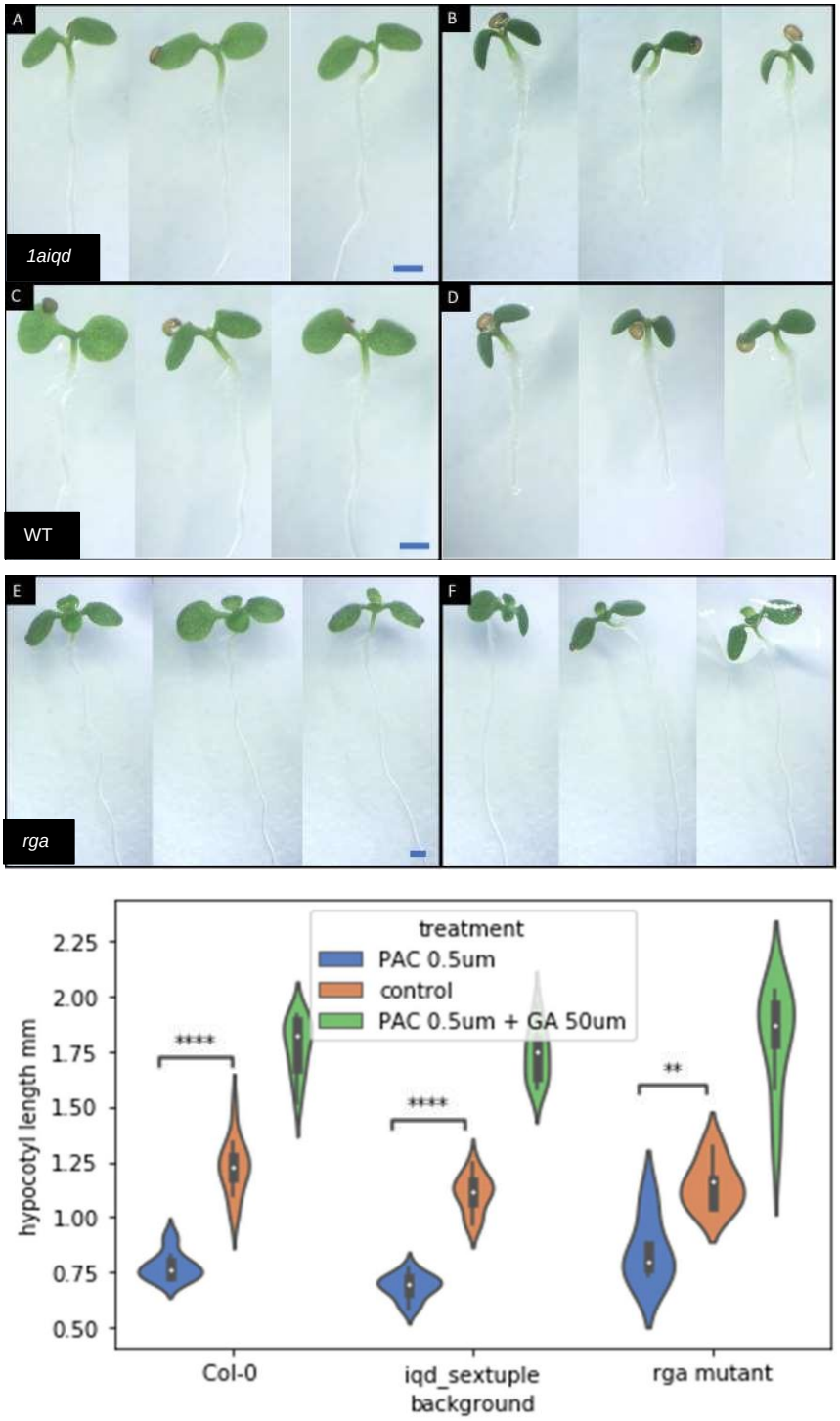

Figure 6. 10 Hypocotyl elongation was severely repressed in WT and *1aiqd* lines by PAC treatment. WT (A.B), *1aiqd* mutant (C,D) and *rga* single mutant (E,F) seedlings grown for 7 days on 0.01% ethanol control (left panel) vs 0.5 µM PAC plates (right panel). scale bars 0.1 mm. Graph represents hypocotyl length measurements collected from paclobutrazol (PAC) and control treated plants. Graph shows GA treatment able to not only rescue but enhance growth in all backgrounds when applied alongside PAC. Statistics for hypocotyl length for each genotype under PAC or control treatment with difference in length and significance were: **WT** n=15, 0.5 µm PAC 0.78 mm, Control 1.23 mm, difference: 0.45 mm, 36.6 % proportion difference, *p*=7.468e-06; ***1aiqd*** n=11, 0.5 µm PAC 0.69 mm, Control 1.11 mm, difference: 0.42, 37.8% proportion difference, *p*= 5.548e-05; ***rga* mutant** n=8: 0.5 µm PAC 0.85 mm, Control 1.15 mm, difference : 0.3, 26 % proportion difference, *p*=4.924e-03. All p values by two sided Mann-Whitney tests with Bonferroni correction; * $p < 0.05$, ** $p < 0.01$, *** $p < 0.001$,**** $p<0.0001$.

Whilst the literature and my own research focused on a link between *1a IQDs* and the DELLA protein RGA, hypocotyl elongation is likely controlled by multiple *DELLA* genes, therefore the specific effect of *RGA* was also investigated using the single *rga* mutant. Without RGA function, PAC still reduced hypocotyl elongation by 26%, compared to 37% in wild type 1a *IQD* background. If 1a IQDs were a large contributor to growth restriction downstream of RGA, the *1aiqd* mutants would mirror the partial insensitivity to PAC seen in the *rga* mutant, but this is not the case.

Nonetheless, these results corresponded only to very early seedling development and IQDs contribution specifically to hypocotyl elongation. To investigate how *1a IQDs* and *RGA* interacted in leaf and stem growth, where previous research demonstrated a function for 1a IQDs (Chapter 3,4), the *rga-Δ17* gain of function mutation was introduced in the *1aiqd* background. To ensure that all plants had only one copy of the *rga-Δ17* allele, I crossed a plant heterozygous for *rga-Δ17* and homozygous for *1aiqd* mutations with either the homozygous *1aiqd* line or the WT Col-0 line. The effect of the *rga-Δ17* mutation was then compared in progeny plants that were fully homozygous or fully heterozygous for all 1a *IQD* loci. In both backgrounds, the *rga-Δ17* mutation caused dwarfed rosettes. While individual leaves were slightly broader and more serrated in the full loss of *1a IQD* function background (Figure 6.11A,B top versus bottom panel), consistent with phenotypes presented Chapter 4, the *1aiqd* background did not suppress the leaf blade phenotype caused by *rga-Δ17*.

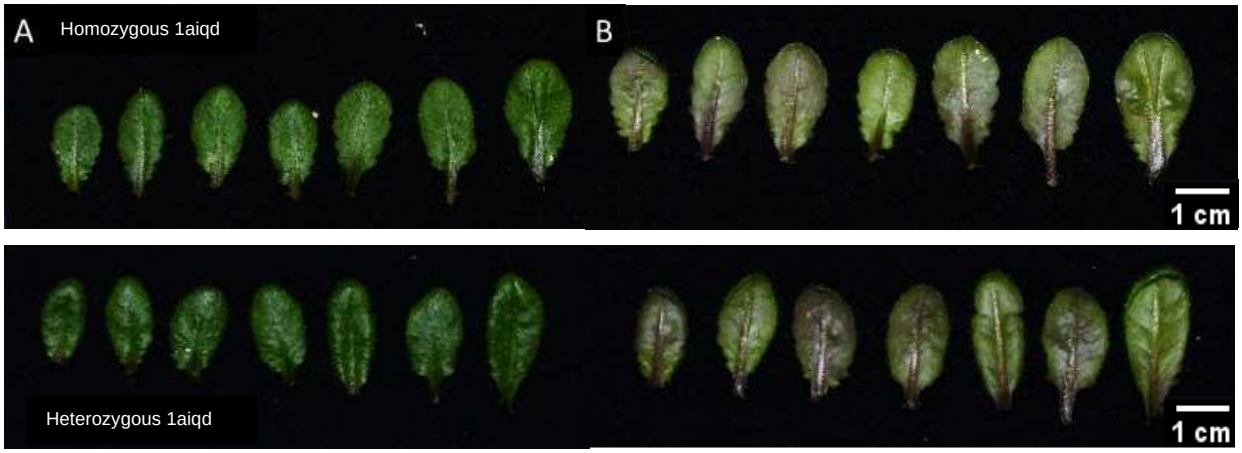

Figure 6. 11. The *rga-Δ17* mutation restricted leaf expansion similarly in full loss of 1a IQD function versus heterozygous background. Images of the adaxial (A) and abaxial (B) surface of the 9th leaf initiated in rosettes of plants with *rga-Δ17* mutation and homozygous for *1aiqd* (top panel) or heterozygous for all 1a *iqd* mutations (bottom panel).

Following the floral transition, the homozygous and heterozygous *1aiqd* populations carrying the *rga-Δ17* mutation showed delayed bolting and reduced stature. There was no visible divergence between plants heterozygous and homozygous for the 1a *iqd* mutations, ruling out that 1a IQDs are essential downstream factors in the growth restriction caused by RGA (Figure 6.12).

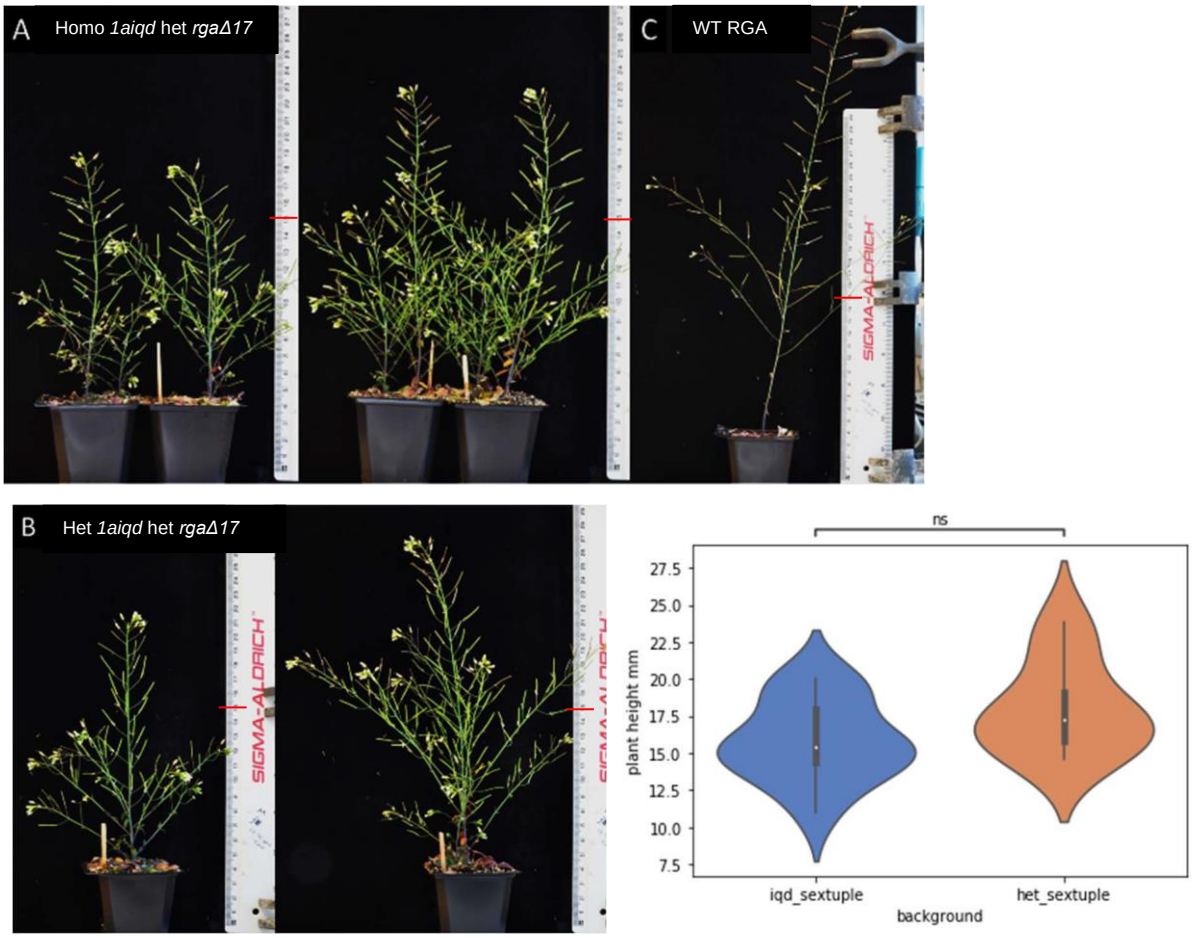

Figure 6. 12: plant height was similarly reduced in *rga-Δ17* with and without 1a IQD function. *rga-Δ17* plants homozygous (A) and heterozygous (B) for all 1a *iqd* mutations had similarly reduced stature compared to the *RGA* WT (C). On average, plants heterozygous for IQD function had marginally greater height, but the difference was not significant (two sided Mann-Whitney tests with Bonferroni correction), *p*=1.032e-01, *1aiqd* line n=13, heterozygous *1aiqd* line n=8. Red line indicates 15cm on ruler.

6.3 Discussion

In this chapter, I investigated whether 1a IQDs interact functionally with DELLA proteins in the control of shoot organ growth. I tested two main hypotheses: first, that 1a IQDs could participate in a feedback loop to regulate DELLA activity, and second, that 1a IQDs mediate growth repressive effects of DELLAs.

Biochemical reduction of DELLA function through GA treatment was able to promote some elongation growth in leaves of the ectopic *IQD22* line, however they remained reduced in size with additional petiole and shape defects compared to controls. This result could suggest either that IQD22 represses growth independently of DELLA proteins, or that IQD22 interferes with DELLA degradation. Repressed growth following induction of ectopic IQD22 protein levels in the shoot apex of plants without functional DELLA proteins demonstrated that gain of 1a IQD function is independent of DELLA activity. Conversely, GA application was used in conjunction with the loss of function *1aiqd* line to probe whether sensitivity to GA was affected, subsequently contributing to increased shoot growth. GA3 treatment induced premature bolting and flowering as well as leaf elongation and curling in both WT and *1aiqd* lines indicating DELLA protein function is equally active in both lines.

The hypothesis that IQD proteins contribute to growth repression downstream of DELLA proteins was tested biochemically through paclobutrazol treatments and genetically using the *rga-Δ17* background. Growth was equally restricted without functional 1a IQDs, rendering the hypothesis null.

Thus, through a thorough analysis, DELLA proteins appear to retain restrictive growth function in absence of 1a IQD function as well as IQDs themselves still retaining ability to repress shoot growth in absence of DELLA function. These results combined suggest similar functions in growth repression involving moderation of fundamental growth processes such as cell division and or expansion but through independent mechanisms. It cannot be excluded, however, that DELLA and IQD activity could be coordinated by regulatory links, which could be related to the binding of RGA to 1a *IQD* gene regions seen in ChIP-seq experiments.

A particularly interesting result was that GA treatment appeared to promote greater increase in stem thickness in WT lines compared to *1aiqd* plants. One

interpretation of this is that 1a IQDs are necessary to carry out the effects of GA, on stem thickening. This would contrast with the apparently independent function in all other aspects of organ growth analysed. Another interpretation is that GA and *1a IQDs* might converge on similar processes, such as oriented cell growth and division, and that thickening of the stem through these processes has reached its limit in the *1aiqd* mutant. This would be in line with the idea that GA/DELLAs and IQDs function independently but target common cellular processes.

In conclusion, what was unveiled from my experimental findings is that signalling involving DELLA and GA appeared undisrupted in gain and loss of function mutant backgrounds, contrary to what could be predicted from the literature (Zhou, X. and Sun, T.-P. 2011). Whilst on cursory inspection loss and gain of 1a IQD function caused phenotypes similar to loss and gain of DELLA function, respectively, multiple aspects of the role of 1a IQDs in growth regulation cast doubt on this link and suggest separate mechanisms. Questions can be raised whether *IQD22*, which is an important 1a member previously linked to DELLA regulation, could have residual function in the *1aiqd* line. However, my results strongly support that no overarching link exists between the whole 1a subfamilly and DELLA function.

Chapter 7 General Discussion

7.1 Introduction

The *IQDs* are a large gene family with numerous links to master regulators of plant growth such as phytohormones and transcription factors (Möller, B.K. 2012, Bencivenga, S. et al 2016; Serrano-Mislata, A. et al. 2017). Indeed, the extent of these links would likely be greatly expanded by a thorough analysis of publicly available transcription datasets. Therefore, it could be hypothesised that IQD proteins have widespread roles in fundamental cellular processes involved in growth. This idea is further supported by expression in stem cell niches (Wendrich, J. et al. 2018, Chapter 5), early in organ development during the largely proliferative growth phase (Dou, J. et al. 2018) as well as early in serration initiation (Chapter 4).

Individual IQD family members have been associated with the control of specific cell types' shape via local concentration of microtubules (Mitra,D. et al. 2019, Sugiyama, Y., et. al., 2017). Regulation of organ shape in fleshy fruit crops is also attributed to IQD proteins, although with little understanding of the molecular basis for this (Wu, S et al 2011; Pan, Y. et al. 2017; Dou, J. et al 2018). A conserved link to subfamily 1a IQDs in cucumber, melon and watermelon fruit shape regulation (Jin, B. et al. 2017) is an additional motivation to investigate their molecular function to further the understanding of plant growth regulation in an organ vital for crop species' profitability.

Phylogenetic grouping into subfamilies points to conserved functions, although in most cases these remain to be identified. Studies are lacking where macroscopic plant growth phenotypes are unveiled in loss of function mutants, with these largely restricted to ectopic *IQD* expression lines. Evidence for substantial growth modification upon loss of whole subfamily function has been provided by the *iqd14-c* mutant in rice (Yang et al., 2018). This study supported a similar approach in a model plant species with more extensive experimental tools to characterise proteins' molecular functions. My PhD research sought to first establish that subfamily 1a IQD proteins have redundant functions contributing to regulation of plant shoot growth in Arabidopsis through both loss and gain of function plant lines. If confirmed, I hoped to use the experimental tools available in this species to reveal the underlying cellular processes. Finally, investigation into IQD's molecular interactions with cellular and other molecular components, such

as microtubules and auxin transporters, aimed to uncover molecular mechanisms underlying *IQDs*' function in plant growth. This information in turn could be used to reassess *IQDs* regulation of growth processes in crop species, directing further research that may have yield implications.

My results supported that subfamily1a *IQD* genes have overlapping functions in multiple aspects of shoot growth (Chapter 2). Further study of differential stem growth in the *1aiqd* mutant implicated IQD function was important for restricting organ radial growth through controlled division plane placement in RZ cells, which generate the stem's central pith zone (Chapter 3). Study of leaf shape supported the role for IQDs in restriction of radial organ growth and highlighted ties between 1a IQD function and auxin transport/gradients due to apparent function in restricting leaf margin complexity (Chapter 4), a trait which auxin gradients regulate.

7.2 Function of 1a *IQD*s in organ shape

IQD proteins could restrict radial organ growth through their identified function in division plane orientation. Work on Cucurbitaceae fruit shape has implied that altered cell divisions in longitudinal or radial directions, regulated by 1a IQD function, underlies differing fruit shapes (Dou, J. et al. 2018). My research in Arabidopsis stems highlighted that IQD function promotes occurrence of majority longitudinal divisions in the RZ; in the absence of IQD function divisions that contribute to increased stem thickness appeared to result from more random orientation of divisions, rather than a specific increase in the frequency of radial divisions (Chapter 3). Further work investigating division plane orientation in *1aiqd* plants' leaf blade and petiole, where radial expansion also occurred, as well as in leaf serrations, where enhanced length and upper serration width were apparent, could strengthen the link between 1a IQD function and division plane orientation. A similar mechanism could be investigated in ovary growth of the Cucurbitaceae family where a divergence in radial expansion was noted prior to fruit growth (Dou, J. et al. 2018).

A role for 1a *IQD* genes in the balance of fruit length and width, in an inverse relationship where increase in length decreases width, has been proposed (Pan, Y. et al. 2017) however, research presented in this thesis supports that 1a IQDs function specifically in the control of organ width rather than length (Chapter

3,4). The exception was leaf serration growth, where both length and distal width increased (Chapter 4), but this again contrasted to the proposed increase in length at a cost to width. My research into 1a IQD function was more detailed than in fruit crops and was based on introduced mutations in 1a *IQD* genes and subsequent study of growth. Current research in fruit crops involves QTL analysis of varieties differing in organ shape and strength of association to *IQD* loci, whilst large genetic variation exists throughout the genome. As methods for genetic manipulation advance, including use of CRISPR in crops (Zhang, Y. et al. 2020), it could be interesting to perturb function of all 1a *IQD* genes in members of the Cucurbitaceae family, particularly in lines with elongated fruits, and monitor the consequences on radial as well as elongation growth.

Apparent variation in IQD regulation of organ shape control also exists across subfamilies, with subfamily two member *SUN12* strongly associated with organ length in tomato (Xiao et al. 2009). Moving forward, research is required to identify variation in IQD function that could account for differing organ shape control. It remains possible that identical functions may underlie *1aiqd* organ growth in Arabidopsis and fruit growth in crop species with loss of 1a *IQD* function, with different local regulation causing variation in the consequences of IQD function for shape and size in stems versus fruits.

7.3 Molecular function involving microtubule behaviour

IQD function is largely associated with microtubule behaviour in the literature (Yang et al., 2018; Mitra,D. et al. 2019, Sugiyama, Y., et. al., 2017) and this was hypothesised to underly the divergence in cell division planes in the *1aiqd* line. Although cell geometry is a major factor directing cell division planes (S. Besson, S. Dumais, J. 2011) it was not visibly altered preceding aberrant division plane orientation in the *1aiqd* mutant. Modelling of cortical MT dynamics, including effects of auxin gradients and stability at cell edges, supported its importance for correct division plane orientation (Chakrabortty B, Weijers D, et al. 2018). Other important roles of MTs in division plane orientation are the formation of the PPB prior to cytokinesis and of the phragmoplast during formation of the cell plate (Rasmussen C. G. et al. 2013). Whilst associated with the CMT array, imaging has not detailed IQD proteins localised at the PPB or phragmoplast. This could be more closely monitored at high magnification and resolution however, varied CMT

dynamics, as predicted by modelling, could be a factor contributing to division plane formation.

CMT arrays also have a central role in the control of directional cell expansion, and consequently cell shape. The importance of microtubule behaviour in establishing the interdigitated PC shape led to the hypothesis that altered microtubule behaviour was involved in the *1aiqd* line's PC shape phenotype. *IQD* function in microtubule behaviour was investigated in PC lobe development, however, the results were limited and inconclusive (Chapter 5). Sites of altered division planes, such as the RZ, lie too deep in plant tissue for live imaging, therefore dynamic live capture in accessible PCs could be complemented by immuno-localisation to capture microtubule organisation in stem sections, or through thin leaf lamina at serrations. The results could correlate changes in microtubule organisation with division plane orientation and shed light on what behavioural difference in microtubule dynamics could underly the altered CMT organisation.

Differential decoration of CMT arrays have been reported to contribute to varied ectopic growth phenotypes in *IQD* members of Arabidopsis (Burstenbinder, K. et al. 2017). Unique functions in microtubule behaviour across different subfamilies could be one reason for differing impacts on plant growth and could be revealed by expanding similar research to other *IQD* subfamilies linked to plant growth, such as 1c and 2. This would again require higher order mutants in Arabidopsis. Microtubule immuno-staining, which has been utilised in tomato (Zhao, F. et al. 2020), could be utilised in tomato *iqd12* NILs with fruit shape defects, allowing assessment of microtubule organisation at early ovary stages where variation in shape occur.

7.4 IQD function and phytohormones

Further research presented in Chapter 4 supported an interplay between 1a IQDs and establishment of auxin gradients. IQDs were until now not known to be molecular players in leaf margin complexity, but their expression pattern in early leaves and the phenotype in serration growth in the *1aiqd* line showed a clear role. This directed my research into questions on how IQDs impact on either the generation of auxin maxima or on the sensitivity of responses to auxin. Experiments on PIN1 protein localisation in early serrations of a partial 1a *IQD* mutant supported the prior (Chapter 4). It was concluded that increased growth

rate of serrations, and subsequently the area of mature serrations, was likely through increased cell proliferation, directed by altered auxin maxima. In turn, this research also validated the differential growth theory as causal for restriction of defined serrations to the leaf base in Arabidopsis, advancing understanding of leaf margin complexity. It would be interesting to further investigate IQD function in leaf complexity of plant species with compound leaves such as tomato.

The striking similarity between *IQD24* expression and auxin transport/ concentration in leaves incites the question as to whether the 1a IQD-auxin functional link is more extensive than just in serrations. Increased cell proliferation was also causal of thick stems in the *1aiqd* line (Chapter 3). Auxin concentration is linked both to induction of division and regulating division plane orientation, for example in lateral root growth a stress signal precedes PIN patterning and auxin gradient generation that is required for the substantial change in division plane orientation (Lucas, M., Swarup, K. et al. 2013). A change in auxin gradients could therefore be positioned upstream of changes in proliferation and division plane orientation in altered stem growth of the *1aiqd* line. Recently, research also re-implicated auxin transport in regulation of PC lobing (Grones, P. et al. 2020), so disruption to auxin transporters could also contribute to altered PC shape in the *1aiqd* line.

Preliminary investigation of the 1a IQD-auxin functional link in the stem could be performed through DR5:GFP imaging or auxin immunostaining in the loss of function line. Support for altered auxin gradients / distribution in the stem, particularly in the RZ, where the stem growth phenotype appears to initiate, could warrant further experimentation probing PIN localisation. This could include PIN3, which has been implicated as a key player in auxin gradient changes during PC lobing, and also transports auxin in the xylem (Waldie, T. and Leyser, O. 2018). The protein is therefore a good candidate to further investigate the link between IQD function and PIN protein patterning as a primary underlying molecular means to regulate plant growth.

Serration outgrowth could, however, be seen as separate to whole organ growth, under less complex regulation with a well-defined mechanism involving auxin transport presented in the literature. Further experimentation into PIN patterning in organ initiation from the SAM in the *1aiqd* line was also not conclusive and supporting evidence of high-resolution images in initiating primordia is required. That being said, a large proportion of research into *IQD* organ shape control in tomato has revolved around links to auxin (Wang, Y. et al.

2019). While the *sun12* NIL had varied transcript levels of several auxin related genes, auxin level itself was not significantly different compared to WT (Wu S., Clevenger J.P., et al. 2015). This, however, is consistent with results presented in Chapter 4 and 5, where no large change in concentration of transporters was seen in primordia or serrations of loss of function lines, with the change restricted to PM localisation and directionality of auxin transport. My research therefore warrants revisiting whether IQDs moderate growth in tomato through changes in the distribution of auxin transporters.

Research into subfamily 1c *IQDs* has also been prompted by their ties to regulation by the auxin response factor MP (Wendrich, J. et al. 2018) and work presented in this thesis extended the auxin link to 1a IQDs, indicating all three subfamilies associated most strongly with plant growth interact with auxin signalling. Auxin has not been investigated in respect to Cucurbitacea fruit shape regulation. Further work investigating auxin function in early fleshy fruit development, in conjunction with IQD function, could be important to advance our understanding of fruit development and may confer unknown differences between fleshy fruit species and seed pod species like Arabidopsis, where no fruit growth defect occurred in the *1aiqd* line.

7.5 IQD function and calcium signalling

As potentially the largest calmodulin interacting family in land plants, another hugely versatile signalling molecule regulating IQDs' function is the ion Ca++. Research undertaken early in this thesis agreed with recently published findings that cytoplasmic calcium concentration does not disrupt IQD cellular localisations through calmodulin binding. Instead, IQD cellular localisations could be important for positioning calcium sensor proteins such as calmodulin at sites where highly localised calcium concentrations are established, rapidly modifying IQD function.

The literature reports interaction of IQDs with other important MAPs, such as CMU and SPR2 (Kolling, M. et al. 2019; Wendrich, J. et al. 2018), with the prospect that these interactions could be moderated by calcium signalling. This would implicate whilst IQDs are MAPs themselves, their function at microtubules may involve transducing calcium signalling messages to other MAPs that subsequently modulate microtubule behaviour. As well as regulating microtubule behaviour, links between calcium signalling and auxin have been established, for example rapid calcium influx and upregulation of CMs followed exogenous auxin

application (Di et al., 2015) and calcium signals appeared to direct PIN-polarity (Zhang et al., 2011). IQD function could be interlinking these processes.

The prospect of calcium moderating IQD function by changing binding partners prompts investigation into novel interactor partners with 1a IQDs that could confer divergent growth functions from other subfamilies. This could be performed through immunoprecipitation-mass spectrometry (IP-MS) using the IQD24-YFP fusion. If interesting binding partners are identified, reporters could be generated to investigate if the interaction is dynamic and varies under different cytoplasmic calcium levels. Inability to rescue normal growth by complementation with a 1a IQD protein mutated in the IQ67 domain could highlight a calmodulin binding mechanism to disrupt other protein interactors. IP-MS on the mutated IQD24-YFP could investigate strengthening of association with binding proteins other than calmodulins as their interaction is no longer competing with CM binding.

7.6 IQD function and biomechanical signals

The research field linking mechanical stress to modulation of plant growth is ever expanding (Zhu, M. and Roeder, HK. A. 2020; Zhao, F. et al. 2020) and this growth modulation is associated with cellular processes in which 1a IQDs are implicated, such as microtubule behaviour (Landrien, B., Hamant, O. 2013), division plane orientation and PIN1 PM polarity (Louveaux, M. Hamant, O. et.al. 2016; Heisler, MG. Hamant O. et al. 2010). One postulated mechano-sensing mechanism involves calcium influx. Boundary regions are known to be under high stress and high expression of IQDs in this region overlaps with high concentrations of cytoplasmic calcium (Chapter 5). Inner tissues, where 1a IQDs were preferentially expressed in leaves and stems, are also under compressive stress from the outer epidermis. Thus, it could be proposed that IQDs are molecular components restricting growth in response to mechanical stress transduced by calcium signals, which modify their function either at microtubules or in auxin gradient regulation. IQDs could therefore be an important molecular component to study in understanding plant growth response to mechanical stress.

The study of stem growth in the *1aiqd* mutant has Implications for further understanding of plant growths' response to stress patterns. All cell types including the epidermis were reduced in diameter following the increase in radial cell population in the pith, suggesting a mechanism stimulated in the plant to restrict

the overall increase in radial growth. A likely signal stimulating this response would be mechanical stress. The results support coordinated growth of inner and outer stem tissues, as well as tension exerted on outer epidermis by inner tissue and compression of outer tissue on inner tissue. Novel elements may exist that are able to interact with the cell expansion machinery and terminate expansion when excessive stress is detected. As implicated, IQDs may be a component that functions to limit stress on outer tissues through regulation of division direction and number. Compensation via reduced cell radius in the *1aiqd* line is not complete, perhaps due to loss of *IQD* function and interference with the plant's responses to mechanical stress.

IQDs' functional interaction with PIN patterning was proposed to be stress-mediated, as it was non-cell autonomous. Loss of PIN patterning was hypothesised as either a direct response to loss of IQD function or indirect, following disruption to division planes that caused less ordered stress patterns in growing tissues. An experiment to probe a direct IQD requirement for PIN patterning could be performed by monitoring the ability of PIN1 protein to re-orientate around an ablation site in loss of 1a IQD function background. If, however, the protein orientates similarly, it would be more indicative that loss of IQD function alters tissue stress patterns to which PIN proteins are responding. Modelling could be performed in which divisions planes are simulated as occurs in the mutant line to predict the impact on stress throughout the tissue. If IQDs are important molecular components for plants to adapt growth to mechanical stress, the sensitivity of the mutant line to a sustained mechanical stress throughout growth could be tested, such as a restrictive force the plant must push against to grow.

Future research in the *1aiqd* line can be enhanced by further attempts to CRISPR gene locus where T-DNA lines disrupt reporters, *IQD22* and *IQD26,* for imaging experiments spanning multiple proposed future work in a full loss of function background. This could also unveil further IQD function if the location of the T-DNA insert upstream of *iqd22-1* does leave limited functionality.

7.7 Current model

Rapid cell division stimulates early organ growth, and this is when *IQD* expression is greatest. In the case of serrations and stems, *IQD* expression appears higher in inner tissues of the growing structures. Based on these results,

functions can be inferred in the orientation of division planes, important for directing shape of the growing structure, and in directing auxin gradients, important for total cell population in this growth phase. Thus, IQDs contribute to control mechanisms in organ shape and size.

Summarising models can be proposed based on current findings, interlinking IQD function with calcium signalling, auxin transport and microtubule behaviour, governed by mechanical stress patterns in the growing tissue. However, these require much future work as detailed above. Whilst the models below are presented in the context of serration outgrowth, a similar mechanism could be transferred to stem growth, where *IQDs* are also expressed in inner tissue and auxin transport likely functions in growth regulation.

7.7.1 Mechanism 1

Through CUC2 and PIN1's relationship, an auxin maximum is generated, where the tip of the serration will form, stimulating outgrowth from the leaf perimeter through changing cell wall plasticity and induced cell division. As the serration grows, compressive stress from the epidermis on inner tissue would be differential, and potentially less where the auxin maxima is located, relaxing wall tension. It could be postulated through calcium signalling this stress directs IQD function involving microtubules in inner tissues, restricting disordered division planes. The ordered pattern of divisions throughout growth transduces stress patterns from the inner tissue to the epidermis where PIN1 patterning is directed. Loss of IQD function impairs restriction of random division planes, leading to less ordered growth. Altered stress patterns in the growing tissue impact PIN patterning, extending the auxin maximum and proliferative region, resulting in larger serrations with altered shape.

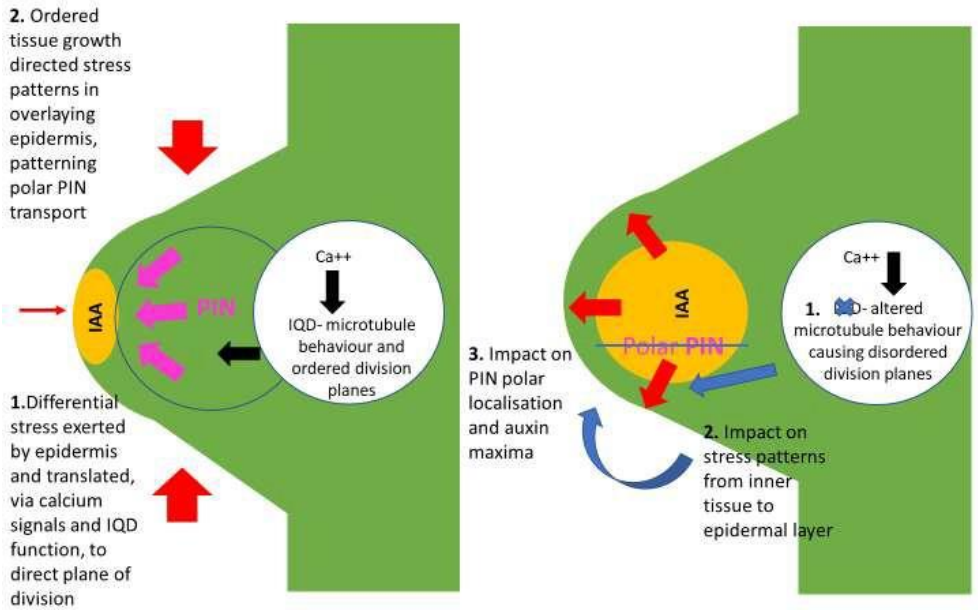

Figure 7. 1 Mechanism **where primary IQD function involves microtubule organisation and division planes. Auxin maxima depicted by yellow region.** Mechanical stress by outer (left of Figure) and inner (right of Figure) tissues is represented by red arrows. The region of calcium signalling and IQD function in the central region is displayed as the white circle to the right

7.7.2 Mechanism 2

Alternately, IQDs could be a molecular component transducing calcium signals stimulated by stress in the inner tissues, to direct PIN1 polar orientation in the epidermis. In this instance, disruption to PIN1 PM patterning would occur first and subsequent changes to auxin distribution could cause altered microtubule behaviour and division plane orientation, as well as frequency of proliferation. Again, changes to tissue growth pattern and auxin gradients may impact stress patterns in the growing tissue itself, fortifying growth modification caused by loss of IQD function. It may well be that inner tissues are sensitised to calcium signalling mediated by stress, but not the outer epidermis, which is constantly under much higher stress and therefore may be less sensitive to minor changes in that stress.

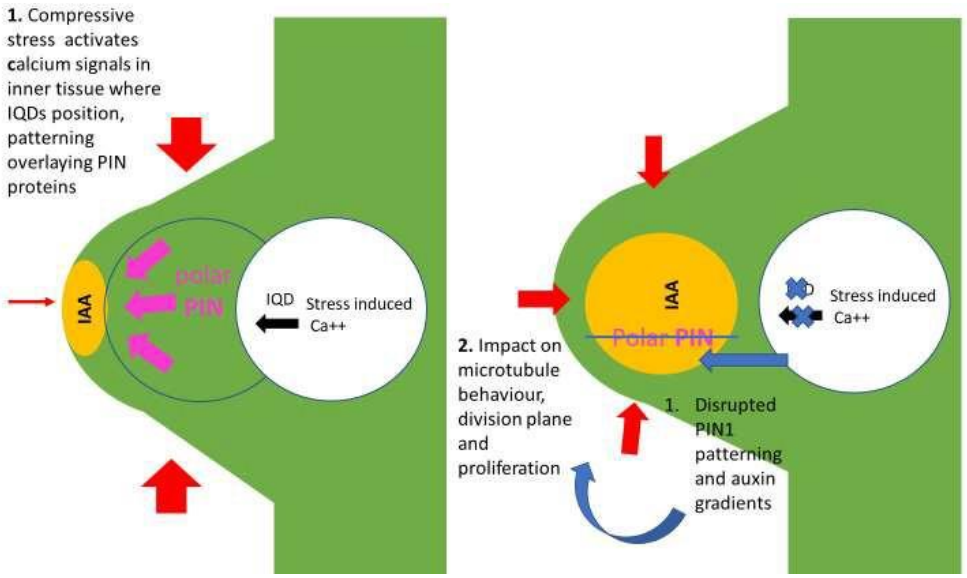

Figure 7. 2 Mechanisms where primary IQD function involves polar PIN patterning. Auxin maxima depicted by yellow region. Mechanical compressive stress from epidermis is represented by red arrows, becoming more uniform following change to auxin maxima. The region of calcium signalling and IQD function in the central region of serration is displayed as the white circle to the right

Overall, this research has advanced understanding of IQD function in plant growth and highlighted avenues worth further research in both Arabidopsis and crop plant species that could tie master growth regulators such as phytohormones, transcription factors, calcium signalling and mechanical stress to growth regulation.

Chapter 8 Methods

8.1 Plant material

8.1.1 Plant lines

T-DNA insertion lines *iqd22-1* (SALK 103903.55.75.x), *iqd23-2* (SALK_073090), *iqd25- 1* (SALK_058876.25.70.x), *iqd26-3* (GK-728F02) and *iqd27-2* (SALK_103602.28.55.X) were provided by Katharina Burstenbinder, Leibniz Institute for Plant Biochemistry, Halle, with analysis of insertion site compared to annotation and functionality performed in Chapter 2. A new mutant allele of *IQD24* was generated by CRISPR-Cas9 mutagenesis as detailed in construct assembly. Reporter constructs pIQD17::IQD17:YFP and pIQD18::IQD18:YFP were provided by collaborator Dolf Weijers, Wageningen University. pIQD24::IQD24:YFP was generated as detailed in construct assembly and transformed in *Arabidopsis thaliana,* Columbia (Col) accession. The RFP-tubulin line was obtained from Dr Jodi Chan, John innes centre, originally received from Dr Ehrhardt (Gutierrez, R. et al. 2009). The PIN1-GFP line was received from Professor Lars Ostegaard, John innes centre, originally from Professor Dolf WeijersWageningen Univeristy. All *Arabidopsis thaliana* lines above were in Col background and accordingly, their respective controls were in the same background.

The RPS5a:LhGR line in *Arabidopsis thaliana* was Landsberg-*erecta* (L-*er*) background, produced by Dr. Stefano Bencivenga and available from within the research group. RPS5a:LhGR plants were re-transformed with a pWOL-based construct (Siligato, R. et al. 2015) directing cDNAs of *IQD22* and *IQD17* as detailed in construct assembly. The pentuple DELLA mutant *gai-t6, rga-t2, rgl1-1, rgl2-1, rgl3-1* (Lee et al., 2002; Peng et al., 2002; Cheng et al., 2004; Koini et al., 2009) was in in L-*er* background. The *GFP-rga-Δ17* in L-er background was provided by Prof. Tai-ping Sun (Duke University)(Dill et al., 2001 for details). For all lines in L-er background, control plants were L-*er*.

The R-GECO calcium reporter was provided in both Columbia and Landsberg background, received through collaboration with Dr Myriam Charpentier, John Innes Centre, along with calcium channel mutants used in a screen for shoot growth defects. All 66 lines listed in table 8.1 were screened; only

annat4 (SALK_121732, NL0115) and *cngc4* (SALK_081369, NL0152) showed promising phenotypes.

Gene	Number	accession
CNGC05	NL0087	SALK_149893C
CNGC05	NL0088	SALK_053354C
CNGC08	NL0089	SALK_004230C
CNGC11	NL0091	SM_3.15048
CNGC13	NL0092	SALK_013536C
CNGC19	NL0093	SALK_027306C
glr1.1	NL0094	SALK_057748.54.75.x
glr2.1	NL0095	GK-897G01.05
glr2.4	NL0096	SALK_010571
glr2.5	NL0097	SAIL_1243_E09
glr2.6	NL0098	SALK_066558
glr2.7	NL0099	SALK_121990C
glr2.8	NL0100	CS374123
glr2.9	NL0101	CS27314 GT1486
glr3.4	NL0103	SALK_016904
glr3.5	NL0104	SALK_035264
glr3.5	NL0105	SALK_023880
glr3.6	NL0106	SALK_035353
glr3.7	NL0108	SALK_101122
ANNAT1	NL0110	SALK_132169.32.15.x
ANNAT3	NL0113	SALK_075525
ANNAT3	NL0114	SALK_082344.34.25
ANNAT4	NL0115	SALK_121732C
CNGC01	NL0150	SAIL_443_B11
CNGC03	NL0151	SALK_056832
CNGC04	NL0152	SALK_081369
CNGC09	NL0153	SALK_026086
glr3.6	NL0156	SALK_032051
glr3.7	NL0157	SALK_022757
ANNAT1	NL0158	SALK_015426
ANNAT1	NL0159	WiscDsLox477-480P11
ANNAT2	NL0160	SALK_054223.49.70.x
glr1.1	NL0162	SALK_117347
glr1.2	NL0163	SALK_114821.36.95.n
glr2.2a	NL0166	GABI_436H08
glr2.6b	NL0167	SALK_115448
glr3.3b	NL0169	SALK_082194
glr1.1 x glr1.2	NL0170	SALK_117347 X SALK_114822

glr1.1 x glr1.4b	NL0171	SALK_117347 X SALK_129955
glr1.2 x glr1.4a	NL0172	SALK_114822 X SALK_124605
glr1.4a x glr3.3b	NL0173	SALK_124605 X SALK_082194
glr2.2a x glr3.3a	NL0174	GABI_436H08 X SALK_077608
glr1.4a x glr2.2a x glr3.3a	NL0176	SALK_124605 X GABI_436H08 X SALK_077608
glr1.2 x glr3.3a	NL0193	SALK_114822 X SALK_077608
glr1.2 x glr2.2 x glr3.3a	NL0195	SALK_114822 X GABI_43H08 X SALK_077608
glr1.2 x glr1.4a x glr2.2 x glr3.3a	NL0197	SALK_114822 X SALK_124605 x GABI_436H08 X SALK_077608
CNGC16	NL0199	SAIL_726_B04 (CS876303)
CNGC07	NL0201	SAIL_59_F03
CNGC12	NL0203	SALK_092622
OSCA1.1-3	NL0206	WiscDsLox331H10
glr2.9	NL0207	SALK_125496
glr1.4a	NL0208	SALK_124605
glr1.4b	NL0209	SALK_129955
glr1.2 x glr1.4a x glr3.3a	NL0211	SALK_114822 X SALK_124605 X SALK_077608
OSCA1.3	NL0670	SALK_134381
CNGC17	NL0674	SALK_014005
glr3.2	NL0717	SALK_150710.17.40.x
glr3.1 x glr3.3 x glr3.6	NL0722	SALK_063873 X SALK_099757 X SALK_091801
glr3.3a	NL0724	SALK_077608
glr3.1	NL0725	SALK_063873C
glr3.6	NL0727	SALK_091801C
glr3.3	NL0728	SALK_099757C
glr3.2 x glr3.3 x glr3.6	NL0855	SALK_150710 X SALK_099757 X SALK_091801
glr3.1*glr3.2	NL1241	SALK_063873 X SALK_150710
CNGC14	NL525	WiscDsLox437E09
CNGC17	NL323	SALK_041923

Table 8. 1: All single and combination calcium channel mutants screened for drastic shoot developmental defects, including line annotation and T-DNA line.

8.1.2 Growth conditions

Sterilised seeds were planted on JIC Arabidopsis Soil Mix Levington F2 compost with a 6:1 ratio of intercept and grit and stratified for 48 hr at 4 °C in the dark, before moving to respective controlled environment room (CER) growth conditions. For experiments phenotyping the *1aiqd* line, growth conditions were at 16 °C under continuous light or, where stated in the results text, at 20 °C under short days (8 h light 16 h dark) and 70% humidity.

In experiments phenotyping leaves of ectopic *IQD22* line at early growth stages, for antibiotic selection after transformation or for confocal imaging experiments on cotyledons or early leaves at fixed DAG, seeds were plated on GM medium [1 litre containing 1% glucose, 4.4 g Murashige and Skoog salts and vitamins (Duchefa), 3 ml of 0.85 M 4-morhpolineethanesulfonic acid (MES) buffer pH 5.7, adjusted to pH 5.7 with 1 M KOH, 0.9% agar added] and stratified before germination and growth under long day conditions (16 h light and 8 h dark) at 21 ° C. For seedlings grown on selection media, 50 µg/ml Kanamycin, 100 µg/ml Gentamycin or 10 µg/ml Phosphinothricin were added to cooled liquid GM, according to the resistance. Positive seedlings under selection were transferred to JIC Arabidopsis Soil Mix Levington F2 compost and grown at 16 °C under continuous light.

For phenotyping after *IQD22* activation in early leaves, seeds of *RPS5a:LhGR Op:IQD22* plants were germinated on GM supplemented with 10 µM dexamethasone (D1756; Merck) and 0.01% ethanol, with respective ethanol controls; for interaction with DELLA proteins, 10 µM GA3 was added to the medium. In assay using paclobutrazol (PAC; Merch, Sigma-Aldrich), seeds were germinated on plates with 0.5 µM PAC and 0.01% ethanol, as well as additional 50 µM GA3 in rescue controls.

8.2 Seed sterilisation

8.2.1 Seed sterilisation for growth on plates

Up to 100 µl of seeds were sterilised by inversion in 1.5 ml of 70% ethanol solution in a 1.7 ml Eppendorf tube for 5 minutes. Tubes were opened under a sterile flow hood and transferred to sterile filter paper to dry.

8.2.2 Sterilisation of T0 transgenic seeds after floral dip transformation

Seeds harvested from Agrobacterium transformed plants (Zhang, X. et al. 2006) were sterilised using Dichloroisocyanuric Acid Sodium Salt. Seeds (300-500 µl) were placed into Eppendorf tubes (2 ml) and 1 ml of Dichloroisocyanuric sterilisation solution was added. 10 ml of Dichloroisocyanuric sterilisation solution was prepared; 5 ml 100% ethanol and 5 ml sterile water containing 0.063g

Dichloroisocyanuric Acid Sodium Salt. Seeds were mixed in the Dichloroisocyanuric sterilisation solution by inversion for 12- 14 min before sterilisation solution was replaced by 1 ml 100% ethanol. Seeds were washed one more time with 100 % ethanol before being piepetted onto sterile filter paper and left to dry under a sterile flow hood.

8.3 DNA extraction

A Quick DNA extraction protocol was used both for genotyping and to obtain template DNA for cloning. Two small leaves were collected in each Eppendorf tube (2 ml) containing a ~2.5 mm steel ball. Leaf tissue was ground for 1 min to fine tissue using TissueLyser LT (QIAGEN) set at 50 oscillations /s. Subsequently 400 µl of extraction buffer containing 250 mM NaCl, 25 mM EDTA pH 8.0, 0.5% SDS, 200 mM Tris-HCl pH 8.0 was added and tubes inverted to homogenise the ground plant tissue and buffer. Samples were then centrifuged at 4,000 rpm for 15 minutes. During centrifugation, fresh labelled tubes (1.7 ml) containing 250 µl of isopropanol were prepared. Subsequently, 250 µl (1 part) supernatant was transferred to fresh tubes, avoiding transfer of pellet containing plant material. Following several inversions to mix, tubes were transferred to -20 °C for 20 minutes. Tubes were then further centrifuged at 4,000 rpm for 10 minutes and the supernatant discarded. 700 ul of 75% ethanol was added to tubes before being centrifuged at 4,000 rpm for 5 minutes to wash the pellet. Supernatants were discarded and after 1 minute the remaining ethanol wash, collected at the bottom of the tube, was removed by pipetting. Pellets were left to air dry at room temperature for 20 – 30 min. Finally, the DNA pellet was resuspended in 100 µl of water or TE buffer and stored at -20 °C for further use.

8.4 Genotyping

8.4.1 PCR genotyping

Genomic DNA was used as template to genotype plant lines by PCR. PCRs were performed in 15 µl reactions: 2 µl gDNA template, 2 µl 10 mM dNTPs diluted in water, 2 µl forward and reverse oligo 10 µM diluted in water, 2 µl CoralLoad 10x Taq Buffer and 5 µl $MgCl_2$ 25 mM buffer, 0.15 µl Taq polymerase (Qiagen). The PCR programme was: 94 °C for 3 min as an initial denaturation step, followed by a

denaturation step at 94 °C for 30 sec, annealing step for 30 sec at 54 °C and extension step at 72 °C for 1 min, repeated for 30 cycles with a final elongation step at 72 °C for 3 min. The oligonucleotide combinations used for genotyping are listed below.

In order to genotype SALK and GABI T-DNA insertion lines, the primer design software tool from the SALK institute http://signal.salk.edu/tdnaprimers.2.html was used. To genotype the CRISPR *iqd24* mutant, primers were designed spanning the deletion site, amplifying a 250 bp product in WT and 183 bp product in mutant with band size separation visible after agarose gel electrophoresis.

8.4.2 Genotyping Oligonucleotides

SALK lines

LBb1.3 ATTTTGCCGATTTCGGAAC used with respective RP's bellow for T-DNA band 550-800bp in length

iqd22-1

LP GACGAAAAACGGAGTAGGGAC RP ACCGTGCCTTAACAGGACTTC

iqd23-2

LP ACTTTAACCGACGCCCTTTAG RP AACTTGGCCCATCTGACAAC

iqd25-1

LP TGGTTTGCAGAAAATGGAAAG RP AACGCTTTTCTCGCCTTTTAC

iqd27-2

LP TCCACCAACACTCTTAGCTGG RP ATTCTTCCAAATCGAGATGGG

annat4

LP ATAGGTCCATGTGTGTTTCGC RP AGCTTGAGGTGTCTGACGAAG

rgl3-1

LP ATGAAACGAAGCCATCAAGAAACGTC RP CGTATCTACCGCCGCAACTCC

GABI lines

o8409 ATATTGACCATCATACTCATTGC primer used with RP for T-DNA band, 550-880 bp.

iqd26-3

LP ACCATCCTCACACCACTAACG RP AGATTGAATTTTGCCATGTGG

DELLA mutant genotyping

DS3-2 T-DNA border used with denoted primer of mutant locus bellow, CCGGTATATCCCGTTTTCG

rgl1-1

FP AAGCTAGCTCGAAACCCCAATG RP CCACAGAGCGCGTAGAGGATAAC, RP with DS3-2

rgl2-1

FP GCTGGTGAAACGCGTGGGAACA RP ACGCCGAGGTTGTGATGAGTG, FP with DS3-2

rga-t2

FP GCCGGAGCTATGAGAAAAGTGG RP GACCTACCAAAACGATATATATAAG, FP with DS3-2

gai-t6

FP CCTAGATCCGACATTGAAGG RP AGCATCAAGATCAGCTAAAGTG FP with T-DNA primer TCGGTACGGGATTTTCGCAT

CRISPR IQD24 site

FP TTGTAGGCAAAGAGAGCGTT RP ACAAGGCTTACAGGGTTTTGG WT 250 bp *iqd24* 183 bp

WT bands 1000-1200 bp product except CRISPR line as denoted above.

8.5 Generating transgenic lines

8.5.1 Cloning of pWOL constructs

Inducible ectopic expression lines for *IQD22* and *IQD17* were established by transforming dexamethasone inducible *RPS5a* driver lines with constructs based on the pWOL pU-6Op vector (Siligato R, 2015; p1R4-pWOL:XVE), which contains 6 Op sequences followed by the Tmv Ω sequence and a region of unique restriction sites prior to a CaMV polyA termination sequence.

The adjacent *ApaI* and *KpnI* restriction sites in pWOL pU-6Op were used for directional cloning of the coding sequences of *IQD22* and *IQD17,* with forward primers designed to introduce an ApaI site upstream of the start codon of the gene and reverse primer a *KpnI* site after the stop codon. Coding sequences were amplified from WT Columbia cDNA, obtained as detailed in the methods for RT-

qPCR. pWOL vector and PCR fragments were digested seperately using NEB CutSmart enzymes in CutSmart buffer (NEB: B7204S) for 1 hr at 37 °C, after which the DNA fragments were separated by agarose gel electrophoresis and purified from the gel with the Macherey-Nagel PCR clean up kit according to the manufacturer's instructions.

The DNA concentration was established using a Nanodrop (ThermoFischer) and a 3:1 ratio of inset to vector used in a 25 µl ligation reaction with 1.5 µl T4 ligase (New England Biolabs Ltd), 2.5 µl of corresponding buffer and final reaction volume made up by sterile water. Ligation reactions were left at room temperature for 1 hr and subsequently overnight at 5 °C. Selection was on LB medium containing Spectinomycin (100 µg/ml). Correct constructs were confirmed by restriction digestion, using *ApaI* and *KpnI*, then sequenced before they were transformed into *Agrobacterium* for plant transformation.

8.5.2 Cloning of CRISPR construct

CRISPR-Cas9 constructs were made using the GoldenGate method, based on type II enzyme restriction digestion and ligation cloning, as described by Weber et al. (2011). DNA modules and the protocol were provided by the Sainsbury Laboratory (TSL SynBio, synbio.tsl.ac.uk).

An initial PCR product was generated using plasmid piCSL70001 as the template, with the forward primer matching the RNA scaffold and introducing the RNA guide sequences adjacent to the PAM site (protospacer adjacent motif where cas9 enzyme cuts; 5′-NGG-3′ where N can be any nucleotide base) and a *Bsa1* site with ATTG overhang. A common reverse primer was used to amplify from the RNA scaffold sequence and introduce a *Bsa1* site with AGCG overhang. PCR reaction and conditions were as described for genotyping, except that 1 µl plasmid (50 ng/µl) was used as template DNA. Products (160bp) were separated by agarose gel electrophoresis, purified with Macherey-Nagel PCR clean up kit according to the manufacturer's instructions and eluted in 25 µl elution buffer. Using a GoldenGate *BsaI* reaction (identical to *BpiI* reaction below, except for the restriction enzyme), the PCR product was combined with the U6-26 promoter of the vector piCSL90002 into destination vectors (piCH47751,61,71) with unique overhang cuts for ligation to *BpiI* sites. The resulting promoter guide scaffold modules were assembled into their entry vectors with selection on LB medium with

carbenicillin (100 µg/ml), IPTG (Isopropyl β- d-1-thiogalactopyranoside, 100 µg/ml) and XGAL (5-bromo-4-chloro-3-indolyl-β-D-galactopyranoside, 200 µg/ml).

The level M destination vector pAGM8031 was used in a GoldenGate reaction to combine the FAST RED plant selection marker (pICSL11015), Ubi10:Cas9 in reverse orientation (BCJJ358C) and guide RNA modules (as PCR products with *BpiI* sites rather than plasmid modules, as detailed in Chapter 2). The total reaction volume was 15 µl, with 1 µl T4 ligase (New England Biolabs Ltd), 1.5 µl ligase buffer and 1 µl *Bpi*I restriction enzyme (Invitrogen), with 1.5 µl of the corresponding 10X concentrated buffer. 1 µl of level M destination vector and the same concentration of entry vectors based on size in kb were added (the concentration and and quality of insert DNA were measured using a NanoDrop, Thermofisher). Final reaction volumes were made up by sterile water. The reaction was subjected to 35 cycles (37 °C 3 minutes, 16 °C 4 minutes) followed by 50 °C for 5 minutes and 80 °C 10 minutes. After transformation into E.coli (DH5α,) and selection in LB medium with spectinomycin (100 µg/ml), IPTG (100 µg/ml) and XGAL (200 µg/ml), positive constructs were confirmed by restriction digestion and sequencing.

8.5.3 Cloning of the pIQD24::IQD24-YFP Reporter Construct

pIQD24::IQD24-YFP was also constructed using the GoldenGate method. The IQD24 promoter region (denoted as the genomic region from the 5’ UTR of the upstream flanking gene to the IQD24 start codon), the coding region (from start codon up to but not including stop codon) and the 3’ terminator region (including 3’UTR and genomic sequence up to the start of the downstream flanking gene) were amplified using Q5 high fidelity DNA polymerase (Qiagen). The reaction contained Q5 buffer supplemented with $MgCl_2$ 25 mM, in 50 µl (2 µl gDNA template, 5 µl 10 mM dNTPs, 5 µl forward and reverse oligo 10 µM, 10 µl 5X concentrated buffer, 5 µl $MgCl_2$ 25 mM, remaining vol made up with sterile water). The PCR cycles were: denaturation step at 98 °C for 3 min, followed by a denaturation step at 98 °C for 30 sec, annealing step for 30 sec 60 °C and extension step at 72 °C for 1 min – 3 min according to amplicon length, repeated for 35 cycles, followed by a final elongation step at 72 °C for 5 min. The primers introduced *BsaI* sites with cut site overhangs for subsequent assembly in the destination vector. PCR products were purified after agarose gel electrophoresis, with Macherey-Nagel PCR clean up kit according to the manufacturer’s

instructions and eluted in 25 µl elution buffer. PCR products were cloned first into the pGEM T-easy vector (Promega) using an A-tail PCR reaction and ligation at 16°C overnight as per the manufacturers' instructions. SP6 and T7 sequencing primers were used to confirm the correct sequence before use in the GoldenGate assembly reaction.

The assembly reaction combined promoter, gene region and terminator regions with a C-terminal YFP tag (pICSL50005, TSL synbio) into the final destination vector pICSL86955OD (TSL synbio), which confers BASTA resistance in plants. The total reaction volume was 15 µl, with 1 µl T4 ligase (New England Biolabs Ltd), 1.5 µl buffer and 1 ul *BsaI* HF (New England Biolabs) and 1.5 ul bovine serum albumin (BSA). 1 µl of destination vector used (100-150 ng/µl) and the same concentration of entry vector based on size in kb. The amount and quality of insert and vector DNA were measured using a NanoDrop (Thermofisher). The final reaction volume was made up by sterile water. PCR cycles were: (37 °C 3 minutes, 16 °C 4 minutes) × 35 cycles, 50 °C 5 minutes, 80 °C 10 minutes. After transformation into E.coli **(**strain DH5α) and selection in LB medium with kanamycin (50 µg/ml), positive clones were confirmed by restriction digestion and sequencing.

8.5.4 Cloning oligonucleotides

8.5.4.1 ApaI-CDS-KpnI

Restriction sites introduced by primers denoted in yellow

IQD17

FP: ATATGGGCCCTATGGGTAAGAAGAGCGGTTC

RP: ATATGGTACCATCATCTTAACCATCGCCTAT

IQD22

FP: ATATGGGCCCTATGGGAAAAGCGTCACG

RP: ATATGGTACCAGTACCTATACCCAATTGGC

8.5.4.2 pIQD24::IQD24-YFP

The genomic DNA sequence was checked for *Bsa*I sites and where present, silent mutations were introduced as detailed below. *Bsa*I sites intoduced by primers are denoted in yellow and overhangs in purple.

Promoter IQD24 600 bp no *Bsa*I sites
FP ATATGGTCTCAGGAGGAACAACATTCAGTTCCGAGG
RP ATATGGTCTCACATTCTTAGTTCATTGTATGAACTGAAC

Gene region IQD24
*Bsa*I site 310 bp into gene region
FP1 ATATGGTCTCAAATGGGTTTCTTTGGAAGACTGTTCG
Edited *Bsa*I site; serine TCT codon can be AGC
RP1 ATATGGTCTCAGCTCCACCGACGATTACTCCG 310 bp product
FP2 ATATGGTCTCAGAGCCAAGAGTATAAAGCAGCTATG
RP2 ATATGGTCTCACGAACCTTGAAAGAAAAGAGGATTAGAAC 900 bp product, The additional two bases in green were used to keep the C terminal fusion to YFP (TTCG-GCTT) in frame

Terminator IQD24 385 bp, no *BsaI* sites.
ATATGGTCTCAGCTTTCGAGAAAGGATGAAAAAAG
ATATGGTCTCAAGCGTAAGTAAAGCAACAAGTTTTAC

8.5.4.3 CRISPR guides

The forward primer for the initial PCR product featured the following components:
tgtGGTCTCAATTGNNNNNNNNNNNNNNNNNNGTTTTAAAAAAAGCACCGACT
*Bsa*I site in yellow, overhang in purple, Guide target region downstream of PAM site (N), terminator in blue and 5' end to anneal to RNA scaffold in piCSL70001 template in green.

Common reverse primer:
TGTGGTCTCAAGGTCTCTAGCGAAAAAAAGCACCGACT introducing a *Bsa*I site and amplifying from 3' end of RNA scaffold.

The following pairs of guide targets (position N in FP) adjacent to PAM sites were used to introduce targets for *IQD22, IQD23* and *IQD24*; gDNA position of adjacent PAMs noted, identifying spacing of guides:

IQD22

ACATTTCTCTTTCTTTCGATA (PAM 12089250),
TCTGCGCAGGATGCACGCTT (PAM 12089295) target regions located in second exon within 50 bp of one another.

IQD23

GAAAGATGGGCTTTTTC (PAM 24932445), TTTCATCGTCGGAAAATCGT (PAM 24932460) target regions before and after the start codon within 20 bp one another.

IQD24

ATAGCAGCACGATGCTCA (PAM 14379170), ATGTGCCTTTAGAGGCTACT (PAM 14379205) target regions in first exon within 40 bp of one another.

Additional guides targeting different regions of *IQD22* and *IQD23* were used in a second round of CRISPR-Cas9 mutagenesis:

IQD22

ATGCTGCTGCTGCGGTCGTC (PAM 12087610),
TTCAGCAACCGCAGCAGTCG (PAM 12087670), located in first exon.

IQD23

TGACAAACATGCGATAGCTG (PAM 24932210), CTCTTACTGCTGCTCATG (PAM 24932290), closer to the end of first exon than round one.

8.5.5 Electroporation of E. coli and Agrobacterium

Plasmid DNA was transformed by electroporation into *Escherichia coli* strain DH5α, for selection of positive constructs during cloning, or *Agrobacterium tumefaciens* strain GV3101, for stable plant transformation. For transformation, 40 µl of electro-competent cells (Untergasser A. 2008) were thawed on ice and 1 µl of plasmid DNA, either from mini-preps or GoldenGate ligation reaction were added.

The cells were then transferred to a pre-cooled transformation cuvette (Geneflow ltd.) and placed into a Biorad Genepulser for elctroporation using the following settings: capacitance extender 250 µFD, capacitance 25 µFD, Voltage 2.5 KV and pulse controller set at 200 Ω resistance for *E.coli* and 400 Ω for *Agrobacterium*. After electroporation, 460 µl of LB medium were added to the cuvette and the bacteria suspension was transferred to a 1.5 ml Eppendorf tube. Subsequently, transformed *E. coli* were incubated at 37 °C for 1 hr and transformed *Agrobacteria* were incubated at 28 °C for 2 hr. Half the 500 µl Bacterial suspension was pipetted onto LB plates with antibiotic selection and distributed evenly using a sterile plastic spreader. Plates were incubated at 37 °C overnight for E.coli and at 30 °C for 2 days for Agrobacterium.

For confirmation of positive cloning constructs, single E. coli colonies were picked and transferred to 10 ml of liquid LB medium supplemented with antibiotics for selection. Liquid cultures were incubated in a shaker (200 rpm speed) at 37 °C and 24 hr for E.coli. Plasmid DNA was purified from *E.coli* cultures using Macherey-Nagel Nucleospin plasmid kit following the manufacturers' instructions.

8.5.6 Plant transformation

For plant transformation the floral dipping method (Zhang, X. et al. 2006) was used. To grow *Agrobacterium* for transformation, 10 ml of LB medium was innoculated with one colony of transformed *Agrobcterium* and incubated for 48 hours at 28°C with shaking. Following growth, 500 ml LB flasks were inoculated with 5 ml of the grown 10 ml culture and incubated with shaking for a further 24 hours at 28 °C. To harvest the *Agrobacterium* cells, the liquid culture was centrifuged in 2 X 250 ml sterile plastic bottles at 3000 rpm and 4 °C for 20 min without centrifuge brakes. The supernatant was discarded and the pellet resuspended in 500 ml transformation media containing 25 g sucrose, and 150 µl Silwet L-77. Any siliques were removed from plants prior to dipping and the main shoot and side branch apices were submerged in the bacterial suspension for 30 sec to 1 min. Dipped plants were transferred to plastic bags sealed, with micropore tape, but not air tightly, and left for 24 hr in the dark. For seed collection, plants were grown in a containment glasshouse until mature.

8.6 Quantitative reverse transcription-polymerase chain reaction (qRT-PCR)

8.6.1 RNA extraction and DNAse treatment

RNA was extracted from 6-10 shoot apices per biological replicate with older flowers and buds removed, which were immediatly frozen in liquid nitrogen and stored at -70 °C. Extraction was performed using the RNEASY PLANT MINI KIT (74904 QIAGEN) according to the manufacturer's instructions and eluted in RNAse-free water before quantifying with Nanodrop (ThermoFischer). RNA was DNaseI treated with AMBION DNA free (AM1906, Invitrogen). In order to obtain 2 µg of treated RNA, 5 µg of eluted RNA were DNAse-treated in a 30 µl reaction containing 3 µl of 10X buffer and 2 µl of DNAseI for 1 h at 37° C, according to the manufacturer's instruction. After DNAse treatment samples were re-checked using the Nanodrop.

8.6.2 Reverse Transcription using DNAse-treated RNA

Subsequently, reverse transcription (cDNA synthesis) was performed using 2 µg of DNAse treated RNA in an 80 µl reaction. For this, 2 µg of RNA was incubated with 3 µl of Oligo dT (12-18) of concentration of 0.5 µg/µl (18418-012I, Invitrogen) and 3 µl of dNTPs of concentration 10 µM (Roche). Final volume was made to 50 µl using RNAse free water. This reaction was incubated for 5 min at 65° C. Once oligos were annealed, the reaction was placed on ice for 1 min. Subsequently, 12 µl of 5X First Strand Buffer (supplied with the Superscript III enzyme), 3 µl of RNasin RNAse inhibitor (N2111, Promega), 3 µl of 0.1 M DTT (supplied with the Superscript III enzyme), 10 µl of RNAse free water, and 3 µl of SuperScript III Reverse Transcriptase (Invitrogen 18080-044) were added, making the final reaction volume 80 µl. For reverse transcription, the reactions were incubated at 50° C for 50 min in a PCR machine with a heated lid, followed by 15 min at 70° C for deactivation of the reverse transcriptase.

8.6.3 qRT–PCR using the LightCycler LC480 system

For quantification of transcript levels, qRT-PCR was performed in technical triplicates for four biological replicates in the LightCycler 480 System using

LIGHTCYCLER 480 SYBR GREEN I MASTER (04707516001, Roche) in a total reaction volume of 10 µl, containing 5 µl of LIGHTCYCLER 480 SYBR GREEN I MASTER, 2 µl of the forward and reverse oligo mix (10 µM), 1 µl of cDNA template, and 2 µl of PCR-grade water (Roche). The reaction was performed in an LC 480 qPCR cycler (Roche) using a standard programme with 5 min at 95° C, 40 cycles of 10 sec at 95° C, 15 sec at annealing temperature 60 °C and 15 sec at 72 °C. After each cycle, the SYBR GREEN signal was measured. The 40 cycles were followed by a melting curve starting from 65 °C to 98 °C. Data was saved as text file format and analysed in Excel (Microsoft) by applying 2-ΔCt method (ΔCt = Ct gene of interest – Ct ref gene), using TUBULIN alpha 4 chain expression (TUB4-RT_1-F, TUB4-RT_1-R) for normalisation (Livak and Schmittgen, 269 2001).

8.6.4 Designing and testing oligos for qRT-PCR

Primers were designed manually to match sequences downstream of T-DNA insertion sites. Where possible, one primer was designed to span an exon-intron border to disrupt amplification from gDNA, which could be present in low quantities as a contaminant. Oligos were diluted in PCR-grade water to 100 µM stock solutions (Sigma) before further 10 µM working solutions were made . The amplification efficiency of qRT-PCR oligos was tested using a dilution series; 1, 0.5, 0.2, 0.1 and 0.06 of cDNA templates with RNAase free water and a water control in three technical replicates with cycler settings as above. The LC480 software was used to generate standard curves from which the slope was calculated (optimum -3.3) to assess efficiency as well as noting the amplification factor, desirable above 1.85, where 2 corresponded to 100% efficiency. In addition, it was checked that the melting curve gave a single clear peak, denoting a single amplification product.

8.6.5 qRT-PCR oligonucleotides

TUB4 control

FP CTGTTTCCGTACCCTCAAGC RP AGGGAAACGAAGACAGCAAG

IQD22

FP CGATCTCTTCTCGCAGCTCC RP CTTGCCTTCGAACCATTCCTCTTG

IQD23

FP GAACAAAAGAGCGGTGGAGG RP CGAGGAGAGCATTACGCAGCTCC

IQD25

FP CGGCGAGAAAATCCACGGAAAG RP CCCTGTATCTACCTCCACTATC

IQD26

FP CATCCTCGACACTCACTTGAG RP CATCGTACGCATTGTTGTTG

IQD27

FP CGGCCGCAATGTTGCAGAGC RP GCTTCATCAAACTTATCAAAGG

8.7 Imaging

8.7.1 Photography of vegetative and whole plant images

Images presented of mature rosettes, individual leaves, whole plants and seedlings were captured with Nikon D3100 camera, with Nikon DX AF-S NIKKOR 18-55mmb1:3.5-5.6G lens or Nikon N AF-S Micro NIKKOR 60mm 1:2.8G lens.

8.7.2 Photography for stem elongation rates

Images of whole plants were captured next to ruler from the day the third mature flower developed (T0), with landmarks drawn directly on the plants every 2 mm from the shoot apex, marking the top 4 cm of the stem. Landmarked plants were re-imaged after 4 days. Fiji was used to manually place landmarks on the images. To measure the distances between landmarks, plot graphs and perform statistical analysis, custom Python scripts were used as described (Bencivenga et al. 2016).

8.7.3 Brightfield microscopy

Brightfield images (ovary and seeds, PI stained stem sections and early leaf serration pattern) were obtained using a Leica MZFLIII stereo microscope with GXCAM LITE camera using transmission light (with bright field - BF settings). Images of scales were taken at the same magnification, with markings every 0.5 mm for stem thickness quantification and 0.1 mm for seed and ovary dimensions.

8.7.4 Phase Contrast

To analyse outlines of PC cells in the epidermis, mature leaf or young leaves were removed and cut into three segments using a razor blade separating base, mid-section and upper region. These leaf sections were placed into 200-300 µl of melted 3% agarose pipetted onto microscope slides. Once set, the leaf sections were carefully removed using forceps and slides left 24 hr to dry in slide cases. Following this, slides were loaded onto the phase microscope stand (Nikon MICROPHOT-SA with Leica camera DFC450), and focus adjusted for outline of PCs under X10 objective. Leaf sections were visualised in Leica Application Suite V4.4 live and optimised before measurements.

8.7.5 Pseudo-Schiff-propidium iodide staining

The pseudo-Schiff-propidium iodide (mPS-PI) staining was modified after Truernit et al. (2008). In preparation for staining, samples of shoot apices, stem sections and early leaves were treated as follows;

Apices: larger floral buds were removed from the inflorescences using forceps and the stem cut 10 mm bellow the apex using a razor blade. Further bud dissection was performed under the stereomicroscope. The inflorescence stems were inserted into a solidified 2% agarose block in a petri dish and submerged in sterile water. Buds were removed concentrically using a syringe needle until only those surrounding the shoot meristem remained.

Stem: hand sections were cut at the base and position of first silique elongated using forceps to secure a 1 cm stem section in desired vicinity and razor blade to cut around 1 mm thick sections.

Leaf: Seedlings grown on plates for 18 days were transferred to petri dish lids containing sterile water. Cotyledons and roots were removed by syringe needle under the stereomicroscope.

Subsequently, the partially dissected samples were submerged in 15%, 30%, 50%, 70%, 85%, 95% and 100% ethanol for 15 min each at room

temperature, after which they could be safely stored at -20 °C or immediately progressed to next step. The stem and leaf samples required no further dissection. The shoot apices were again secured by 2% agarose in petri dishes and submerged in 100 % ethanol for manual removal of all but the 3-4 buds surrounding the meristem using a syringe needle. The stem was then removed from the set agarose and sample, laid on its side and cut just bellow the base of the meristem and adjoining buds using multiple small incisions around the circumference of the stem with the syringe needle to ensure an even flat surface. This was important to subsequently position the sample upright.

If not previously stored in ethanol, samples were submerged in 100% ethanol in 2 ml Eppendorph tubes were kept at -20 °C overnight. Then, the samples were rehydrated through the same ethanol series, washed in water and incubated at 37 °C for 24 hr, or minimum overnight, in alpha-amylase solution containing 0.3 mg/ml alpha amylase (A4551, Sigma) in 20 mM phosphate buffer pH 7.0, 2 mM NaCl, 0.25 mM $CaCl_2$. Samples were then rinsed twice in water before being submerged in 1% periodic acid (freshly dissolved in sterile water) for 30 minutes, followed by two washes in water. Subsequent steps were performed at room temperature with gentle shaking and protected from light. The samples were incubated for 2 hr in Schiff-PI reagent, which was prepared as follows: 625 µl HCl 12 N added to 49 ml sterile water, before dissolving 0.95 g sodium metabisulfite; propidium iodide (81845, Sigma, stock solution of 1mg/ml in water) was added to this solution to a final concentration of 20 µg/ml as in Truernit et al. (2008). Following staining in Schiff-PI reagent, samples were washed twice in water.

Subsequently, the meristem and early leaf samples were individually placed on single cavity depression slides (76 x 25 x 1.25 mm) (AGL4090, Agar Scientific). Stem section samples were placed laying flat on normal slides and white tape layered on coverslips, creating spacers to separate the coverslip from the sample. Samples were immediately covered with a drop of 25% chloral hydrate solution diluted in sterile water (stock solution 40 g chloral hydrate dissolved in 10 ml sterile water and 5 ml glycerol) and left for 8 min. The solution was carefully removed by filter paper. This step was repeated at a 50% dilution, 75% dilution and finally 100% concentration of chloral hydrate. This step was particularly important for stem sections where changes in osmotic pressure can damage large cells. Then, the samples were covered (100 µl for leaf and meristem samples, 150 µl for stem sections) with Hoyer’s Medium as in Truernit et al. (2008) (40 g chloral hydrate

dissolved in 10 ml sterile water, 5 ml glycerol, 6 g gum Arabic, G9752, Sigma) that was centrifuged for 20 min prior to use. The meristem and leaf samples were arranged using the syringe needle in the centre of the depression with the apices facing upwards and early leaves laying flat, as visualised under a stereomicroscope. Samples were finally covered with a 22 x 22 mm glass cover slip, thickness No 0 (VWR International). Prepared slides were left to dry overnight protected from light and imaged within the following two days.

For imaging, a Zeiss 880 confocal microscope with a 25X mixed immersion objective was used with laser excitation at 561 nm and emission filters set to 580-640 nm for the PI signal. 16-bit images were obtained with 1016x1016 pixel size using 4X mean averaging. For z-stacks, the image thickness was set to 0.5 µm and the pinhole to an optical thickness of airy 1. The detector gain was adjusted according to the signal intensity across samples. Images were saved in .lsm file format and displayed in Fiji (Schindelin, J. et al. 2012).

8.7.6 Confocal live imaging

Live imaging was also performed using a Zeiss 880 confocal microscope. Meristem, cotyledon and early leaf samples were prepared and imaged as follows. For live imaging of meristems, floral apices were dissected under water in 2% agarose with a syringe needle (as described above). Floral apices were left to recover for 24 hr on GM in individual 60 mm petri dishes under normal growth conditions. Samples in GM dishes were submerged in water for imaging with a 40X water dipping lens.

For live imaging of cotyledons, whole seedlings at 2, 5 and 10 DAG were transferred from GM plates to slides with a sterile water drop. A coverslip was positioned to flatten the cotyledons. For live imaging of early leaves, seedlings at 14-18 DAG were dissected on slides in a water drop under a stereomicroscope using a syringe needle. At early time points, cotyledons were removed and early leaves with upper hypocotyl transferred to fresh slide to be imaged. At later time points, the first leaf was detached from the stem and transferred to a separate slide to be imaged. In instances where cell outlines were stained with N-(4-triethylammoniumpropyl)-r-(pdietheylaminophenylhexatrienyl pyridium dibromide) (FM4-64, Invitrogen), early leaves were first transferred to a 0.6 ml tube containing 50-100 µl of FM4-64 solution at 20 µg/ml concentration for 10 min. The early leaves were then washed once in water before transferring to a microscope slide

with drop of water. A coverslip was positioned to create a flat laying leaf. Imaging was performed with a 25X multi-immersion lens.

When imaging *pIQD24::IQD24YFP* , *pIQD18::IQD18YFP*, *pPIN1:PIN1 - GFP*, *DR5:GFP* and *mCherry-TUA5* lines, laser excitation was at 488 nm for GFP, 514 nm for YFP signal and 561 nm for FM4-64 and mCherry. GFP emission signal was detected at 505-540 nm, YFP at 520-560 nm, FM4-64 emission signal at 590-660 nm and mCherry at 570-640 nm. 3D Viewer and Orthogonal Views plugins of Fiji (Schmid et al., 2000) as well as z-stack projection were used in images presented in some Figures.

8.7.7 Nuclei staining with DAPI

Stem sections were hand cut using a razor blade as detailed and immediately transferred to an Eppendorf tube (2 ml) containing 300 µl of water with 100µg/ml fixable version of FM4-64, FM4-64-FX (F34653, ThermoFischer) for 15 min. After staining, the sections were washed once in 1× PBS buffer and transferred to fresh 2 ml tubes containing 1× PBS buffer with 3% formaldehyde and 1µg/ml of DAPI (4', 6-diamidino-2-phenylindole) (10236276001, Roche). The samples were vacuum-infiltrated (80-100 mbar) for 5 minutes before tubes were left in staining solution a further 15 minutes at room pressure on ice. Samples were washed twice in 1× PBS buffer before slide preparation as detailed previously for stem sections, however with water rather than Hoyer's medium. Accordingly, slides were imaged using the 25X mixed immersion objective with water rather than oil. Samples were imaged with laser excitation at 405 nm and captured over the emmission range 405 – 520 nm.

8.7.8 FACS analysis of DAPI-stained nuclei

Stem sections cut from the base of mature plant stems, or young leaves from plants grown on GM plates for 3 weeks, were collected and immediately chopped with a razor blade in 500 µl ice-cold nuclei extraction buffer (CyStain UV precise P, PARTEC) in a small petri dish lid. The solution was filtered through 30-µm nylon mesh into 5 ml round-bottom tubes and stained with 1 ml DAPI staining buffer (×2 vol, CyStain UV precise P, PARTEC). The stained nuclei were analysed by flow

cytometry (BD FACSMelody system) and the data were processed with the BD FACSChorus software to determine the ploidy distribution.

8.8 Chemical plant treatments

8.8.1 Dexamethasone induction treatment for phenotyping

For activation of dex-inducible transgenes in the shoot apex, a 0.015% Silwet L-77 (De Sangosse) solution supplemented with 0.1% ethanol (control treatment) or with 10 µM dexamethasone (D4902, Sigma) solution and 0.1% ethanol (induction treatment) was used to treat *RPS5a:LhGR Op:IQD22* and *RPS5a:LhGR Op:IQD17* lines. As a further control, wild-type L-*er* plants were treated with dex as per the induction treatment. All treated plants had the respective solutions applied to the centre of the inflorescence using a paint brush, with applications every other day for 4 treatments. For activation throughout development, seeds were germinated on GM plates containing dex 10 µM as detailed in plant growth.

8.8.2 Dexamethasone treatment for calcium signalling

To investigate downstream response of calcium realease events following induction of the *IQD22*, *RPS5a:LhGR Op:IQD22* line, meristems were dissected under a stereomicroscope as described above and incubated for 24 hr in 60 mm petri dishes containing GM and 10 µM of dexamethasone. Additionally, the solution used to submerge the samples during live imaging contained 10 µM dex and 0.1% ethanol. Respective 0.1% ethanol controls were performed with inducible lines or dex with 0.1% ethanol for L-*er* controls.

8.8.3 Flg22 induction for calcium signalling

Dissected shoot apices in assays using the calcium response elicitor flg22 (Sigma-Aldrich: SRP8029-10UG) were initially imaged while submerged in water, which was then replaced with 10 µM flg22 solution containing 0.01% Silwet-77 and imaged immediately and at 1 hr and 1.5 hr intervals. Due to disruption to IQD localisation caused by Silwet-77, the assay was subsequently performed with only 10 µM flg22 elicitor.

8.8.4 2,4-dichlorophenoxyacetic acid (2,4-D) induction

To activate auxin responses in early leaves of plants expressing *IQD24-YFP* or *DR5:GFP*, whole seedlings at 18 DAG were submerged for 24 hr in 2 ml of 10 µM 2,4-D solution (D7299, SIGMA), alongside controls submerged in water only. Following this treatment, early leaves were dissected, stained with FM4-64 and loaded to slides as detailed above for imaging.

8.8.5 Oryzalin treatments

In confocal experiment where microtubule stability under oryzalin treatment was assayed in PCs of early leaves seedlings were grown on plates for 14 days. Subsequently, first leaf was dissected as detailed in live imaging section above, and submerged in 2 ml wells containing 0.5% DMSO for control, 2 µM oryzalin (36182, SIGMA) in 0.2% DMSO solution and 5 µM oryzalin in 0.5% DMSO solution for 1 hr, prior to washing in water, loading to microscope slides and imaging immediately as detailed in live imaging.

8.8.6 Mannitol solution osmotic treatment

Meristems on PIN1-GFP plants were dissected and left to recover for 24 hr in GM as detailed above. Prior to imaging, meristems were submerged for 1.5 hr in a 0.2 M mannitol solution aimed to mirror osmotic potential of meristem cells. Following this, meristems were imaged under settings as detailed for the GFP reporter above and then moved to hypo-osmotic water solution for 1 hr, before re-imaging under identical microscope settings for comparison of signal intensity.

8.9 Data analysis

8.9.1 Analysis of oriented divisions in mPS-PI images

Image processing of mPS-PI-stained meristems was performed by Robert Sablowski with Fiji macros and custom python scripts as described (Bencivenga et al 2016). Briefly, 3D segmentation used the morphological watershed algorithm implemented in SimpleITK, with a Gaussian blur of the cell walls image to prevent

oversegmentation (i.e., splitting of real cells into may artifactual, smaller cells). To select cells in the RZ, the latter was defined as a region between 25 and 150 µm of the meristem summit, contained within a radius from the main stem axis that increased linearly from 10 µm near the summit to 30 µm at the bottom. Segmented cells whose centre of mass was contained in the region defined as RZ had their volumes calculated from the number of voxels and voxel size. Their sphericity was measured as the coefficient of variation of the distances between the cell's centre of mass and each voxel on the cell surface. Recently made cell walls identified assuming that the mPS-PI signal was proportional to wall thickness; a new wall was flagged when two neighboring cells shared the same wall as their wall with lowest intensity. Once new walls were selected, their orientation was calculated. "Angle to the main axis" was defined as the angle between the main stem axis (defined by manually chosen landmarks) and the vector normal to a plane best fitting each new wall. "Angle to the radial axis" was the angle between the vector normal to best fitting plane and a vector perpendicular to the main axis that crossed the wall's center of mass (Bencivenga, S. et al 2016).

8.9.2 Morpholeaf

Morpholeaf (Biot, E. et al. 2016; Andrey, P. & Maurin, Y. 2005) was used to outline leaves, including serrations, and add landmarks at the top of the petiole, petiole base, leaf apex and each identified serrations’ sinus and peak in Free D. All landmarks were placed automatically and adjusted manually. Markings subsequently allowed readouts of leaf area, serration area, as well as width and height measurements (Biot et al., Practical Guide for MorphoLeaf).

8.9.3 Fiji

Metadata and pixel size in µm or scales were used to quantify diameter of stem as well as cells in stem cross sections, seed width, ovary and silique size through manually drawing ROIs in Fiji (Schindelin, J. et al. 2012).

8.10 Statistics

The Kolmogorov–Smirnov test was used to compare distributions of new division plane angles, RZ cell volume and sphericity and report significance of differences between WT and *1aiqd* lines. Data were plotted using Matplotlib in Python and seaborn (Hunter, J.D., 2007; Waskom, M et al. 2020). A two-sided Mann-Whitney test with Bonferroni correction was used to test for significance of differences in plant measurements, including the extensive analysis of leaf shape performed in Morpholeaf. Stem diameter thickness data presented using DABEST (Ho, J. et al. 2019) was also assessed using the Mann-Whitney test and also Hedge's g analysis, to indicate the power of the analysis.

Bibliography

Abel, S., Savchenko, T. and Lev, M. (2005). Genome-wide comparative analysis of the IQD gene families in Arabidopsis thaliana and Oryza sativa. BMC Evolutionary Biology, 20055:72. DOI: 10.1186/1471-2148-5-727

Aida, M., Ishida, T. and Tasaka, M. (1999). Shoot apical meristem and cotyledon formation during Arabidopsis embryogenesis: interaction among the CUP-SHAPED COTYLEDON and SHOOT MERISTEMLESS genes Development, 126, pp. 1563–1570

Allard, J. F., Wasteneys, G. O., & Cytrynbaum, E. N. (2010). Mechanisms of self-organization of cortical microtubules in plants revealed by computational simulations. *Molecular biology of the cell*, *21*(2), 278–286.

Altartouri, B., Bidhendi, A.J. Tani, T., Suzuki, J., Conrad, C., Chebli, Y., Liu, N., Karunakaran, C., Scarcelli, G., Geitmann, A. (2019). Pectin Chemistry and Cellulose Crystallinity Govern Pavement Cell Morphogenesis in a Multi-Step Mechanism. Plant Physiology, 181 (1) 127-141; DOI: 10.1104/pp.19.00303.

Amir J. Bidhendi, A.J., Geitmann, A. (2019). Geometrical Details Matter for Mechanical Modeling of Cell Morphogenesis. Developmental Cell, Volume 50, Issue 1, 1, Pages 117-125.e2

Ando K, Grumet R. (2010). Transcriptional profiling of rapidly growing cucumber fruit by 454-pyrosequencing analysis. J Amer Soc Hortic Sci, 135: 291-302.

Andrey P & Maurin Y (2005). *Free-D*: an integrated environment for three-dimensional reconstruction from serial sections. *Journal of Neuroscience Methods*, 145, 233-244

Achard P., Gusti A., Cheminant S., Alioua M., Dhondt S., Coppens F., Beemster G. T. S., Genschik P (2009). Gibberellin signaling controls cell proliferation rate in Arabidopsis. Curr. Biol. **19**, 1188–1193

Badmi, R., Payyavula, R. S., Bali, G., Guo, H. B., Jawdy, S. S., Gunter, L. E., Yang, X., Winkeler, K. A., Collins, C., Rottmann, W. H., Yee, K., Rodriguez, M., Jr, Sykes, R. W., Decker, S. R., Davis, M. F., Ragauskas, A. J., Tuskan, G. A., & Kalluri, U. C. (2018). A New Calmodulin-Binding Protein Expresses in the Context of Secondary Cell Wall Biosynthesis and Impacts Biomass Properties in *Populus*. *Frontiers in plant science*, *9*, 1669. https://doi.org/10.3389/fpls.2018.01669)

Bahler, M. and Rhoads, A. (2002). Calmodulin signaling via the IQ motif. FEBS Letters. Volume 513, Issue 1, 20, Pages 107–113.

Banasiak, A., Biedroń, M., Dolzblasz, A., & Berezowski, M. A. (2019). Ontogenetic Changes in Auxin Biosynthesis and Distribution Determine the Organogenic Activity of the Shoot Apical Meristem in *pin1* Mutants. *International journal of molecular sciences*, *20*(1), 180. https://doi.org/10.3390/ijms20010180

Baskin,T. I. (2005). Anisotropic Expansion of the Plant Cell Wall. Annu. Rev. Cell Dev. Biol, 21:203–22.

Bencivenga, S., Serrano-Mislata, A., Bush, M., Fox, S., & Sablowski, R. (2016). Control of Oriented Tissue Growth through Repression of Organ Boundary Genes Promotes Stem Morphogenesis. *Developmental Cell*, *39*(2), 198–208. http://doi.org/10.1016/j.devcel.2016.08.013

Belteton, SA., Sawchuk, MG., Donohoe, BS., Scarpella, E., Szymanski, DB. (2018). Reassessing the Roles of PIN Proteins and Anticlinal Microtubules during Pavement Cell Morphogenesis. Plant Physiol.

Bennett, T. and Leyser, O. (2006). Something on the side: axillary meristems and plant development. Plant Mol Biol 60: 843. doi:10.1007/s11103-005-2763-4

Besson, S. Dumais, J. (2011). Universal rule for the symmetric division of cells. Proc. Natl. Acad. Sci. U.S.A., 108 , pp. 6294-6299)

Biedroń, M., & Banasiak, A. (2018). Auxin-mediated regulation of vascular patterning in Arabidopsis thaliana leaves. *Plant cell reports*, *37*(9), 1215–1229.

Biot E, Cortizo M, Burguet J, Kiss A, Oughou M, Maugarny-Calès A, Gonçalves B, Adroher B, Andrey P, Boudaoud A, Laufs P. (2016). Multiscale quantification of morphodynamics: MorphoLeaf software for 2D shape analysis *Development* 143, 3417-3428; doi: 10.1242/dev.134619

Bilsborough, G.D, Runions, A., Barkoulas, M., Jenkins, H.W., Hasson, A., Galinha, C., Laufs, P., Hay, A., Prusinkiewicz, P., Tsiantis, M. (2011). Model for the regulation of *Arabidopsis thaliana* leaf margin development PNAS, 108 (8) 3424-3429; DOI: 10.1073/pnas.1015162108

Boller, T., and Felix, G. (2009). A renaissance of elicitors: perception of microbe-associated molecular patterns and danger signals by pattern-recognition receptors. Annu. Rev. Plant Biol.60, 379–406

Boudaoud, A., Burian, A., Borowska-Wykręt, D., Uyttewaal, M., Wrzalik, R., Kwiatkowska, D., Hamant, O. (2014). FibrilTool, an ImageJ plug-in to quantify fibrillar structures in raw microscopy images. Nature Protocols.

Boudolf, V., Vlieghe, K., Beemster, G.T., Magyar, Z., Torres Acosta, J.A., Maes, S., Van Der Schueren, E., Inzé, D. and De Veylder, L. (2004). The plant-specific cyclin-dependent kinase CDKB1;1 and transcription factor E2Fa-DPa control the balance of mitotically dividing and endoreduplicating cells in Arabidopsis. The Plant Cell. 16, 2683–2692.

Bourdon M., Frangne N., Mathieu-Rivet E., Nafati M., Cheniclet C., Renaudin J.P., Chevalier C. (2010). Endoreduplication and growth of fleshy fruits. *Progress in Botany,* 71, 101-132.

Boruc, J. Weimer, A.K., Stoppin-Mellet, V., Mylle, E., Kosetsu,K., Cedeño,C., Jaquinod, M., Njo, M., De Milde,L., Tompa,P., Gonzalez, N., Inzé, D., Beeckman, T., Vantard, M. Van Damme, D. (2017). Phosphorylation of MAP65-1 by Arabidopsis Aurora Kinases Is Required for Efficient Cell Cycle Progression. Plant Physiology, 173 (1) 582-599; DOI: 10.1104/pp.16.01602

Bowman, J.L. and Eshed, Y. (2000). Formation and maintenance of the shoot apical meristem. Trends Plant Sci. 5(3):110-5.

Braam, J. (2005), In touch: plant responses to mechanical stimuli. New Phytologist, 165: 373-389. https://doi.org/10.1111/j.1469-8137.2004.01263.x

Braun, N., Wyrzykowska, J., Muller, P., David, K., Couch, D., Perrot-Rechenmann, C., Fleming, A.J. (2008). Conditional Repression of AUXIN BINDING PROTEIN1 Reveals That It Coordinates Cell Division and Cell Expansion during Postembryonic Shoot Development in *Arabidopsis* and Tobacco. The Plant Cell, 20 (10) 2746-2762; DOI**:** 10.1105/tpc.108.059048

Bryant, J.A. and Francis, D. (1985). The cell division cycle in plants. SEB Seminar Series, No. 26. Cambridge: Cambridge University Press

Byrne, M.E., Groover, A.T., Fontana, J.R. and Martienssen, R.A. (2003). Phyllotactic pattern and stem cell fate are determined by the Arabidopsis homeobox gene BELLRINGER. Development, 130, pp. 3941–3950.

Bürstenbinder,K., Möller, B., Plötner, R., Stamm, G., Hause, G., Mitra, D. and Abel, S. (2017). The IQD Family of Calmodulin-binding proteins Links Calmodulin Signaling to Microtubules, Membrane Microdomains, and the Nucleus. Plant Physiology. 73 (3) 1692-1708; DOI: 10.1104/pp.16.01743

Bürstenbinder K, Savchenko T, Müller J, Adamson AW, Stamm G, Kwong R, Zipp BJ, Dinesh DC, Abel S. (2013). Arabidopsis calmodulin-binding protein IQ67-domain 1 localizes to microtubules and interacts with kinesin light chain-related protein-1. J Biol Chem 288: 1871-1882.

Buschmann H, Fabri CO, Hauptmann M, Hutzler P, Laux T, Lloyd CW, Schaffner AR. (2004). Helical growth of the Arabidopsis mutant tortifolia1 reveals a plant-specific microtubule-associated protein. Curr Biol 14: 1515-1521.

Buschmann H, Dols J, Kopischke S, Peña EJ, Andrade-Navarro MA, Heinlein M, Szymanski DB, Zachgo S, Doonan JH, Lloyd CW. (2015). Arabidopsis KCBP interacts with AIR9 but stays in the cortical division zone throughout mitosis via its MyTH4-FERM domain. J Cell Sci 128: 2033–2046.

Busov V. B., Brunner A. M., Strauss S. H.(2008). Genes for control of plant stature and form. New Phytol. **177**, 589–607.

Cai, R. H., Zhang, C. S., Zhao, Y., Zhu, K. J., Wang, Y. F., Jiang, H. Y., Xiang, Y. and Cheng, B. J. (2016). Genome-wide analysis of the IQD gene family in maize. Molecular Genetics and Genomics. Vol. 291, issue 2, pg 543-558.

Castel, B., Tomlinson, L., Locci, F., Yang, Y., & Jones, J. (2019). Optimization of T-DNA architecture for Cas9-mediated mutagenesis in Arabidopsis. *PloS one*, *14*(1), e0204778. https://doi.org/10.1371/journal.pone.0204778

Chakrabortty B, Willemsen V, de Zeeuw T, Liao C-Y, Weijers D, et al. (2018). A plausible microtubule-based mechanism for cell division orientation in plant embryogenesis. Curr. Biol. 28:3031–43.E2).

Champagne, C., Sinha, N. (2004). Compound leaves: equal to the sum of their parts? Development 131: 4401-4412; doi: 10.1242/dev.01338

Cockcroft, C.E., Bart, G. W., den Boer J. M., Healy, S. & Murray J.A. (2000). Cyclin D control of growth rate in plants. Nature. 405, 575-579

Collins TJ. (2007). ImageJ for microscopy. *BioTechniques* 43:S25-S30.

Colón-Carmona A. et al. (1999). Spatio-temporal analysis of mitotic activity with a labile cyclin-GUS fusion protein. *Plant J.*; 20: 503-508

Crowell, E.F. Gonneau, M. Vernhettes, S. Höfte,H. (2010). Regulation of anisotropic cell expansion in higher plants, Comptes Rendus Biologies, Volume 333, Issue 4, Pages 320-324, ISSN 1631-0691, https://doi.org/10.1016/j.crvi.2010.01.007.

Cyr, R.J. and Palevitz, B.A. (1995). Organization of cortical microtubules in plant cells. Current Opinion in Cell Biology. Volume 7, Issue 1, 1995, Pages 65–71

Cyr, J.A. (1991). Calcium/Calmodulin Affects Microtubule Stability in Lysed Protoplasts. Journal of Cell Science. 1991 100: 311-317

Czesnick, H.and Lenhard, M. (2015). Size control in plants — lessons from leaves and flowers. Cold Spring Harb. Perspect Biol, 7, p. a019190

Dana, H., Mohar, B., Sun, Y., Narayan, S., Gordus, A., Hasseman, J. P., et al. (2016). Sensitive red protein calcium indicators for imaging neural activity. *Elife* 5:e12727. doi: 10.7554/eLife.12727

Davies, P. J. (2010). The Plant Hormones: Their Nature, Occurrence, and Functions. Springer Netherlands. P 1-15. Doi. 10.1007/978-1-4020-2686-7_1

Deinum, E.E., Tindemans, S.H., Lindeboom, J.J. and Mulder, B.M. (2017). How katanin severing aligns cortical microtubules. Proceedings of the National

Academy of Sciences Jul 2017, 114 (27) 6942-
6947; DOI: 10.1073/pnas.1702650114

Desvoyes B, Gutierrez C. (2020). Roles of plant retinoblastoma protein: cell cycle and beyond. EMBO J. 1;39(19):e105802. doi: 10.15252/embj.2020105802. Epub. PMID: 32865261; PMCID: PMC7527812.

Dhonukshe, P., Tanaka, H., Goh, T., Ebine, K., Mahonen, A.P., Prasad, K., Blilou, I., Geldner, N., Xu, J., Uemura, T., Chory, J. Ueda, T., Nakano, A., Scheres, B. and Friml, J. (2014). Retraction: Generation of cell polarity in plants links endocytosis, auxin distribution and cell fate decisions. Nature. Vol.511, issue 7509,370.

Di, D. W., C. Zhang and G. Q. Guo (2015). “Involvement of secondary messengers and small organic molecules in auxin perception and signaling.” Plant Cell Rep 34(6): 895-904.

Dill, A., Thomas, S., Hu, J., Steber, C & Sun, T-P. (2004). The Arabidopsis F-box protein SLEEPY1 targets GA signaling repressors for GA-induced degradation. The Plant cell. 16. 1392-405. 10.1105/tpc.020958.

Ding Z, Galván-Ampudia CS, Demarsy E, Łangowski Ł, Kleine-Vehn J, Fan Y, Morita MT, Tasaka M, Fankhauser C, Offringa R, Friml J. (2011). Light-mediated polarization of the PIN3 auxin transporter for the phototropic response in Arabidopsis. Nat Cell Biol. ;13(4):447-52. doi: 10.1038/ncb2208. Epub 2011 Mar 13. PMID: 21394084

Dinneny,J.R., Yadegari, R., Fischer, R.L., Yanofsky, M.F. and Weigel, D. (2004). The role of JAGGED in shaping lateral organs. Development. 131: 1101-1110; doi: 10.1242/dev.00949

Dixit, R., Cyr, R. (2004). The Cortical Microtubule Array: From Dynamics to Organization. The Plant Cell, 16 (10) 2546-2552; DOI: 10.1105/tpc.104.161030

Dobney, S., Chiasson, D., Lam, P., Smith, S.P., Snedden, W.A. (2009). The calmodulin-related calcium sensor CML42 plays a role in trichome branching. J. Biol. Chem., 284, pp. 31647-31657

Dou, J., Zhao, S., Lu, X., He, N., Zhang, L., Ali, A., Kuang, H., Lui, W. (2018). Genetic mapping reveals a candidate gene (*ClFS1*) for fruit shape in watermelon

(*Citrullus lanatus* L.). *Theor Appl Genet* 131**,** 947–958. https://doi.org/10.1007/s00122-018-3050-5

Douady, S. Couder, Y. (1996) Phyllotaxis as a Dynamical Self Organizing Process Part II: The Spontaneous Formation of a Periodicity and the Coexistence of Spiral and Whorled Patterns. Journal of Theoretical Biology. Volume 178, Issue 3, Pages 275-294.

Drevensek S, Goussot M, Duroc Y, Christodoulidou A, Steyaert S, Schaefer E, Duvernois E, Grandjean O, Vantard M, Bouchez D, et al. (2012). The *Arabidopsis* TRM1-TON1 interaction reveals a recruitment network common to plant cortical microtubule arrays and eukaryotic centrosomes. Plant Cell 24: 178–191.

Edel, K.H., Marchadier, E., Brownlee, C., Kudla, J., Hetherington, A.M. (2017). The Evolution of Calcium-Based Signalling in Plants,Current Biology,Volume 27, Issue 13,Pages R667-R679,ISSN 0960-9822,https://doi.org/10.1016/j.cub.2017.05.020.

Engler, C; Kandzia, R; Marillonnet, S (2008). "A One Pot, One Step, Precision Cloning Method with High Throughput Capability". *PLOS ONE*. **3** (11): e3647. Bibcode: 2008PLoSO 3.3647E. ISSN 1932-6203. PMC 2574415. PMID 18985154.

Fàbregas, N., Formosa-Jordan, P., Confraria, A., Siligato, R., Alonso, J.M., Swarup, R., Bennett, M.J., Mähönen, P.A., Caño-Delgado, A.I. Ibañes,M. (2015). Auxin Influx Carriers Control Vascular Patterning and Xylem Differentiation in *Arabidopsis thaliana.*.PLOS genetics.

Farquharson, K. L. (2009). Cortical Microtubules Regulate the Insertion of Cellulose Synthase Complexes in the Plasma Membrane. The Plant Cell, 21(4), 1028. http://doi.org/10.1105/tpc.109.210411

Faulkner, C, Zhou, J, Evrard, A, Bourdais, G, Maclean, D, Haweker, H, Eckes, P and Robatzek, S. (2017). An automated quantitative image analysis tool for the identification of microtubule patterns in plants. *Traffic*; 18: 683– 693. https://doi.org/10.1111/tra.12505

Ferjani A, Ishikawa K, Asaoka M, Ishida M, Horiguchi G, Maeshima M, Tsukaya H. (2013. Class III compensation, represented by KRP2 overexpression, depends on V-ATPase activity in proliferative cells. Plant Signal Behav.; 8:11. pmid:24305734

Feng, L., Chen, Z., Ma, H., Chen, X., Li, Y. (2014). The IQD Gene Family in Soybean: Structure, Phylogeny, Evolution and Expression. PLoS ONE. 9(10): e110896. doi:10.1371/journal.pone.0110896

Fletcher, J.C., Brand, U., Running, M.P., Simon, R. and Meyerowitz, E.M. (1999). Signaling of cell fate decisions by CLAVATA3 in Arabidopsis shoot meristems. Science, 283, pp. 1911–1914

Fridman, Y. Savaldi-Goldstein, S. (2013). Brassinosteroids in growth control: how, when and where. *Plant Science* 209, 24–31.

Fu Y*,* Gu Y*,* Zheng Z*,* Wasteneys G*,* Yang Z. *(*2005*).* Arabidopsis interdigitating cell growth requires two antagonistic pathways with opposing action on cell morphogenesis*.* Cell 120*:* 687–700.

Fu H.Q., Mao W.H., Shi K., Zhou Y.H., Yu J.Q. (2010). Spatio-temporal changes in cell division, endoreduplication and expression of cell cycle-related genes in pollinated and plant growth substances-treated ovaries of cucumber. *Plant Biology,* 12, 98-107.

Fujikura U, Ezaki K, Horiguchi G, Seo M, Kanno Y, Kamiya Y, et al. (2020). Suppression of class I compensated cell enlargement by *xs2* mutation is mediated by salicylic acid signaling. PLoS Genet 16(6): e1008873. https://doi.org/10.1371/journal.pgen.1008873

Gaillochet, C., Daum, G., Lohmann, J.U. (2015). O Cell, Where Art Thou? The mechanisms of shoot meristem patterning, Current Opinion in Plant Biology, Volume 23, Pages 91-97, ISSN 1369-5266, https://doi.org/10.1016/j.pbi.2014.11.002.

Gallavotti, A. (2013). The role of auxin in shaping shoot architecture. J. Exp. Bot.; 64 (9): 2593-2608. doi: 10.1093/jxb/ert141

Gardiner J (2013) The evolution and diversification of plant microtubule-associated proteins. Plant Journal 75: 219-229.

Gendron, J.M., Liu, J.S., Fan, M., Bai, M.Y., Wenkel, S., Springer, P.S. Barton, M.K. and Wang Z.Y. (2012). Brassinosteroids regulate organ boundary formation in the shoot apical meristem of Arabidopsis. Proceedings of the National Academy of Sciences, USA 109, 21152–21157.

Genschik, P., Marrocco, K., Bach, L., Noir, S., Criqui, M.C. (2014). Selective protein degradation: a rheostat to modulate cell cycle phase transitions. Journal of

Experimental Botany. 65, 2603–2615.

Glover, B.J. (2000). Differentiation in plant epidermal cells. Journal of Experimental Botany 51:497505

Gonzalez, N., Vanhaeren, H. and Inzé, D. (2012). Leaf size control: complex coordination of cell division and expansion. Cell press. Volume 17, Issue 6, Pages 332–340.

Grandjean, O., Vernoux, T., Laufs, P., Belcram, K., Mizukami, Y. and Traas, J. (2004). In vivo analysis of cell division, cell growth, and differentiation at the shoot apical meristem in Arabidopsis. The Plant Cell 16, 74–87.

Grones, P., Majda,M., Doyle, S.M., Van Damme, D., Robert, S. (2020). Fluctuating auxin response gradients determine pavement cell-shape acquisition. Proceedings of the National Academy of Sciences, 117 (27) 16027-16034; DOI: 10.1073/pnas.2007400117

Grunewald, W., Friml, J. (2010). The march of the PINs: developmental plasticity by dynamic polar targeting in plant cells. The EMBO Journal.vol.29. issue 16. Pg 2700-2714. 10.1038/emboj.2010.181

Gutierrez, R., Lindeboom, J.J., Paredez, A.R., Emons, A.M.C., Ehrhardt, D.W. (2009). Arabidopsis cortical microtubules position cellulose synthase delivery to the plasma membrane and interact with cellulose synthase trafficking compartments. Nat. Cell Biol., 11, pp. 797-806.

Haas K.T. Wightman R. Meyerowitz E.M. Peaucelle A. (2020). Pectin homogalacturonan nanofilament expansion drives morphogenesis in plant epidermal cells. *Science.*; 367: 1003-1007.

Hall, H., Ellis, B. (2012). Developmentally equivalent tissue sampling based on growth kinematic profiling of Arabidopsis inflorescence stems. New Phytol, 194, pp. 287-296.

Hamada T (2014). Microtubule organization and microtubule-associated proteins in plant cells. Int Rev Cell Mol Biol 312: 1–52.

Hamant, O., Heisler, M.G., Jönsson, H., Krupinski, P., Uyttewaal, M., Bokov, P., Corson, F., Sahlin, P., Boudaoud, A., Meyerowitz, E.M. *et al* (2008). Developmental patterning by mechanical signals in Arabidopsis. Science, 322, pp. 1650-1655.

Hang, Y and Showalter, A. M. (2020). CRISPR/Cas9 Genome Editing Technology: A Valuable Tool for Understanding Plant Cell Wall Biosynthesis and Function. Frontiers in Plant Science. Volume 11, pg 1779. https://www.frontiersin.org/article/10.3389/fpls.2020.589517

Heisler, M.G., Hamant, O., Krupinski, P., Uyttewaal, M., Ohno, C., Jönsson, H., Traas, J. and Meyerowitz. (2010). Alignment between PIN1 polarity and microtubule orientation in the shoot apical meristem reveals a tight coupling between morphogenesis and auxin transport. PLoS Biol, 8, p. e1000516

Heisler, M.G., Byrne, M.E. (2020). Progress in understanding the role of auxin in lateral organ development in plants, Current Opinion in Plant Biology, Volume 53, Pages 73-79, ISSN 1369-5266, https://doi.org/10.1016/j.pbi.2019.10.007.

Hejnowicz, Z. Sievers, A. (1995b). Tissue stresses in organs of herbaceous plants. II. Determination in three dimensions in the hypocotyl of sunflower. *Journal of Experimental Botany* 46, 1045–1053.

Hepler, P.K. (2016). The cytoskeleton and its regulation by calcium and protons. Plant Physiol., 170, pp. 3-22

Ho, J., Tumkaya, T., Aryal, S., Choi, H., Claridge-Chang, A. (2019). Moving beyond P values: Everyday data analysis with estimation plots**.** *Nature Methods*, 1548-7105. doi:10.1038/s41592-019-0470-3

Houdusse, A., Gaucher, J.F., Krementsova, E., Mui, S., Trybus, K.M. and Cohen, C. (2006). Crystal structure of apo-calmodulin bound to the first two IQ motifs of myosin V reveals essential recognition features. PNAS vol. 103, No. 51. 19326 – 19331

Hunter, J.D. (2007). Matplotlib: A 2D graphics environment. Computing in science & engineering, 9(3), pp.

Hyun, Y., Kim, J., Cho, S. W., Choi, Y., Kim, J.-S., & Coupland, G. (2015). Site-directed mutagenesis in Arabidopsis thaliana using dividing tissue-targeted RGEN of the CRISPR/Cas system to generate heritable null alleles. Planta, 241, 271–284. http://doi.org/10.1007/s00425-014-2180-5

Ishida T, Kaneko Y, Iwano M, Hashimoto T. (2007). Helical microtubule arrays in a collection of twisting tubulin mutants of Arabidopsis thaliana. Proc Natl Acad Sci USA 104: 8544-8549

Jarsch I.K., Konrad S.S.A., Stratil T.F., Urbanus S.L., Szymanski W., Braun, P., Braun, K.H. and Ott, T. (2014). Plasma membranes are subcompartmentalized into a plethora of coexisting and diverse microdomains in Arabidopsis and Nicotiana benthamiana. Plant Cell 26: 1698-1711

Jian-Jun, T. Hao-Wei, C. Biao,M. Wan-Ke, Z. Shou-Yi, C. and Jin-Song, Z. (2015). The Role of Ethylene in Plants Under Salinity Stress. Frontiers in Plant Science. VOL 6. Pages 1059. https://www.frontiersin.org/article/10.3389/fpls.2015.01059

Jin, B. Kim, J. Jung, J. Kim, D. and Park, Y. (2017).Characterization of IQ Domain Gene Homologs as Common Candidate Genes for Elongated Fruit Shape in Cucurbits. HORTICULTURAL SCIENCE and TECHNOLOGY 36(1):85-97, 2018)

Jonsson H, Heisler M. G, Shapiro B. E, Mjolsness E, Meyerowitz E. M. (2006). An auxin-driven polarized transport model for phyllotaxis. Proc Natl Acad Sci U S A 103: 1633–1638.

Johnson, K. and Lenhard, M. (2011), Genetic control of plant organ growth. New Phytologist, 191: 319-333. https://doi.org/10.1111/j.1469-8137.2011.03737.x

Kang, J., Tang, J., Donnelly,P., Dengler, N. (2003). Primary vascular pattern and expression of *ATHB-8* in shoots of *Arabidopsis.* New phytologist

Kasprzewska A, Carter R, Swarup R, Bennett M, Monk N, Hobbs JK, Fleming A. Auxin influx importers modulate serration along the leaf margin. (2015). Plant J.;83(4):705-18. doi: 10.1111/tpj.12921. Epub 2015 Jul 27. PMID: 26111009; PMCID: PMC4949643.

Keijzer, J., Mulder, B. and Janson, M. (2014). Microtubule Networks for Plant Cell Division. Systems and Synthetic Biology. 8.3: 187–194. PMC. Web. 31 Mar. 2017

Kölling, M., Kumari, P., Bürstenbinder, K. (2019) Calcium- and calmodulin-regulated microtubule-associated proteins as signal-integration hubs at the plasma membrane–cytoskeleton nexus, *Journal of Experimental Botany*, Volume 70, Issue 2, Pages 387–396, https://doi.org/10.1093/jxb/ery397

Kremers G.J., Goedhart J., van Munster E.B., Gadella T.W., Jr. (2006). Cyan and yellow super fluorescent proteins with improved brightness, protein folding, and FRET forster radius. Biochemistry;45:6570–6580. doi: 10.1021/bi0516273

Kugler, A., Hoth, S. and Dietrich, P. (2013). An IQ Domain Mediates the Interaction with Calmodulin in a Plant Cyclic Nucleotide-Gated Channel. Cornelia Fischer, Plant Cell Physiol. 54(4): 573–584.

Kushwaha, R., Singh, A., Chattopadhyay, S. (2008). Calmodulin7 plays an important role as transcriptional regulator in *Arabidopsis* seedling developmentPlant Cell, 20, pp. 1747-1759.

Kusumi, A., Fujiwara, T.K., Chadda, R., Xie, M., Tsunoyama, T.A., Kalay, Z., Kasai, R.S. and Suzuki, K.G. (2012). Dynamic organizing principles of the plasma membrane that regulate signal transduction: commemorating the fortieth anniversary of Singer and Nicolson's fluid-mosaic model. Annu Rev Cell Dev Biol 28: 215-250.

Kutschera, U. and Niklas,K. J. (2013). Cell division and turgor-driven stem elongation in juvenile plants: A synthesis, Plant Science, Vol: 207, Page: 45-56.

Kwaaitaal M, Huisman R, Maintz J, Reinstädler A, Panstruga R. (2011). Ionotropic glutamate receptor (iGluR)-like channels mediate MAMP-induced calcium influx in *Arabidopsis thaliana*. Biochemical Journal 440: 355–365.

Lampropoulos, A., Sutikovic, Z., Wenzl, C., Maegele, I., Lohmann, J.U. and Forner, J. (2013). GreenGate - A Novel, Versatile, and Efficient Cloning System for Plant Transgenesis. PLoS ONE 8(12): e83043. doi:10.1371/journal.pone.0083043.

Landrein, B., Hamant, O. (2013). How mechanical stress controls microtubule behavior and morphogenesis in plants: history, experiments and revisited theories. The Plant Journal.

Latchman, D.S. (1997). Transcription factors: an overview. The International Journal of Biochemistry & Cell Biology. 29 (12): 1305–12. doi:10.1016/S1357-2725(97)00085-X. PMID 9570129

Lazzaro M.D., Wu S, Snouffer A, Wang Y, van der Knaap E. (2018). Plant Organ Shapes Are Regulated by Protein Interactions and Associations With Microtubules. Frontiers in Plant Science.VOL 9 Pg 1766. https://www.frontiersin.org/article/10.3389/fpls.2018.01766 DOI=10.3389/fpls.2018.01766

Lee, B. H., Johnston, R., Yang, Y., Gallavotti, A., Kojima, M., Travençolo, B. A., Costa, L., Sakakibara, H., & Jackson, D. (2009). Studies of aberrant phyllotaxy1 mutants of maize indicate complex interactions between auxin and cytokinin signaling in the shoot apical meristem. Plant physiology, 150(1), 205–216. https://doi.org/10.1104/pp.109.137034

Levy, M., Wang, Q., Kaspi, R., Parrella, M. P., and Abel, S. (2005). Arabidopsis IQD1, a novel calmodulin-binding nuclear protein, stimulates glucosinolate accumulation and plant defense. Plant J. 43, 79–96. doi: 10.1111/j.1365-313X.2005.02435.x

Li J, Wang X, Qin T, Zhang Y, Liu X, Sun J, Zhou Y, Zhu L, Zhang Z, Yuan M, et al (2011). MDP25, a novel calcium regulatory protein, mediates hypocotyl cell elongation by destabilizing cortical microtubules in Arabidopsis. Plant Cell 23: 4411–4427.

Li, T., Yan, A., Bhatia, N., Altinok, A., Afik, E., Durand-Smet, P., Tarr, P.T., Schroeder, J.I., Heisler, M.G., & Meyerowitz, E.M. (2019). Calcium signals are necessary to establish auxin transporter polarity in a plant stem cell niche. Nat Commun . 13;10(1):726. doi: 10.1038/s41467-019-08575-6.

Liu, K.,Rajareddy, S., Liu, L., Jagarlamudi, K., Boman, K., Selstam, G. and Reddy, P. (2006). Control of mammalian oocyte growth and early follicular development by the oocyte PI3 kinase pathway: New roles for an old timer. Developmental Biology, 299, pp. 1-11.

Liu ZY, Persson S, Zhang Y (2015). The connection of cytoskeletal network with plasma membrane and the cell wall. Journal of Integrative Plant Biology 57: 330-340.

Long, J.A. and Barton, M.K.(1998). The development of apical embryonic pattern in Arabidopsis Development, 125, pp. 3027–3035.

Louveaux, M. Julien, J-D., Mirabet, V. Boudaoud, A. and Hamant, O. (2016). Cell division plane orientation based on tensile stress in *Arabidopsis thaliana*. PNAS July 26, 2016 113 (30) E4294-E4303; first published July 19, 2016; https://doi.org/10.1073/pnas.1600677113

Maeda, S., Gunji, S., Hanai, K., Hirano, T., Kazama, Y., Ohbayashi, I., Abe, T., Sawa, S., Tsukaya, H., Ferjani, A. (2014). The Conflict Between Cell Proliferation

and Expansion Primarily Affects Stem Organogenesis in Arabidopsis *Plant and Cell Physiology*, Volume 55, Issue 11, Pages 1994–2007

Maugarny-Calès, A., Laufs, P. (2018). Getting leaves into shape: a molecular, cellular, environmental and evolutionary view.. Development 2018 145: dev161646 doi: 10.1242/dev.161646

Mayer, F.F.X., Schoof, H., Haecker, A., Lenhard, M., Jürgens, G. and Laux, T. (1998). Role of WUSCHEL in regulating stem cell fate in the Arabidopsis shoot meristem. Cell, 95, pp. 805–815.

McCormack E., Braam J. (2003). Calmodulins and related potential calcium sensors of *Arabidopsis*. New Phytol. 159, 585–598. 10.1046/j.1469-8137.2003.00845.x

Mitra, D., Kumari, P., Quegwer, J., Klemm, S., Möller, B., Poeschl, Y., Pflug, P., Stamm, G., Abel, S., and Bürstenbinder, K. (2019). Microtubule-associated protein IQ67 DOMAIN5 regulates interdigitation of leaf pavement cells in Arabidopsis thaliana. *Journal of Experimental Botany*, Volume 70, Issue 2, Pages 529–543.

Mirabet, V. Jas, P. Bondaoud, A. Hamant, O. (2011). The role of mechanical forces in plant morphogenesis. Annu. Rev. Plant Biol., 62, pp. 365-385.

Mirabet V, Krupinski P, Hamant O, Meyerowitz EM, Jönsson H, Boudaoud A (2018) The self-organization of plant microtubules inside the cell volume yields their cortical localization, stable alignment, and sensitivity to external cues. PLoS Comput Biol 14(2): e1006011. https://doi.org/10.1371/journal.pcbi.1006011

Möller, B. K. (2012). Identification of novel MONOPTEROS target genes in embryonic root initiation. Thesis Wageningen University.

Moon, D-O., Kim, M-O., Choi, Y. H., Kim, G-Y. (2008). β-Sitosterol induces G2/M arrest, endoreduplication, and apoptosis through the Bcl-2 and PI3K/Akt signaling pathways. Cancer Letters, Elsevier

Müller D, Leyser O. (2011). Auxin, cytokinin and the control of shoot branching. Ann Bot. ;107(7):1203-12. doi: 10.1093/aob/mcr069. Epub 2011 Apr 18. PMID: 21504914; PMCID: PMC3091808.

Murray, J. A. H. et al. (1998). in Plant Cell Division (eds Francis, D., Dudits, D. &

Inzé, D.) 99–127 Portland, London

Nakamura, M., Lindeboom, J.J., Saltini, M., Mulder, B.M., Ehrhardt, D.W. (2018). SPR2 protects minus ends to promote severing and reorientation of plant cortical microtubule arrays. *J Cell Biol* 5; 217 (3): 915–927. doi: https://doi.org/10.1083/jcb.201708130

Nakashima, K., Yamaguchi-Shinozaki, K. (2013). ABA signaling in stress-response and seed development. *Plant Cell Rep* 32, 959–970. https://doi.org/10.1007/s00299-013-1418-1

Nakayama, N., Smith, R.S., Mandel, T., Robinson, S., Kimura, S., Boudaoud, A., Kuhlemeier, C. (2012). mechanical regulation of Auxin mediated growth. Current biology Volume 22, Issue 16, Pages 1468-1476.

Narasimhulu, S.B and Reddy, A. S. N. (1998). Characterization of microtubule binding domains in the Arabidopsis kinesin-like calmodulin-binding protein. Plant Cell. 10; 957-965.

Nicotra A. B., Leigh A., Boyce, K.C., Jones C.S., Niklas K.J., Royer D. L., Tsukaya H. (2011). The evolution and functional significance of leaf shape in the angiosperms. *Functional Plant Biology* **38**, 535-552.

Niculescu, A.B., Chen, X., Smeets, M., Hengst, L., Prives, C., Reed, S.I. (1998). Effects of p21(Cip1/Waf1) at both the G_1/S and the G_2/M cell cycle transitions: pRb is a critical determinant in blocking DNA replication and in preventing endoreduplication Mol. Cell. Biol., 18, pp. 629-643.

Niklas K.J. Paolillo D.J. Jr . (1998). Preferential states of longitudinal tension in the outer tissues of *Taraxacum officinale* (Asteraceae) peduncles. *American Journal of Botany* 85, 1068–1081.

Nikovics, K., Blein, T., Peaucelle, A., Ishida, T., Morin, H., Aida, M., Laufs, P. (2006). The Balance between the *MIR164A* and *CUC2* Genes Controls Leaf Margin Serration in *Arabidopsis*. The Plant Cell, 18 (11) 2929-2945; DOI: 10.1105/tpc.106.045617

Palatnik, J.F. et al. (2003). Control of leaf morphogenesis by microRNAs. Nature, 425, pp. 257–263

Pan, Y. Liang, X. Gao, M. Liu, H.· Meng, H. Weng, Y. Cheng, Z. (2017). Round fruit shape in WI7239 cucumber is controlled by two interacting quantitative trait

loci with one putatively encoding a tomato SUN homolog. Theor Appl Genet 130:573–586

Park, J., Nguyen, K. T., Park, E., Jeon, J. S., & Choi, G. (2013). DELLA proteins and their interacting RING Finger proteins repress gibberellin responses by binding to the promoters of a subset of gibberellin-responsive genes in Arabidopsis. *The Plant cell*, *25*(3), 927–943. https://doi.org/10.1105/tpc.112.108951

Peaucelle, A., Braybrook, S.A. Le Guillou, L., Bron, E., Kuhlemeier, C. and Höfte, H. (2011). Pectin-induced changes in cell wall mechanics underlie organ initiation in Arabidopsis. Current Biology 21, 1720–1726.

Pelletier, S., Van Orden,J., Wolf, S., Vissenberg, K., Delacourt,J., Assoumou, Y. *et al.* (2010). A role for pectin de-methylesterification in a developmentally regulated growth acceleration in dark-grown *Arabidopsis* hypocotyls.New Phytol., 188, pp. 726-739

Perrot-Rechenmann, C. (2010). Cellular responses to auxin: division versus expansion. Cold Spring Harb. Perspect Biol. **2**, a001446. doi:10.1101/cshperspect.a001446

Peter W.S. Tomos A.D. (2000). The mechanic state of ‘inner tissue’ in the growing zone of sunflower hypocotyls and the regulation of its growth rate following excision. *Plant Physiology* 123, 605–612.

Petrovska, B., Cenklova, V., Pochylova, Z., Kourova, H., ilova, A.D., Binarova O.e.P.H.L. and Binarova, P. (2012). Plant Aurora kinases play a role in maintenance of primarymeristems and control of endoreduplication. New Phytologist 193: 590–604doi: 10.1111/j.1469-8137.2011.03989.x

Ranf S, Eschen-Lippold L, Pecher P, Lee J, Scheel D. (2011). Interplay between calcium signalling and early signalling elements during defence responses to microbe- or damage-associated molecular patterns. Plant Journal 68: 100–113.

Ranty, B., Aldon, D. and Galaud, J.P. (2006). Plant Calmodulins and Calmodulin-Related Proteins Multifaceted Relays to Decode Calcium Signals. Plant Signal Behav. 1(3): 96–104.

Rashotte, A.M., Carson, S.D.B, To, J.P.C. and Kieber, J.J. (2003). Expression Profiling of Cytokinin Action in Arabidopsis. Plant Physiology. 132(4):1998-2011. doi:10.1104/pp.103.021436.

Rasmussen, C.G., Wright, A.J., Müller, S. (2013). Review: The role of the cytoskeleton and associated proteins in determination of the plant cell division plane. Plant J. 75(2):258-69.

Rast, M.I. and Simon, R. (2012). Arabidopsis JAGGED LATERAL ORGANS acts with ASYMMETRIC LEAVES2 to coordinate KNOX and PIN expression in shoot and root meristems. The Plant Cell. 24, 2917–2933

Riou-Khamlichi, C., Huntley, R., Jacqmard, A. & Murray, J.A.H. (1999). Cytokinin activation of *Arabidopsis* cell division through a D-type cyclin. *Science* 283, 1541–1544.

Reinhardt, D., Pesce, E., Stieger, P. *et al.* (2003). Regulation of phyllotaxis by polar auxin transport. *Nature* 426**,** 255–260. https://doi.org/10.1038/nature02081

Roeder, A.H., Ferrándiz, C., Yanofsky, M.F. (2003). The Role of the REPLUMLESS Homeodomain Protein in Patterning the Arabidopsis Fruit. Current Biology, Volume 13, Issue 18, 1630–1635.

Sablowski, R. and Dornelas, M.C. (2014). Interplay between cell growth and cell cycle in plants. J Exp Bot. 65 (10): 2703-2714. doi: 10.1093/jxb/ert354

Sachs, R.M. Stem elongation. Annu Rev Plant Physiol, 16 (1965), pp. 73-95

Sampathkumar, P. Krupinski, R. Wightman, P. Milani, A. Berquand, A. Boudaoud, O. Hamant, H. Jönsson, E.M. Meyerowitz. (2014). Subcellular and supracellular mechanical stress prescribes cytoskeleton behavior in *Arabidopsis* cotyledon pavement cells. eLife, 3, p. e01967

Sapala A., Runions A., Routier-Kierzkowska A.L., Das Gupta M., Hong L., Hofhuis H., Verger S., Mosca G., Li C.B., and Hay A. et al. (2018). Why plants make puzzle cells, and how their shape emerges. *eLife.*; 7e32794

Satina, S. et al. (1940). Demonstrations of the three germ layers in the shoot apex of Datura by means of induced polyploidy in periclinal chimerasAm. J. Bot., 27, pp. 895–905.

Schaller, E. Street, I.H. and Kieber, J.J. (2014). Cytokinin and the cell cycle, Current Opinion in Plant Biology, Volume 21, Pages 7-15, ISSN 1369-5266, https://doi.org/10.1016/j.pbi.2014.05.015.

Schiessl, K., Muiño, J.M. and Sablowski, R. (2014).Arabidopsis JAGGED links floral organ patterning to tissue growth by repressing Kip-related cell cycle

inhibitors. PNAS 2014 111 (7) 2830-2835.

Schiessl, K. Kausika, S. Southam, P. Bush, M. Sablowski, R. (2012). JAGGED controls growth anisotropy and coordination between cell size and cell cycle during plant organogenesis. Current Biology 22, 1739–1746.

Schindelin, J.; Arganda-Carreras, I. & Frise, E. et al. (2012), "Fiji: an open-source platform for biological-image analysis", Nature methods 9(7): 676-682, PMID 22743772.

Schlereth, A., B. Moller, W. Liu, M. Kientz, J. Flipse, E. H. Rademacher, M. Schmid, G. Jurgens and D. Weijers (2010). “MONOPTEROS controls embryonic root initiation by regulating a mobile transcription factor.” Nature 464(7290): 913-916.

Schmid et. Al (2005). Data from Gene Expression Map of Arabidopsis Development Nat. Gen. 37.501.

Schopfer, P. (2006). Biomechanics of plant growth. Am. J. Bot., 93, pp. 1415-1425.

Scott AM, Antal CE, Newton AC (2013). Electrostatic and hydrophobic interactions differentially tune membrane binding kinetics of the C2 domain of protein kinase Cα. J Biol Chem 288: 16905–16915.

Sedbrook, J.C., Ehrhardt, D.W., Fisher, S.E., Scheible, W.R. and Somerville, C.R. (2004). The Arabidopsis sku6/spiral1 gene encodes a plus endlocalized microtubule-interacting protein involved in directional cell expansion. Plant Cell 16: 1506-1520.

Serrano-Mislata, A. Sablowski, R. (2018). The pillars of land plants: new insights into stem development. Current Opinion in Plant Biology. Volume 45, Part A, Pages 11-17.

Serrano-Mislata, A., Bencivenga, S., Bush, M. Schiessl,K. Boden, S. Sablowski, R. (2017). DELLA genes restrict inflorescence meristem function independently of plant height. Nat Plants, 3, p. 749.

Shapiro, B.E., Tobin, C., Mjolsness, E. and Meyerowitz, E.M. (2015). Analysis of cell division patterns in the Arabidopsis shoot apical meristem. Proc Natl Acad Sci USA, 112, pp. 4815–4820

Shen, Q., Wang, Y.T., Tian, H., Guo, F.Q. (2013). Nitric oxide mediates cytokinin functions in cell proliferation and meristem maintenance in Arabidopsis. Mol Plant, 6, pp. 1214-1225.

Shi, H., Wang,L.L. Sun, L.T. Dong, L.L., Liu, B., Chen, L.P.(2012)Cell division and endoreduplication play important roles in stem swelling of tuber mustard (*Brassica juncea* Coss. var. *tumida* Tsen et Lee) Plant biology.

Shirley, N.J., Aubert, M.K., Wilkinson, L.G., Bird, D.C., Lora, J., Yang,X., Tucker, M.R. (2018). Translating auxin responses into ovules, seeds and yield: Insight from *Arabidopsis* and the cereals Journal of Integrative Plant Biology. https://doi.org/10.1111/jipb.12747

Siligato R, Wang X, Yadav SR, Lehesranta S, Ma G, Ursache R, Sevilem I, Zhang J, Gorte M, Prasad K, Wrzaczek M, Heidstra R, Murphy A, Scheres B, Mähönen AP. (2015). MultiSite Gateway compatible cell type-specific gene inducible system for plants. Plant Physiol. pii: pp.01246.2015.

Singh, A.P. Savaldi-Goldstein, S. (2015). Growth control: brassinosteroid activity gets context, *Journal of Experimental Botany*, Volume 66, Issue 4, Pages 1123–1132, https://doi.org/10.1093/jxb/erv026

Skylar, A., Hong, F., Chory, J., Weigel, D., Wu, X. (2010). *STIMPY* mediates cytokinin signaling during shoot meristem establishment in *Arabidopsis* seedlings. Development 137: 541-549; doi: 10.1242/dev.041426

Smith, R.S. Kuhlemeier, C. and Prusinkiewicz,P. (2006). Inhibition fields for phyllotactic pattern formation: a simulation study. Canadian Journal of Botany, 84:1635-1649, https://doi.org/10.1139/b06-133

Smith, R.S. Guyomarc'h, S., Mandel, T., Reinhardt, D., Kuhlemeier, C. and Prusinkiewicz, P. (2006). A plausible model of phyllotaxis PNAS January 31, 103 (5) 1301-1306

Soni, R., Carmichael, J.P., Shah, Z.H. & Murray, J.A.H. (1995). A family of cyclin D homologs from plants differentially controlled by growth regulators and containing the conserved retinoblastoma protein interaction motif. Plant Cell 7, 85–103.

Sotiriou, P., Giannoutsou. E., Panteris, E., Galatis, B., Apostolakos, P. (2018). Local differentiation of cell wall matrix polysaccharides in sinuous pavement cells:

its possible involvement in the flexibility of cell shape Plant Biology, 10.1111/plb.12681, 29247575.

Strauss, S., Lempe, J., Prusinkiewicz, P., Tsiantis, M. and Smith, R.S. (2020), Phyllotaxis: is the golden angle optimal for light capture? New Phytol, 225: 499-510. doi:10.1111/nph.16040.

Su, L., Bassa, C., Audran, C., Mila, I., Cheniclet, C., Chevalier, C., Roustan,J-P. Chervin, C. (2014). The Auxin *Sl-IAA17* Transcriptional Repressor Controls Fruit Size Via the Regulation of Endoreduplication-Related Cell Expansion *Plant and Cell Physiology*, Volume 55, Issue 11, Pages 1969–1976.

Sugimoto-Shirasu, K., Roberts, K. (2003). “Big it up”: endoreduplication and cell-size control in plants, Current Opinion in Plant Biology,Volume 6, Issue 6,Pages 544-553,ISSN 1369 5266, https://doi.org/10.1016/j.pbi.2003.09.009

Sugiyama, Y., Wakazaki, M., Toyooka, K., Fukuda, H. and Oda, Y. (2017) A Novel Plasma Membrane-Anchored Protein Regulates Xylem Cell-Wall Deposition through Microtubule-Dependent Lateral Inhibition of Rho GTPase Domains. Current Biology 27, 2522–2528

Suzuki, N. Koussevitzky, S. Mittler, R. Miller, G. (2011). ROS and redox signalling in the response of plants to abiotic stress. Plant, Cell and Environment 35, 259–270

Swain, S.M. and Singh, D.P. (2005). Tall tales from sly dwarves: novel functions of gibberellins in plant development. Volume 10, Issue 3, Pages 123–129 http://dx.doi.org/10.1016/j.tplants.2005.01.007

Swarup, R. Benjamin, P. (2012). AUX/LAX family of auxin influx carriers—an overview. Frontiers in Plant Science. Vol 3. Pages 225. DOI 10.3389/fpls.2012.00225

Tae-Wuk K. and Zhi-Yong W. (2010). Brassinosteroid Signal Transduction from Receptor Kinases to Transcription Factors. Annu. Rev. Plant Biol. 61:681–704.

Tianxiao, Y., Yongyan, W., Sachin, T., Zhanhui, Z., Guiliang, T. (2018). The Making of Leaves: How Small RNA Networks Modulate Leaf Development. Frontiers in Plant Science.

Townsley, B., Sinha, N. (2012). A new development: evolving concepts in leaf ontogeny. Annu Rev Plant Biol, 63, pp. 535-562.

Tsai, Y.C., Delk, N.A., Chowdhury, N.I., Braam, J. (2007). *Arabidopsis* potential calcium sensors regulate nitric oxide levels and the transition to flowering.Plant Signal. Behav., 2, pp. 446-454.

Tsukaya H. (2002). Interpretation of mutants in leaf morphology: genetic evidence for a compensatory system in leaf morphogenesis that provides a new link between cell and organismal theories. Int Rev Cytol.; 217: 1–39. pmid:12019561

Tsuda, K. Abraham-Juarez, M.J. Maeno, A., Dong, Z. Aromdee, D. Meeley, R. Shiroishi, T., Nonomura,K.I. Hake. S. (2017). KNOTTED1 cofactors, BLH12 and BLH14, regulate internode patterning and vein anastomosis in maizePlant Cell, 29, pp. 1105-1118.

Tuteja,N. and Mahajan, S. (2007). Calcium Signaling Network in Plants An Overview. Plant Signal Behav. 2(2): 79–85

Ubeda-Tomas S., Swarup R., Coates J., Swarup K., Laplaze L., Beemster G. T. S., Hedden P., Bhalerao R., Bennett M. J.(2008). Root growth in Arabidopsis requires gibberellin/DELLA signalling in the endodermis. Nat. Cell Biol. **10**, 625–628

Untergasser A. 2008 “Preparation of Electro-Competent Cells” Untergasser's Lab. http://www.untergasser.com/lab/protocols/competent_cells_electro_v1_0.pdf

Vale, R.D., Funatsu, T., Pierce, D.W., Romberg, L., Harada, Y., & Yanagida, T. (1996). Direct observation of single kinesin molecules moving along microtubules. Nature, 380(6573), 451–453. http://doi.org/10.1038/380451a0

Van Damme, D. De Rybel, B., Gudesblat, G., Demidov,D., Grunewald, W., De Smet,I., Houben, A., Beeckman, T., Russinova, E.(2011). *Arabidopsis* α Aurora Kinases Function in Formative Cell Division Plane Orientation. The Plant Cell, 23 (11) 4013-4024; DOI:10.1105/tpc.111.089565

Wakelam, M.J.O. and Berridge, M.J (2007). Inositol trisphosphate and calcium oscillations. *Biochem Soc Symp* 12; 74 1–7. doi: https://doi.org/10.1042/BSS2007c01

Waldie, T., Leyser, O. (2018). Cytokinin Targets Auxin Transport to Promote Shoot Branching. Plant Physiology, 177 (2) 803-818; DOI: 10.1104/pp.17.01691

Wang, F., Cui, X., Sun, Y. *et al.* (2013). Ethylene signaling and regulation in plant growth and stress responses. *Plant Cell Rep* 32, 1099–1109. https://doi.org/10.1007/s00299-013-1421-6

Wang X. Wilson L. Cosgrove D.J. (2020). Pectin methylesterase selectively softens the onion epidermal wall yet reduces acid-induced creep. *J. Exp. Bot.*; https://doi.org/10.1101/766931.

Wang, Y. Clevenger, J.P. Illa-Berenguer, E. Meulia, T. van der Knaap, E. and Sun, L. (2019). A Comparison of sun, ovate, fs8.1 and Auxin Application on Tomato Fruit Shape and Gene Expression. Plant and Cell Physiology.

Waskom, M. and the seaborn development team, (2020). mwaskom/seaborn, Zenodo, latest version. Doi 10.5281/zenodo.592845,https://doi.org/10.5281/zenodo.592845.

Weber, E., Engler, C., Gruetzner, R., Werner, S. Marillonnet, S. (2011). A modular cloning system for standardized assembly of multigene constructs. PLoS One, 6, p. e16765.

Wechter W.P., Levi A., Harris K.R., Davis A.R., Fei Z., Katzir N., Giovannoni J.J., Salman-Minkov A., Hernandez A., Thimmapuram J., Tadmor Y., Portnoy V., Trebitsh T. (2008). Gene expression in developing watermelon fruit. BMC Genomics. 9: 275-10.1186/1471-2164-9-275.

Wendrich, J.R., Yang, B-J., Mijnhout, P., Xue, H-W., Rybel, B.D. and Weijers, D. (2018). IQD proteins integrate auxin and calcium signaling to regulate microtubule dynamics 5 during Arabidopsis development. BioRxiv.

Willige, B. C., Ghosh, S., Nill, C., Zourelidou, M., Dohmann, E. M., Maier, A., & Schwechheimer, C. (2007). The DELLA domain of GA INSENSITIVE mediates the interaction with the GA INSENSITIVE DWARF1A gibberellin receptor of Arabidopsis. *The Plant cell*, *19*(4), 1209–1220. https://doi.org/10.1105/tpc.107.051441

Wolf, S., Hématy, K., Höfte, H. (2012). Growth control and cell wall signaling in plants. Annual Review of Plant Biology 63, 381–407.

Wu, M.L., Yuan, C., Danmei, L., Huanlong, Z. and Dongyue, X.Y. (2016). Genome-wide identification and expression analysis of the IQD gene family in

moso bamboo (Phyllostachys edulis) Scientific Reports 6, Article number: 24520. doi:10.1038/srep24520

Wu S., Clevenger J.P., Sun L., Visa S., Kamiya Y., Jikumaru Y., et al. (2015). The control of tomato fruit elongation orchestrated by *sun*, *ovate* and *fs8.1* in a wild relative of tomato. *Plant Sci*. 238 : 95–104

Wu, S., Xiao, H., Cabrera, A., Meulia, T. and van der Knaap, E. (2011). SUN regulates vegetative and reproductive organ shape by changing cell division patterns. Plant Physiol 157: 1175-1186

Xiao, H., Jiang, N., Schaffner, E., Stockinger, E.J. and van der Knaap, E. (2008). A retrotransposon-mediated gene duplication underlies morphological variation of tomato fruit. Science 319: 1527-1530

Xiong, Y., McCormack, M., Li, L., Hall, Q., Xiang, C. and Sheen, J. (2013). Glucose-TOR signalling reprograms the transcriptome and activates meristems. Nature. 496, 181–186.

Xu, T. Wen, M. Nagawa, S. Fu,Y. Chen, J. Wu, M-J. Perrot-Rechenmann, C. Friml, J. Jones, A.M. Yang, Z. (2010) Cell Surface- and Rho GTPase-Based Auxin Signaling Controls Cellular Interdigitation in *Arabidopsis.* Cell. Volume 143, Issue 1, 1 October 2010, Pages 99-110

Xu, Q., Krishnan, S., Merewitz, E., Xu, J., & Huang, B. (2016). Gibberellin-Regulation and Genetic Variations in Leaf Elongation for Tall Fescue in Association with Differential Gene Expression Controlling Cell Expansion. *Scientific reports*, *6*, 30258. https://doi.org/10.1038/srep30258

Yang, B., Wendrich, J.R., Rybel, B.D., Weijers, D. and Xue1, H. (2018). *OsIQD14* regulates rice grain shape through modulating the microtubule cytoskeleton. BioRxiv

Yang, T., Poovaiah, B.W. (2002). Hydrogen peroxide homeostasis: Activation of plant catalase by calcium/calmodulin. Proceedings of the National Academy of Sciences, 99 (6) 4097-4102; DOI: 10.1073/pnas.052564899

Yanai, O., Shani, E., Dolezal, K., Tarkowski, P., Sablowski, R., Sandberg, G., Samach, A. and Ori, N. (2005). *Arabidopsis* KNOXI Proteins Activate Cytokinin Biosynthesis Volume 15, Issue 17, p1566–1571.

Yang T., Davies P. J., Reid J. B. (1996). Genetic dissection of the relative roles of auxin and gibberellin in the regulation of stem elongation in intact light-grown peas. Plant Physiol. 110, 1029–1034.

Ye ,J., Tian, R., Meng, X., Tao, P., Li, C., Liu, G., Chen, W., Wang, Y., Li, H., YeYuyang, Z. (2020). Tomato *SD1*, encoding a kinase-interacting protein, is a major locus controlling stem development. Journal of *Experimental Botany*, Volume 71, Issue 12, 22 June 2020, Pages 3575–3587, https://doi.org/10.1093/jxb/eraa144

Yen, L., Lee, C., Hou, X., Fang, L., Fan, S., Kumar, P.P., Yu, H. (2012*) STUNTED* mediates the control of cell proliferation by GA in *Arabidopsis* Development 139: 1568-1576; doi: 10.1242/dev.079426

Yoshida S, Barbier de Reuille P, Lane B, Bassel GW, Prusinkiewicz P, et al. 2014. Genetic control of plant development by overriding a geometric division rule.Dev.Cell 29:75–87

Yoshida, H., Hirano, K., Sato, T., Mitsuda, N., Nomoto, M., Maeo, K., Koketsu, E., Mitani, R., Kawamura, M., Ishiguro, S., Tada, Y., Ohme-Takagi, M., Matsuoka, M., M Ueguchi-Tanaka, M. (2014) DELLA acts as a coactivator using IDD proteins. Proceedings of the National Academy of Sciences, 111 (21) 7861-7866; DOI: 10.1073/pnas.1321669111

Yu, H., Ito, T., Zhao, Y., Peng, J., and Kumar, P. (2004). Floral homeotic genes are targets of gibberellin signaling in flower development. Proceedings of the National Acad. Sciences.

Zhang, J., S. Vanneste, P. B. Brewer, M. Michniewicz, P. Grones, J. Kleine-Vehn, C. Lofke, T. Teichmann, A. Bielach, B. Cannoot, K. Hoyerova, X. Chen, H. W. Xue, E. Benkova, E. Zazimalova and J. Friml (2011). “Inositol trisphosphate-induced Ca2+ signaling modulates auxin transport and PIN polarity.” Dev Cell 20(6): 855-866.

Zhang, Q.-Q., Wang, J.-G., Wang, L.-Y., Wang, J.-F., Wang, Q., Yu, P., Bai, M.-Y. and Fan, M. (2020), Gibberellin repression of axillary bud formation in *Arabidopsis* by modulation of DELLA-SPL9 complex activity. J. Integr. Plant Biol., 62: 421-432. https://doi.org/10.1111/jipb.12818

Zhang, X., Henriques, R., Lin, SS. *et al.* (2006) *Agrobacterium*-mediated transformation of *Arabidopsis thaliana* using the floral dip method. *Nat Protoc* 1, 641–646. https://doi.org/10.1038/nprot.2006.97

Zhang, Y., Pribil, M., Palmgren, M. *et al.* (2020) A CRISPR way for accelerating improvement of food crops. *Nat Food* 1, 200–205. https://doi.org/10.1038/s43016-020-0051-8

Zentella, R., Zhang, Z.-L., Park, M., Thomas, S.G., Endo, A., Murase, K., Fleet, C.M., Jikumaru, Y., Nambara, E., Kamiya, Y. and Sun, T.-P. (2007). Global Analysis of DELLA Direct Targets in Early Gibberellin Signaling in Arabidopsis. The Plant Cell.

Zhao, F., Du, F., Oliveri, H., Zhou, L., Ali, O., Chen, W., Feng, S., Wang, Q., Lü, S., Long, M., Schneider, R., Sampathkumar, A., Godin, C., Traas, J., Jiao. Y. (2020) Microtubule-Mediated Wall Anisotropy Contributes to Leaf Blade Flattening. Current Biolog. Volume 30, Issue 20, Pages 3972-3985

Zhao, Y. & Mooney, S.D. (2009). A study on synthetic regional environmental policies for utilising biomass resources. Int. J. Environ. Sci. Te 11, 102–117.

Zhao, Y., Araki, S., Wu, J., Teramoto, T., Chang, Y.-F., Nakano, M. and Campbell, R. E. (2011). An Expanded Palette of Genetically Encoded Ca2+ Indicators. Science (New York, N.Y.), 333(6051), 1888–1891. http://doi.org/10.1126/science.1208592

Zhou, X. and Sun, T.-P. (2011). IQD, a negative regulator of GA response, plays a role in the regulatory network among the GA, calcium and auxin pathways. 22nd international conference on Arabidopsis research, abstract.

Zhu, M. and HK Roeder, HK. A. 2020. Plants are better engineers: the complexity of plant organ morphogenesis, Current Opinion in Genetics & Development, Volume 63, Pages 16-23, ISSN 0959-437X, https://doi.org/10.1016/j.gde.2020.02.008.